UNIVERSIDADE FEDERAL DO RIO GRANDE DO NORTE
CENTRO DE CIÊNCIAS EXATAS E DA TERRA – CCET
PROGRAMA DE PÓS-GRADUAÇÃO EM GEODINÂMICA E GEOFÍSICA

DISSERTAÇÃO DE MESTRADO

CARACTERIZAÇÃO QUÍMICA E MINERALÓGICA DE FOSFATOS DE ALUMÍNIO DA FALHA DE SAMAMBAIA, RIO GRANDE DO NORTE

Autor:
ADRIANO HENRIQUE ANDRADE DE AGUIAR

Orientador:
PROF. DR. FREDERICO CASTRO JOBIM VILALVA

Coorientadora:
DRA. CRISTIANE PAULINO DE MENEZES

Dissertação nº 306/PPGG

Agosto de 2025
Natal / RN, Brasil

ADRIANO HENRIQUE ANDRADE DE AGUIAR

CARACTERIZAÇÃO QUÍMICA E MINERALÓGICA DE FOSFATOS DE ALUMÍNIO NA FALHA DE SAMAMBAIA, RIO GRANDE DO NORTE

Dissertação apresentada no dia 13 de Agosto de 2025 ao Programa de Pós-Graduação em Geodinâmica e Geofísica (PPGG) da Universidade Federal do Rio Grande do Norte (UFRN) como requisito à obtenção do título de Mestre em Geodinâmica e Geofísica, Área de Concentração Geodinâmica.

BANCA EXAMINADORA:

Prof. Dr. Frederico Castro Jobim Vilalva
Presidente e orientador – (PPGG/UFRN)

Profª. Dra. Raquel Franco de Souza
Membro Externo – (PRODEMA/UFRN)

Prof. Dr. Fabio Ramos Dias de Andrade
Membro Externo – (IGc/USP)

Universidade Federal do Rio Grande do Norte - UFRN
Sistema de Bibliotecas - SISBI
Catalogação de Publicação na Fonte. UFRN - Biblioteca Setorial Prof. Ronaldo Xavier de Arruda - CCET

Aguiar, Adriano Henrique Andrade de.
Caracterização química e mineralógica de fosfatos de alumínio da falha de Samambaia, Rio Grande do Norte / Adriano Henrique Andrade de Aguiar. - Natal, 2025.
150 f.: il.

Dissertação (mestrado) - Universidade Federal do Rio Grande do Norte, Centro de Ciências Exatas e da Terra, Programa de Pós-Graduação em Geodinâmica e Geofísica. Natal, RN, 2025.
Orientação: Prof. Dr. Frederico Castro Jobim Vilalva.
Coorientação: Dra. Cristiane Paulino de Menezes.

1. Aluminofosfatos - Dissertação. 2. Alteração hidrotermal - Dissertação. 3. Neotectônica - Dissertação. I. Vilalva, Frederico Castro Jobim. II. Menezes, Cristiane Paulino de. III. Título.

RN/UF/CCET CDU 631.851(043.3)

Elaborado por Joseneide Ferreira Dantas - CRB-15/324

AGRADECIMENTOS

Ao passo em que finalizo mais uma conquista e uma etapa da minha vida, tenho refletido sobre os desafios que enfrentamos ao longo do nosso crescimento pessoal e profissional. Começar algo do zero e ter todas as condições para finalizar já é desafiador, e fazer ciência no Brasil poderia ser considerado como um ato de rebeldia, tamanho o menosprezo e sucateamento que a pesquisa científica enfrenta todos os dias em nosso país. Mas difícil mesmo é ter um alicerce construído e sólido que te dê condições de construir a sua própria versão do que é ser humano.

Nesse ciclo que encerro, alguns alicerces foram fundamentais para que eu pudesse fechá-lo com sucesso, e eu os agradeço aqui. Primeiramente à minha mãe, que vem pavimentando essa estrada desde os seus 16 anos. Graças a ela, posso dizer que estou me tornando o primeiro mestre da minha família.

Ao meu orientador Fred, que nos últimos dois anos se mostrou sereno, compreensivo, apoiador e maior entusiasta de meu trabalho. Me deu a certeza de que eu não poderia ter feito escolha melhor para aquele por quem eu já nutria profunda admiração enquanto professor desde a graduação, mas que também se tornou meu mentor, amigo, e pai (um pai da geologia, digamos assim).

À minha coorientadora Cristiane, que contribuiu significativamente com a evolução do meu trabalho em todas as vezes que discutimos, solucionamos e avançamos juntos no conhecimento científico, por dividir o fardo e os problemas, os momentos difíceis e desafiadores, e torná-los mais leves nessa trajetória.

Aos meus amigos da UFRN, de gradução e pós-graduação, que sempre estiveram comigo desde 2016, e aos que também fiz pelo caminho.

À minha família e minha namorada, pela torcida, apoio, compreensão e carinho que nunca faltou e sempre esteve presente.

Ao Prof. Francisco Hilário, por acreditar em meu potencial durante o projeto, e juntamente com a Fundação Norte-riograndense de Pesquisa e Cultura (Funpec), o Programa de Pós-graduação em Geodinâmica e Geofísica (PPGG) e à Shell Brasil, pelo subsídio financeiro dedicado ao meu trabalho. Sem ele, eu não poderia e nem conseguiria ter produzido resultados tão significativos.

À UFRN, minha casa há 12 anos, que sempre me acolheu e mais uma vez fez parte da minha formação e qualificação enquanto Geólogo.

Às professoras Paola Barbosa e Gláucia Queiroga, pelas importantes contribuições que fizeram ao meu trabalho. Por fim, agradeço a todos os profissionais, servidores, laboratórios e universidades que prestaram apoio e impactaram diretamente ao meu trabalho e não foram aqui mencionados.

LISTA DE FIGURAS

Figura 1.1: Mapa de localização e acessos à região de estudo desta pesquisa..14

Figure 4.1: Geological setting for Samambaia fault. A) Geological background and host rocks of Samambaia fault with registered earthquake epicenters recording NE-SW fault trend; B) Arizona quarry quartz veins outcrop; C), D) and E) Location of W1, W6 and W7 walls used for sample acquisition and outcrop analyses (Modified from Bezerra et al. 2021)..29

Figure 4.2: D) and A) Walls 6 and 7 of Arizona quarry, respectively showing heavily fractured Si- and P-rich veins exposure with breccia pipes and fault core. B) Detailed image of breccia pipe in W7 showing quartz breccia with APM-rich matrix; C) Detailed image of fault core in W7 showing APM-rich fault gouge; E) Detailed image of APM-filled vein in W6; F) Detailed image of APM-filled porous material..32

Figure 4.3: Multiple textures identified in variscite. A) Colloidal variscite; B) Clast-filling variscite-rich material with Fe-rich crusts showing compositional alternation affecting Al-phosphate precipitation; C) Vein-filling variscite; D) Sheaf-like variscite; E) Vug-filling syntaxial-like growth; F) Vug-filling under cross polarized light showing cryptocrystalline and prysmatic variscite variation along with distinct interference colors and wavy extinction; G) and H) Pore-filling fibrous to prysmatic variscite..34

Figure 4.4: Textural diversity and occurence modes. A) and B) Millisite-rich breccia matrix with variscite-rich recrystallized edges and clast-filling material; C) Breccia matrix composed of crandallite-rich borders and variscite-rich veins; D) Colloidal crandallite with recrystallized spherulitic variscite; E) and F) Calcite/Dolomite pseudomorphs substituted by Si-rich fluid; G) Kaolinite coatings filling porous material and quartz; H) Alteration of kaolinite to variscite...............36

Figure 4.5: Textural evidence of reworked material and multiple fluid injection. A) and B) Thin section image and schematic drawing showing variscite-rich cockade textures with Fe-variscite cockade core inside variscite-rich matrix; C) and D) Cockade texture showing quartz clast surrounded by crandallite borders with recrystallized variscite edges; E and F) Clast-cortex aggregates with quartz clasts inside crandallite-rich material; G) and H) Clast-cortex aggregate with quartz clasts inside variscite-rich material..38

Figure 4.6: Unified diffractograms for 19 analyzed samples showing main intensity peaks and all mineral phases identified based on each respective 2theta angles (Cran = Crandallite; Var = Variscite; HAp/Dol = Hydroxylapatite/Dolomite; Qtz = Quartz; Dia/Mc = Diaspore/Microcline; Cal = Calcite; FAp = Fluorapatite)..40
Figure 4.7: QEMSCAN analyses. A) W5-D1 hand sample; B) Thin section image showing variscite-rich matrix with Fe-rich crusts; C) QEMSCAN mapping with Fe-rich crusts in Orange, variscite-rich matrix in red, quartz in light pink; D) W7-A3 hand sample; E) Thin section image of crandallite and variscite-rich breccia matrix; F) QEMSCAN mapping with crandallite-rich matrix and clasts with vein-like recrystallized variscite; G) W6-C6 hand sample; H) Thin section showing millisite-rich matrix with recrystallized variscite-rich edges and clast-filling material; I) QEMSCAN mapping showing millisite-rich matrix in pink, variscite-rich edges and fillings in red, and quartz in light pink; J) W7-A5 hand sample; K) Thin section image showing kaolinite coatings altered to variscite-rich material; L) QEMSCAN mapping showing kaolinite coatings in brown, variscite in red, quartz in light pink..41
Figure 4.8: SEM analysis imaging. A) W5-F1b thin section; B) SEM image showing pore-filling variscite-rich prysmatic crystals with zoned compositional alternation; C) Schematic drawing showing zoned composition with Fe-rich crusts and Al-rich crystal edges...42
Figure 4.9: Chemical mapping of W6-B2 sample. A) W6-B2 thin section showing variscite and crandallite-rich matrix; B) Chemical mapping of W6-B2 thin section highlighting Ca-rich material in orange; C) Detailed image of thin section showing crandallite crust and variscite vein filling; D) and E) Chemical mapping showing Fe and Al concentrations, respectively..43
Figure 4.10: Si vs Al binary diagram showing compositional variation for clays in analyzed samples. Composition clusters near dickite end-member and is interpreted as clays from kaolinite-group minerals..44
Figure 4.11: Ternary and binary plots of chemistry data. A) Al-Ca-Fe ternary plot showing two main trends and compositional clusters for variscite and crandallite; B) Fe vs Al. Binary diagram showing $Al^{3+} \rightleftharpoons Fe^{3+}$ substitution mechanism on analyzed samples; C) PCA diagram of Al-phosphates with respective end

members; D) Ca vs Al binary diagram highlighting Al-rich variscite and Ca-bearing crandallites...45
Figure 4.12: Schematic diagram showing textural diversity identified in Al-phosphates. Multiple textures identification demonstrates time and space-dependent precipitation evolution..49
Figure 4.13: Schematic drawing of multiple fluid injection and Al-phosphates precipitation stages identified at Samambaia fault..51

LISTA DE TABELAS

Tabela 1.1: Aluminofosfatos encontrados mais comuns. Fonte: mindat.org..18

Table 4.2: Percentage of average oxide composition for each analyzed sample through EPMA (excluding clays)...46

SUMÁRIO

LISTA DE FIGURAS..4

LISTA DE TABELAS...7

RESUMO...9

ABSTRACT..10

1. INTRODUÇÃO..11

1.1. Apresentação e estruturação...11

1.2. Justificativa e objetivos..12

1.3. Localização e vias de acesso..13

2. REVISÃO BIBLIOGRÁFICA - MINERALOGIA DOS FOSFATOS DE ALUMÍNIO...13

2.1 Introdução..14

2.2 Processos de Formação..15

2.3 Fatores Geoquímicos e Controle da Precipitação.............................15

2.4 Propriedades Minerais e Estabilidade..16

2.5 Diversidade Mineralógica...17

2.6 Modos de Ocorrência..18

3. MATERIAIS E MÉTODOS..18

3.1 Coleta de Amostras e Estratégia Analítica...19

3.2 Análise Petrográfica..19

3.3 Análise por Difração de Raios-X...19

3.4 Mineralogia Automatizada (QEMSCAN)..20

3.5 Análise MEV-EDS de Alta Resolução..21

3.6 Análise por Microssonda Eletrônica (EPMA)......................................22

4. ARTIGO CIENTÍFICO SUBMETIDO À PERIÓDICO INDEXADO...23

5. CONSIDERAÇÕES FINAIS..61

6. REFERÊNCIAS...62

RESUMO

A Falha de Samambaia, no Rio Grande do Norte, representa uma estrutura sismogênica de relevância no contexto tectônico do Brasil, caracterizada por intensa atividade neotectônica e alterações hidrotermais em zonas de fratura. Nesse cenário, foram identificadas mineralizações de fosfatos de alumínio com potencial papel na selagem e evolução diagenética dessas zonas. Esta pesquisa visa caracterizar textural e quimicamente as fases fosfatadas presentes em veios e brechas da Falha de Samambaia, compreender seus mecanismos de formação e discutir suas implicações na história de alteração hidrotermal e supergênica da região. Foram utilizadas análises integradas de DRX, QEMSCAN, MEV/EDS e EPMA em amostras coletadas em diferentes zonas da falha. Os dados permitiram identificar mineralogia, composição química e relações texturais entre fases fosfatadas e minerais associados. Os principais aluminofosfatos identificados foram variscita, crandallita e millisita/wardita, associados a caulinita e quartzo. A variscita é o mineral predominante, com ampla variação composicional (substituições $Al^{3+} \rightleftharpoons Fe^{3+}$). Crandallita e millisita/wardita ocorrem subordinadamente, sugerindo evolução sob diferentes pulsos de fluido. Evidências texturais indicam que os fosfatos precipitaram em ambientes ácidos e de baixa temperatura, com predominância de fluidos meteóricos. A presença de aluminofosfatos na Falha de Samambaia resulta de múltiplos eventos de alteração química, com forte controle do pH e atividade de fósforo. Esses minerais podem ter papel relevante na redução da permeabilidade em zonas fraturadas. Estudos futuros devem integrar dados isotópicos, petrofísicos e experimentais para elucidar a origem dos fluidos, estabilidade mineral e impactos na dinâmica de falhas.

Palavras-chave: Aluminofosfatos; alteração hidrotermal; neotectônica.

ABSTRACT

The Samambaia Fault in Rio Grande do Norte represents a seismogenic structure of relevance in the tectonic context of Brazil, characterized by intense neotectonic activity and hydrothermal alterations in fracture zones. In this scenario, aluminum phosphate mineralizations with potential role in sealing and diagenetic evolution of these zones were identified. This research aims to characterize texturally and chemically the phosphate phases present in veins and breccias of the Samambaia Fault, understand their formation mechanisms, and discuss their implications in the hydrothermal and supergene alteration history of the region. Integrated analyses of XRD, QEMSCAN, SEM/EDS, and EPMA were employed on samples collected from different fault zones. The data allowed identification of mineralogy, chemical composition, and textural relationships between phosphate phases and associated minerals. The main aluminophosphates identified were variscite, crandallite, and millisite/wardite, associated with kaolinite and quartz. Variscite is the predominant mineral, with wide compositional variation ($Al^{3+} \rightleftharpoons Fe^{3+}$ substitutions). Crandallite and millisite/wardite occur subordinately, suggesting evolution under different fluid pulses. Textural evidence indicates that phosphates precipitated in acidic and low-temperature environments, with predominance of meteoric fluids. The presence of aluminophosphates in the Samambaia Fault results from multiple chemical alteration events, with strong pH control and phosphorus activity. These minerals may play a relevant role in permeability reduction in fractured zones. Future studies should integrate isotopic, petrophysical, and experimental data to elucidate fluid origin, mineral stability, and impacts on fault dynamics.

Keywords: Al-phosphates; hydrothermal alteration; neotectonics.

1. INTRODUÇÃO

1.1. Apresentação e estruturação

O objetivo do trabalho é caracterizar as ocorrências de fosfato de alumínio na Falha de Samambaia, localizada em João Câmara, RN, com foco em compreender os processos de precipitação mineral associados a sistemas de falhas silicificadas. A pesquisa está vinculada ao projeto "*Processos e Caracterização de Rotas de Fluxo de Fluidos em Reservatórios Carstificados, Fraturados e Silicificados do Pré-sal – Porocarste Fase II*", financiado pela Shell Brasil, que investiga análogos de reservatórios silicificados e fraturados com ênfase em propriedades petrofísicas e implicações para migração de hidrocarbonetos nesses sistemas.

A Falha de Samambaia é uma estrutura sismogênica ativa, caracterizada superficialmente por veios massivos de quartzo de direção NE-SW, de dimensões métricas a decamétricas, formados por múltiplos eventos de injeção de fluidos hidrotermais ricos em sílica associados a processos contínuos de fraturamento e reativação tectônica, que favorecem a abertura de condutos e o influxo de fluidos (Bezerra *et al*., 2021). Esses veios estão encaixados no embasamento cristalino pré-cambriano, composto principalmente por rochas metaplutônicas e sequências metavulcanossedimentares do Maciço São José do Campestre (Dantas *et al*., 2013; Souza et al., 2023), e são capeados pelas sequências carbonáticas, siliciclásticas, e pelíticas da Bacia Potiguar. Apresentam-se intensamente fraturados e brechados, com fraturas e brechas preenchidos por material rico em fosfato, objeto de estudo desta pesquisa.

A pesquisa foi estruturada em duas frentes principais. A primeira inclui as etapas de campo, coleta de amostras, confecção de seções delgadas e descrição petrográfica, visando integrar essas informações aos dados existentes para realizar a caracterização textural e mineralógica detalhada. A segunda frente é analítica, abrangendo análises de difração de raios X, QEMSCAN, microscopia eletrônica de varredura e microssonda eletrônica de grãos selecionados. O foco está na caracterização textural e química dos fosfatos, além de interpretações iniciais sobre as possíveis fontes e gênese do fluido mineralizante.

Os resultados e discussões preliminares estão detalhados no Capítulo 4 desta dissertação como artigo científico submetido à periódico indexado.

1.2. Justificativa e objetivos

Os fosfatos de alumínio são minerais amplamente estudados devido à sua ocorrência em diversos contextos geológicos e sua relevância como indicadores de processos de alteração química e circulação de fluidos. Eles geralmente se formam em condições associadas a intemperismo intenso em bacias sedimentares e depósitos de fosforitos marinhos, estando ligados a interações químicas complexas entre fluidos e substratos rochosos. Exemplos notáveis incluem depósitos como Bone Valley, na Flórida (Altschuler *et al.*, 1973), Thiès, no Senegal (Flicoteaux e Lucas, 1984), e outros registros significativos na Austrália, Sibéria e Egito (Nriagu, 1976; Zanin, 1968; El Agami, 2019). Esses depósitos ilustram a variabilidade paragenética dos aluminofosfatos e sua relação com ambientes geológicos específicos.

Na Falha de Samambaia, os fosfatos de alumínio são encontrados associados a sistemas de falhas silicificadas, onde ocorrem como cimentos em brechas, preenchendo fraturas e cavidades em veios de quartzo. Esses veios são o resultado de múltiplos episódios de silicificação hidrotermal, que redistribuíram elementos químicos e criaram condições favoráveis para a precipitação mineral (Bezerra *et al*. 2021). Entender as condições de formação desses minerais é essencial para desvendar os processos de percolação de fluidos em sistemas tectonicamente ativos e suas implicações para a evolução estrutural e geoquímica da região.

Essa investigação está diretamente relacionada aos objetivos do projeto Porocarste Fase II, que busca caracterizar os fatores que afetam a porosidade e permeabilidade de reservatórios carstificados, fraturados e silicificados no contexto do Pré-sal. Os aluminofosfatos da Falha de Samambaia podem atuar como marcadores importantes da interação entre fluidos mineralizantes e a rocha hospedeira, oferecendo subsídios para a modelagem de fluxos de fluidos e a evolução de sistemas de reservatórios.

Apesar de sua relevância, as ocorrências de fosfatos de alumínio na Bacia Potiguar ainda são pouco estudadas em termos de composição química, sequência paragenética e espessura da zona fosfatada. Trabalhos anteriores, como Matsuda (1988) e Advíncula e Silva *et al*. (2022), apontam a necessidade de investigações detalhadas para compreender as fontes de fósforo, a gênese dos fluidos mineralizantes e os mecanismos responsáveis pela formação dessas mineralizações. A ausência de minerais indicadores clássicos de hidrotermalismo, como sulfetos, na região, também levanta questões sobre o papel dos processos supergênicos e epigenéticos na formação desses depósitos.

Diante desse cenário, este trabalho busca integrar análises texturais, mineralógicas e geoquímicas para caracterizar as ocorrências de fosfatos de alumínio e interpretar as condições de formação desses minerais. Os resultados esperados contribuirão para a compreensão dos processos de circulação de fluidos e para o avanço das investigações relacionadas aos objetivos do projeto Porocarste Fase II.

Com base nisso, os objetivos específicos do trabalho são:

1. Caracterizar do ponto de vista mineralógico, textural e químico as ocorrências de fosfato de alumínio na Falha de Samambaia, RN.
2. Identificar e distinguir as diferentes fases minerais presentes, propondo um modelo evolutivo para a sequência paragenética.
3. Investigar as possíveis fontes de fósforo e a gênese dos fluidos mineralizantes, utilizando dados geoquímicos.
4. Discutir as implicações da formação desses fosfatos na porosidade e permeabilidade de sistemas de reservatórios análogos, alinhando-se aos objetivos do projeto Porocarste Fase II.

1.3. Localização e vias de acesso

A área de estudo está localizada no Rio Grande do Norte, na região do município de João Câmara, a cerca de 5 km do centro da cidade. Trata-se de uma pedreira inativa em propriedade privada, acessada pela Fazenda Arizona através de estradas carroçáveis e acessos secundários que se conectam à rodovia federal BR-406, e à rodovia estadual RN-120 (Figura 1.1). O município de João Câmara está localizado na mesorregião do Agreste Potiguar e na microrregião de Baixa Verde, inserida na Folha homônima (SB.25-V-C-IV), distante 81 km da capital Natal.

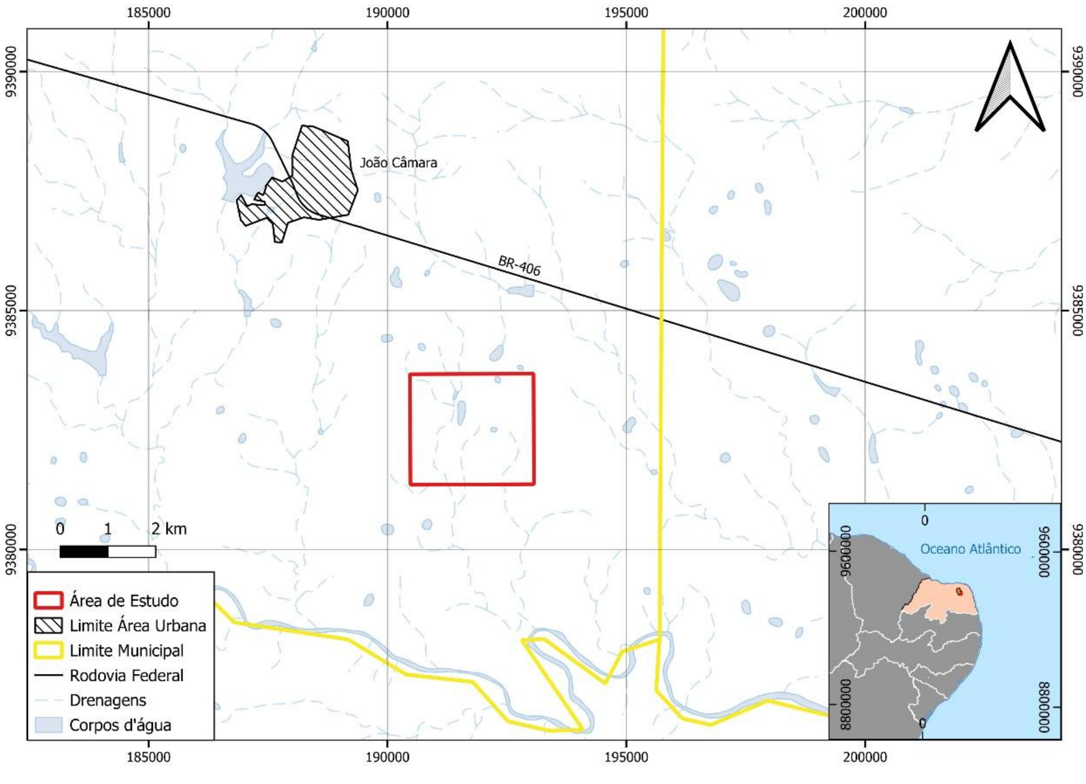

Figura 1.1: Mapa de localização e acessos à região de estudo desta pesquisa.

2. REVISÃO BIBLIOGRÁFICA - MINERALOGIA DOS FOSFATOS DE ALUMÍNIO

2.1. Introdução

Os fosfatos de alumínio, ou aluminofosfatos, constituem um grupo mineral com ampla distribuição em ambientes geológicos distintos. Embora sua ocorrência seja comum em diferentes contextos, predominam em horizontes de solo submetidos a variados graus de intemperismo, bacias sedimentares e depósitos de fosforitos marinhos, além de sequências carbonáticas e argilosas (Dill, 2001). As principais ocorrências globais incluem Bone Valley (Flórida), Fairfield (Utah), Thiès, Lam Lam e Tobene (Senegal), Nigéria, Congo, China, Vietnã, Sibéria, Austrália, Costa do Marfim e Upper Volta (Altschuler et al., 1956, 1958; Capdecomme, 1952, 1953; Slansky et al., 1964; Riedel, 1959; Lucas et al., 1980).

Essas ocorrências compartilham características sedimentares comuns: formação em bacias marinhas rasas com intercalações de litotipos fosfáticos, carbonáticos e siliciclásticos, majoritariamente do Eoceno ao Mioceno. A alta produtividade biogênica e a diagenética precoce desses ambientes geraram condições geoquímicas favoráveis à precipitação dos aluminofosfatos, especialmente em zonas de acúmulo de matéria orgânica (Filippelli, 2008).

2.2. Processos de Formação

A formação dos aluminofosfatos ocorre predominantemente por dois processos principais: (i) intemperismo químico em ambientes supergênicos, e (ii) interação de fluidos hidrotermais com rochas hospedeiras enriquecidas em Al e P (Flicoteaux e Lucas, 1980). Em depósitos como os de Bone Valley (EUA) e Thiès (Senegal), observa-se a substituição progressiva de apatita e argilominerais por aluminofosfatos secundários, como crandallita e millisita, frequentemente acompanhados por variscita, wavellita e augelita (Altschuler, 1973; Nriagu, 1976).

A alteração supergênica de minerais de argila, como a caulinita, em ambientes ácidos, também favorece a precipitação de aluminofosfatos, comumente em fraturas e zonas porosas de rochas silicatadas alteradas.

2.3. Fatores Geoquímicos e Controle da Precipitação

A estabilidade e precipitação dos aluminofosfatos são fortemente controladas por variáveis geoquímicas como pH do fluido, temperatura, pressão e composição química da solução e do substrato. De forma geral, ambientes com pH neutro a levemente alcalino (6–8) favorecem a formação de minerais ricos em Ca, como crandallita e millisita, enquanto ambientes ácidos ($pH < 5$) propiciam a formação de variscita, Fe-variscita e outros aluminofosfatos ricos em Al (Nriagu, 1976; Altschuler, 1964).

A remoção de sílica do sistema é outro fator determinante, promovendo a transformação de argilominerais em aluminofosfatos, especialmente a conversão de caulinita em variscita mediante reação com HPO_4^{2-} (Nriagu, 1976). Além disso, altas atividades de Ca e a interação com substratos carbonáticos ou lateríticos alteram os campos de estabilidade desses minerais.

2.4. Propriedades Minerais e Estabilidade

Crandallita ($CaAl_3(PO_4)_2(OH)_5 \cdot H_2O$)

A crandallita é estável sob condições de pH entre 5,5 e 6,5, embora sua precipitação seja favorecida por ambientes neutros a alcalinos, frequentemente em solos lateríticos (Mach et al., 2021). Ensaios hidrotérmicos indicam que a crandallita pode se formar a até 200 °C e 15 bar, mas fases puras e ricas em cálcio não são estáveis acima de 139 °C, e sua estabilidade diminui com o aumento da temperatura (Schwab et al., 1990a; Dill, 2001; Frost, 2012). Em solução, variações discretas de pH próximas a 7 controlam a competição entre precipitação de crandallita e apatita.

A crandallita apresenta ampla capacidade de substituição isomórfica, com Ca sendo parcialmente substituído por Sr, Ba e Pb, resultando em fases mistas ou crandallitas pobres em Ca, como observado na Falha de Samambaia.

Variscita ($AlPO_4 \cdot 2H_2O$)

Considerada o aluminofosfato menos solúvel a temperatura ambiente (25 °C) e sob pH ácido (3–6), a variscita atua como regulador da concentração de fosfato em águas naturais fracamente ácidas (Roncal-Herrero, 2008, 2011). Apresenta estabilidade mesmo em ambientes extremamente ácidos, como cavernas (Audra et al., 2021), sendo instável em condições com alta atividade de Ca e sílica dissolvida (Nriagu, 1976).

Modelagens indicam que a variscita pode manter um campo de estabilidade mais amplo em ambientes superficiais com leve acidez. A estabilidade térmica é limitada, com tolerância até 113 °C sob pressão atmosférica, e início de desidratação formando berlinita a partir de 186 °C e 500 bar (Druppel, 2007). A variscita também forma solução sólida com a strengita, permitindo substituição parcial de Al por Fe^{3+}.

Millisita ($CaAl(PO_4)(OH)\cdot 2H_2O$)

A millisita ocorre geralmente por alteração de apatita em ambientes de pH neutro a alcalino, com precipitação favorecida por temperaturas baixas em perfis de intemperismo e lateritas (Nriagu e Moore, 1984). Sua estabilidade depende da concentração de Al e Ca; sua alteração para crandallita pode ocorrer com baixos teores de fósforo e em pH mais elevado. Em ambientes ricos em ferro, a formação de Fe-millisita pode ocorrer, como nos depósitos de Lam Lam e El Hefuf (El Agami, 2019).

Caulinita ($Al_2Si_2O_5(OH)_4$)

A caulinita é estável em ambientes ácidos, podendo ser alterada para aluminofosfatos mediante acúmulo relativo de Al (por lixiviação de sílica) e enriquecimento em P e Fe. Esse processo, identificado em Samambaia, envolve a alteração direta de caulinita para variscita ou Fe-millisita sob forte acidez. Quando em ambiente hidrotermal, a sua formação e estabilidade são controladas principalmente pela temperatura do fluido.

2.5. Diversidade Mineralógica

A Tabela 1 resume os principais aluminofosfatos descritos na literatura, suas fórmulas, ambientes de formação, condições de precipitação e ocorrências típicas. Dentre os minerais listados, destacam-se ainda a wavellita, augelita, wardita, florencita, trolleíta, senegalita, goyazita e montgomeryita, os quais refletem a diversidade cristalino-química e ambiental dos aluminofosfatos. Cada um deles possui condições geoquímicas específicas, como a presença de flúor (wavellita), interação com sódio (wardita), altos teores de terras raras (florencita), ou Mg (montgomeryita), que controlam sua estabilidade e ocorrência.

2.6. Modo de Ocorrência

Os aluminofosfatos geralmente ocorrem como massas criptocristalinas, revestimentos em fraturas, preenchimento de poros e brechas ou como produtos de substituição de minerais primários. Na Falha de Samambaia, sua ocorrência em brechas e fraturas associadas a veios de quartzo hidrotermalizados indica episódios de circulação de fluidos ricos em fósforo e alumínio. No entanto, a ausência de sulfetos e a predominância de minerais supergênicos sugerem condições meteóricas ácidas como principal agente formador, em detrimento de sistemas hidrotermais clássicos.

Mineral	Fórmula Química	Ambiente de Formação	Fatores de Precipitação	Exemplo de Ocorrência	Características Texturais
Crandallita	$CaAl_3(PO_4)_2(OH)_5 \cdot H_2O$	Intemperismo em solos lateríticos	pH neutro a alcalino (6-8)	Bone Valley, Flórida	Cimento em brechas; revestimento de poros
Millisita	$CaAl(PO_4)(OH) \cdot 2H_2O$	Alteração de apatitas em solos ácidos	pH neutro a alcalino (6-8)	Thiès, Senegal	Preenchimento de fraturas
Variscita	$AlPO_4 \cdot 2H_2O$	Intemperismo em substratos argilosos	pH ácido (<5)	Fairfield, Utah	Massas criptocristalinas; cavidades
Wavellita	$Al_3(PO_4)_2(OH,F)_3 \cdot 5H_2O$	Lateritas e solos ricos em matéria orgânica	pH ácido (<5); presença de flúor	Austrália	Radiações fibrosas em matrizes de brechas
Augelita	$Al_2(PO_4)(OH)_3 \cdot H_2O$	Alteração em rochas pelíticas	pH ácido (<5)	Thiès, Senegal	Substituição de argilominerais
Wardita	$NaAl_3(PO_4)_2(OH)_4 \cdot 2H_2O$	Solos lateríticos e áreas de intemperismo químico	pH alcalino; interação com sódio	Fairfield, Utah	Revestimento de fraturas e cavidades
Florencita	$CeAl_3(PO_4)_2(OH)_6$	Intemperismo em rochas ricas em terras raras	pH neutro a ligeiramente ácido	Bahia, Brasil	Inclusões em minerais de terras raras
Trolleíta	$Al_4(PO_4)_3(OH)_3$	Alteração hidrotermal de apatitas	pH ácido a neutro; alta pressão	Escandinávia	Agregados massivos em brechas
Senegalita	$Al_2(PO_4)(OH)_3 \cdot 3H_2O$	Intemperismo em zonas lateríticas	pH ácido; solos ricos em alumínio	Thiès, Senegal	Camadas microcristalinas em solos
Goyazita	$SrAl_3(PO_4)_2(OH)_5 \cdot H_2O$	Depósitos lateríticos ricos em estrôncio	pH neutro a alcalino	Goiás, Brasil	Massas criptocristalinas
Montgomeryita	$Ca_4MgAl_4(PO_4)_6(OH)_4 \cdot 12H_2O$	Depósitos secundários em cavidades vulcânicas	pH alcalino; presença de Mg	Montgomery, EUA	Agregados fibrosos em cavidades

Tabela 1.1: Aluminofosfatos encontrados mais comuns. Fonte: mindat.org

3. MATERIAS E MÉTODOS

Este capítulo detalha as etapas e ações realizadas durante a pesquisa, divididas em: etapa preliminar, etapa de campo, etapa de tratamento e aquisição de dados, e etapa de integração e interpretação de dados.

3.1 Coleta de Amostras e Estratégia Analítica

Quatorze amostras foram coletadas durante trabalho de campo sistemático e integradas com 53 amostras previamente coletadas da mesma localidade. Coordenadas GPS, medidas estruturais e fotografias de campo detalhadas documentaram as relações espaciais entre a mineralização fosfática e a arquitetura da zona de falha.

O fluxo de trabalho analítico foi primariamente projetado para caracterizar minerais fosfáticos de alumínio e suas fases associadas. Este fluxo seguiu uma abordagem sistemática e multiescalar que abrangeu petrografia óptica, mineralogia total (DRX), mineralogia automatizada (QEMSCAN), imageamento de alta resolução (MEV-EDS) e química mineral quantitativa (EPMA). Esta estratégia integrada permitiu a correlação dos dados de mineralogia total com características texturais em microescala e variações químicas.

3.2 Análise Petrográfica

Quarenta e três seções delgadas polidas foram preparadas. Dezenove seções correspondem a amostras recentemente coletadas, enquanto 24 derivaram do arquivo de amostras adquirido na 1º fase do projeto Porocarste. Analisamos a mineralogia e microestruturas relacionadas às rochas de falha portadoras de fosfato usando seções delgadas cortadas perpendicular e paralelamente às superfícies de deslizamento, examinadas com microscópio petrográfico sob luz plano-polarizada (PPL) e luz polarizada cruzada (XPL). A documentação focou nas relações de corte entre *fabrics* de deformação e mineralização fosfática, variações de tamanho de grão, relações de crescimento e substituição, e padrões de distribuição espacial. Os dados preliminares de DRX, QEMSCAN e MEV, obtidos na 1º fase do projeto, guiaram a análise focada e seleção de áreas para trabalho microanalítico detalhado.

3.3 Análise de Difração de Raios X

Trinta amostras representativas foram submetidas à análise de DRX de pó de rocha total para estabelecer assembleias mineralógicas totais e identificar fases criptocristalinas. A preparação de amostras envolveu moagem a <63 μm em almofarizes de ágata seguida de montagem de pó aleatório.

Vinte e duas amostras foram analisadas no Laboratório de Caracterização Tecnológica – LCT, Universidade de São Paulo – USP (São Paulo-SP, Brasil) usando um difratômetro Malvern Panalytical Empyrean com radiação CuKα (λ = 1,542 Å, 2,2 kW). A coleta de dados abrangeu 2-50° 2θ com tamanho de passo de 0,01° e tempo de contagem de 29,8 s por passo. O detector PIXcel3D operou com monocromador ou filtros Kβ. A identificação de fases utilizou o software X'Pert HighScore Plus v.4.8 com bancos de dados PDF-4+ (2021) e ICSD (2021.1).

O instrumento foi equipado com detector sensível à posição PIXcel3D com monocromador ou filtros Kβ. Os dados foram coletados em ângulos 2θ variando de 0 a 50º. As fases cristalinas foram identificadas usando os softwares X'Pert Data Collector e X'Pert High Score Plus 4.8, referenciando os bancos de dados PDF2 do ICDD (International Centre for Diffraction Data) e ICSD (Inorganic Crystal Structure Database).

Oito amostras adicionais foram analisadas no Instituto de Geociências – IG, Universidade de Brasília – UnB (Brasília-DF, Brasil), usando difratômetro Rigaku Ultima IV com radiação Cu (40 kV, 40 mA). A coleta de dados cobriu 5-70° 2θ usando passos de 0,02° e taxa de varredura de 1° min^{-1}. A identificação mineral empregou software Jade 9.0 com banco de dados ICDD PDF-2 (versão 2010). A análise semi-quantitativa utilizou métodos de razão de intensidade de referência (RIR). A reprodutibilidade interlaboratorial, verificada usando três amostras de referência, demonstrou <3% de variação na quantificação de fases maiores.

3.4 Mineralogia Automatizada (QEMSCAN)

A avaliação quantitativa de minerais foi conduzida usando técnica QEMSCAN, que integra imageamento por microscopia eletrônica de varredura (MEV) com espectroscopia de energia dispersiva (EDS) (Gottlieb et al., 2000; Goodall et al., 2005). Onze seções delgadas polidas foram examinadas utilizando microscópio eletrônico de varredura ThermoNoran-FEI FEGSEM 650F equipado com detectores EDS duplos QuantaX Bruker no IG-UnB.

As análises utilizaram varreduras de 'imagem de campo' para mapeamento contínuo por pixel a 25 kV, 10 nA, magnificação de 1000× e espaçamento de 2-μm. Cada pixel foi atribuído com coordenadas X/Y e dados químicos EDS. O software iDiscover (v.5.3.2) comparou espectros com banco de dados personalizado SIP LIST de mais de 200 espectros de referência portadores de fosfato, atribuindo cores para fases minerais e produzindo mapas quantitativos de fases convertidos em dados modais.

Os mapas brutos foram processados com filtros morfológicos para segmentação de partículas e limpeza de limites. Os cálculos modais omitiram epóxi e reportaram intervalos de confiança estatística. A precisão de medição foi ±1% para fases >5 vol%, ±0,5% para 1–5 vol%, e ±0,1% para <1 vol%. As relações de limite de grão foram quantificadas usando matrizes de liberação e associação, e as distribuições de tamanho de partícula foram baseadas em diâmetros circulares equivalentes.

3.5. Análise MEV-EDS de Alta Resolução

Duas amostras representativas foram analisadas por MEV-EDS usando microscópio eletrônico de varredura de emissão de campo Tescan MIRA4 no Laboratório de Peneiras Moleculares – LABPEMOL, Universidade Federal do Rio Grande do Norte – UFRN (Natal-RN, Brasil), para observar contrastes composicionais e padrões de zoneamento e selecionar pontos analíticos para análise adicional por microssonda eletrônica. A análise foi conduzida com voltagem de aceleração de 20 kV, corrente do feixe de 200 pA e revestimento de carbono de 15 nm. Um detector Bruker XFlash 410-M foi usado para imageamento por elétrons retroespalhados e mapeamento elemental qualitativo, permitindo identificação de variações composicionais e seleção de localizações adequadas para análise quantitativa por microssonda.

3.6. Análise por Microssonda Eletrônica (EPMA)

Oito amostras selecionadas foram submetidas à análise quantitativa de química mineral usando JEOL JXA-8230 Superprobe equipado com cinco espectrômetros dispersivos por comprimento de onda (WDS) e um espectrômetro dispersivo por energia (EDS) no Laboratório de Microscopia e Microanálises – LMic, Universidade Federal de Ouro Preto – UFOP (Ouro Preto-MG, Brasil). A análise examinou primariamente APM e argilas minerais associadas para avaliar possíveis origens relacionadas à alteração. Grãos representativos identificados por métodos anteriores foram selecionados, com atenção dada ao zoneamento químico e relações de reação. Traversos através de limites de grão registraram gradientes químicos e reações de substituição entre minerais primários e fases secundárias.

As análises utilizaram voltagem de aceleração de 15 kV, corrente do feixe de 20 nA (~2,0 × 10^{-8} A) e diâmetro do feixe de 5 µm. Os tempos de contagem de pico e background foram 10 s e 5 s por elemento. Cinco espectrômetros WDS com cristais otimizados cobriram: Canal 1 (TAPH): Na Kα, F Kα; Canal 2 (TAP): Si Kα, Al Kα, Mg Kα; Canal 3 (PETH/LIFH): Ba Lα, Fe Kα, Cl Kα, V Kα, Sr Lα; Canal 4 (PETJ): Ti Kα, Ca Kα, P Kα; Canal 5 (PETL/LIFL): Cr Kα, K Kα, Mn Kα.

Padrões naturais e sintéticos da coleção da Smithsonian Institution incluíram anortoclásio (Na_2O), CaF_2 (F), quartzo (SiO_2), coríndon (Al_2O_3), olivina (MgO), $BaSO_4$ (BaO), magnetita (FeO), escapolita (Cl), vidro riolítico IR-W (V_2O_3), estroncianita (SrO), rutilo (TiO_2), fluorapatita (CaO, P_2O_5), cromita (Cr_2O_3), microclínio (K_2O) e Mn metálico (MnO). As intensidades brutas foram submetidas a correções de matriz ZAF (Z – número atômico, A – absorção, F – fluorescência). As fórmulas estruturais para APM assumiram 4 oxigênios para variscita e 8 para crandallita. As proporções catiônicas em argilas minerais foram calculadas baseadas em 22 oxigênios para balanço de carga. O conteúdo total de ferro foi reportado como Fe_2O_3 para APM e como FeO para argilas minerais.

A precisão analítica alcançou ±1% relativo para elementos maiores (>10 wt%) e ±5-10% relativo para elementos traço (<1 wt%). Os limites de detecção variaram de 0,01-0,03 wt% para elementos maiores a 0,05-0,10 wt% para elementos traço.

4. ARTIGO CIENTÍFICO SUBMETIDO À PERIÓDICO INDEXADO

Mineralogy, chemistry, and textural characterization of Al-phosphates: examples from Samambaia intraplate fault system, Brazil

Adriano H.A. Aguiar[1*], Frederico C.J. Vilalva[2], Cristiane P. Menezes[1], Francisco H.R. Bezerra[2], Glaucia N. Queiroga[3], Vincenzo La Bruna[1], Paola F. Barbosa[4], Marco Paulo de Castro[3]

1 – Programa de Pós-Graduação em Geodinâmica e Geofísica, Universidade Federal do Rio Grande do Norte, Campus Central, Natal-RN, Brazil
2 – Departamento de Geologia, Universidade Federal do Rio Grande do Norte, Campus Central. Rua das Engenharias s/n, 59078-970, Natal-RN, Brazil
3 – Departamento de Geologia, Campus Morro do Cruzeiro, Universidade Federal de Ouro Preto, 35400-000, Ouro Preto-MG, Brazil
4 – Instituto de Geociências, Universidade de Brasília, Campus Universitário Darcy Ribeiro ICC, 70.910-900, Brasília-DF, Brazil
*corresponding author: adrianoaaguiar@gmail.com

Abstract

Aluminum-phosphate minerals (APM) commonly form under low-temperature conditions and can record fluid-rock interactions in dynamic geological settings such as active faults. This study investigates the mineralogy, chemistry, and textures of APMs from the Samambaia intraplate fault system, northeastern Brazil, aiming to reconstruct the precipitation history and geochemical conditions of mineralizing fluids. Fourteen samples from hydrothermal breccias and fault gouges were analyzed using an integrated approach combining X-ray diffraction (XRD), QEMSCAN, SEM-EDS, and EPMA. Results reveal that variscite, crandallite, and minor millisite/wardite occur predominantly in uncemented breccias and fault gouges, filling pores, fractures, and vugs. Variscite is the dominant phase, while crandallite appears in restricted samples. Distinct textures (e.g., fibrous sheaves, cockades, and zoned crystals) record multiple fluid pulses and structural reactivations. EPMA and PCA analyses demonstrate compositional fields consistent with pH-controlled precipitation, with variscite forming under acidic conditions (pH 1.5–2.5) and crandallite under extremely acidic to acidic pH (3.0–5.0). Estimated temperatures (<113–139°C) contrast with earlier high-temperature silicification (91–388°C), suggesting late-stage APM formation. These findings highlight APMs as sensitive indicators of fluid evolution, fault sealing, and seismic cycles. Their textures and compositions may aid in reconstructing paleo-fluid conditions and evaluating fault behavior in crystalline basement terranes.

Introduction

Aluminum-phosphate minerals (APM) are common in diverse geological settings, indicating chemical alteration and precipitation. These minerals can provide valuable insights into fluid pathways and circulation from weathering profiles to fault zones (Nriagu 1976; Dill 2001). In dynamic systems, APM are particularly important because their distinct textural relationships and compositional variations record specific conditions of fluid evolution and chemical exchange. Understanding these processes is essential for interpreting APM distribution in geological settings and their significance as indicators of fluid-rock interaction.

In seismogenic fault zones, fluid circulation and mineral precipitation link closely to faulting events (Saishu et al. 2017; Smeraglia et al. 2018; Bezerra et al. 2021). While previous research broadly recognizes the role of mineral precipitation in fault healing and weakening (e.g., Yehya and Rice 2020; Bezerra et al. 2021), the specific conditions and mechanisms governing the formation of APM during active faulting in crystalline basement settings are not yet well understood. APM offer sensitive geochemical fingerprints of transient fluid conditions, making their detailed characterization crucial for deciphering complex fluid histories in such dynamic environments.

This study investigates APM precipitation within the Arizona quarry exposures of the Samambaia Fault zone, Rio Grande do Norte, Brazil. The fault intersects the Precambrian basement of the Potiguar Basin and is characterized at the surface by brecciated quartz and chalcedony–opal vein swarms that record hydrothermal activity along reactivated structures (Bezerra et al. 2007; 2021). The Arizona quarry provides exceptional three-dimensional exposure of fault-hosted mineralization, allowing for detailed investigation of fluid–rock interaction processes (Bezerra et al. 2007; Bezerra et al. 2021).

Although APM occur in various geological settings including caves, lateritic profiles and hydrothermal systems (e.g., Altschuler 1973; Audra et al. 2021), paragenetic and textural studies remain limited (e.g., Dill 2001; El-Agami et al. 2005; Spier et al. 2020). This gap is problematic for fault-hosted systems, where APM precipitation may preserve episodic fluid flow, pressure-temperature fluctuations, and chemical evolution associated with seismic cycles. The cryptocrystalline nature of most APM further complicates their study (El Agami 2019; Díaz-Acha 2019), requiring integrated micro-analytical approaches.

Our primary objective is to characterize APM assemblages to better understand fluid evolution, source, and migration within the Samambaia Fault zone. Specifically, the study aims to: (1) describe APM textural variability as indicators of changing fluid conditions; (2) establish the sequence of APM precipitation to reconstruct fluid–rock interaction history; and (3) determine APM chemical compositions to infer fluid provenance and flow pathways.

Background: Al-Phosphate Characteristics and Formation Processes

APM primarily form through alteration where P-rich fluids interact with Al-rich rock substrates, with apatite, whether sedimentary, igneous, or metamorphic, as the main phosphate source (Vieillard et al. 1979; Nriagu and Moore 1984; Flicoteaux and Lucas 1984). Alteration fluids originate from meteoric water, groundwater, or low-temperature hydrothermal systems, often mixed and circulated through deep fracture networks and fault zones (Schwab et al. 1990a, b; Dill 1991, 2001; El Agami 2019). Fluid compositions reflect elements dissolved from primary host-rock minerals: Al from aluminosilicates and P from apatite dissolution under varying physicochemical conditions (Toledo 1999). Additional elements, including Ca, K, Na, Sr, Ba, Pb, and REEs, incorporate through fluid interaction with carbonate, argillaceous, or igneous rocks (Toledo, 1999), forming common Al-phosphates such as variscite ($AlPO_4{\cdot}2H_2O$), crandallite

($CaAl_3(PO_4)(PO_3OH)(OH)_6$), millisite ($(Na,K)CaAl_6(PO_4)_4(OH)_9 \cdot 3H_2O$), wardite ($NaAl_3(PO_4)_2(OH)_4 \cdot 2H_2O$), and strengite ($FePO_4 \cdot 2H_2O$).

A key process in Al-phosphate formation is the phosphatolysis of clay minerals such as illite and montmorillonite, where phosphate ions destabilize clay structures, releasing Al (Nriagu 1976; Dill 2001). This interaction often leads to the conversion of mixed-layer clays to kaolinite and subsequent phosphate minerals. APM frequently form at shallow depths and near-surface temperatures in intense weathering profiles (Druppel et al. 2007). Their precipitation is sensitive to a range of physicochemical variables, including temperature, pH, depth, fluid composition, and element solubility (Vieillard et al. 1979; Schwab et al. 1989; Toledo 1999).

Key Physicochemical Controls on Precipitation

The mineralization process involves fluid infiltration, dissolution of primary minerals, mobilization of ions into solution, and their subsequent recombination to form secondary precipitates. The specific conditions, particularly temperature, pH, and redox state, control the type and stability of the forming APM.

Temperature influences precipitation rates, generally decreasing at higher temperatures. For instance, optimal Al-phosphate formation can occur around 50–100°C. Amorphous phases formed at these temperatures can transform into crystalline forms like variscite and metavariscite at 100°C over time (Roncal-Herrero et al. 2009). Conversely, low-temperature environments, such as caves, favor the crystallization of hydrated Al-phosphates (Frost et al. 2011; Audra et al. 2021). Crandallite, often found as a cave mineral, is stable at these low temperatures, though studies show it becomes unstable above approximately 139°C, undergoing dehydration (Gilkes and Palmer 1983). Synthetic crandallite, however, can be crystallized at higher temperatures, for example, 200°C under pressure (Francisco et al. 2007).

pH is a critical control due to its influence on aluminum and phosphate speciation and mineral solubility, thereby affecting the stability and precipitation pathways of APM. At low pH (e.g., 1.5-2.5), Al^{3+} predominates, favoring the formation of well-crystallized variscite, especially at elevated temperatures (90-100°C) (Hsu and Sikora 1993; Ulrich and Pöthig 2000; Roncal-Herrero et al. 2009). At acidic pH (3.0-5.0), amorphous Al-phosphate phases form via surface complexation (Del Nero et al. 2010; Rosseto et al. 2006), while crandallite-group minerals become stable, making the APM precipitation sequence a valuable paleo-pH indicator (Roncal-Herrero et al. 2009). In natural settings like caves, acidic leachates from bat guano play a significant role in controlling the precipitation of crandallite and other phosphates (Audra et al. 2021). APM solubility minimizes between pH 6.0-7.0, marking optimal precipitation conditions where Al-phosphate solubility reaches a minimum between pH 6.0-7.0 where Al^{3+} and PO_4^{3-} ion activities are balanced (Goldshmid and Rubin 1988; Barros et al. 2024). Above pH 7.0, solubility increases due to the formation of soluble $Al(OH)_4^-$ complexes, while at even higher pH values, increased alkali concentrations favor millisite and wardite formation (Larsen 1942; Nriagu 1970).

The formation of APM involves aluminum mobilization from mineral frameworks (chlorite, smectite, albite) under acidic conditions or CO_2 acidification (Wang et al. 2019). Simultaneously, phosphate protonation equilibria yield reactive anions (H_3PO_4, $H_2PO_4^-$, HPO_4^{2-}, PO_4^{3-}) across pH 2-9, with each form interacting differently with aluminum (Matula and Wojtkowska 2025). Once supersaturation is achieved, nucleation and subsequent crystal growth drive APM formation. Heterogeneous nucleation, often favored on existing mineral surfaces like quartz or clay minerals, is common, especially under elevated temperatures (>80 °C) and high ionic strengths (Roncal-Herrero et al. 2009). Increasing temperatures (e.g., 50 °C to >150 °C) can also drive crystal growth through sequential transformations, such as variscite to metavariscite, ultimately leading to berlinite (Roncal-Herrero et al. 2009).

Beyond pH, fluid Fe/Al ratios also influence solid solution stability in the variscite-strengite series (Gaboreau et al. 2005), and trace elements such as Cu can dictate specific mineral varieties (e.g., turquoise; Reid and Macintyre 2000).

Geological Setting

Tectonic and geological context

The Samambaia Fault, situated along the Potiguar Basin margin in northeastern Brazil, represents a well-documented example of fluid-controlled intraplate seismicity and associated hydrothermal mineralization (Bezerra et al. 2007; 2011; 2021). This NE–SW-trending fault system, comprising segments 5 to 26 km long and extending to depths of 1 to 9 km, is characterized by recurrent seismic activity (Figure 4.1a, b). The Potiguar Basin is notably one of the most seismically active intraplate regions in South America, with instrumental records showing events up to 5.2 Mb, and paleoseismic evidence suggesting past earthquakes of at least magnitude 7.0 (Bezerra et al. 2011). Seismicity is concentrated within a ∼27 km linear zone, with hypocenters located in the crystalline basement at depths of 1–9 km (Bezerra et al. 2007, 2011, 2021). Focal mechanisms indicate dextral strike-slip motion with a normal component, driven by E–W maximum horizontal compression. Fault reactivation is linked to elevated fluid pressures that reduce effective stress, thereby promoting rupture and, in extreme cases, hydraulic fracturing (Bezerra et al. 2021).

The broader geological framework encompasses encompasses the Precambrian Borborema Province crystalline basement, specifically the São José do Campestre Domain the São José do Campestre Domain (Figure 4.1a) which includes Archean nuclei (up to 3.2 Ga, zircon U-Pb), and Neoproterozoic orthogneisses and granitoid plutons, deformed during the Brasiliano cycle (Dantas et al. 2013; Souza et al. 2023). Overlying sequences include Late Cretaceous siliciclastic (Açu Formation) and carbonate (Jandaíra Formation) rocks, Miocene siliciclastics (Barreiras Formation), Quaternary alluvial sediments, and lateritic soils (Bezerra et al. 2007, 2021; Rossetti et al. 2013). The area also contains volcanic plugs dated between 45 and 6 My (Souza et al. 2022).

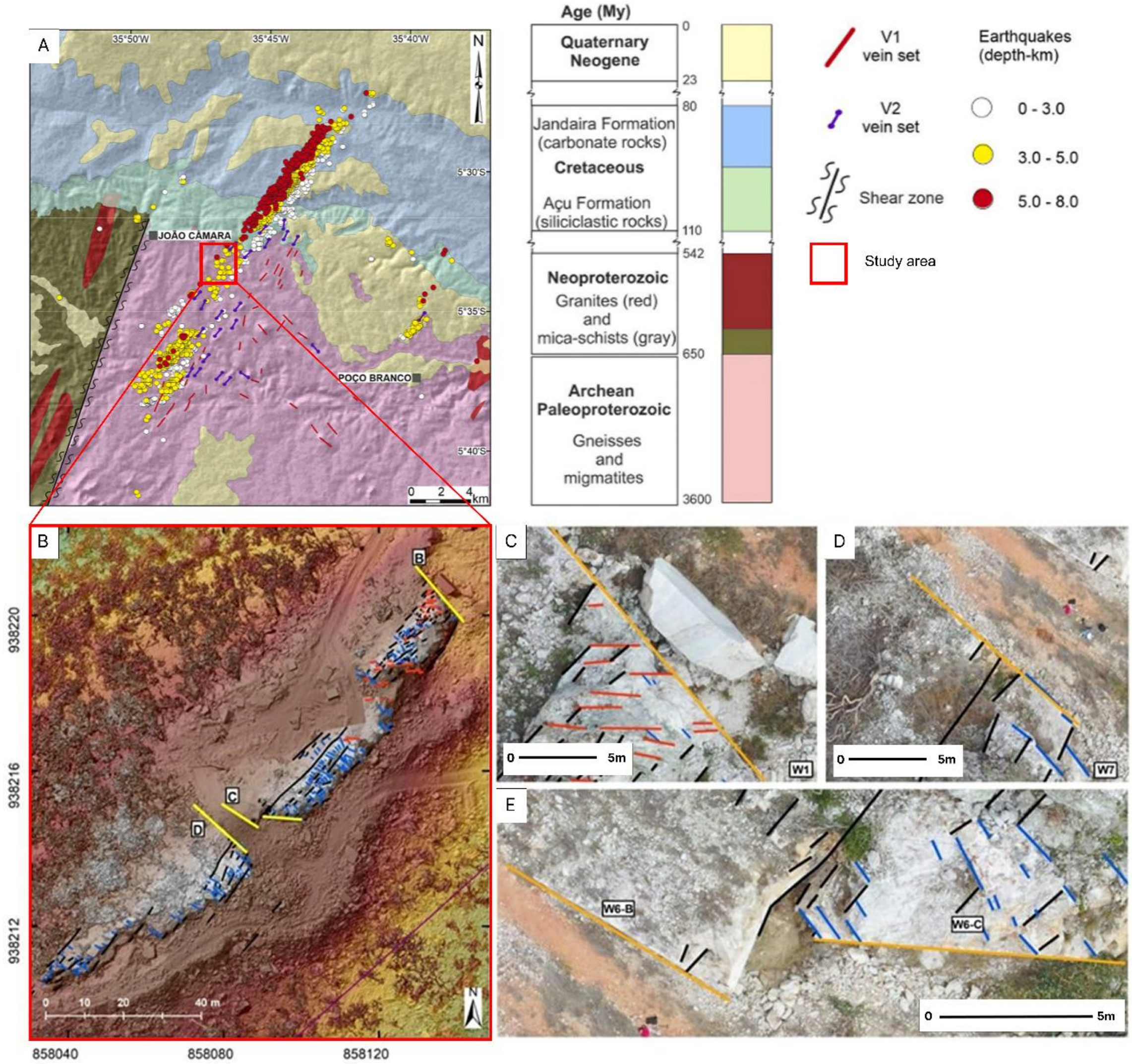

Figure 4.1: Geological setting for Samambaia fault. A) Geological background and host rocks of Samambaia fault with registered earthquake epicenters recording NE-SW fault trend; B) Arizona quarry quartz veins outcrop; C), D) and E) Location of W1, W6 and W7 walls used for sample acquisition and outcrop analyses. Samples from W5 wall were acquired but later fieldwork revealed its destruction. (Modified from Bezerra et al. 2021).

Hydrothermal Processes and Mineralization

Hydrothermal fluid involvement in Samambaia Fault seismicity was initially reported by Henderson et al. (1994), with subsequent studies by Bezerra et al. (2007, 2021) detailing extensive silicification. The fault zone is characterized at surface by metric to decametric silicified quartz veins, often bounded by breccias with earlier quartz fragments cemented by Al-phosphate-, opal-, and chalcedony-rich matrices (Figure 4.2). Two vein generations are distinguished: V1 quartz veins parallel to Proterozoic-Archean basement foliation, and V2 chalcedony-opal-quartz veins crosscutting Cretaceous sediments. Fluid inclusion microthermometry indicates magmatic fluid origin, with V1 and V2 veins recording trapping temperatures of 91–336°C and 147–388°C, respectively (Bezerra et al., 2021).

The fault zone shows progressive structural-mineralogical evolution through four fault rock groups (Bezerra et al. in prep):

- Group 1: White and Gray Quartz Veins - earliest silicification via primary gray quartz formation and white quartz recrystallization.
- Group 2: Silica-Cemented Breccias - brittle deformation onset with fragmented Group 1 veins cemented by opal and chalcedony.
- Group 3: Uncemented Fault Breccias - porous sandy to clay-rich matrices with APM from fluid-mediated dissolution and clay formation.
- Group 4: Fault Gouge - advanced fault core deformation with fine-grained, porous matrices enriched in APM.

Hydrothermal processes and conceptual model

The Samambaia Fault functions as a valve-like system where fluid pressure regulates fracture opening and sealing (Bezerra et al. 2021). Rising pressure triggers hydraulic fracturing, enabling silica- and phosphorus-rich fluid migration through the fault zone. Subsequent mineral precipitation seals these fractures, temporarily halting fluid flow until renewed pressure accumulation generates new ruptures (Bezerra et al. 2021). This cyclic process of structural reactivation, fluid flow, and mineral sealing represents a classic crack-seal mechanism characteristic of intraplate fault systems (e.g., Berger and Herwegh 2019).

Materials and Methods

For this study, we collected 14 samples from the Arizona quarry within the Samambaia Fault System, integrating them with an existing database of 53 samples. These samples were characterized through a multi-analytical approach combining X-ray Diffraction (XRD) for bulk mineralogy, Quantitative Evaluation of Minerals by Scanning Electron Microscopy (QEMSCAN) for mineralogical mapping and identification, Scanning Electron Microscopy with Energy Dispersive Spectroscopy (SEM-EDS) for detailed textural and elemental analysis, and Electron Probe Microanalysis (EPMA) for precise quantitative chemical analysis of individual mineral grains, particularly phosphates and clay minerals. This comprehensive suite of techniques allowed for a detailed understanding of the mineralogical composition, textural relationships, and chemical variations within the fault rocks. Detailed descriptions of all analytical procedures, instrument settings, and data processing protocols are provided in the Supplementary Material 1.

Results

Field and Macroscopic Characteristics

Aluminum phosphate minerals (APM) occur predominantly within brecciated zones and fault gouges of the Samambaia Fault system as porous (Figure 4.2f), fine-grained, powdery beige masses, forming a breccia matrix with quartz, opal, and chalcedony clasts (Figure 4.2b). APM also fill fractures and veins within quartz, appearing as friable, yellowish-gray to brown crusts coating cavities and fracture walls (Figures 4.2e). These minerals are commonly associated with clay minerals and reach their highest abundance in uncemented fault breccias (Group 3) and fault gouges (Group 4) (Figure 4.2c), as defined by Bezerra et al. (in prep.).

Group 3 breccias contain a porous, cohesive matrix ranging from sandy-sized to clay-rich, incorporating microcrystalline quartz and kaolinite, with APM as a major constituent. Group 4 gouges form lenses up to 1.5 m wide within quartz vein cores, consisting of a loosely consolidated, fine sand-sized matrix with a yellowish-gray coloration dominated by microcrystalline APM and scattered relict quartz grains.

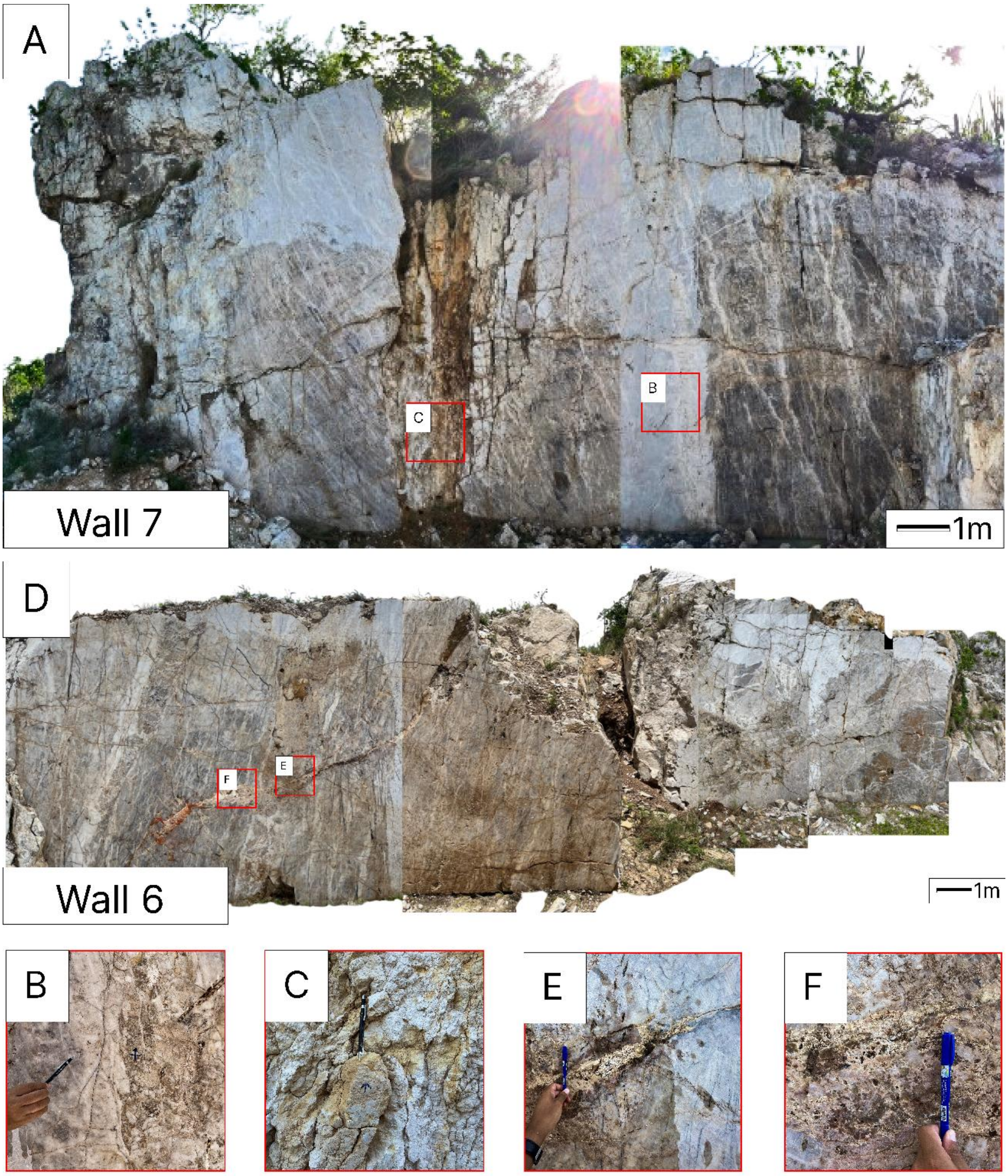

Figure 4.2: D) and A) Walls 6 and 7 of Arizona quarry, respectively showing heavily fractured Si- and P-rich veins exposure with breccia pipes and fault core. B) Detailed image of breccia pipe in W7 showing quartz breccia with APM-rich matrix; C) Detailed image of fault core in W7 showing APM-rich fault gouge; E) Detailed image of APM-filled vein in W6; F) Detailed image of APM-filled porous material.

Textural characterization by petrograhic analysis

Petrographic analysis complemented the X-ray diffraction data to refine the characterization of Al-phosphate minerals. There is broad information available about petrographic descriptions of these minerals, particularly at the microscopic scale (e.g., Nriagu and Moore 1984; Goldbery and Loughnan 1977), but textural variations in function of their distinct precipitation sources are not well detailed. Due to its cryptocrystalline nature and modes of occurence, Al-phosphates are hard to distinguish using only macro or microscopic observation. Most recently, El Agami (2019) and Díaz-Acha (2019) made notable progress in discriminate texturally some of the Al-phosphates minerals, establishing relationships with its precipitation sequence and discussing a feasible evolution path. The petrographic description below is mostly based on these findings, and the previous x-ray analysis results were also considered.

Petrographic description of Al-phosphates modes of occurence

Variscite is the most abundant aluminum phosphate and occurs as colorless, beige, and brown cryptocrystalline masses that compose the breccia matrix and fill cavities, fractures, and clasts (Figures 4.2a, b, c). It exhibits fibrous, sheaf-like, colloidal and spherulitic textures (Figures 4.2a, d, g, h, 4.3d). Under cross-polarized light, cryptocrystalline masses show low interference colors (white to yellow, 1st order), wavy extinction, and locally isotropic behavior (Figures 4.2f, h). In vugs and cavities, variscite forms prismatic subhedral to euhedral microcrystals up to 25 μm, appearing white to colorless without pleochroism and showing punctual wavy extinction (Figures 4.2e, f).

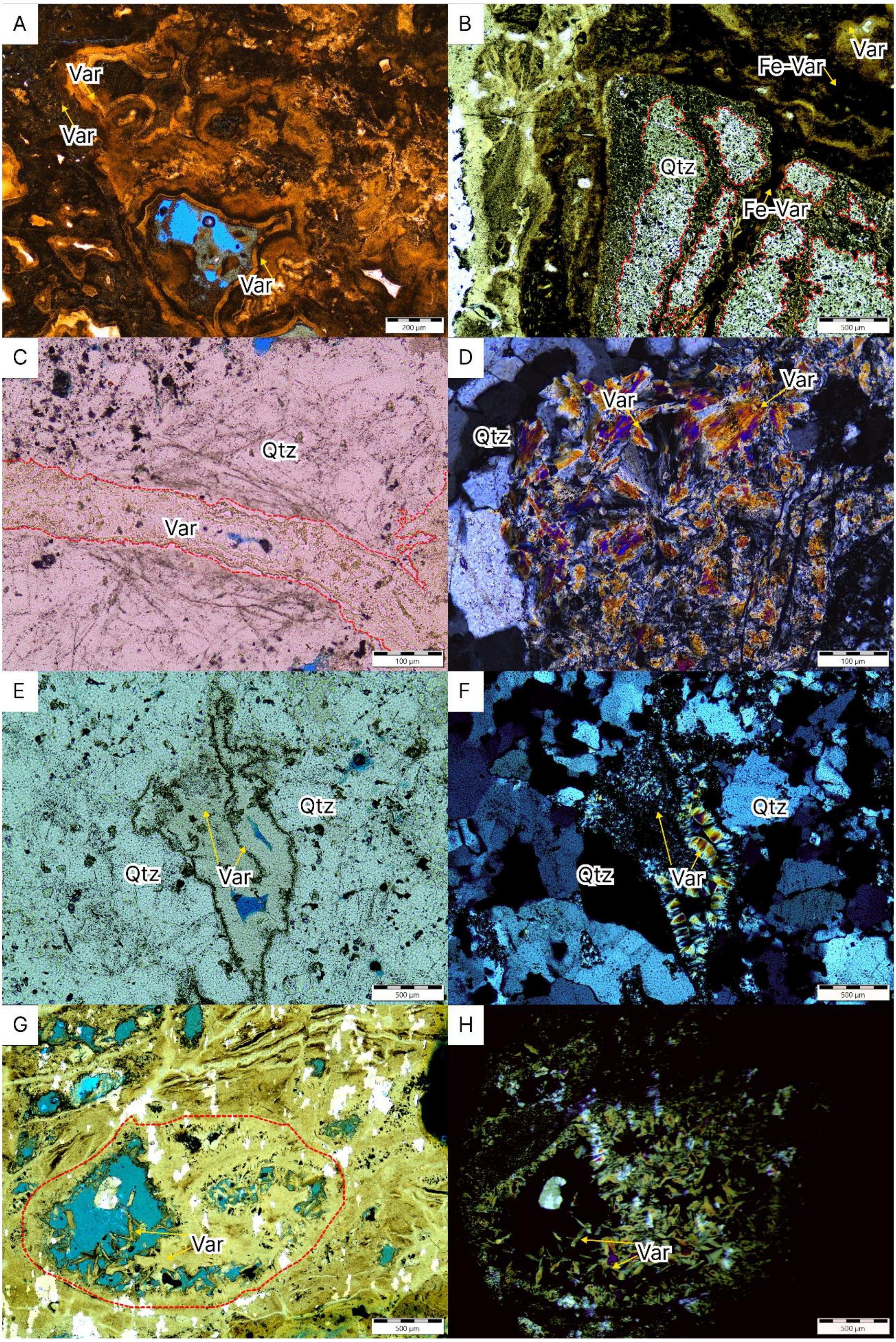

Figure 4.3: Multiple textures identified in variscite. A) Colloidal variscite; B) Clast-filling variscite-rich material with Fe-rich crusts showing compositional alternation affecting Al-phosphate precipitation; C) Vein-filling variscite; D) Sheaf-like variscite; E) Vug-filling syntaxial-like growth;

F) Vug-filling under cross polarized light showing cryptocrystalline and prysmatic variscite variation along with distinct interference colors and wavy extinction; G) and H) Pore-filling fibrous to prysmatic variscite.

Crandallite occurs as colorless to brown cryptocrystalline masses without pleochroism, showing low birefringence and first-order grayish to white interference colors under polarized light, making it challenging to distinguish from millisite/wardite (4.3 c, d). Crandallite composes the breccia matrix, fills cavities and pores, and occurs along clast edges (Figures 4.3c, d, 4.4c). Locally, it appears as a filling material in clast-cortex aggregates and exhibits colloidal textures in veins (Figures 4.4e, f, 4.3d).

Millisite/wardite minerals occur as brown cryptocrystalline masses without pleochroism, appearing isotropic under polarized light with low birefringence and first-order grayish-to-white interference colors (Figure 4.3a, b). The cryptocrystalline appearance and optical properties indicate a heterogeneous mineralogical composition with mixtures of clay minerals and other phosphates such as crandallite.

Kaolinite fills veins, fractures, and porous materials associated with quartz, as well as in fragments of dissolved primary material from crystalline basement remnants that maintain original form (Figures 4.3d, g, h). Hydroxyapatite and fluorapatite, which were subsequently identified by XRD, were not observed in the thin sections or hand samples. Dolomite and calcite occur as pseudomorphs with preserved cleavage planes, crystal shapes, and edges, which are mostly replaced by silicification and phosphate-rich fluids (Figures 4.3e, f).

Textural relationships show that crandallite is frequently associated with variscite, which shows precipitation borders in crandallite-rich cemented breccias filling pores and open cracks (Figures 4.3c, d, 4.6e, 4.8c). Millisite occasionally occurs as crusts with recrystallization edges of distinct compositions such as variscite. Kaolinite occurs in association with variscite (Figure 4.3a).

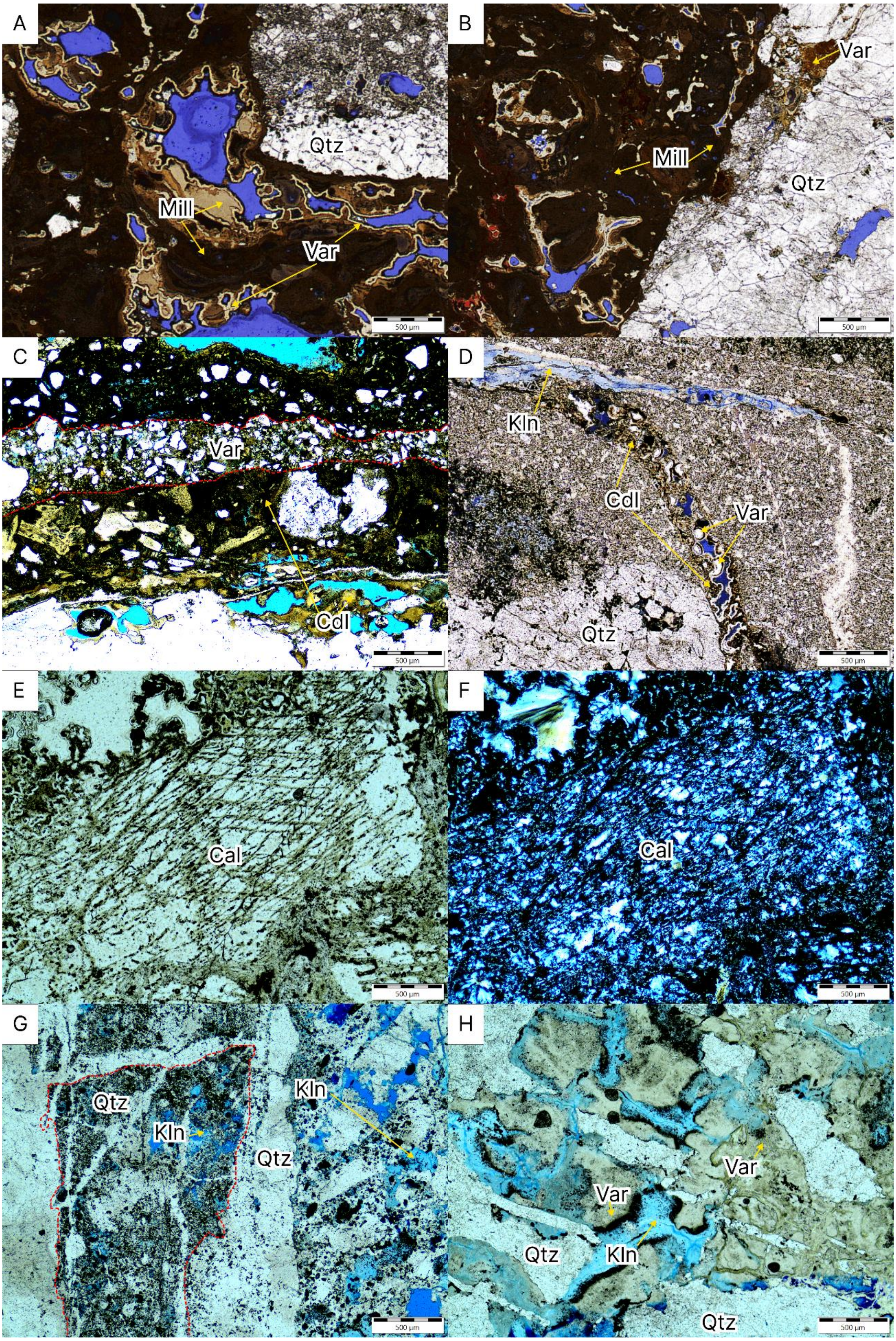

Figure 4.4: Textural diversity and occurence modes. A) and B) Millisite-rich breccia matrix with variscite-rich recrystallized edges and clast-filling material; C) Breccia matrix composed of crandallite-rich borders and variscite-rich veins; D) Colloidal crandallite with recrystallized

spherulitic variscite; E) and F) Calcite/Dolomite pseudomorphs substituted by Si-rich fluid; G) Kaolinite coatings filling porous material and quartz; H) Alteration of kaolinite to variscite.

Textural identification of multiple fluid injection and tectonic reactivation dynamics

Some textures observed shows reworked material or multi-stage precipitation. Vug-fillings show syntaxial-like variscite growth with intermediate birefringence and 2nd order pink to yellow interference colors under cross-polarized light (Figures 4.2e, f). Additionally, variscite locally shows zoned growth, cockade and clast-cortex aggregates textures with a variscite-rich matrix and quartz and calcite pseudomorphs replaced by variscite-rich masses (Figures 4.4a, b, c, d). Crandallite replacement of primary material clasts in fault breccias is demonstrated also by clast-cortex aggregates and cockade textures in fault breccias (Figures 4.4c, d, e, f).

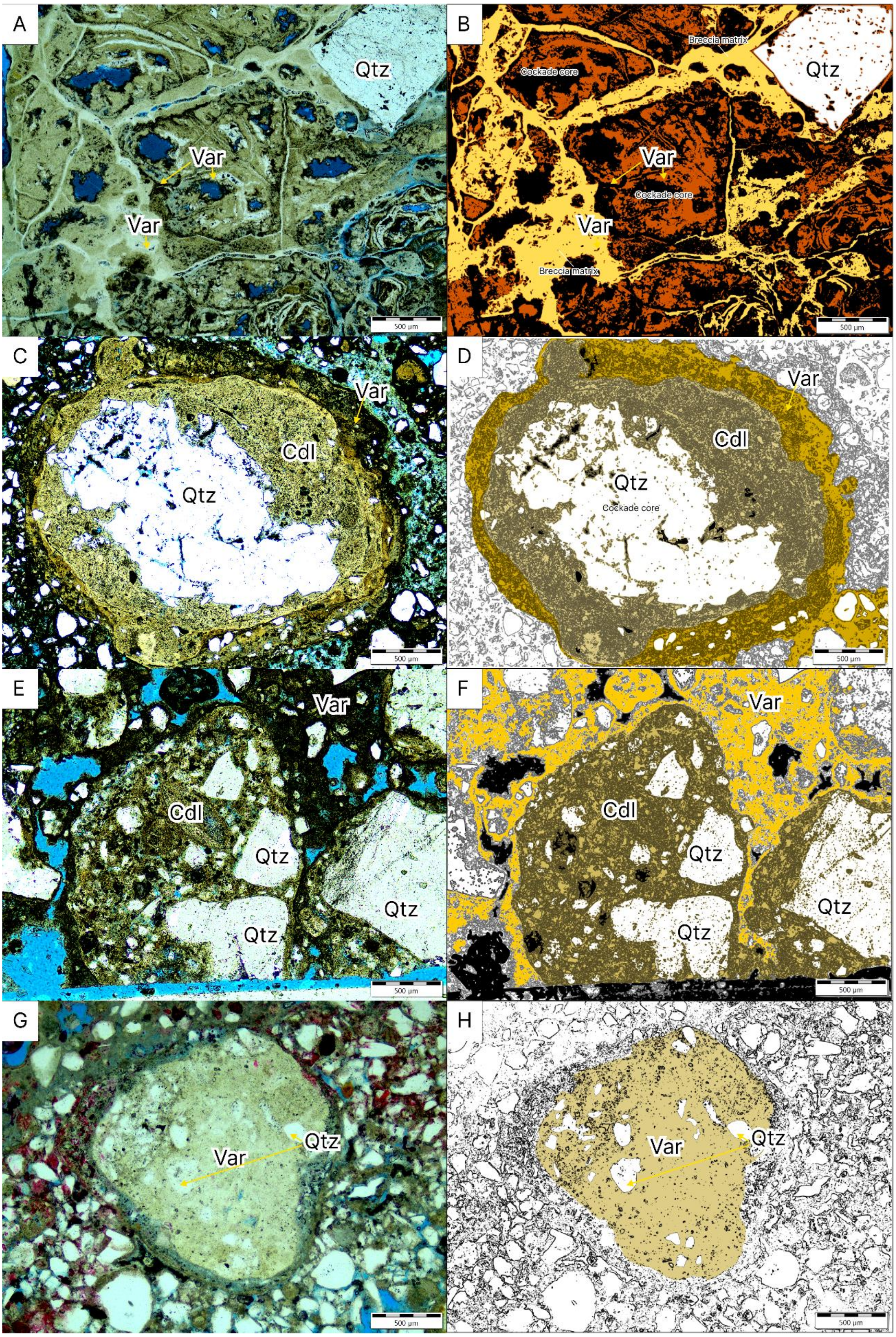

Figure 4.5: Textural evidence of reworked material and multiple fluid injection. A) and B) Thin section image and schematic drawing showing variscite-rich cockade textures with Fe-variscite cockade core inside variscite-rich matrix; C) and D) Cockade texture showing quartz clast

surrounded by crandallite borders with recrystallized variscite edges; E and F) Clast-cortex aggregates with quartz clasts inside crandallite-rich material; G) and H) Clast-cortex aggregate with quartz clasts inside variscite-rich material.

Mineralogical analysis by X-ray diffraction

X-ray diffraction analysis confirmed the mixed mineral assemblage observed petrographically: secondary Al-phosphate minerals (variscite, crandallite, and millisite/wardite), clay minerals (kaolinite), and accessory phases (quartz, diaspore, hydroxylapatite, fluorapatite, dolomite, and calcite). Secondary phosphate assemblages are the dominant mineralization (Figure 4.5).

Variscite (ICDD file 00-025-0018) occurs in four associations: (1) quartz, (2) quartz + crandallite, (3) quartz + crandallite ± millisite/wardite, and (4) quartz + millisite/wardite ± diaspore. Crandallite (ICDD file 01-070-2069) occurs with quartz, quartz + variscite, and quartz + variscite ± millisite/wardite assemblages. Millisite and wardite (ICDD files 00-013-0370 and 01-070-2154) could not be distinguished because of overlapping diffractometric peaks, but they were associated with quartz + crandallite + variscite ± diaspore.

Kaolinite was confirmed as the sole clay mineral phase (ICDD file 01-078-1996), occurring with quartz and quartz + variscite ± crandallite. Hydroxyapatite, fluorapatite, dolomite, and calcite (ICDD files 01-074-0566, 01-073-2445, 01-075-1687, 01-072-1937) were identified in three samples; calcite and fluorapatite appeared in one sample.

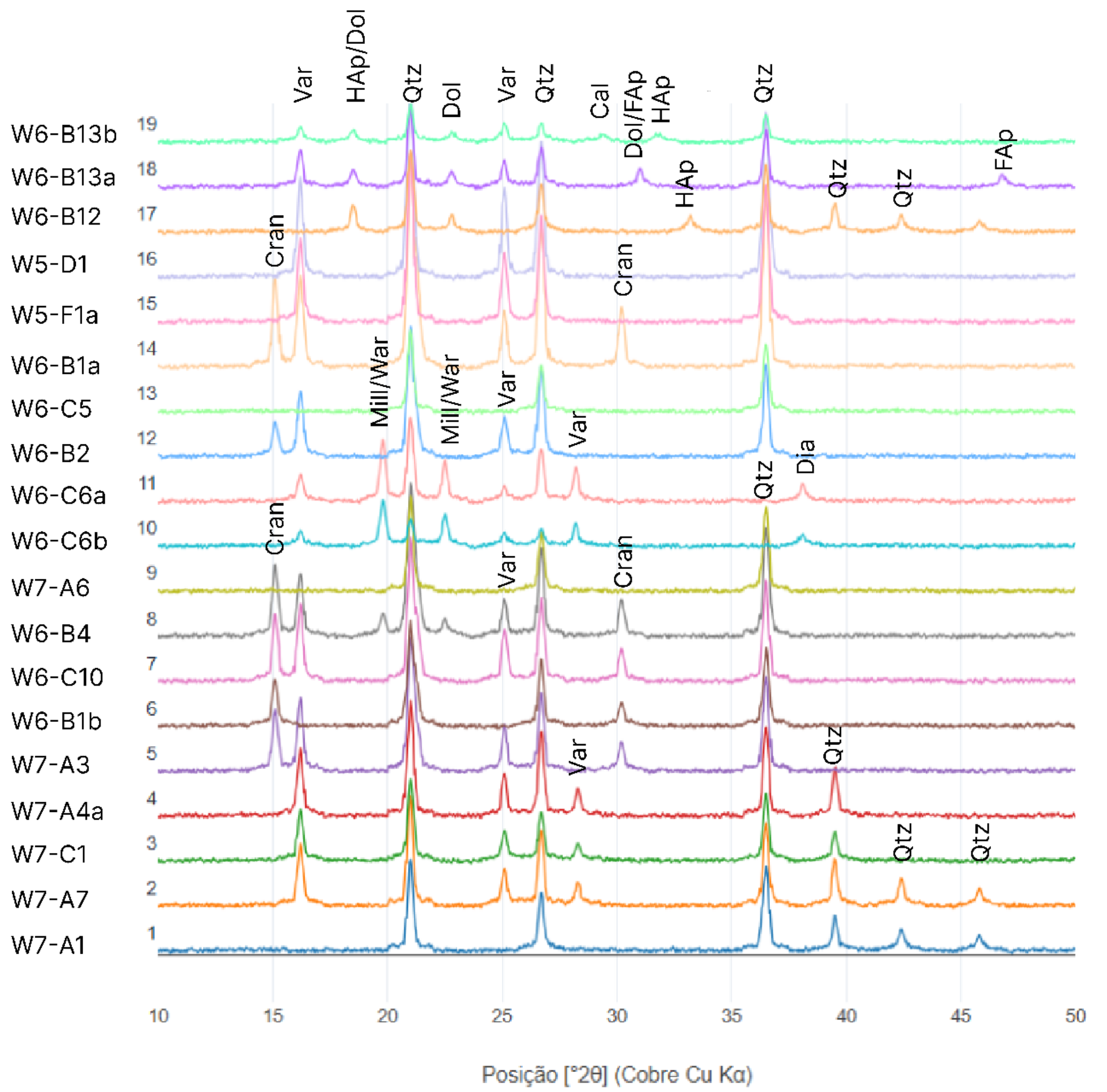

Figure 4.6: Unified diffractograms for 19 analyzed samples showing main intensity peaks and all mineral phases identified based on each respective 2theta angles (Cran = Crandallite; Var = Variscite; HAp/Dol = Hydroxylapatite/Dolomite; Qtz = Quartz; Dia/Mc = Diaspore/Microcline; Cal = Calcite; FAp = Fluorapatite).

Quantitative Evaluation of Minerals by Scanning Electron Microscopy (QEMSCAN)

QEMSCAN analysis of 11 samples provided detailed mineral distribution mapping that corroborated the XRD identifications and petrographic observations. Al-rich variscite (red) predominantly fills the cavity walls, veins, fractures, and breccia matrix (Figures 4.6c, e, f, l). Fe-rich variscite coatings (orange) fill cavities and open spaces at clast edges within the Al-rich phosphate matrix (Figure 4.6c). Crandallite (pink) occurs as veins, fracture fillings, and breccia matrices in association with variscite and quartz (Figure 4.6f).

Millisite/wardite (pink) was identified in one sample as a breccia matrix, with variscite coatings in cavities observed in association with millisite (Figure 4.6i).

Kaolinite (brown) occurs as pore-filling material associated with variscite, commonly in zones of increased porosity (Figure 4.6l). Calcite pseudomorphs were recognized as crystals filled with quartz and aluminum phosphate crusts.

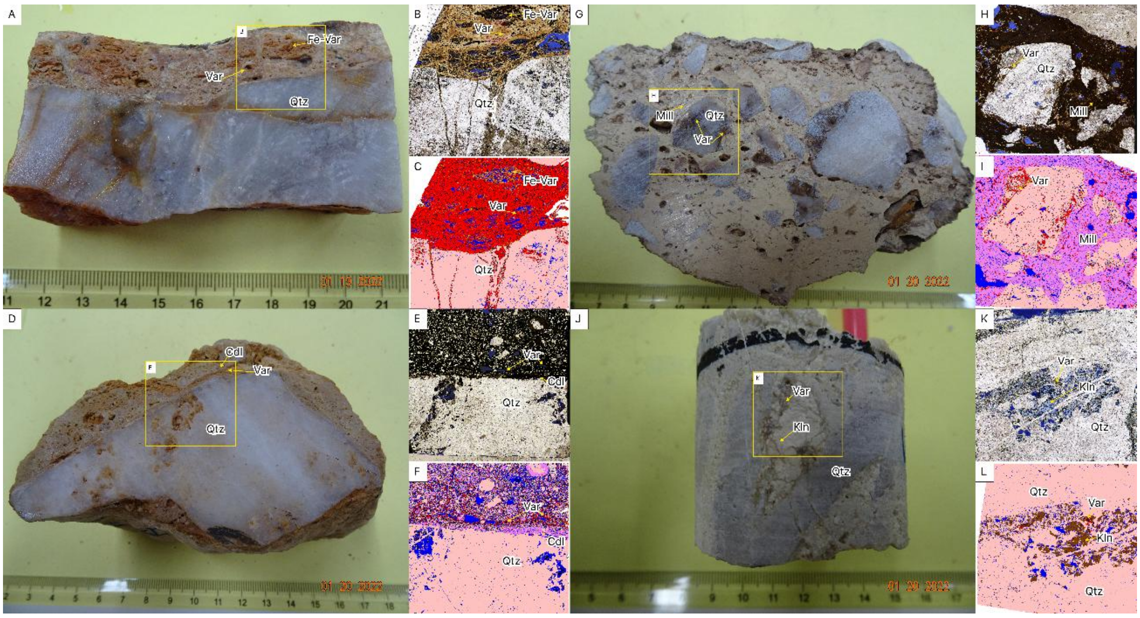

Figure 4.7: QEMSCAN analyses. A) W5-D1 hand sample; B) Thin section image showing variscite-rich matrix with Fe-rich crusts; C) QEMSCAN mapping with Fe-rich crusts in Orange, variscite-rich matrix in red, quartz in light pink; D) W7-A3 hand sample; E) Thin section image of crandallite and variscite-rich breccia matrix; F) QEMSCAN mapping with crandallite-rich matrix and clasts with vein-like recrystallized variscite; G) W6-C6 hand sample; H) Thin section showing millisite-rich matrix with recrystallized variscite-rich edges and clast-filling material; I) QEMSCAN mapping showing millisite-rich matrix in pink, variscite-rich edges and fillings in red, and quartz in light pink; J) W7-A5 hand sample; K) Thin section image showing kaolinite coatings altered to variscite-rich material; L) QEMSCAN mapping showing kaolinite coatings in brown, variscite in red, quartz in light pink.

Microstructural analysis by Scanning Electron Microscopy (SEM)

The SEM images enabled the detailed microstructural characterization of the Al-phosphate phases identified by previous methods. Variscite was observed in several occurrence modes, including cryptocrystalline masses as well as acicular and prismatic growth within vugs and pores (Figures 4.2e, g, 4.7b). The images also revealed zoned crystals with Fe-rich and Al-rich inner and outer rims, respectively (Figures 4.7b, c).

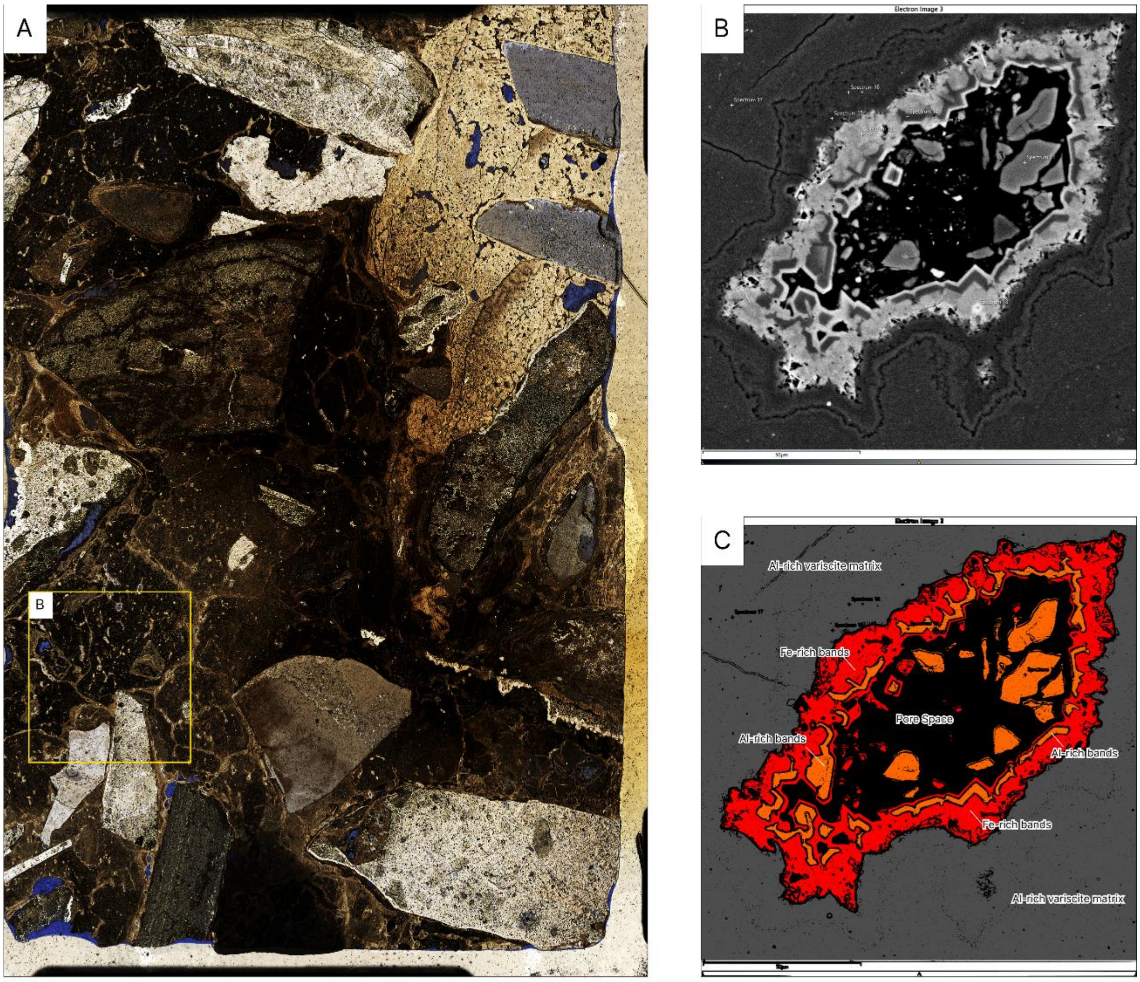

Figure 4.8: SEM analysis imaging. A) W5-F1b thin section; B) SEM image showing pore-filling variscite-rich prysmatic crystals with zoned compositional alternation; C) Schematic drawing showing zoned composition with Fe-rich crusts and Al-rich crystal edges.

Chemical mapping of thin sections identified crandallite by Ca levels and variscite by Al and Fe in vein fillings, defining their distribution in the vein fillings (Figures 4.8b, d, e). Although XRD and petrographic analyses identified millisite/wardite, kaolinite, carbonates, and other phosphates, these minerals were not detected in the samples investigated using SEM/EDS.

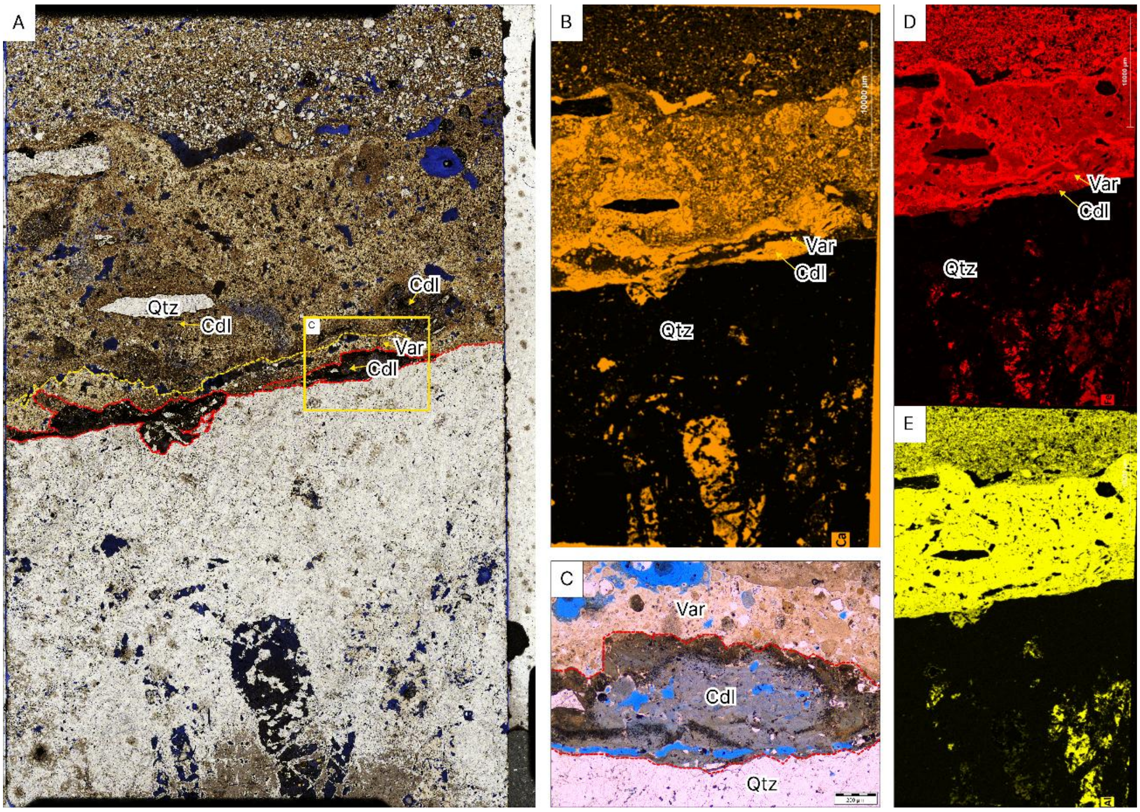

Figure 4.9: Chemical mapping of W6-B2 sample. A) W6-B2 thin section showing variscite and crandallite-rich matrix; B) Chemical mapping of W6-B2 thin section highlighting Ca-rich material in orange; C) Detailed image of thin section showing crandallite crust and variscite vein filling; D) and E) Chemical mapping showing Fe and Al concentrations, respectively.

Major elements chemical analysis by electron probe microanalyzer

Principal component analysis (PCA) of 189 EPMA individual spots distinguished two main aluminum phosphates using Euclidean distances to ideal end-members and a 2.0 wt% CaO threshold. Samples above this threshold were classified as crandallite (in a broad sense), and those below as variscite. The PCA plot shows distinct compositional clusters with minimal phase overlap (Figure 4.10c). Phases identified by XRD (millisite, wardite) were not detected in the EPMA dataset, consistent with limited Na and Sr substitution and potential analytical challenges from submicron intergrowths or detection limits for alkali-bearing phosphates (Table 4.1). Furthermore, analyses of the associated clay minerals (our unpublished data) confirmed compositions consistent with kaolinite-group minerals clustering near the dickite end-member (Figure 4.9).

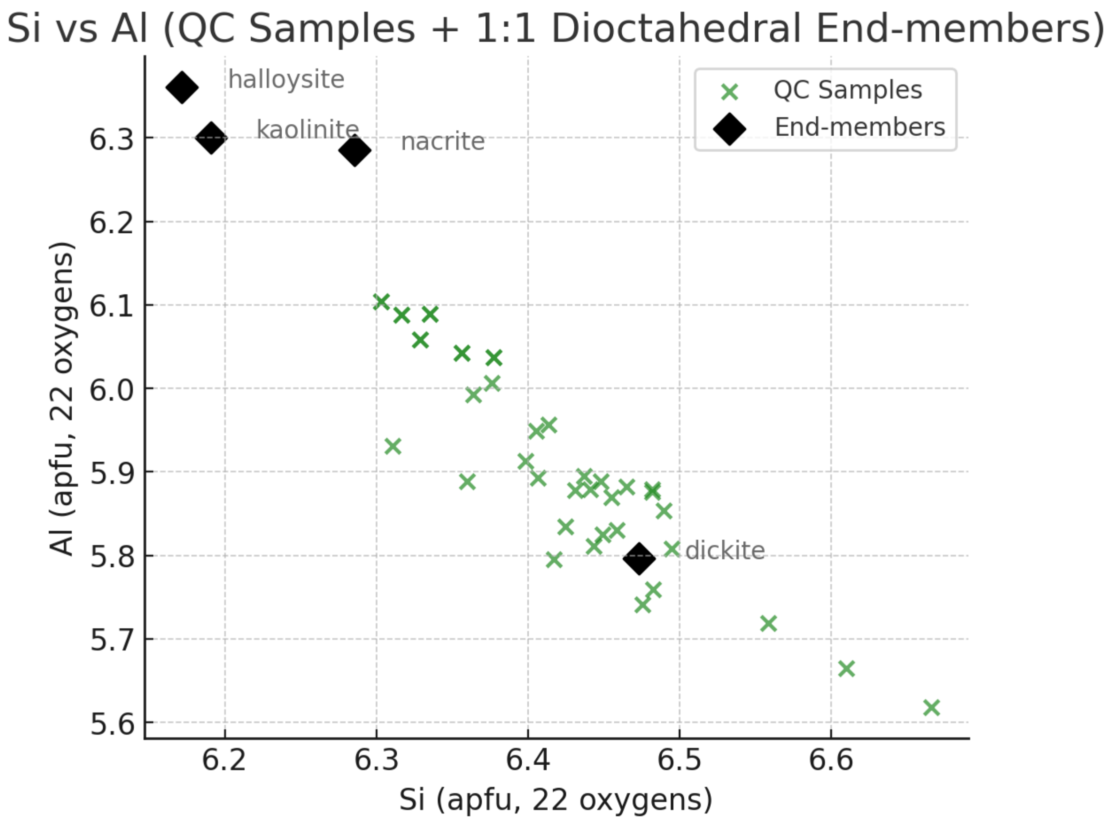

Figure 4.10: Si vs Al binary diagram showing compositional variation for clays in analyzed samples. Composition clusters near dickite end-member and is interpreted as clays from kaolinite-group minerals.

Variscite represented 83.6% of the analyses (n=158) across seven samples, showing close conformity to the ideal $AlPO_4 \cdot 2H_2O$ stoichiometry with mean P/Al ratios of 1.036 ± 0.135 (apfu); 51.9% of the analyses approached near-ideal compositions. Major oxide ranges include P_2O_5 (32.5-49.3 wt%, mean 41.5%), Al_2O_3 (14.0-33.9 wt%, mean 29.1%), and CaO (0.0-2.5 wt%, mean 0.13%), with minimal Ca enrichment (Ca/Al: 0.004 ± 0.010) and variable Fe^{3+} substitution (Fe^{3+}/Al: 0.129 ± 0.144).

Crandallite comprised 16.4% of the analyses (n=31) and was concentrated in sample W6-C6 (66.7%) with subordinate occurrences in three other samples. The compositions deviated from the ideal $CaAl_3(PO_4)_2(OH)_5 \cdot H_2O$ stoichiometry, with mean P/Al ratios of 0.733 ± 0.078 (theoretical value: 0.667) and Ca/Al ratios of 0.241 ± 0.052 (theoretical value: 0.333). However, 45.2% of the samples had compositions close to the ideal values. Major oxide compositions include P_2O_5 (22.0-32.6 wt%, mean 30.1%), Al_2O_3 (25.2-36.3 wt%, mean 29.7%), and CaO (2.2-10.2 wt%, mean 7.7%).

The Fe^{3+} versus Al plot demonstrates $Al^{3+} \rightleftharpoons Fe^{3+}$ substitution operating in both phases, with variscite showing greater compositional variability (Fe^{3+}: 0.004-0.542 apfu) than crandallite (Fe^{3+}: 0.038-0.393 apfu) (Figure 4.10b). The Al–Fe^{3+}–Ca ternary diagram reveals compositional fields concentrated near the Al apex, with variscite plotting closer to the Al corner and crandallite extending toward the Ca corner (Figure 4.10a). No composition approaches the Fe-rich end members despite extensive Fe^{3+} substitution.

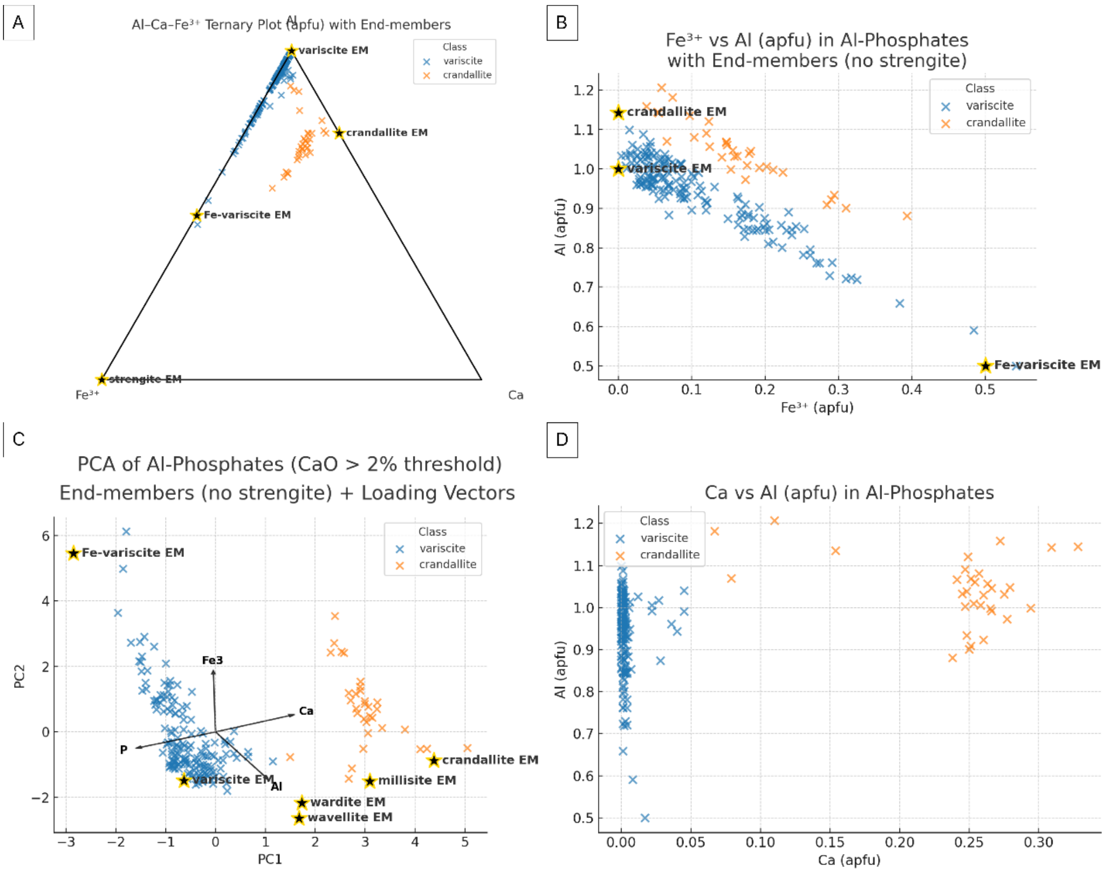

Figure 4.11: Ternary and binary plots of chemistry data. A) Al-Ca-Fe ternary plot showing two main trends and compositional clusters for variscite and crandallite; B) Fe vs Al. Binary diagram showing $Al^{3+} \rightleftharpoons Fe^{3+}$ substitution mechanism on analyzed samples; C) PCA diagram of Al-phosphates with respective end members; D) Ca vs Al binary diagram highlighting Al-rich variscite and Ca-bearing crandallites.

The $Al/(Al+Fe^{3+})$ versus $P/(Al+Fe^{3+})$ plot reveals fundamental structural controls on the composition (Figure xD). The $P/(Al+Fe^{3+})$ ratio achieved near-perfect separation: variscite clusters at 0.85-1.05 (approaching the theoretical

1.0), while crandallite formed a distinct field at 0.50-0.70 (approaching the ideal 0.667). A pronounced compositional gap at P/(Al+Fe^{3+}) = 0.75-0.85 separates the phosphate fields.

Sample Oxide	W5-D1A	W5-F1A	W6-B7A	W6-B7B	W6-C6	W7-A5	W7-C1A	W7-C2B
P2O5	41.23	41.79	43.47	40.64	34.36	37.25	37.93	38.94
V2O3	0.01	0.01	0.01	0.02	0.01	0.01	0.01	0.01
SiO2	0.25	0.44	0.56	0.69	0.08	1.16	2.73	1.38
Al2O3	26.19	27.54	30.98	31.38	29.05	29.25	32.68	30.68
Cr2O3	0.01	0.01	0.02	0.00	0.02	0.01	0.01	0.00
TiO2	0.45	0.17	0.01	0.01	0.19	0.01	0.02	0.02
Fe2O3	8.17	8.13	3.54	2.03	6.80	4.29	3.58	2.96
MgO	0.02	0.02	0.02	0.03	0.03	0.02	0.09	0.03
MnO	0.03	0.03	0.02	0.01	0.05	0.03	0.03	0.03
CaO	0.08	0.07	0.04	0.47	5.51	0.65	2.29	0.30
BaO	0.00	0.01	0.00	0.01	0.15	0.07	0.01	0.01
SrO	0.05	0.04	0.01	0.05	0.42	0.18	0.00	0.01
Na2O	0.00	0.00	0.00	0.03	0.01	0.00	0.19	0.00
K2O	0.09	0.06	0.02	0.06	0.07	0.11	0.09	0.08
F	0.48	0.50	0.51	0.50	0.44	0.49	0.42	0.51
Cl	0.04	0.01	0.01	0.01	0.03	0.01	0.02	0.02
Total 1	76.45	78.20	78.57	75.29	76.57	72.91	79.45	74.33
O=F=Cl	0.21	0.21	0.21	0.21	0.19	0.21	0.18	0.22
Total 2	76.23	77.99	78.35	75.08	76.38	72.70	79.27	74.11
H2O FTIR semiquant	21.70	21.70	21.70	21.70	21.70	21.70	20.03	21.33
Total 3	97.93	99.69	100.05	96.78	98.08	94.40	99.29	95.44

Table 4.2: Percentage of average oxide composition for each analyzed sample through EPMA (excluding clays).

Discussions

Structural and textural controls on mineralization

Al-phosphate minerals exhibit varied morphological and textural characteristics across geological settings. Goldbery and Loughnan (1977) described crandallite occurrences as cryptocrystalline masses, globular aggregates, acicular assemblages, and prismatic crystals. The Lam Lam deposit in Senegal displays tabular crystal growth for Ca-millisite and needle-like, sheaf-like, and arrow-head textures for crandallites (Flicoteaux and Lucas 1984). Similar textural variations occur in the El Hefuf deposit in Egypt, where crandallite textural diversity reflects in situ recrystallization of Ca-millisite (El Agami 2019).

Variscite typically forms spherical aggregates of prismatic and tabular crystals, fine-grained masses, crusts and nodules (Larsen 1942; Onac et al. 2004; Druppel et al. 2007), with associated kaolinite appearing as fine-grained, vermicular aggregates and zoned coatings (Shelton 1964; Flicoteaux and Lucas 1984).

This documented diversity provides context for the Al-phosphate assemblages at Samambaia, whereas apatites and carbonate minerals were locally poorly described. These comparable morphological expressions record the dynamic conditions of fault-controlled hydrothermal systems (Figure 4.11). While apatites were only observed in XRD analysis, description shows calcite/dolomite pseudomorphs substituted by quartz and APM (Figures 4.3e, f). This limited occurence indicates a previously existing primary mineralogy, later dissolved or replaced by aluminum phosphates during fluid circulation. The localized presence of these primary minerals suggests an environment of intense alteration, with geochemical control dominated by acid pH and mobilization of Al, Fe and P, which is in agreement with previous deposit descriptions (e.g., Dill 1991; El Agami 2019). These Ca-bearing minerals would have precipitated in more alkaline conditions, but increased acidity induced by fluid-rock interaction caused mineral dissolution and later substitution by Al-phosphates and quartz.

Al-phosphates occur preferentially in uncemented breccias (Group 3) and fault gouges (Group 4) (Bezerra et al. In prep.), as fault structure controls Al-phosphate distribution through systematic relationships with fault rock architecture, demonstrating that fault-generated porosity and permeability controlled fluid access and mineral precipitation. QEMSCAN mapping coupled with petrographic description reveals systematic spatial relationships where Al-rich variscite predominantly fills cavity walls, veins, fractures, and breccia matrix, while Fe-rich variscite coatings occupy open spaces at clast edges (Figures 4.2, 4.5). This spatial pattern indicates episodic fluid access controlled by fault-generated porosity evolution, with different textural domains recording distinct stages of the seismic cycle.

Texture variations documented in variscite and crandallite also reflect crystallization conditions, as the matrix-forming character of cryptocrystalline Al-phosphates in Groups 3 and 4 contrasts with vug-filling euhedral crystals in fractured quartz veins (Figures 4.2, 4.3, 4.4). Cryptocrystalline masses and breccia matrix fillings indicate more space with less time for precipitation, while well-crystallized prismatic, drusiform, fibrous and sheaf-like textures in pores and vugs show precipitation with more time in less space. Millisite-rich matrix with variscite-filled recrystallized borders also indicate changes in crystallization conditions, and small fractures, joints and intraclast fissures exhibit quick precipitation rates with limited space. This dynamism reflects multiple changes of precipitation parameters during fault reactivation, revealing alternating stages of seismic activity with interseismic periods.

Rhythmic features in Al-phosphates document and support this multiple seismic activity model for Samambaia. The syntaxial-like variscite growth patterns in vugs indicate episodic fluid injection associated with fault reactivation events (Figures 4.2e, f). These systematic crystallographic orientations reflect precipitation from static or slowly moving fluids in fracture networks established during fault movement, contrasting with chaotic growth patterns that characterize dynamic flow during active faulting episodes.

Growth zoning provides the strongest evidence for seismic control. The cockade and clast-cortex textures - observed both in variscite and crandallite - and rhythmic zoning documented in variscite directly record the crack-seal mechanism proposed for the Samambaia Fault (Bezerra et al., 2021) (Figure 4.4). SEM analysis reveals alternating Fe-rich and Al-rich compositional bands in variscite crystals, with Fe^{3+} contents ranging from 0.004-0.542 apfu. Each band represents a discrete fracture-seal cycle, with compositional alternations recording changing fluid access to basement lithologies during successive fault reactivation events.

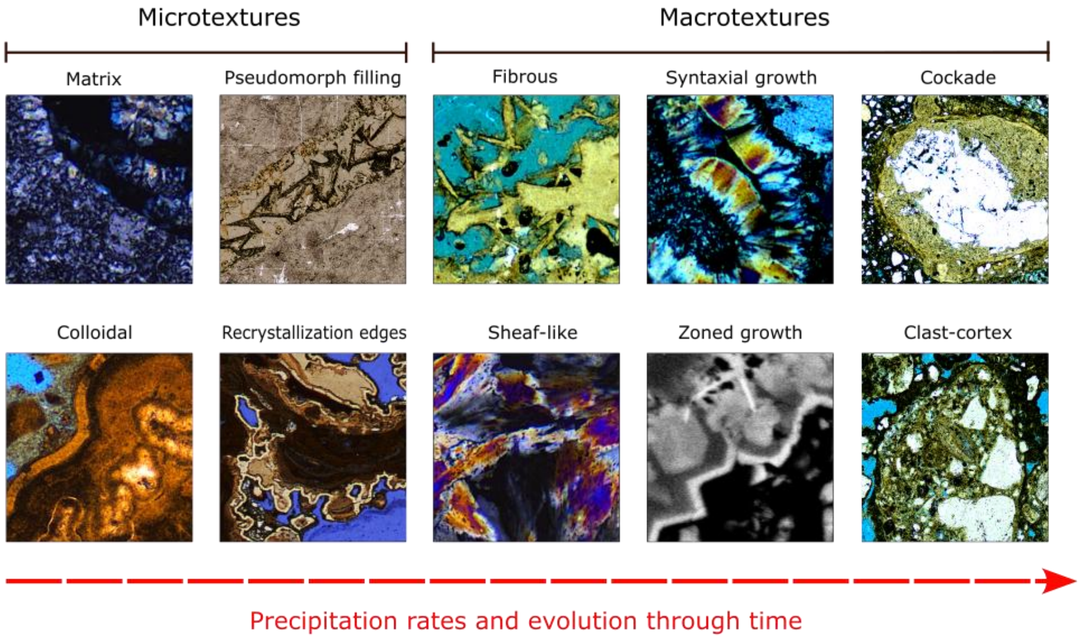

Figure 4.12: Schematic diagram showing textural diversity identified in Al-phosphates. Multiple textures identification demonstrates time and space-dependent precipitation evolution.

Temperature and pH controls on mineral stability

Structural processes clearly influence fluid access and basement alteration, and these structural and textural relationships control the chemical evolution preserved in the mineral assemblages, as mineral stability data constrain formation temperatures and pH values. The preservation of variscite and crandallite without dehydrated phases (metavariscite, berlinite) restricts formation temperatures to <113°C and <139°C, respectively (Druppel et al., 2007; Gilkes & Palmer, 1983). Dehydration reactions in variscite begin at 186°C and 500 bar, forming berlinite (Druppel 2007). These limits conflict with fluid inclusion microthermometry from associated quartz veins, which records trapping temperatures of 91-336°C (V1) and 147-388°C (V2) (Bezerra et al., 2021). This temperature discrepancy suggests Al-phosphate precipitation during late-stage cooling or as a separate, lower-temperature event following initial silicification.

Chemical data provide complementary evidence. The systematic compositional clustering revealed by PCA analysis, with a sharp 2.0 wt% CaO threshold discriminating variscite from crandallite compositions, directly reflects pH-controlled precipitation. Variscite dominance indicates predominantly acidic conditions (pH 1.5-2.5) where Al^{3+} species predominate, consistent with experimental data showing optimal variscite crystallization under these conditions (Hsu and Sikora, 1993). Conversely, the restricted occurrence of crandallite in specific samples (particularly W6-C6) records localized acidic pH conditions (3.0-5.0) where crandallite-group minerals achieve stability.

Textural and chemical data establish a three-stage paragenetic evolution documenting fluid-rock interaction history within the Samambaia Fault zone (Figure 4.12). Petrographic observations combined with chemical mapping (EPMA and SEM) reveal clear contacts between variscite and crandallite, documenting sequential paragenesis driven by pH and elemental composition changes in the fluids. Three generations of Al-phosphates precipitated in Samambaia, revealing compositional variation of mineralizing fluids through time.

Integrated paragenetic history

Stage 1 (Early Ca-Bearing Phase): The host rock initially contained apatite, calcite, dolomite, K-feldspar, and clay minerals exposed to weathering under near-neutral to slightly alkaline conditions. Crandallite formed as one of the first alteration products from interaction between fluids, clays and apatites or from dissolution of Ca-millisite. Though crandallite can form distinct textures including clast-cortex aggregates, breccia and cataclasite matrix, spherulitic vein-fillings and crusts, only cryptocrystalline masses were preserved at Samambaia. Substrate relationships of crandallite to later variscite borders indicate formation under acidic pH conditions (3.0-5.0) when Ca availability from carbonate or plagioclase dissolution maintained higher pH conditions. Simultaneously, K-feldspar alteration under acidic conditions facilitated kaolinite formation during initial basement weathering.

Stage 2 (Main Variscite Event): Changing pH conditions and decreasing Ca and Al availability favored partial dissolution and replacement of crandallite by variscite under increasingly acidic conditions (pH 1.5-2.5). Contact relationships show variscite precipitation associated with recrystallization or alteration of crandallite, consistent with physicochemical conditions evidenced by previous work (Dill 1997; Toledo 1999). Unlike the Fairfield, Utah deposit where variscite-rich nodules represent primary Al-phosphate precipitates (Larsen 1942), at Samambaia variscite functions as both primary product (when precipitated directly from kaolinite alteration) and secondary product (through recrystallization from crandallite and millisite).

Stage 3 (Late Fe-Rich Event): Continued fracturing and fluid influx enabled interaction with weathered lateritic crusts, increasing Fe activity in solution and favoring precipitation of Fe-rich variscite in cavities, fractures, and breccia matrices. QEMSCAN analysis confirms that Fe-rich variscite coatings preferentially occupy clast edges within Al-rich phosphate matrices, indicating limited Fe mobility and local precipitation control. Tectonic reworking of previously precipitated material formed clast-cortex aggregates of both crandallite and variscite, with textures such as cockade breccias, rhythmic zoning, and Fe–Al banding reflecting multiple episodes of fluid injection, fracture sealing, and fluctuations in element availability. Millisite shows limited stability under the acidic conditions that dominated the system, with nearly complete substitution by variscite representing the final equilibrium assemblage.

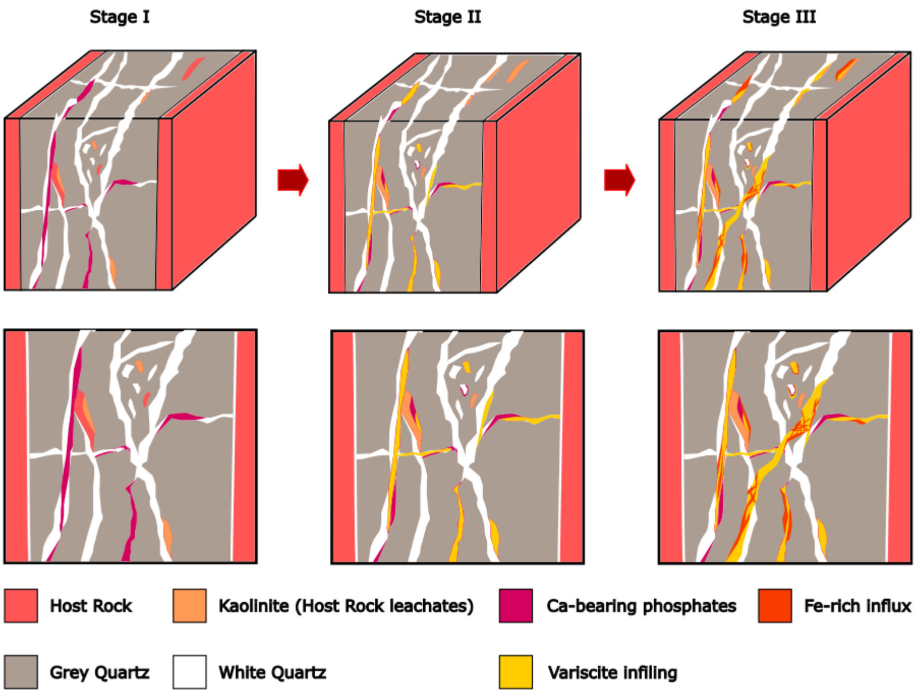

Figure 4.13: Schematic drawing of multiple fluid injection and Al-phosphates precipitation stages identified at Samambaia fault.

Chemical evolution and fluid source

Crystal structure of variscite controls the final composition, as this mineral participates in a solid solution series with strengite, allowing Fe incorporation through Al-Fe interchange in its isostructural framework. Exceptional discrimination by P/(Al+Fe^{3+}) ratios reflects fundamental structural controls on composition, with variscite clustering near theoretical ratios of 1.0 and crandallite near 0.667. The complete absence of compositions approaching Fe-variscite end-members suggests thermodynamic constraints on Fe-rich phosphate stability under the specific pH-Eh conditions at Samambaia.

Additionally, analytical data provide evidence for complex precipitation. XRD, QEMSCAN and petrographic analyses identified crandallite and millisite/wardite, but stoichiometric closure values for these Ca-bearing Al-phosphates were below average. Higher Fe contents and lower Ca values suggest compositional mixtures and multiple precipitation phases, consistent with Samambaia's multiple phases of reactivation, fluid percolation, and reworked material. This compositional heterogeneity indicates that Ca-bearing phosphates were unstable under increasingly acidic conditions, with these mixtures representing transitional settings containing remnants of initial precipitation phases.

Variscite compositions cluster near ideal $AlPO_4 \cdot 2H_2O$ stoichiometry with minimal Ca enrichment and limited Fe^{3+} substitution (0.004-0.542 apfu), indicating formation from highly evolved, Al- and P-rich hydrothermal solutions derived from extensive water-rock interaction with Precambrian basement rocks. Fe enrichment in both calcium Al-phosphates and variscite results from interaction with iron oxide-bearing fluids that modified the chemical balance during mineral precipitation (Figure 4.10b).

Widespread variscite, functioning as a pH buffer, confirms that acidic precipitation conditions prevailed for extended periods, creating conditions for dissolution of crandallite and millisite while leaching Ca from the system. This evolution reflects progressive acidification of initially neutral fluids through extensive water-rock interaction and meteoric water input.

Initial intermediate conditions, with alkaline to slightly acidic solutions, allowed dissolution of Ca-bearing minerals from host rocks and their precipitation in fractures. As acidic conditions developed, these Ca-bearing phosphates became unstable and dissolved, with mobile elements leached out, preserving only relicts and crystal shapes. Porosity from dissolution was later filled by new precipitation of Al-richer phosphates and Al-rich clays such as kaolinite.

Element mobilization likely required multiple sources, with a possible contribution from regional units. Apatites identified through XRD analyses likely represent a major phosphorus source, while calcium derived from primary carbonate minerals such as calcite and dolomite. Heterogeneous distribution of crandallite, concentrated primarily in sample W6-C6 with subordinate occurrences in three other samples, indicates spatially variable fluid compositions within the fault zone. Other potential sources include sedimentary units from the Potiguar Basin such as carbonates from the Jandaíra Formation, sandstones from the Açu Formation, and lateritic coverings from the Barreiras Formation, or apatite-bearing igneous and metamorphic rocks of the crystalline basement. High iron content observed in analyzed samples results from fluid interaction with iron oxides and hydroxides formed within heavily weathered rock profiles, supporting near-surface formation conditions (Spier 2020), although Fe inheritance from other iron bearing silicate minerals is not discarded.

The coexistence of final and intermediate phases in the paragenetic sequence, characterized by variations in mineralizing fluid chemistry, reflects the dynamic nature of this geochemical system. These compositional behaviors, as illustrated in ternary and binary diagrams, emphasize the importance of fluid chemical conditions and substrate interactions in controlling the paragenetic evolution of the Samambaia Fault system. Understanding these relationships is essential for interpreting the formation mechanisms and broader geochemical implications of this complex mineral assemblage.

The percolation of meteoric water was likely the source for increased acidity through time, as sulphide minerals weren’t detected in Samambaia in our analysis, supporting predominance of supergene or late low-temperature hydrothermal processes. Diverse occurrence modes identified through SEM and petrographic analysis influence fractures, veins, pores and fault rock geometry, likely affecting secondary porosity and permeability in this tectonically active environment.

Implications

Scientific Contributions and Process Understanding

This study contributes to understanding Al-phosphate formation in fault systems through formation conditions, precipitation mechanisms, and structural controls. The findings establish a framework for interpreting similar hydrothermal systems in active tectonic settings. Notably, Al-phosphate assemblages preserve records of pH evolution, fluid chemistry changes, and episodic fluid injection, which may provide tools for reconstructing hydrothermal system evolution in fault zones.

Combining experimental thermodynamic constraints with natural mineral assemblages offers an approach for constraining formation conditions. The documented temperature gap between high-temperature silicification (147-388°C) and low-temperature Al-phosphate precipitation (<113-139°C) illustrates the importance of thermal evolution in controlling mineral precipitation sequences. This approach could be applied to other fault systems to understand temporal relationships between different hydrothermal events and their connection to tectonic activity.

The systematic mineral associations (quartz → quartz+crandallite → quartz+crandallite+variscite) suggest a model for progressive basement alteration under acidifying fluid conditions, potentially applicable to interpretation of comparable mineral assemblages in other crystalline basement settings. The documented sensitivity of Al-phosphate formation to pH, temperature, and fluid chemistry changes suggests these minerals may serve as indicators for paleoenvironmental reconstruction in continental settings.

Paleoseismic Applications

Rhythmic precipitation textures and compositional zoning in Al-phosphates record individual fault reactivation events, potentially contributing to paleoseismic research. The crack-seal mechanism documented through variscite growth patterns provides a mineralogical record of seismic cycles that may extend beyond conventional paleoseismic indicators. Growth zones potentially represent discrete fault movement events, which could contribute to reconstruction of earthquake frequency and temporal clustering over geological timescales in intraplate settings. The transition from cryptocrystalline masses to euhedral crystals offers a framework for interpreting deformation history from mineral textures, potentially supplementing structural analysis in regions where fault activity history is poorly constrained.

Understanding these relationships may contribute to assessing long-term fault behavior and earthquake hazards in crystalline basement terranes, particularly in intraplate regions where seismic hazard assessment is challenging due to limited historical records.

Applications to Basement Hydrothermal Systems

The process model developed here may inform basement-hosted hydrothermal systems, particularly for understanding permeability evolution in fracture-controlled environments. The relationship between fault architecture, fluid flow patterns, and mineral precipitation suggests how secondary mineralization modifies fluid pathways in crystalline rocks. Al-phosphate distribution patterns might serve as indicators of past hydrothermal activity and fluid flow directions in fault systems.

Thermal constraints from Al-phosphate stability relationships may complement conventional geothermometry. The mineralogical record of temperature evolution from initial silicification to late-stage phosphate precipitation contributes insights into hydrothermal longevity and thermal history, with potential applications for understanding fluid circulation in basement terranes.

The Samambaia system demonstrates how secondary mineralization can create complex porosity and permeability structures in fractured crystalline rocks. The documented spatial heterogeneity in mineral distribution and the evolution from permeable breccias to mineral-sealed fault gouges may provide insights relevant to geothermal systems, basement-hosted resources, and fluid circulation in tectonically active crystalline terranes.

Acknowledgements

This research was carried out in association with the ongoing R&D Project registered as ANP 23505-1, “Processos e Caracterização de Rotas de Fluxo de Fluidos em Reservatórios Carstificados, Fraturados e Silicificados do Pré-Sal –

Porocarste Fase II” (UFRN/UNB/UFPE/UFC/UFRA/IFRN/IFPB/Shell Brasil/ANP) – Porokarst Phase II – Processes and Characterization of fluid pathways in Karstified, Fractured and Silicified Reservoirs of the Presalt, sponsored by Shell Brasil under the ANP R&D levy. The authors also thank FAPEMIG APQ-02529-24 project, coordinated by G. Queiroga, who kindly helped us with the chemical analyses through EPMA.

References cited

Altschuler, Z.S. (1973) The weathering of phosphate deposits - geochemical and environmental aspects. In Griffith, E.J., Beeton, A., Spencer, J.M., and Mitchell, D.T., Eds., Environmental Phosphorus Handbook, p. 33-96. John Wiley, New York.

Audra, P., Häuselmann, P., Bigot, J.Y., and Nobécourt, J.C. (2021) The role of condensation-corrosion in thermal speleogenesis: Study of a hypogenic sulfidic cave in Brazil. International Journal of Speleology, 50, 125-145.

Barros, L.V., Silva, F.C., and Santos, R.N. (2024) Geochemical controls on aluminum-phosphate mineral stability in weathering profiles. Chemical Geology, 635, 121615.

Berger, A., and Herwegh, M. (2019) Cockade textures in veins and their bearing on fracture-seal processes. Tectonophysics, 751, 56-72.

Bezerra, F.H.R., Ferreira, J.M., and Sousa, M.O.L. (2007) Review of seismicity and Neogene tectonics in northeastern Brazil. Revista Brasileira de Geofísica, 25, 379-396.

Bezerra, F.H.R., Rossetti, D.F., Oliveira, R.G., Medeiros, W.E., Neves, B.B.B., Balsamo, F., Nogueira, F.C.C., Dantas, E.L., Andrades Filho, C., and Góes, A.M. (2011) Neotectonic reactivation of shear zones and implications for faulting style and geometry in the continental margin of NE Brazil. Tectonophysics, 614, 78-90.

Bezerra, F.H.R., Lima-Filho, F.P., Amaral, R.F., Caldas, L.H.O., and Costa-Neto, L.X. (2021) Pliocene-Quaternary fault control of sedimentation and coastal plain morphology in NE Brazil. Journal of South American Earth Sciences, 14, 61-75.

Dantas, E.L., Souza, Z.S., Wernick, E., Hackspacher, P.C., Martin, H., Xiaodong, D., and Li, J.W. (2013) Crustal growth in the 3.4-2.7 Ga São José de Campestre Massif, Borborema Province, NE Brazil. Precambrian Research, 227, 120-156.

Del Nero, M., Galindo, C., Barillon, R., Halter, E., and Madé, B. (2010) Surface reactivity of α-Al2O3 and mechanisms of phosphate sorption: In situ ATR-FTIR spectroscopy and ζ potential studies. Journal of Colloid and Interface Science, 342, 437-444.

Díaz-Acha, C. (2019) Caracterização mineralógica e geoquímica de fosfatos de alumínio da jazida El Hefuf, Egito. M.S. thesis, Universidade de São Paulo, Brazil, 89 p.

Dill, H.G. (1991) Geological and mineralogical characteristics of the Fairfield nodular phosphate deposit, Utah County, Utah. Economic Geology, 86, 1084-1098.

Dill, H.G. (1997) A comparative study of uranium-thorium-bearing and barren leucogranites from the Bohemian Massif (Austria). Ore Geology Reviews, 12, 75-93.

Dill, H.G. (2001) The geology of aluminium phosphates and sulfates of the alunite group minerals: a review. Earth-Science Reviews, 53, 35-93.

Druppel, K., Littmann, S., Rohn, R., and Klemd, R. (2007) Petrology and isotope geochemistry of the Mesoproterozoic anorthosite massifs of Kunene Complex, NW Namibia. Precambrian Research, 156, 1-31.

El Agami, N.L. (2019) Aluminum phosphate minerals from the El Hefuf deposit, Qena, Egypt: Mineralogy and genetic implications. Applied Clay Science, 182, 105285.

El-Agami, N.L., El-Naggar, A.Y., and Madani, A.A. (2005) Aluminum phosphate minerals from lateritized carbonatites of Qena district, Egypt. Applied Clay Science, 28, 63-74.

Flicoteaux, R., and Lucas, J. (1984) Weathering of phosphate minerals. In Nriagu, J.O., and Moore, P.B., Eds., Phosphate Minerals, p. 292-317. Springer-Verlag, Berlin.

Francisco, P.C.M., Louro, V.H.A., and Silva, M.R.R. (2007) Synthesis and characterization of crandallite at high temperature and pressure conditions. American Mineralogist, 92, 1521-1529.

Frost, R.L., López, A., Scholz, R., and Xi, Y. (2011) Infrared and Raman spectroscopic characterization of the phosphate mineral crandallite - CaAl3(PO4)2(OH)5·H2O from Brazil. Spectrochimica Acta Part A, 78, 1260-1264.

Gaboreau, S., Vieillard, P., Ehrenberg, S.N., Aagaard, P., and Klitgaard-Kristensen, D. (2005) Aluminum phosphate-sulfate minerals associated with Proterozoic unconformities in the Athabasca Basin (Saskatchewan, Canada). Chemical Geology, 230, 41-54.

Gilkes, R.J., and Palmer, B. (1983) Synthesis, thermal stability and infrared spectroscopy of crandallite. Mineralogical Magazine, 47, 465-468.

Goldbery, R., and Loughnan, F.C. (1977) Dawsonite and crandallite from the Liddell Coal Measures, New South Wales, Australia. American Mineralogist, 62, 1237-1242.

Goldshmid, J., and Rubin, H. (1988) Aluminum-phosphate interactions in saturated kaolinitic soils. Soil Science Society of America Journal, 52, 1089-1094.

Henderson, T.R., Gomes, P.S., Ferreira, J.M., and Assumpcao, M. (1994) Seismicity, volcanism and neotectonics of northeastern Brazil. In Sauck, W.A., Ed., Neotectonics of South America, 19, 201-214. Penrose Conference Series, Geological Society of America.

Hsu, S.C., and Sikora, E. (1993) Synthesis and characterization of variscite and metavariscite. American Mineralogist, 78, 1358-1361.

Larsen, E.S. (1942) The mineralogy and paragenesis of the variscite nodules from near Fairfield, Utah. American Mineralogist, 27, 281-300.

Matula, J., and Wojtkowska, M. (2025) Phosphate speciation in aqueous solutions: A comprehensive thermodynamic analysis. Chemical Geology, 642, 121789.

Nriagu, J.O. (1976) Phosphate-clay mineral relations in soils and sediments. Canadian Journal of Earth Sciences, 13, 717-736.

Nriagu, J.O., and Moore, P.B. (1984) Phosphate Minerals, 442 p. Springer-Verlag, Berlin.

Onac, B.P., Effenberger, H., and Breban, R.C. (2004) Brushite and taranakite from Cioclovina Cave (Romania): Occurrence and paragenetic sequence. Mineralogical Magazine, 68, 395-403.

Palacios, E., García-Guinea, J., Crespo-Feo, E., González-Martín, R., and Tormo, L. (2013) Phosphate biomineralization in acidic solutions and the formation of aluminum phosphate phases. Chemical Geology, 347, 1-11.

Reid, A.M., and Macintyre, R.M. (2000) Carbonate and organic matter in Olduvai Bed I: Possible source for turquoise at the FLK Zinj site. Journal of Human Evolution, 38, 609-620.

Roncal-Herrero, T., Rodríguez-Blanco, J.D., Oelkers, E.H., and Benning, L.G. (2009) Precipitation of iron and aluminum phosphates directly from aqueous solution as a function of temperature from 50 to 200°C. Crystal Growth & Design, 9, 5197-5205.

Rossetti, D.F., Bezerra, F.H.R., and Dominguez, J.M.L. (2013) Late Oligocene-Miocene transgressions along the equatorial and eastern margins of Brazil. Earth-Science Reviews, 123, 87-112.

Saishu, H., Okamoto, A., and Tsuchiya, N. (2017) The significance of silica precipitation on the formation and evolution of slow slip events. Nature Geoscience, 10, 447-451.

Schwab, R.G., Herold, H., and Götz, C. (1989) Compounds of the crandallite type: Synthesis and properties of pure goyazite, gorceixite and plumbogummite. Neues Jahrbuch für Mineralogie Monatshefte, 3, 113-126.

Schwab, R.G., Herold, H., Götz, C., and de Oliveira, N.P. (1990a) Crandallite and goyazite from Catalão I carbonatite complex, Goiás, Brazil, and their industrial applications. Applied Clay Science, 5, 33-43.

Schwab, R.G., Herold, H., de Oliveira, N.P., and Götz, C. (1990b) Plumbogummite and corkite from Catalão I carbonatite complex, Goiás, Brazil, and their industrial applications. Neues Jahrbuch für Mineralogie Abhandlungen, 161, 265-276.

Shelton, K.L. (1964) Variscite occurrences in Arkansas. Arkansas Geological Commission Bulletin, 19, 34 p.

Smeraglia, L., Aldega, L., Billi, A., Carminati, E., Di Paolo, L., Giordano, G., and Rossetti, F. (2018) Development of an intracontinental transcurrent fault system: The Mattinata Fault Zone, Apulia, southern Italy. Journal of Structural Geology, 116, 179-195.

Souza, Z.S., Kalsbeek, F., Deng, X.D., Frei, R., Kokfelt, T.F., Dantas, E.L., Li, J.W., Pimentel, M.M., and Galindo, A.C. (2022) Generation of continental crust in the northern part of the Borborema Province, northeastern Brazil, from Archaean to Neoproterozoic. Journal of South American Earth Sciences, 68, 68-96.

Souza, Z.S., Vasconcelos, P.M., Nascimento, M.A.L., Silveira, F.V., Paiva, H.S., Dias, L.G.S., Thiede, D., and Carmo, I.O. (2023) Ar-Ar ages of Brazilian intraplate magmatism and regional implications. Lithos, 349, 105221.

Spier, C.A., Vasconcelos, P.M., and Oliveira, S.M.B. (2020) 40Ar/39Ar geochronological constraints on the evolution of lateritic bauxite deposits in the Quadrilátero Ferrífero, Minas Gerais, Brazil. Chemical Geology, 528, 119286.

Toledo, M.C.M. (1999) Geochemical aspects of the formation of aluminum-phosphate minerals in lateritic environments. Applied Geochemistry, 14, 931-945.

Ulrich, A., and Pöthig, R. (2000) Solid-state structures and solution behavior of aluminum phosphate complexes. European Journal of Inorganic Chemistry, 8, 1681-1688.

Vieillard, P., Tardy, Y., and Nahon, D. (1979) Stability fields of clays and aluminum phosphates: Parageneses in lateritic weathering of argillaceous phosphatic sediments. American Mineralogist, 64, 626-634.

Wang, L., Chen, Y., Liu, X., and Zhang, H. (2019) Aluminum mobilization from feldspar by organic acids: Kinetics and mechanisms. Geochimica et Cosmochimica Acta, 248, 255-270.

Yehya, A., and Rice, J.R. (2020) Fault healing promotes earthquake clustering: Evidence from a viscoelastic earthquake simulator. Geophysical Research Letters, 47, e2020GL089056.

5. CONSIDERAÇÕES FINAIS

A presente pesquisa contribuiu significativamente para a caracterização mineralógica e geoquímica de fosfatos de alumínio presentes na Falha de Samambaia, revelando a importância desses minerais no contexto de evolução pós-tectônica e alteração química de zonas de falha. A predominância da variscita, sua variação composicional e a associação com crandallita, millisita/wardita e caulinita indicam um sistema de alteração complexo, onde a circulação de fluidos ácidos meteóricos desempenhou papel decisivo na precipitação dos aluminofosfatos.

As observações texturais e os dados analíticos sugerem que os fosfatos atuaram como agentes de selagem em fraturas abertas, influenciando a permeabilidade da zona de falha. Tal dinâmica tem implicações diretas na evolução mecânica e hidráulica do sistema fraturado, podendo afetar a reativação sísmica e a migração de fluidos. Nesse sentido, os aluminofosfatos representam não apenas produtos de alteração, mas também registradores de processos geológicos tardios.

Contudo, persistem lacunas importantes no entendimento dos processos que governaram a precipitação e estabilidade dessas fases minerais. A ausência de dados isotópicos e termodinâmicos limita a interpretação da origem dos fluidos e das condições físico-químicas precisas de formação dos aluminofosfatos. Além disso, aspectos petrofísicos, como porosidade, permeabilidade e conectividade de fraturas antes e após a mineralização permanecem pouco explorados.

Como sugestões para trabalhos futuros, destacam-se: (i) a aplicação de análises isotópicas (como $\delta^{18}O$) nos aluminofosfatos para identificação da assinatura dos fluidos envolvidos; (ii) testes experimentais em laboratório para definição de estabilidade térmica e química das fases identificadas em diferentes condições de pH e temperatura; (iii) análises petrofísicas de amostras alteradas e não alteradas para avaliação do impacto da mineralização na dinâmica de fluxo; (iv) estudos comparativos com outras zonas de falha sismogênicas com presença de fosfatos.

Tais abordagens integradas permitirão uma compreensão mais robusta do papel dos aluminofosfatos na evolução tectono-hidrotermal de zonas fraturadas, com possíveis aplicações em modelagens de reservatórios, geomecânica de falhas e exploração mineral.

6. REFERÊNCIAS

ALTSCHULER, Z. et al. Bone Valley: The Fluoride and Phosphate Deposits of Florida. Economic Geology, v. 51, p. 1361-1381, 1956.

ALTSCHULER, Z. et al. Phosphate mineralization in the Bone Valley area, Florida. Economic Geology, v. 53, p. 1044-1063, 1958.

ALTSCHULER, Z. S. The weathering of phosphate deposits - geochemical and environmental aspects. In Griffith, E.J., Beeton, A., Spencer, J.M., and Mitchell, D.T., Eds., Environmental Phosphorus Handbook, p. 33-96. John Wiley, New York, 1973.

AUDRA, P.; HÄUSELMANN, P.; BIGOT, J.Y.; NOBÉCOURT, J.C. The role of condensation-corrosion in thermal speleogenesis: Study of a hypogenic sulfidic cave in Brazil. International Journal of Speleology, v. 50, p. 125-145, 2021.

BARROS, L.V.; SILVA, F.C.; SANTOS, R.N. Geochemical controls on aluminum-phosphate mineral stability in weathering profiles. Chemical Geology, v. 635, 121615, 2024.

BERGER, A.; HERWEGH, M. Cockade textures in veins and their bearing on fracture-seal processes. Tectonophysics, v. 751, p. 56-72, 2019.

BEZERRA, F. H. R. et al. Coseismic reactivation of the Samambaia fault, Brazil. Tectonophysics, v. 430, n. 1–4, p. 27–39, fev. 2007.

BEZERRA, F.H.R.; FERREIRA, J.M.; SOUSA, M.O.L. Review of seismicity and Neogene tectonics in northeastern Brazil. Revista Brasileira de Geofísica, v. 25, p. 379-396, 2007.

BEZERRA, F. H. R. et al. Review of active faults in the Borborema Province, Intraplate South America — Integration of seismological and paleoseismological data. Tectonophysics, v. 510, n. 3–4, p. 269–290, out. 2011.

BEZERRA, F.H.R. et al. Neotectonic reactivation of shear zones and implications for faulting style and geometry in the continental margin of NE Brazil. Tectonophysics, v. 614, p. 78-90, 2011.

BEZERRA, F. N. et al. Caracterização mineralógica e isotópica de fosfatos de alumínio em rochas da Falha de Samambaia, RN. Geosul, v. 56, p. 183-202, 2021.

BEZERRA, F.H.R.; LIMA-FILHO, F.P.; AMARAL, R.F.; CALDAS, L.H.O.; COSTA-NETO, L.X. Pliocene-Quaternary fault control of sedimentation and coastal plain morphology in NE Brazil. Journal of South American Earth Sciences, v. 14, p. 61-75, 2021.

CAPDECOMME, P. Les phosphates d'aluminium dans les roches sédimentaires. Comptes Rendus de l'Académie des Sciences, Paris, v. 235, p. 1136-1138, 1952.

CAPDECOMME, P. Les phosphates d'aluminium de Thiès (Sénégal). Comptes Rendus de l'Académie des Sciences, Paris, v. 237, p. 1677-1680, 1953.

CHARPY, L. et al. Phosphate mineralization in the Ivory Coast. Economic Geology, v. 73, p. 1850-1867, 1978.

DANTAS, E. M. et al. Geologia do Maciço São José do Campestre, RN. Revista Brasileira de Geociências, v. 43, p. 89-101, 2013.

DANTAS, E.L. et al. Crustal growth in the 3.4-2.7 Ga São José de Campestre Massif, Borborema Province, NE Brazil. Precambrian Research, v. 227, p. 120-156, 2013.

DEL NERO, M. et al. Surface reactivity of α-Al2O3 and mechanisms of phosphate sorption: In situ ATR-FTIR spectroscopy and ζ potential studies. Journal of Colloid and Interface Science, v. 342, p. 437-444, 2010.

DÍAZ-ACHA, C. Caracterização mineralógica e geoquímica de fosfatos de alumínio da jazida El Hefuf, Egito. M.S. thesis, Universidade de São Paulo, Brazil, 89 p., 2019.

DILL, H.G. Geological and mineralogical characteristics of the Fairfield nodular phosphate deposit, Utah County, Utah. Economic Geology, v. 86, p. 1084-1098, 1991.

DILL, H.G. A comparative study of uranium-thorium-bearing and barren leucogranites from the Bohemian Massif (Austria). Ore Geology Reviews, v. 12, p. 75-93, 1997.

DILL, H. G. The geology of aluminium phosphates and sulfates of the alunite group minerals: a review. Earth-Science Reviews, v. 53, p. 35-93, 2001.

DRUPPEL, K. et al. Petrology and isotope geochemistry of the Mesoproterozoic anorthosite massifs of Kunene Complex, NW Namibia. Precambrian Research, v. 156, p. 1-31, 2007.

EL AGAMI, N.L. Aluminum phosphate minerals from the El Hefuf deposit, Qena, Egypt: Mineralogy and genetic implications. Applied Clay Science, v. 182, 105285, 2019.

EL-AGAMI, N.L.; EL-NAGGAR, A.Y.; MADANI, A.A. Aluminum phosphate minerals from lateritized carbonatites of Qena district, Egypt. Applied Clay Science, v. 28, p. 63-74, 2005.

FILIPPELLI, S. Phosphate rock in the global economy. Economic Geology, v. 103, p. 665-687, 2008.

FLICOTEAUX, E. et al. Les minéraux argileux dans les phosphates. Comptes Rendus de l'Académie des Sciences, Paris, v. 291, p. 167-170, 1980.

FLICOTEAUX, E.; LUCAS, R. Aluminofosfatos em solos lateríticos. Geochimica et Cosmochimica Acta, v. 44, p. 1871-1880, 1980.

FLICOTEAUX, R.; LUCAS, J. Weathering of phosphate minerals. In Nriagu, J.O., and Moore, P.B., Eds., Phosphate Minerals, p. 292-317. Springer-Verlag, Berlin, 1984.

FRANCISCO, P.C.M.; LOURO, V.H.A.; SILVA, M.R.R. Synthesis and characterization of crandallite at high temperature and pressure conditions. American Mineralogist, v. 92, p. 1521-1529, 2007.

FROST, R.L. et al. Infrared and Raman spectroscopic characterization of the phosphate mineral crandallite - CaAl3(PO4)2(OH)5·H2O from Brazil. Spectrochimica Acta Part A, v. 78, p. 1260-1264, 2011.

GABOREAU, S. et al. Aluminum phosphate-sulfate minerals associated with Proterozoic unconformities in the Athabasca Basin (Saskatchewan, Canada). Chemical Geology, v. 230, p. 41-54, 2005.

GILKES, R.J.; PALMER, B. Synthesis, thermal stability and infrared spectroscopy of crandallite. Mineralogical Magazine, v. 47, p. 465-468, 1983.

GOLDBERY, R.; LOUGHNAN, F.C. Dawsonite and crandallite from the Liddell Coal Measures, New South Wales, Australia. American Mineralogist, v. 62, p. 1237-1242, 1977.

GOLDSHMID, J.; RUBIN, H. Aluminum-phosphate interactions in saturated kaolinitic soils. Soil Science Society of America Journal, v. 52, p. 1089-1094, 1988.

GOODALL, W. R.; SCALES, P. J.; RYAN, C. G. Applications of PIXE and diagnostic leaching in the characterisation of complex gold ores. Minerals Engineering, v. 18, n. 10, p. 1010-1019, 2005.

GOTTLIEB, P. et al. Using quantitative electron microscopy for process mineralogy applications. Jom, v. 52, n. 4, p. 24-25, 2000.

HENDERSON, T.R. et al. Seismicity, volcanism and neotectonics of northeastern Brazil. In Sauck, W.A., Ed., Neotectonics of South America, 19, p. 201-214. Penrose Conference Series, Geological Society of America, 1994.

HSU, S.C.; SIKORA, E. Synthesis and characterization of variscite and metavariscite. American Mineralogist, v. 78, p. 1358-1361, 1993.

LARSEN, E. S. The mineralogy and paragenesis of the variscite nodules from near Fairfield, Utah. American Mineralogist, v. 27, p. 281-300, 1942.

LI, X. et al. CO2-induced aluminum mobilization from feldspar: Implications for carbon sequestration. Geochimica et Cosmochimica Acta, v. 318, p. 112-128, 2022.

LUCAS, R. et al. Sur l'origine des phosphates d'aluminium dans les sols et roches. Geochimica et Cosmochimica Acta, v. 44, p. 106-114, 1980.

LUCAS, R.; PREVOT, L. Les phosphates d'aluminium en Afrique de l'Ouest. Geochimica et Cosmochimica Acta, v. 45, p. 2083-2095, 1981.

MATULA, J.; WOJTKOWSKA, M. Phosphate speciation in aqueous solutions: A comprehensive thermodynamic analysis. Chemical Geology, v. 642, 121789, 2025.

NRIAGU, J. O. Phosphate-clay mineral relations in soils and sediments. Canadian Journal of Earth Sciences, v. 13, p. 717-736, 1976.

NRIAGU, J.O.; MOORE, P.B. Phosphate Minerals, 442 p. Springer-Verlag, Berlin, 1984.

ONAC, B.P.; EFFENBERGER, H.; BREBAN, R.C. Brushite and taranakite from Cioclovina Cave (Romania): Occurrence and paragenetic sequence. Mineralogical Magazine, v. 68, p. 395-403, 2004.

REID, A.M.; MACINTYRE, R.M. Carbonate and organic matter in Olduvai Bed I: Possible source for turquoise at the FLK Zinj site. Journal of Human Evolution, v. 38, p. 609-620, 2000.

RIEDEL, M. E. Phosphate deposits in Congo. Economic Geology, v. 54, p. 881-900, 1959.

RONCAL-HERRERO, T. et al. Precipitation of iron and aluminum phosphates directly from aqueous solution as a function of temperature from 50 to 200°C. Crystal Growth & Design, v. 9, p. 5197-5205, 2009.

ROSSETTI, D.F.; BEZERRA, F.H.R.; DOMINGUEZ, J.M.L. Late Oligocene-Miocene transgressions along the equatorial and eastern margins of Brazil. Earth-Science Reviews, v. 123, p. 87-112, 2013.

ROSSETO, R.; SANTOS, A.C.; GALEMBECK, F. Hydrous non-crystalline phosphates: structure, function and a new white pigment. *Journal of the Brazilian Chemical Society*, v. 17, n. 8, p. 1465-1472, 2006. DOI:10.1590/S0103-50532006000800002.

RUSS, M.; ANDREW, F. B. Phosphate deposits in the Nigerian region. Journal of African Earth Sciences, v. 1, p. 85-100, 1924.

RUSSELL, F. L.; TRUEEMAN, G. W. The mineralogy of phosphate deposits in Australia. Economic Geology, v. 66, p. 1180-1200, 1971.

SAISHU, H.; OKAMOTO, A.; TSUCHIYA, N. The significance of silica precipitation on the formation and evolution of slow slip events. Nature Geoscience, v. 10, p. 447-451, 2017.

SCHWAB, R.G.; HEROLD, H.; GÖTZ, C. Compounds of the crandallite type: Synthesis and properties of pure goyazite, gorceixite and plumbogummite. Neues Jahrbuch für Mineralogie Monatshefte, v. 3, p. 113-126, 1989.

SCHWAB, R.G. et al. Crandallite and goyazite from Catalão I carbonatite complex, Goiás, Brazil, and their industrial applications. Applied Clay Science, v. 5, p. 33-43, 1990a.

SCHWAB, R.G. et al. Plumbogummite and corkite from Catalão I carbonatite complex, Goiás, Brazil, and their industrial applications. Neues Jahrbuch für Mineralogie Abhandlungen, v. 161, p. 265-276, 1990b.

SHELTON, K.L. Variscite occurrences in Arkansas. Arkansas Geological Commission Bulletin, v. 19, 34 p., 1964.

SLANSKY, J. et al. Phosphate mineralization in Senegal. Economic Geology, v. 59, p. 1210-1234, 1964.

SMERAGLIA, L. et al. Development of an intracontinental transcurrent fault system: The Mattinata Fault Zone, Apulia, southern Italy. Journal of Structural Geology, v. 116, p. 179-195, 2018.

SOUZA, Z. S. et al. Generation of continental crust in the northern part of the Borborema Province, northeastern Brazil, from Archaean to Neoproterozoic. Journal of South American Earth Sciences, v. 68, p. 68-96, 2022.

SOUZA, Z. S. et al. Zircon U-Pb dating and petrogenesis of the São José do Campestre Granite Complex, NE Brazil: an example of neoarchean mantle-derived post-collisional magmatism. Brazilian Journal of Geology, v. 53, n. 2, p. e20220079, 2023.

SOUZA, Z.S. et al. Ar-Ar ages of Brazilian intraplate magmatism and regional implications. Lithos, v. 349, 105221, 2023.

SPIER, C.A.; VASCONCELOS, P.M.; OLIVEIRA, S.M.B. 40Ar/39Ar geochronological constraints on the evolution of lateritic bauxite deposits in the Quadrilátero Ferrífero, Minas Gerais, Brazil. Chemical Geology, v. 528, 119286, 2020.

SYKES, L. R. Intraplate seismicity, reactivation of preexisting zones of weakness, alkaline magmatism, and other tectonism postdating continental fragmentation. Reviews of Geophysics, v. 16, n. 4, p. 621–688, nov. 1978.

TAKEYA, M. et al. The 1986–1988 intraplate earthquake sequence near João Câmara, northeast Brazil—evolution of seismicity. Tectonophysics, v. 167, n. 2–4, p. 117–131, out. 1989.

TOLEDO, M.C.M. Geochemical aspects of the formation of aluminum-phosphate minerals in lateritic environments. Applied Geochemistry, v. 14, p. 931-945, 1999.

ULRICH, A.; PÖTHIG, R. Solid-state structures and solution behavior of aluminum phosphate complexes. European Journal of Inorganic Chemistry, v. 8, p. 1681-1688, 2000.

VIEILLARD, P.; TARDY, Y.; NAHON, D. Stability fields of clays and aluminum phosphates: Parageneses in lateritic weathering of argillaceous phosphatic sediments. American Mineralogist, v. 64, p. 626-634, 1979.

WANG, L. et al. Aluminum mobilization from feldspar by organic acids: Kinetics and mechanisms. Geochimica et Cosmochimica Acta, v. 248, p. 255-270, 2019.

YEHYA, A.; RICE, J.R. Fault healing promotes earthquake clustering: Evidence from a viscoelastic earthquake simulator. Geophysical Research Letters, v. 47, e2020GL089056, 2020.

ZANIN, A. Phosphate mineralization in Siberia. Mineralogical Journal, v. 7, p. 175-189, 1968.

Anexo A - Supplementary Material 1

samples	anion prop basis 4O		P	V	Si	Al	Cr	Ti	Fe3	Mg
W5-D1A	W5-D1A_campo4-1	variscite	0.979	0.000	0.002	0.761	0.000	0.007	0.274	0.000
W5-D1A	W5-D1A_campo4-2	variscite	0.975	0.000	0.001	0.659	0.000	0.002	0.383	0.001
W5-D1A	W5-D1A_campo4-3	variscite	0.980	0.000	0.000	0.876	0.000	0.000	0.166	0.001
W5-D1A	W5-D1A_campo4-4	variscite	0.992	0.000	0.001	0.815	0.000	0.002	0.211	0.001
W5-D1A	W5-D1A_campo4-5	variscite	0.987	0.000	0.001	0.846	0.000	0.010	0.171	0.001
W5-D1A	W5-D1A_campo4-6	variscite	0.875	0.001	0.024	0.500	0.001	0.104	0.542	0.000
W5-D1A	W5-D1A_campo4-7	variscite	0.956	0.000	0.002	0.721	0.000	0.034	0.310	0.001
W5-D1A	W5-D1A_campo4-8	variscite	0.991	0.000	0.002	0.956	0.000	0.001	0.068	0.002
W5-D1A	W5-D1A_campo4-9	variscite	0.991	0.001	0.004	0.896	0.000	0.003	0.119	0.001
W5-D1A	W5-D1A_campo4-10	variscite	0.979	0.000	0.001	0.724	0.000	0.002	0.317	0.000
W5-D1A	W5-D1A_campo4-11	variscite	0.999	0.000	0.001	0.810	0.000	0.000	0.204	0.000
W5-D1A	W5-D1A_campo4-12	variscite	0.987	0.000	0.001	0.801	0.000	0.003	0.223	0.001
W5-D1A	W5-D1A_campo4-13	variscite	0.928	0.000	0.002	0.591	0.001	0.036	0.484	0.000
W5-D1A	W5-D1A_campo4-14	variscite	0.983	0.000	0.001	0.844	0.000	0.008	0.183	0.001
W5-D1A	W5-D1A_campo4-15	variscite	0.963	0.000	0.003	0.968	0.000	0.003	0.099	0.000
W5-D1A	W5-D1A_campo4-16	variscite	0.974	0.001	0.007	0.914	0.000	0.005	0.121	0.000
W5-D1A	W5-D1A_campo4-17	variscite	0.985	0.000	0.000	0.782	0.000	0.003	0.252	0.001
W5-D1A	W5-D1A_campo3-2	variscite	0.941	0.001	0.004	0.930	0.001	0.005	0.162	0.000
W5-D1A	W5-D1A_campo3-3	variscite	0.983	0.000	0.002	0.979	0.000	0.000	0.060	0.001
W5-D1A	W5-D1A_campo3-4	variscite	0.992	0.000	0.000	0.858	0.000	0.002	0.163	0.000
W5-D1A	W5-D1A_campo3-6	variscite	0.971	0.000	0.000	1.035	0.000	0.000	0.026	0.001
W5-D1A	W5-D1A_campo3-7	variscite	0.982	0.000	0.008	0.977	0.000	0.002	0.049	0.001
W5-D1A	W5-D1A_campo3-9	variscite	0.982	0.000	0.007	1.014	0.000	0.000	0.025	0.000
W5-D1A	W5-D1A_campo3-10	variscite	1.000	0.000	0.002	1.001	0.000	0.000	0.011	0.000
W5-D1A	W5-D1A_campo2-1	variscite	0.943	0.001	0.071	0.896	0.000	0.013	0.100	0.001
W5-D1A	W5-D1A_campo2-3	variscite	0.969	0.000	0.015	0.961	0.000	0.011	0.069	0.001
W5-D1A	W5-D1A_campo2-4	variscite	0.997	0.000	0.001	0.927	0.000	0.000	0.089	0.000
W5-D1A	W5-D1A_campo2-5	variscite	0.972	0.000	0.031	0.930	0.001	0.014	0.063	0.001
W5-F1A	W5-F1A_campo4-1	variscite	0.964	0.000	0.002	0.897	0.000	0.003	0.167	0.001
W5-F1A	W5-F1A_campo4-2	variscite	0.972	0.000	0.001	0.883	0.000	0.005	0.168	0.001
W5-F1A	W5-F1A_campo4-3	variscite	0.964	0.000	0.001	1.033	0.000	0.000	0.040	0.002
W5-F1A	W5-F1A_campo4-4	variscite	0.968	0.000	0.004	0.965	0.000	0.006	0.089	0.002
W5-F1A	W5-F1A_campo4-5	variscite	0.956	0.001	0.002	1.051	0.000	0.001	0.026	0.001
W5-F1A	W5-F1A_campo4-6	variscite	0.955	0.000	0.011	0.981	0.000	0.006	0.088	0.001

W5-F1A	W5-F1A_campo4-7	variscite	0.979	0.000	0.005	0.934	0.000	0.003	0.108	0.003
W5-F1A	W5-F1A_campo4-8	variscite	0.972	0.000	0.008	0.952	0.000	0.003	0.089	0.002
W5-F1A	W5-F1A_campo4-9	variscite	0.948	0.000	0.000	1.058	0.000	0.001	0.043	0.000
W5-F1A	W5-F1A_campo4-10	variscite	0.990	0.001	0.002	0.929	0.000	0.001	0.093	0.000
W5-F1A	W5-F1A_campo4-11	variscite	0.981	0.001	0.002	0.977	0.000	0.000	0.063	0.001
W5-F1A	W5-F1A_campo4-12	variscite	0.991	0.000	0.002	0.943	0.000	0.000	0.084	0.000
W5-F1A	W5-F1A_campo1-1	variscite	0.977	0.001	0.005	0.761	0.000	0.007	0.270	0.000
W5-F1A	W5-F1A_campo1-2	variscite	0.974	0.000	0.012	0.848	0.000	0.009	0.177	0.000
W5-F1A	W5-F1A_campo1-3	variscite	0.981	0.001	0.003	0.844	0.000	0.006	0.188	0.000
W5-F1A	W5-F1A_campo1-5	variscite	0.871	0.001	0.195	0.681	0.000	0.017	0.259	0.000
W5-F1A	W5-F1A_campo1-6	variscite	0.980	0.000	0.029	0.828	0.000	0.003	0.172	0.001
W5-F1A	W5-F1A_campo1-7	variscite	0.922	0.000	0.071	0.781	0.000	0.002	0.261	0.000
W5-F1A	W5-F1A_campo1-8	variscite	0.972	0.000	0.005	0.762	0.000	0.003	0.291	0.000
W5-F1A	W5-F1A_campo1-9	variscite	0.923	0.000	0.085	0.729	0.000	0.005	0.288	0.001
W5-F1A	W5-F1A_campo2-7	variscite	0.941	0.002	0.041	0.719	0.000	0.003	0.325	0.000
W5-F1A	W5-F1A_campo2-8	variscite	0.963	0.000	0.013	0.844	0.001	0.008	0.200	0.000
W5-F1A	W5-F1A_campo3-3	variscite	0.964	0.000	0.005	0.853	0.000	0.009	0.198	0.001
W5-F1A	W5-F1A_campo3-4	variscite	0.958	0.000	0.003	0.876	0.000	0.009	0.184	0.001
W5-F1A	W5-F1A_campo3-5	variscite	0.972	0.000	0.003	0.846	0.000	0.001	0.205	0.000
W5-F1A	W5-F1A_campo3-7	variscite	0.952	0.000	0.005	0.955	0.000	0.000	0.131	0.000
W5-F1A	W5-F1A_campo3-8	variscite	0.990	0.000	0.004	1.003	0.000	0.000	0.024	0.000
W5-F1A	W5-F1A_campo3-9	variscite	0.952	0.000	0.006	0.875	0.000	0.002	0.199	0.001
W5-F1A	W5-F1A_campo3-10	variscite	0.954	0.000	0.004	0.846	0.001	0.003	0.236	0.000
W5-F1A	W5-F1A_campo3-11	variscite	0.969	0.000	0.009	0.848	0.001	0.006	0.190	0.000
W5-F1A	W5-F1A_campo3-12	variscite	0.928	0.000	0.034	0.844	0.000	0.004	0.229	0.000
W5-F1A	W5-F1A_campo3-13	variscite	0.953	0.000	0.012	0.862	0.000	0.005	0.202	0.000
W5-F1A	W5-F1A_campo3-14	variscite	0.950	0.001	0.000	0.854	0.000	0.000	0.242	0.000
W6-B7A	W6-B7A_campo3-6	variscite	0.843	0.000	0.153	0.958	0.000	0.001	0.111	0.002
W6-B7A	W6-B7A_campo3-8	variscite	0.953	0.001	0.012	0.833	0.000	0.000	0.236	0.000
W6-B7A	W6-B7A_campo3-11	variscite	0.918	0.000	0.065	0.944	0.000	0.002	0.113	0.002
W6-B7A	W6-B7A_campo1-13	variscite	0.580	0.000	0.246	0.960	0.001	0.002	0.334	0.003
W6-B7A	W6-B7A_campo1-14	variscite	0.976	0.000	0.002	0.795	0.000	0.000	0.261	0.002
W6-B7A	W6-B7A_campo1-15	variscite	0.976	0.000	0.001	1.032	0.000	0.000	0.025	0.001
W6-B7A	W6-B7A_campo1-17	variscite	0.969	0.000	0.002	1.003	0.000	0.000	0.060	0.000
W6-B7A	W6-B7A_campo1-18	variscite	0.946	0.000	0.001	0.848	0.000	0.000	0.253	0.000

W6-B7A	W6-B7A_campo1-19	variscite	0.960	0.000	0.002	1.043	0.000	0.000	0.036	0.000
W6-B7A	W6-B7A_campo1-21	variscite	0.877	0.000	0.146	0.975	0.000	0.000	0.046	0.002
W6-B7A	W6-B7A_campo1-22	variscite	0.970	0.000	0.002	1.006	0.000	0.000	0.063	0.000
W6-B7A	W6-B7A_campo1-23	variscite	0.956	0.000	0.001	0.925	0.000	0.000	0.163	0.000
W6-B7A	W6-B7A_campo1-24	variscite	0.973	0.000	0.001	1.040	0.000	0.001	0.016	0.001
W6-B7A	W6-B7A_campo2-25	variscite	0.955	0.001	0.003	1.056	0.000	0.000	0.032	0.001
W6-B7A	W6-B7A_campo2-28	variscite	0.952	0.000	0.000	1.056	0.000	0.000	0.038	0.001
W6-B7A	W6-B7A_campo2-29	variscite	0.937	0.001	0.000	1.088	0.000	0.000	0.034	0.000
W6-B7A	W6-B7A_campo2-31	variscite	0.968	0.000	0.001	0.993	0.000	0.000	0.067	0.001
W6-B7A	W6-B7A_campo2-32	variscite	0.930	0.000	0.025	1.011	0.000	0.001	0.084	0.001
W6-B7A	W6-B7A_campo2-33	variscite	0.870	0.001	0.103	0.989	0.000	0.000	0.100	0.001
W6-B7A	W6-B7A_campo4-43	variscite	0.949	0.001	0.012	0.910	0.001	0.000	0.173	0.001
W6-B7B	W6-B7B_campo1_01-1	variscite	0.907	0.000	0.056	0.981	0.000	0.000	0.102	0.003
W6-B7B	W6-B7B_campo1_01-7	variscite	0.987	0.000	0.001	1.033	0.000	0.000	0.004	0.001
W6-B7B	W6-B7B_campo1_01-9	variscite	0.985	0.000	0.005	0.999	0.000	0.000	0.026	0.001
W6-B7B	W6-B7B_campo1_01-12	variscite	0.978	0.001	0.006	1.008	0.000	0.000	0.037	0.000
W6-B7B	W6-B7B_campo1_01-14	variscite	0.959	0.000	0.009	1.035	0.000	0.000	0.036	0.000
W6-B7B	W6-B7B_campo1_01-15	variscite	0.778	0.000	0.021	1.207	0.000	0.001	0.059	0.004
W6-B7B	W6-B7B_campo1_01-16	variscite	0.995	0.001	0.003	1.008	0.000	0.000	0.010	0.000
W6-B7B	W6-B7B_campo1_01-17	variscite	0.981	0.000	0.001	1.035	0.000	0.000	0.010	0.001
W6-B7B	W6-B7B_campo1_01-19	variscite	0.986	0.001	0.002	1.016	0.000	0.000	0.018	0.001
W6-B7B	W6-B7B_campo2_01-1	variscite	0.971	0.000	0.004	1.035	0.000	0.001	0.016	0.002
W6-B7B	W6-B7B_campo2_01-6	variscite	0.856	0.000	0.191	0.968	0.000	0.000	0.025	0.001
W6-B7B	W6-B7B_campo2_01-9	variscite	0.827	0.000	0.138	1.040	0.000	0.000	0.038	0.005
W6-B7B	W6-B7B_campo2_01-10	variscite	0.985	0.001	0.003	0.950	0.000	0.000	0.087	0.002
W6-B7B	W6-B7B_campo2_01-11	variscite	0.766	0.000	0.259	1.025	0.000	0.001	0.029	0.001
W6-B7B	W6-B7B_campo3_01-8	variscite	0.976	0.000	0.022	0.982	0.000	0.000	0.040	0.000
W6-B7B	W6-B7B_campo3_01-9	variscite	0.925	0.001	0.005	0.991	0.000	0.000	0.109	0.001
W6-B7B	W6-B7B_campo3_01-10	variscite	0.984	0.000	0.011	0.979	0.000	0.000	0.047	0.001
W6-C6	W6-C6_campo1-1	variscite	0.974	0.001	0.000	0.874	0.001	0.008	0.149	0.001
W6-C6	W6-C6_campo1-2	variscite	0.985	0.000	0.000	0.920	0.000	0.001	0.118	0.000
W6-C6	W6-C6_campo1-9	variscite	1.002	0.000	0.000	0.927	0.000	0.000	0.085	0.001
W6-C6	W6-C6_campo1-10	variscite	0.984	0.000	0.001	0.914	0.000	0.002	0.120	0.000
W6-C6	W6-C6_campo1-11	variscite	0.999	0.000	0.001	0.925	0.000	0.000	0.089	0.001
W6-C6	W6-C6_campo1-15	variscite	0.988	0.000	0.000	0.946	0.000	0.000	0.092	0.000

W6-C6	W6-C6_campo1-17	variscite	0.958	0.000	0.004	1.006	0.000	0.002	0.041	0.001
W6-C6	W6-C6_campo1-18	variscite	1.001	0.000	0.001	0.946	0.000	0.000	0.061	0.000
W6-C6	W6-C6_campo2-9	variscite	0.973	0.000	0.001	1.009	0.000	0.000	0.047	0.000
W6-C6	W6-C6_campo2-10	variscite	0.994	0.000	0.000	0.974	0.000	0.000	0.049	0.000
W6-C6	W6-C6_campo3-1	variscite	1.001	0.000	0.002	0.979	0.000	0.000	0.030	0.000
W6-C6	W6-C6_campo3-2	variscite	0.973	0.001	0.000	1.024	0.000	0.000	0.030	0.000
W6-C6	W6-C6_campo3-11	variscite	0.972	0.001	0.002	0.879	0.000	0.001	0.177	0.002
W7-A5	W7-A5_campo1-3	variscite	0.957	0.001	0.007	1.061	0.000	0.000	0.019	0.000
W7-A5	W7-A5_campo1-4	variscite	0.940	0.001	0.003	1.099	0.000	0.000	0.015	0.000
W7-A5	W7-A5_campo1-6	variscite	0.956	0.000	0.002	0.857	0.000	0.000	0.222	0.000
W7-A5	W7-A5_campo1-8	variscite	0.924	0.000	0.054	0.885	0.001	0.000	0.177	0.001
W7-A5	W7-A5_campo1-14	variscite	0.926	0.000	0.035	1.011	0.000	0.000	0.077	0.001
W7-A5	W7-A5_campo1-15	variscite	0.812	0.001	0.152	1.079	0.000	0.000	0.041	0.002
W7-A5	W7-A5_campo2_02-1	variscite	0.980	0.000	0.017	0.981	0.000	0.000	0.042	0.000
W7-A5	W7-A5_campo2_02-7	variscite	0.960	0.000	0.005	1.030	0.000	0.001	0.041	0.001
W7-A5	W7-A5_campo2_04-19	variscite	0.926	0.000	0.031	1.040	0.000	0.000	0.052	0.001
W7-A5	W7-A5_campo2_04-21	variscite	0.912	0.000	0.048	1.025	0.000	0.001	0.068	0.001
W7-A5	W7-A5_campo2_04-23	variscite	0.934	0.000	0.010	1.068	0.001	0.000	0.043	0.001
W7-A5	W7-A5_campo3_01-3	variscite	0.815	0.001	0.196	0.955	0.001	0.000	0.095	0.002
W7-A5	W7-A5_campo3_01-4	variscite	0.738	0.000	0.266	0.934	0.000	0.003	0.154	0.001
W7-A5	W7-A5_campo3_01-11	variscite	0.765	0.000	0.224	0.957	0.000	0.014	0.124	0.004
W7-A5	W7-A5_campo3_01-13	variscite	0.914	0.001	0.024	0.891	0.000	0.000	0.232	0.002
W7-A5	W7-A5_campo3_01-14	variscite	0.946	0.001	0.004	0.903	0.001	0.000	0.192	0.001
W7-C1A	W7-C1A_campo1-5	variscite	0.912	0.000	0.096	0.947	0.000	0.000	0.075	0.002
W7-C1A	W7-C1A_campo1-16	variscite	0.873	0.000	0.127	0.970	0.000	0.001	0.078	0.003
W7-C1A	W7-C1A_campo2-11	variscite	0.717	0.000	0.124	1.182	0.000	0.000	0.074	0.006
W7-C1A	W7-C1A_campo3-8	variscite	0.956	0.000	0.022	1.002	0.000	0.001	0.047	0.001
W7-C2B	W7-C2B_campo2-4	variscite	0.855	0.000	0.115	1.026	0.000	0.001	0.063	0.001
W7-C2B	W7-C2B_campo2-8	variscite	0.882	0.000	0.103	0.992	0.000	0.002	0.056	0.002
W7-C2B	W7-C2B_campo2-13	variscite	0.864	0.000	0.141	1.000	0.000	0.000	0.044	0.002
W7-C2B	W7-C2B_campo2-16	variscite	0.990	0.000	0.002	0.960	0.000	0.000	0.068	0.002
W7-C2B	W7-C2B_campo2-18	variscite	0.970	0.000	0.000	1.026	0.000	0.000	0.036	0.001
W7-C2B	W7-C2B_campo3-5	variscite	0.944	0.001	0.014	1.041	0.000	0.000	0.045	0.000
W7-C2B	W7-C2B_campo3-6	variscite	0.949	0.001	0.001	1.012	0.000	0.001	0.086	0.000
W7-C2B	W7-C2B_campo3-7	variscite	0.961	0.000	0.005	0.998	0.000	0.001	0.073	0.000

W7-C2B	W7-C2B_campo1-1	variscite	0.947	0.000	0.001	1.037	0.000	0.000	0.063	0.001
W7-C2B	W7-C2B_campo1-4	variscite	0.957	0.000	0.002	1.024	0.000	0.000	0.057	0.000
W7-C2B	W7-C2B_campo1-6	variscite	0.960	0.000	0.003	1.021	0.000	0.000	0.055	0.002
W7-C2B	W7-C2B_campo1-9	variscite	0.946	0.001	0.003	1.014	0.000	0.000	0.085	0.001
W7-C2B	W7-C2B_campo1-11	variscite	0.921	0.000	0.050	1.013	0.000	0.000	0.062	0.001
W7-C2B	W7-C2B_campo1-14	variscite	0.947	0.000	0.017	1.032	0.000	0.001	0.047	0.001
W7-C2B	W7-C2B_campo1-17	variscite	0.863	0.000	0.096	1.017	0.000	0.000	0.073	0.003
W7-C2B	W7-C2B_campo1-19	variscite	0.828	0.000	0.079	1.070	0.000	0.002	0.066	0.002
W7-C2B	W7-C2B_campo1-21	variscite	0.929	0.000	0.049	0.980	0.000	0.000	0.086	0.002
W7-C2B	W7-C2B_campo1-22	variscite	0.959	0.000	0.001	1.020	0.000	0.000	0.063	0.001
W7-A5	W7-A5_campo2_02-3	Ca-rich	0.585	0.000	0.212	1.159	0.000	0.000	0.038	0.004
W6-B7A	W6-B7A_campo2-34	Ca-rich	0.405	0.002	0.152	0.750	0.002	0.004	0.898	0.005
W7-C1A	W7-C1A_campo2-1	Ca-rich	0.738	0.001	0.073	1.135	0.000	0.001	0.097	0.006
W7-C1A	W7-C1A_campo2-10	Ca-rich	0.708	0.000	0.243	1.010	0.000	0.001	0.066	0.016
W7-C1A	W7-C1A_campo2-13	Ca-rich	0.705	0.000	0.069	1.121	0.000	0.000	0.123	0.003
W7-C1A	W7-C1A_campo2-14	Ca-rich	0.649	0.000	0.204	1.067	0.000	0.000	0.106	0.009
W6-C6	W6-C6_campo1-3	Ca-rich	0.788	0.000	0.003	1.009	0.000	0.007	0.175	0.001
W6-C6	W6-C6_campo1-4	Ca-rich	0.788	0.000	0.002	1.081	0.001	0.001	0.103	0.001
W6-C6	W6-C6_campo1-5	Ca-rich	0.789	0.000	0.003	1.030	0.001	0.005	0.141	0.001
W6-C6	W6-C6_campo1-6	Ca-rich	0.784	0.000	0.002	1.057	0.000	0.005	0.124	0.002
W6-C6	W6-C6_campo1-7	Ca-rich	0.795	0.001	0.005	0.973	0.001	0.006	0.173	0.002
W6-C6	W6-C6_campo1-8	Ca-rich	0.783	0.000	0.002	0.999	0.001	0.010	0.153	0.001
W6-C6	W6-C6_campo1-12	Ca-rich	0.774	0.001	0.002	1.032	0.001	0.008	0.158	0.003
W6-C6	W6-C6_campo1-13	Ca-rich	0.780	0.000	0.003	1.033	0.000	0.010	0.162	0.003
W6-C6	W6-C6_campo1-14	Ca-rich	0.733	0.001	0.000	1.143	0.001	0.000	0.055	0.000
W6-C6	W6-C6_campo1-16	Ca-rich	0.733	0.000	0.000	1.145	0.001	0.000	0.053	0.001
W6-C6	W6-C6_campo1-19	Ca-rich	0.775	0.000	0.002	1.067	0.000	0.003	0.147	0.002
W6-C6	W6-C6_campo2-1	Ca-rich	0.764	0.001	0.004	1.006	0.001	0.005	0.202	0.002
W6-C6	W6-C6_campo2-2	Ca-rich	0.765	0.000	0.023	1.003	0.000	0.004	0.192	0.002
W6-C6	W6-C6_campo2-3	Ca-rich	0.763	0.001	0.002	1.039	0.000	0.008	0.178	0.001
W6-C6	W6-C6_campo2-4	Ca-rich	0.768	0.000	0.002	1.061	0.000	0.012	0.148	0.003
W6-C6	W6-C6_campo2-5	Ca-rich	0.767	0.000	0.003	0.998	0.000	0.008	0.211	0.003
W6-C6	W6-C6_campo2-6	Ca-rich	0.747	0.000	0.000	1.091	0.000	0.000	0.120	0.001
W6-C6	W6-C6_campo2-7	Ca-rich	0.763	0.000	0.001	0.992	0.000	0.006	0.224	0.001
W6-C6	W6-C6_campo2-11	Ca-rich	0.763	0.000	0.000	1.069	0.000	0.003	0.147	0.001

W6-C6	W6-C6_campo2-12	Ca-rich	0.750	0.001	0.001	1.046	0.000	0.003	0.180	0.002
W6-C6	W6-C6_campo3-3	Ca-rich	0.781	0.001	0.007	0.909	0.002	0.006	0.284	0.001
W6-C6	W6-C6_campo3-4	Ca-rich	0.765	0.000	0.003	0.901	0.002	0.011	0.310	0.002
W6-C6	W6-C6_campo3-6	Ca-rich	0.664	0.001	0.003	0.760	0.004	0.007	0.631	0.002
W6-C6	W6-C6_campo3-7	Ca-rich	0.601	0.002	0.006	0.645	0.008	0.015	0.857	0.001
W6-C6	W6-C6_campo3-8	Ca-rich	0.739	0.001	0.001	0.881	0.004	0.005	0.393	0.001
W6-C6	W6-C6_campo3-9	Ca-rich	0.757	0.000	0.000	0.934	0.003	0.015	0.294	0.001
W6-C6	W6-C6_campo3-10	Ca-rich	0.767	0.000	0.003	0.923	0.002	0.006	0.290	0.000
W6-C6	W6-C6_campo3-12	Ca-rich	0.764	0.000	0.003	1.048	0.000	0.005	0.156	0.003
variscite E	variscite EM	variscite EM	1.000	0.000	0.000	1.000	0.000	0.000	0.000	0.000
crandallite	crandallite EM	crandallite EM	1.524	0.000	0.000	2.286	0.000	0.000	0.000	0.000
strengite E	strengite EM	strengite EM	1.000	0.000	0.000	0.000	0.000	0.000	1.000	0.000
millisite EM	millisite EM	millisite EM	4.682	0.000	0.000	7.025	0.000	0.000	0.000	0.000
wardite EM	wardite EM	wardite EM	1.600	0.000	0.000	2.400	0.000	0.000	0.000	0.000
wavellite E	wavellite EM	wavellite EM	1.684	0.000	0.000	2.526	0.000	0.000	0.000	0.000

Mn	Ca	Ba	Sr	Na	K	F	Cl	Al/P	Fe/P	Ca/P	Al/Fe	Na+K/P
0.000	0.001	0.000	0.001	0.000	0.002	0.042	0.000	0.777	0.279	0.001	2.781	0.002
0.001	0.001	0.000	0.000	0.000	0.011	0.031	0.000	0.675	0.393	0.001	1.720	0.011
0.001	0.000	0.000	0.000	0.000	0.002	0.037	0.000	0.894	0.170	0.000	5.264	0.002
0.002	0.001	0.000	0.000	0.000	0.003	0.055	0.001	0.822	0.212	0.001	3.871	0.003
0.000	0.002	0.000	0.001	0.000	0.002	0.040	0.001	0.857	0.173	0.002	4.956	0.003
0.000	0.017	0.000	0.009	0.000	0.004	0.051	0.026	0.571	0.619	0.019	0.922	0.004
0.001	0.004	0.000	0.002	0.000	0.006	0.038	0.002	0.755	0.324	0.004	2.328	0.006
0.001	0.000	0.000	0.000	0.000	0.001	0.044	0.001	0.965	0.068	0.000	14.092	0.001
0.000	0.002	0.000	0.000	0.000	0.002	0.036	0.000	0.904	0.120	0.002	7.537	0.002
0.001	0.001	0.000	0.000	0.000	0.001	0.036	0.000	0.739	0.324	0.001	2.280	0.001
0.001	0.001	0.000	0.000	0.000	0.002	0.045	0.000	0.810	0.204	0.001	3.977	0.002
0.000	0.002	0.000	0.000	0.000	0.002	0.031	0.000	0.812	0.226	0.002	3.595	0.002
0.000	0.008	0.000	0.004	0.000	0.005	0.042	0.005	0.637	0.522	0.008	1.220	0.006
0.000	0.003	0.000	0.001	0.000	0.002	0.038	0.000	0.859	0.186	0.003	4.618	0.002
0.002	0.001	0.000	0.000	0.000	0.002	0.047	0.000	1.005	0.102	0.001	9.823	0.002
0.001	0.002	0.000	0.002	0.000	0.001	0.034	0.000	0.939	0.125	0.002	7.535	0.001
0.000	0.001	0.000	0.000	0.000	0.001	0.040	0.001	0.794	0.255	0.001	3.107	0.001
0.001	0.004	0.000	0.001	0.000	0.005	0.038	0.002	0.987	0.172	0.004	5.743	0.006
0.001	0.001	0.000	0.000	0.000	0.002	0.047	0.001	0.996	0.061	0.001	16.409	0.002
0.001	0.003	0.000	0.000	0.000	0.003	0.040	0.002	0.865	0.164	0.003	5.276	0.003
0.001	0.001	0.000	0.000	0.000	0.004	0.044	0.001	1.066	0.026	0.001	40.297	0.004
0.000	0.001	0.000	0.000	0.000	0.002	0.032	0.000	0.995	0.050	0.001	19.962	0.002
0.000	0.001	0.000	0.000	0.000	0.003	0.061	0.000	1.032	0.026	0.001	40.382	0.003
0.000	0.002	0.000	0.000	0.000	0.006	0.052	0.000	1.001	0.011	0.002	94.137	0.006
0.001	0.003	0.000	0.000	0.000	0.006	0.057	0.002	0.950	0.106	0.003	8.972	0.007
0.002	0.003	0.000	0.001	0.000	0.004	0.054	0.001	0.992	0.071	0.003	14.002	0.004
0.000	0.000	0.000	0.000	0.000	0.001	0.042	0.001	0.930	0.090	0.000	10.362	0.001
0.000	0.005	0.000	0.001	0.000	0.001	0.038	0.001	0.957	0.065	0.005	14.809	0.001
0.000	0.004	0.000	0.001	0.000	0.004	0.049	0.001	0.931	0.173	0.004	5.369	0.004
0.000	0.005	0.000	0.001	0.000	0.002	0.051	0.001	0.909	0.173	0.005	5.245	0.002
0.000	0.000	0.000	0.000	0.000	0.000	0.046	0.000	1.073	0.041	0.000	25.849	0.000
0.000	0.003	0.000	0.001	0.000	0.003	0.053	0.001	0.997	0.091	0.003	10.892	0.003
0.001	0.000	0.000	0.000	0.000	0.000	0.030	0.000	1.099	0.027	0.000	40.358	0.000
0.000	0.003	0.000	0.001	0.000	0.002	0.061	0.000	1.026	0.092	0.003	11.161	0.002

0.001	0.003	0.000	0.001	0.000	0.005	0.070	0.001	0.954	0.110	0.003	8.673	0.005
0.001	0.003	0.000	0.001	0.000	0.002	0.045	0.001	0.979	0.092	0.003	10.637	0.002
0.003	0.000	0.000	0.000	0.000	0.001	0.055	0.000	1.115	0.046	0.000	24.323	0.001
0.001	0.000	0.000	0.000	0.000	0.000	0.037	0.000	0.938	0.094	0.000	9.975	0.000
0.000	0.000	0.000	0.000	0.000	0.000	0.038	0.000	0.995	0.064	0.000	15.555	0.000
0.002	0.000	0.000	0.001	0.000	0.000	0.048	0.000	0.952	0.084	0.000	11.281	0.000
0.001	0.004	0.000	0.001	0.000	0.002	0.044	0.000	0.779	0.277	0.004	2.813	0.002
0.000	0.001	0.000	0.000	0.000	0.004	0.037	0.000	0.871	0.182	0.001	4.783	0.004
0.001	0.002	0.000	0.000	0.000	0.003	0.049	0.000	0.860	0.192	0.002	4.489	0.003
0.000	0.003	0.000	0.000	0.000	0.002	0.033	0.000	0.782	0.297	0.003	2.628	0.003
0.002	0.002	0.000	0.000	0.000	0.005	0.042	0.000	0.845	0.175	0.002	4.821	0.005
0.000	0.004	0.000	0.000	0.000	0.001	0.036	0.000	0.847	0.283	0.004	2.995	0.002
0.000	0.001	0.000	0.000	0.000	0.003	0.051	0.000	0.784	0.299	0.001	2.618	0.003
0.001	0.003	0.000	0.000	0.000	0.004	0.040	0.001	0.789	0.312	0.003	2.531	0.005
0.001	0.002	0.001	0.000	0.000	0.002	0.031	0.000	0.764	0.346	0.002	2.210	0.002
0.000	0.002	0.000	0.001	0.000	0.004	0.044	0.000	0.876	0.207	0.002	4.223	0.004
0.001	0.007	0.000	0.003	0.000	0.004	0.051	0.001	0.885	0.205	0.007	4.312	0.004
0.001	0.002	0.000	0.000	0.000	0.002	0.036	0.000	0.915	0.192	0.002	4.757	0.002
0.000	0.001	0.000	0.000	0.000	0.002	0.031	0.001	0.870	0.211	0.001	4.126	0.002
0.002	0.000	0.000	0.001	0.000	0.001	0.044	0.000	1.003	0.137	0.000	7.307	0.001
0.000	0.000	0.000	0.000	0.000	0.000	0.050	0.000	1.013	0.024	0.000	41.577	0.000
0.000	0.002	0.000	0.001	0.000	0.002	0.026	0.001	0.919	0.209	0.002	4.399	0.003
0.000	0.003	0.000	0.001	0.000	0.004	0.060	0.001	0.887	0.247	0.003	3.587	0.004
0.002	0.004	0.001	0.002	0.000	0.002	0.039	0.000	0.875	0.196	0.004	4.455	0.002
0.002	0.004	0.000	0.000	0.000	0.003	0.026	0.000	0.909	0.246	0.004	3.691	0.003
0.000	0.003	0.000	0.002	0.000	0.003	0.041	0.000	0.904	0.212	0.003	4.264	0.003
0.000	0.000	0.000	0.001	0.000	0.000	0.043	0.000	0.899	0.255	0.000	3.525	0.000
0.000	0.001	0.000	0.000	0.000	0.001	0.041	0.000	1.137	0.132	0.001	8.633	0.001
0.001	0.001	0.000	0.001	0.000	0.001	0.032	0.001	0.874	0.248	0.001	3.527	0.001
0.000	0.002	0.000	0.000	0.000	0.001	0.034	0.001	1.028	0.123	0.002	8.361	0.001
0.000	0.103	0.002	0.005	0.000	0.002	0.009	0.001	1.656	0.577	0.178	2.872	0.004
0.001	0.001	0.000	0.000	0.000	0.003	0.064	0.000	0.814	0.267	0.001	3.049	0.003
0.001	0.001	0.000	0.000	0.000	0.001	0.063	0.001	1.057	0.025	0.001	41.868	0.001
0.001	0.001	0.000	0.000	0.000	0.001	0.049	0.001	1.036	0.062	0.001	16.649	0.001
0.001	0.001	0.000	0.000	0.000	0.001	0.038	0.001	0.897	0.267	0.001	3.357	0.001

0.000	0.001	0.000	0.000	0.000	0.000	0.046	0.000	1.086	0.037	0.001	29.322	0.000
0.001	0.003	0.000	0.000	0.000	0.001	0.041	0.001	1.112	0.053	0.003	21.092	0.001
0.001	0.001	0.000	0.000	0.000	0.000	0.071	0.000	1.037	0.065	0.001	15.863	0.000
0.001	0.001	0.000	0.000	0.000	0.001	0.053	0.000	0.967	0.171	0.001	5.670	0.001
0.001	0.000	0.000	0.000	0.000	0.001	0.043	0.000	1.069	0.016	0.000	65.894	0.001
0.002	0.000	0.000	0.000	0.000	0.000	0.059	0.000	1.106	0.033	0.000	33.059	0.000
0.000	0.000	0.000	0.001	0.000	0.001	0.047	0.000	1.109	0.040	0.000	27.694	0.001
0.001	0.001	0.000	0.000	0.000	0.000	0.059	0.000	1.162	0.036	0.001	31.940	0.001
0.001	0.003	0.000	0.000	0.000	0.000	0.034	0.000	1.025	0.070	0.003	14.742	0.000
0.000	0.000	0.000	0.000	0.000	0.001	0.044	0.000	1.086	0.090	0.000	12.047	0.001
0.001	0.001	0.000	0.000	0.000	0.002	0.041	0.000	1.137	0.115	0.001	9.898	0.002
0.000	0.000	0.000	0.000	0.000	0.001	0.049	0.001	0.958	0.182	0.000	5.259	0.001
0.000	0.001	0.000	0.000	0.000	0.010	0.030	0.000	1.082	0.113	0.001	9.602	0.011
0.000	0.000	0.000	0.000	0.000	0.001	0.051	0.000	1.046	0.004	0.000	281.968	0.001
0.001	0.001	0.000	0.000	0.000	0.001	0.028	0.000	1.014	0.027	0.001	37.751	0.001
0.001	0.002	0.000	0.000	0.000	0.001	0.059	0.000	1.030	0.038	0.002	26.883	0.001
0.000	0.001	0.000	0.000	0.000	0.000	0.048	0.000	1.080	0.038	0.001	28.673	0.000
0.000	0.110	0.000	0.000	0.026	0.001	0.032	0.000	1.552	0.076	0.142	20.326	0.035
0.001	0.001	0.000	0.000	0.000	0.001	0.050	0.000	1.012	0.010	0.001	102.615	0.001
0.000	0.001	0.000	0.000	0.000	0.001	0.050	0.000	1.055	0.010	0.001	102.339	0.001
0.000	0.001	0.000	0.000	0.000	0.001	0.045	0.001	1.031	0.018	0.001	56.631	0.001
0.000	0.001	0.000	0.000	0.000	0.003	0.031	0.000	1.066	0.016	0.001	65.623	0.003
0.000	0.005	0.000	0.000	0.000	0.003	0.036	0.000	1.131	0.029	0.005	38.967	0.004
0.000	0.045	0.001	0.006	0.000	0.004	0.036	0.001	1.258	0.046	0.054	27.461	0.005
0.002	0.000	0.000	0.000	0.000	0.003	0.057	0.000	0.965	0.088	0.000	10.968	0.003
0.001	0.000	0.000	0.000	0.000	0.002	0.032	0.000	1.338	0.037	0.000	35.759	0.003
0.000	0.002	0.000	0.000	0.000	0.001	0.044	0.000	1.007	0.041	0.002	24.360	0.001
0.000	0.045	0.001	0.005	0.000	0.002	0.050	0.001	1.072	0.118	0.049	9.118	0.002
0.000	0.001	0.000	0.000	0.000	0.001	0.046	0.000	0.994	0.048	0.001	20.676	0.001
0.000	0.028	0.001	0.007	0.000	0.002	0.051	0.000	0.897	0.153	0.029	5.882	0.002
0.000	0.000	0.000	0.000	0.000	0.002	0.043	0.000	0.934	0.120	0.000	7.760	0.002
0.000	0.000	0.000	0.001	0.000	0.001	0.050	0.000	0.925	0.085	0.000	10.910	0.001
0.000	0.001	0.000	0.001	0.000	0.002	0.040	0.000	0.928	0.122	0.001	7.597	0.002
0.001	0.001	0.000	0.000	0.000	0.001	0.048	0.000	0.925	0.089	0.001	10.407	0.001
0.002	0.002	0.000	0.000	0.000	0.001	0.064	0.000	0.958	0.093	0.002	10.289	0.001

0.001	0.022	0.001	0.009	0.000	0.002	0.028	0.000	1.050	0.043	0.023	24.671	0.002
0.002	0.001	0.000	0.000	0.000	0.001	0.042	0.000	0.945	0.061	0.001	15.468	0.001
0.000	0.001	0.000	0.000	0.000	0.003	0.043	0.000	1.037	0.048	0.001	21.458	0.003
0.001	0.001	0.000	0.000	0.000	0.001	0.044	0.000	0.981	0.049	0.001	19.867	0.001
0.002	0.000	0.000	0.000	0.000	0.001	0.050	0.000	0.978	0.030	0.000	32.550	0.001
0.001	0.000	0.000	0.000	0.000	0.001	0.035	0.000	1.053	0.031	0.000	34.147	0.001
0.001	0.001	0.000	0.000	0.000	0.002	0.048	0.000	0.904	0.182	0.001	4.954	0.002
0.001	0.001	0.000	0.001	0.000	0.001	0.063	0.000	1.108	0.020	0.001	55.835	0.001
0.000	0.000	0.000	0.001	0.000	0.001	0.059	0.000	1.169	0.015	0.000	75.712	0.001
0.001	0.000	0.000	0.000	0.000	0.002	0.032	0.000	0.896	0.232	0.000	3.856	0.002
0.002	0.000	0.000	0.000	0.000	0.003	0.033	0.000	0.958	0.191	0.000	5.012	0.003
0.001	0.001	0.000	0.000	0.000	0.003	0.048	0.000	1.091	0.084	0.001	13.056	0.003
0.002	0.001	0.000	0.000	0.000	0.004	0.045	0.001	1.328	0.051	0.002	26.198	0.004
0.001	0.000	0.000	0.000	0.000	0.003	0.048	0.000	1.001	0.043	0.000	23.421	0.003
0.000	0.001	0.000	0.000	0.000	0.005	0.042	0.001	1.074	0.043	0.001	24.844	0.005
0.000	0.002	0.000	0.001	0.000	0.004	0.041	0.000	1.123	0.057	0.002	19.809	0.004
0.001	0.003	0.000	0.000	0.000	0.007	0.051	0.000	1.123	0.075	0.003	15.001	0.007
0.000	0.001	0.000	0.000	0.000	0.004	0.052	0.001	1.143	0.046	0.001	25.071	0.004
0.000	0.002	0.000	0.000	0.000	0.006	0.024	0.000	1.172	0.116	0.002	10.077	0.007
0.001	0.002	0.000	0.000	0.000	0.005	0.044	0.001	1.266	0.209	0.002	6.066	0.006
0.000	0.002	0.000	0.000	0.000	0.006	0.034	0.000	1.251	0.162	0.002	7.727	0.008
0.000	0.002	0.000	0.000	0.000	0.005	0.049	0.000	0.975	0.254	0.002	3.845	0.005
0.001	0.001	0.000	0.000	0.000	0.005	0.041	0.000	0.955	0.203	0.001	4.696	0.005
0.001	0.001	0.000	0.000	0.000	0.003	0.024	0.000	1.037	0.082	0.002	12.650	0.003
0.001	0.001	0.000	0.000	0.000	0.004	0.030	0.000	1.112	0.090	0.001	12.414	0.005
0.000	0.067	0.000	0.000	0.050	0.003	0.048	0.000	1.648	0.103	0.093	15.946	0.074
0.001	0.000	0.000	0.000	0.000	0.003	0.021	0.000	1.048	0.049	0.000	21.413	0.003
0.001	0.012	0.001	0.001	0.000	0.004	0.038	0.001	1.200	0.073	0.014	16.379	0.004
0.000	0.022	0.001	0.002	0.000	0.003	0.033	0.002	1.125	0.064	0.025	17.635	0.004
0.000	0.005	0.000	0.000	0.000	0.004	0.035	0.001	1.157	0.051	0.006	22.879	0.005
0.002	0.001	0.000	0.000	0.000	0.002	0.052	0.000	0.970	0.069	0.001	14.121	0.002
0.001	0.001	0.000	0.000	0.000	0.001	0.043	0.000	1.057	0.037	0.002	28.451	0.001
0.000	0.001	0.000	0.000	0.000	0.003	0.045	0.001	1.103	0.048	0.001	22.919	0.003
0.000	0.001	0.000	0.000	0.000	0.002	0.054	0.000	1.066	0.091	0.001	11.778	0.002
0.001	0.000	0.000	0.000	0.000	0.002	0.042	0.000	1.038	0.076	0.000	13.751	0.002

0.000	0.000	0.000	0.000	0.000	0.001	0.046	0.000	1.095	0.067	0.000	16.452	0.002
0.002	0.001	0.000	0.000	0.000	0.001	0.043	0.002	1.069	0.060	0.001	17.965	0.001
0.002	0.001	0.000	0.000	0.000	0.005	0.052	0.000	1.064	0.057	0.001	18.661	0.005
0.000	0.003	0.000	0.000	0.000	0.002	0.052	0.001	1.073	0.090	0.003	11.883	0.002
0.000	0.006	0.000	0.000	0.000	0.004	0.047	0.001	1.100	0.068	0.007	16.258	0.004
0.000	0.001	0.000	0.000	0.000	0.002	0.047	0.000	1.091	0.049	0.001	22.179	0.002
0.002	0.027	0.000	0.000	0.000	0.005	0.035	0.001	1.179	0.084	0.031	13.956	0.006
0.000	0.079	0.000	0.000	0.000	0.003	0.037	0.004	1.293	0.080	0.096	16.165	0.004
0.001	0.001	0.000	0.000	0.000	0.003	0.053	0.000	1.055	0.093	0.001	11.377	0.004
0.000	0.001	0.000	0.000	0.000	0.003	0.054	0.001	1.064	0.066	0.001	16.226	0.003
0.001	0.272	0.011	0.040	0.000	0.009	0.026	0.005	1.981	0.066	0.466	30.141	0.015
0.001	0.215	0.002	0.011	0.000	0.003	0.078	0.002	1.852	2.217	0.530	0.836	0.008
0.001	0.154	0.000	0.000	0.033	0.002	0.039	0.001	1.539	0.132	0.208	11.664	0.048
0.001	0.123	0.000	0.000	0.003	0.005	0.032	0.001	1.426	0.094	0.173	15.193	0.011
0.000	0.249	0.000	0.000	0.000	0.003	0.044	0.001	1.590	0.174	0.353	9.139	0.004
0.000	0.216	0.000	0.000	0.006	0.004	0.039	0.002	1.644	0.164	0.333	10.037	0.015
0.001	0.253	0.000	0.002	0.000	0.002	0.049	0.000	1.280	0.222	0.322	5.778	0.002
0.001	0.257	0.000	0.002	0.000	0.002	0.025	0.004	1.373	0.131	0.326	10.515	0.002
0.002	0.260	0.001	0.002	0.006	0.003	0.036	0.001	1.305	0.179	0.330	7.280	0.011
0.000	0.263	0.000	0.001	0.000	0.001	0.026	0.002	1.347	0.158	0.336	8.512	0.001
0.002	0.277	0.000	0.002	0.000	0.003	0.030	0.007	1.224	0.217	0.348	5.632	0.003
0.000	0.294	0.003	0.016	0.000	0.003	0.042	0.012	1.276	0.195	0.376	6.536	0.003
0.000	0.275	0.000	0.002	0.000	0.001	0.045	0.003	1.333	0.204	0.355	6.534	0.002
0.002	0.245	0.001	0.003	0.000	0.002	0.047	0.000	1.325	0.207	0.314	6.387	0.002
0.000	0.309	0.013	0.057	0.000	0.005	0.029	0.001	1.559	0.076	0.421	20.632	0.006
0.000	0.328	0.010	0.046	0.000	0.003	0.033	0.001	1.562	0.072	0.447	21.764	0.004
0.001	0.241	0.001	0.006	0.000	0.002	0.038	0.001	1.376	0.189	0.310	7.273	0.002
0.003	0.258	0.001	0.003	0.000	0.004	0.017	0.001	1.317	0.264	0.337	4.982	0.005
0.001	0.247	0.001	0.004	0.015	0.005	0.034	0.015	1.312	0.251	0.323	5.226	0.027
0.002	0.248	0.001	0.002	0.000	0.003	0.014	0.002	1.362	0.233	0.325	5.846	0.003
0.002	0.254	0.000	0.002	0.000	0.003	0.049	0.001	1.380	0.193	0.331	7.160	0.004
0.002	0.265	0.000	0.003	0.000	0.003	0.056	0.001	1.301	0.275	0.345	4.724	0.004
0.000	0.247	0.022	0.066	0.000	0.004	0.041	0.004	1.460	0.160	0.331	9.125	0.005
0.002	0.266	0.001	0.003	0.000	0.003	0.043	0.001	1.299	0.293	0.349	4.428	0.005
0.003	0.251	0.007	0.025	0.000	0.005	0.050	0.002	1.401	0.192	0.329	7.287	0.006

0.003	0.266	0.003	0.011	0.000	0.006	0.018	0.002	1.395	0.240	0.355	5.816	0.008
0.001	0.251	0.000	0.001	0.000	0.005	0.057	0.001	1.164	0.364	0.321	3.198	0.006
0.003	0.250	0.000	0.001	0.000	0.002	0.032	0.001	1.178	0.405	0.327	2.909	0.003
0.001	0.222	0.000	0.003	0.013	0.007	0.026	0.001	1.145	0.950	0.335	1.205	0.030
0.001	0.192	0.000	0.002	0.009	0.008	0.033	0.001	1.075	1.427	0.319	0.753	0.029
0.001	0.238	0.000	0.004	0.000	0.002	0.042	0.000	1.193	0.531	0.322	2.245	0.003
0.003	0.248	0.000	0.002	0.000	0.002	0.051	0.000	1.233	0.389	0.328	3.172	0.002
0.000	0.260	0.000	0.002	0.000	0.002	0.043	0.000	1.203	0.378	0.339	3.182	0.002
0.001	0.279	0.000	0.001	0.000	0.004	0.037	0.001	1.373	0.204	0.365	6.722	0.005

0.000	0.000	0.000	0.000	0.000	0.000	0.000	0.000	1.000	0.000	0.000	0.000	0.000
0.000	0.762	0.000	0.000	0.000	0.000	0.000	0.000	1.500	0.000	0.500	0.000	0.000
0.000	0.000	0.000	0.000	0.000	0.000	0.000	0.000	0.000	1.000	0.000	0.000	0.000
0.000	1.172	0.000	0.000	0.821	0.351	0.000	0.000	1.500	0.000	0.250	0.000	0.250
0.000	0.000	0.000	0.000	0.800	0.000	0.000	0.000	1.500	0.000	0.000	0.000	0.500
0.000	0.000	0.000	0.000	0.000	0.000	0.000	0.000	1.500	0.000	0.000	0.000	0.000

Al/Si+P
0.775
0.675
0.894
0.821
0.856
0.556
0.753
0.963
0.901
0.738
0.810
0.811
0.635
0.858
1.002
0.932
0.794
0.983
0.994
0.864
1.066
0.986
1.025
0.999
0.883
0.976
0.929
0.927
0.928
0.908
1.072
0.992
1.096
1.014

0.949
0.971
1.115
0.936
0.993
0.950
0.775
0.860
0.858
0.639
0.821
0.786
0.780
0.723
0.732
0.864
0.880
0.911
0.868
0.998
1.009
0.913
0.883
0.867
0.877
0.893
0.899
0.962
0.863
0.961
1.163
0.813
1.056
1.034
0.896

1.084
0.953
1.035
0.966
1.068
1.102
1.109
1.162
1.024
1.058
1.017
0.946
1.018
1.045
1.009
1.024
1.069
1.511
1.010
1.054
1.029
1.062
0.925
1.078
0.962
1.000
0.984
1.066
0.984
0.897
0.934
0.925
0.928
0.925
0.957

1.045
0.943
1.036
0.980
0.976
1.052
0.903
1.101
1.165
0.894
0.905
1.051
1.119
0.984
1.069
1.087
1.067
1.131
0.945
0.931
0.968
0.950
0.951
0.939
0.971
1.405
1.025
1.057
1.007
0.995
0.968
1.057
1.086
1.064
1.033

1.094
1.068
1.061
1.069
1.043
1.071
1.061
1.180
1.003
1.064
1.455
1.346
1.400
1.061
1.448
1.251
1.275
1.369
1.300
1.344
1.216
1.273
1.329
1.320
1.559
1.562
1.373
1.310
1.274
1.359
1.377
1.296
1.460
1.297
1.401

1.393
1.154
1.174
1.140
1.064
1.191
1.232
1.198
1.368
1.000
1.500
0.000
1.500
1.500
1.500

Sample	W5-D1A_c	W5-D1A_ca	W5-D1A_ca	W5-D1A_ca	W5-D1A_ca	W5-D1A_ca	W5-D1A_ca	W5-D1A_ca	W5-D1A_ca	W5-D1A_ca	W5-D1A_ca	W5-D1A_ca
No.	1	2	3	4	5	6	7	8	9	10	11	12
P2O5	40.91	42.21	40.76	43.21	42.50	34.08	41.66	42.02	43.16	40.16	41.81	42.42
V2O3	0.01	0.01	0.00	0.01	0.00	0.03	0.01	0.00	0.05	0.00	0.00	0.00
SiO2	0.08	0.03	0.00	0.03	0.05	0.79	0.09	0.06	0.14	0.04	0.03	0.02
Al2O3	22.84	20.47	26.17	25.50	26.16	13.99	22.58	29.13	28.04	21.31	24.33	24.74
Cr2O3	0.00	0.01	0.00	0.00	0.00	0.03	0.01	0.00	0.00	0.00	0.01	0.00
TiO2	0.31	0.11	0.02	0.10	0.49	4.58	1.65	0.05	0.16	0.07	0.01	0.16
Fe2O3	12.86	18.64	7.79	10.32	8.27	23.75	15.20	3.24	5.83	14.64	9.58	10.78
MgO	0.01	0.02	0.01	0.02	0.04	0.00	0.01	0.06	0.01	0.00	0.01	0.03
MnO	0.02	0.04	0.05	0.07	0.00	0.00	0.04	0.05	0.02	0.06	0.03	0.00
CaO	0.04	0.02	0.00	0.05	0.08	0.52	0.13	0.01	0.06	0.03	0.02	0.06
BaO	0.00	0.00	0.00	0.00	0.00	0.00	0.00	0.01	0.00	0.00	0.00	0.00
SrO	0.05	0.03	0.00	0.01	0.05	0.50	0.12	0.00	0.03	0.00	0.00	0.03
Na2O	0.00	0.00	0.00	0.00	0.00	0.00	0.00	0.00	0.00	0.00	0.00	0.00
K2O	0.05	0.31	0.06	0.08	0.07	0.10	0.16	0.04	0.05	0.02	0.06	0.05
F	0.47	0.36	0.41	0.65	0.46	0.53	0.44	0.50	0.42	0.39	0.50	0.36
Cl	0.00	0.00	0.00	0.02	0.02	0.51	0.04	0.01	0.01	0.00	0.01	0.00
Total 1	*77.00*	*81.60*	*74.62*	*79.40*	*77.54*	*78.75*	*81.49*	*74.52*	*77.33*	*76.06*	*75.74*	*77.99*
O=F=Cl	0.199	*0.152*	*0.175*	*0.275*	*0.198*	*0.338*	*0.193*	*0.214*	*0.179*	*0.165*	*0.212*	*0.149*
Total 2	**76.80**	**81.45**	**74.45**	**79.12**	**77.34**	**78.41**	**81.29**	**74.31**	**77.15**	**75.89**	**75.53**	**77.84**
moles prop												
P2O5	0.288	0.297	0.287	0.304	0.299	0.240	0.293	0.296	0.304	0.283	0.295	0.299
V2O3	0.000	0.000	0.000	0.000	0.000	0.000	0.000	0.000	0.000	0.000	0.000	0.000
SiO2	0.001	0.000	0.000	0.000	0.001	0.013	0.001	0.001	0.002	0.001	0.001	0.000
Al2O3	0.224	0.201	0.257	0.250	0.257	0.137	0.221	0.286	0.275	0.209	0.239	0.243
Cr2O3	0.000	0.000	0.000	0.000	0.000	0.000	0.000	0.000	0.000	0.000	0.000	0.000
TiO2	0.004	0.001	0.000	0.001	0.006	0.057	0.021	0.001	0.002	0.001	0.000	0.002
Fe2O3	0.081	0.117	0.049	0.065	0.052	0.149	0.095	0.020	0.036	0.092	0.060	0.067
MgO	0.000	0.001	0.000	0.000	0.001	0.000	0.000	0.001	0.000	0.000	0.000	0.001
MnO	0.000	0.001	0.001	0.001	0.000	0.000	0.000	0.001	0.000	0.001	0.000	0.000
CaO	0.001	0.000	0.000	0.001	0.001	0.009	0.002	0.000	0.001	0.001	0.000	0.001
BaO	0.000	0.000	0.000	0.000	0.000	0.000	0.000	0.000	0.000	0.000	0.000	0.000
SrO	0.001	0.000	0.000	0.000	0.000	0.005	0.001	0.000	0.000	0.000	0.000	0.000
Na2O	0.000	0.000	0.000	0.000	0.000	0.000	0.000	0.000	0.000	0.000	0.000	0.000

K2O	0.001	0.003	0.001	0.001	0.001	0.001	0.002	0.000	0.001	0.000	0.001	0.000
F	0.0248	0.0190	0.0218	0.0340	0.0243	0.0279	0.0231	0.0265	0.0222	0.0206	0.0263	0.0187
Cl	0.000	0.000	0.000	0.000	0.001	0.014	0.001	0.000	0.000	0.000	0.000	0.000
cation prop												
P	0.576	0.595	0.574	0.609	0.599	0.480	0.587	0.592	0.608	0.566	0.589	0.598
V	0.000	0.000	0.000	0.000	0.000	0.000	0.000	0.000	0.001	0.000	0.000	0.000
Si	0.001	0.000	0.000	0.000	0.001	0.013	0.001	0.001	0.002	0.001	0.001	0.000
Al	0.448	0.401	0.513	0.500	0.513	0.274	0.443	0.571	0.550	0.418	0.477	0.485
Cr	0.000	0.000	0.000	0.000	0.000	0.000	0.000	0.000	0.000	0.000	0.000	0.000
Ti	0.004	0.001	0.000	0.001	0.006	0.057	0.021	0.001	0.002	0.001	0.000	0.002
Fe3	0.161	0.233	0.098	0.129	0.104	0.297	0.190	0.041	0.073	0.183	0.120	0.135
Mg	0.000	0.001	0.000	0.000	0.001	0.000	0.000	0.001	0.000	0.000	0.000	0.001
Mn	0.000	0.001	0.001	0.001	0.000	0.000	0.000	0.001	0.000	0.001	0.000	0.000
Ca	0.001	0.000	0.000	0.001	0.001	0.009	0.002	0.000	0.001	0.001	0.000	0.001
Ba	0.000	0.000	0.000	0.000	0.000	0.000	0.000	0.000	0.000	0.000	0.000	0.000
Sr	0.001	0.000	0.000	0.000	0.000	0.005	0.001	0.000	0.000	0.000	0.000	0.000
Na	0.000	0.000	0.000	0.000	0.000	0.000	0.000	0.000	0.000	0.000	0.000	0.000
K	0.001	0.007	0.001	0.002	0.002	0.002	0.003	0.001	0.001	0.000	0.001	0.001
F												
Cl												
oxygen prop												
P	1.441	1.487	1.436	1.522	1.497	1.200	1.467	1.480	1.520	1.415	1.473	1.494
V	0.000	0.000	0.000	0.000	0.000	0.001	0.000	0.000	0.001	0.000	0.000	0.000
Si	0.003	0.001	0.000	0.001	0.002	0.026	0.003	0.002	0.005	0.001	0.001	0.001
Al	0.672	0.602	0.770	0.750	0.770	0.412	0.664	0.857	0.825	0.627	0.716	0.728
Cr	0.000	0.000	0.000	0.000	0.000	0.001	0.000	0.000	0.000	0.000	0.000	0.000
Ti	0.008	0.003	0.001	0.003	0.012	0.115	0.041	0.001	0.004	0.002	0.000	0.004
Fe3	0.242	0.350	0.146	0.194	0.155	0.446	0.285	0.061	0.109	0.275	0.180	0.202
Mg	0.000	0.001	0.000	0.000	0.001	0.000	0.000	0.001	0.000	0.000	0.000	0.001
Mn	0.000	0.001	0.001	0.001	0.000	0.000	0.000	0.001	0.000	0.001	0.000	0.000
Ca	0.001	0.000	0.000	0.001	0.001	0.009	0.002	0.000	0.001	0.001	0.000	0.001
Ba	0.000	0.000	0.000	0.000	0.000	0.000	0.000	0.000	0.000	0.000	0.000	0.000
Sr	0.001	0.000	0.000	0.000	0.000	0.005	0.001	0.000	0.000	0.000	0.000	0.000
Na	0.000	0.000	0.000	0.000	0.000	0.000	0.000	0.000	0.000	0.000	0.000	0.000

K	0.001	0.003	0.001	0.001	0.001	0.001	0.002	0.000	0.001	0.000	0.001	0.000
F	0.0248	0.0190	0.0218	0.0340	0.0243	0.0279	0.0231	0.0265	0.0222	0.0206	0.0263	0.0187
Cl	0.000	0.000	0.000	0.000	0.001	0.014	0.001	0.000	0.000	0.000	0.000	0.000
sum_O	2.355	2.439	2.343	2.456	2.427	2.194	2.456	2.391	2.456	2.311	2.358	2.423
normaliz factor (4O)	*1.699*	*1.640*	*1.707*	*1.629*	*1.648*	*1.823*	*1.629*	*1.673*	*1.629*	*1.731*	*1.696*	*1.651*
anion prop basis 4O	**W5-D1A_c**	**W5-D1A_ca**	**W5-D1A_ca**	**W5-D1A_ca**	**W5-D1A_ca**	**W5-D1A_ca**	**W5-D1A_ca**	**W5-D1A_ca**	**W5-D1A_ca**	**W5-D1A_ca**	**W5-D1A_ca**	**W5-D1A_ca**
P	0.979	0.975	0.980	0.992	0.987	0.875	0.956	0.991	0.991	0.979	0.999	0.987
V	0.000	0.000	0.000	0.000	0.000	0.001	0.000	0.000	0.001	0.000	0.000	0.000
Si	0.002	0.001	0.000	0.001	0.001	0.024	0.002	0.002	0.004	0.001	0.001	0.001
Al	0.761	0.659	0.876	0.815	0.846	0.500	0.721	0.956	0.896	0.724	0.810	0.801
Cr	0.000	0.000	0.000	0.000	0.000	0.001	0.000	0.000	0.000	0.000	0.000	0.000
Ti	0.007	0.002	0.000	0.002	0.010	0.104	0.034	0.001	0.003	0.002	0.000	0.003
Fe3	0.274	0.383	0.166	0.211	0.171	0.542	0.310	0.068	0.119	0.317	0.204	0.223
Mg	0.000	0.001	0.001	0.001	0.001	0.000	0.001	0.002	0.001	0.000	0.000	0.001
Mn	0.000	0.001	0.001	0.002	0.000	0.000	0.001	0.001	0.000	0.001	0.001	0.000
Ca	0.001	0.001	0.000	0.001	0.002	0.017	0.004	0.000	0.002	0.001	0.001	0.002
Ba	0.000	0.000	0.000	0.000	0.000	0.000	0.000	0.000	0.000	0.000	0.000	0.000
Sr	0.001	0.000	0.000	0.000	0.001	0.009	0.002	0.000	0.000	0.000	0.000	0.000
Na	0.000	0.000	0.000	0.000	0.000	0.000	0.000	0.000	0.000	0.000	0.000	0.000
K	0.002	0.011	0.002	0.003	0.002	0.004	0.006	0.001	0.002	0.001	0.002	0.002
F	0.042	0.031	0.037	0.055	0.040	0.051	0.038	0.044	0.036	0.036	0.045	0.031
Cl	0.000	0.000	0.000	0.001	0.001	0.026	0.002	0.001	0.000	0.000	0.000	0.000
[A]site (ideally 1)	1.05	1.06	1.05	1.03	1.03	1.18	1.08	1.03	1.02	1.05	1.02	1.03
[T]site (ideally 1)	0.98	0.98	0.98	0.99	0.99	0.90	0.96	0.99	0.99	0.98	1.00	0.99
warning 1 [A]	ok	ok	ok	ok	ok	excess	ok	ok	ok	ok	ok	ok
warning 2 [T]	ok	ok	ok	ok	ok	ok	ok	ok	ok	ok	ok	ok
Fe3>Al	menor	menor	menor	menor	menor	maior	menor	menor	menor	menor	menor	menor

W5-D1A_ca	W5-D1A_ca	W5-D1A_ca	W5-D1A_ca	W5-D1A_ca	W5-D1A_ca	W5-D1A_ca	W5-D1A_ca	W5-D1A_ca	W5-D1A_ca	W5-D1A_ca	W5-D1A_ca	W5-D1A_ca	W5-D1A_ca
13	**14**	**15**	**16**	**17**	**19**	**20**	**21**	**23**	**24**	**26**	**27**	**28**	**30**
38.89	42.64	41.34	41.12	41.35	38.48	42.19	41.17	41.91	43.63	41.77	42.11	38.98	41.06
0.01	0.00	0.00	0.03	0.01	0.04	0.00	0.00	0.01	0.00	0.00	0.01	0.03	0.02
0.08	0.02	0.11	0.24	0.00	0.14	0.07	0.01	0.00	0.31	0.25	0.06	2.48	0.55
17.78	26.30	29.85	27.74	23.58	27.30	30.18	25.57	32.10	31.17	30.97	30.28	26.58	29.25
0.05	0.01	0.00	0.00	0.00	0.02	0.00	0.00	0.00	0.00	0.00	0.00	0.00	0.00
1.69	0.37	0.17	0.23	0.14	0.25	0.01	0.09	0.00	0.08	0.02	0.00	0.61	0.51
22.82	8.92	4.76	5.76	11.88	7.44	2.88	7.59	1.25	2.45	1.20	0.50	4.64	3.27
0.00	0.01	0.01	0.00	0.03	0.01	0.01	0.01	0.02	0.03	0.00	0.00	0.03	0.03
0.00	0.01	0.07	0.04	0.02	0.04	0.05	0.05	0.04	0.00	0.00	0.01	0.04	0.07
0.25	0.10	0.02	0.07	0.02	0.12	0.04	0.11	0.03	0.02	0.03	0.05	0.09	0.10
0.00	0.02	0.00	0.00	0.00	0.00	0.02	0.01	0.00	0.03	0.00	0.00	0.00	0.00
0.23	0.08	0.03	0.12	0.00	0.04	0.00	0.02	0.00	0.02	0.02	0.00	0.01	0.04
0.00	0.00	0.00	0.00	0.00	0.00	0.00	0.00	0.00	0.00	0.00	0.00	0.00	0.00
0.15	0.05	0.04	0.04	0.04	0.15	0.05	0.07	0.11	0.06	0.08	0.17	0.17	0.12
0.47	0.44	0.54	0.39	0.45	0.42	0.54	0.44	0.51	0.38	0.70	0.59	0.63	0.62
0.10	0.01	0.01	0.00	0.01	0.04	0.02	0.04	0.03	0.01	0.01	0.01	0.03	0.02
81.88	*78.34*	*76.29*	*75.14*	*76.87*	*73.84*	*75.39*	*74.51*	*75.38*	*77.53*	*74.40*	*73.15*	*73.68*	*75.00*
0.219	*0.187*	*0.230*	*0.163*	*0.191*	*0.184*	*0.229*	*0.196*	*0.223*	*0.159*	*0.295*	*0.249*	*0.273*	*0.265*
81.66	**78.15**	**76.06**	**74.97**	**76.68**	**73.66**	**75.16**	**74.32**	**75.15**	**77.37**	**74.10**	**72.90**	**73.40**	**74.74**
0.274	0.300	0.291	0.290	0.291	0.271	0.297	0.290	0.295	0.307	0.294	0.297	0.275	0.289
0.000	0.000	0.000	0.000	0.000	0.000	0.000	0.000	0.000	0.000	0.000	0.000	0.000	0.000
0.001	0.000	0.002	0.004	0.000	0.002	0.001	0.000	0.000	0.005	0.004	0.001	0.041	0.009
0.174	0.258	0.293	0.272	0.231	0.268	0.296	0.251	0.315	0.306	0.304	0.297	0.261	0.287
0.000	0.000	0.000	0.000	0.000	0.000	0.000	0.000	0.000	0.000	0.000	0.000	0.000	0.000
0.021	0.005	0.002	0.003	0.002	0.003	0.000	0.001	0.000	0.001	0.000	0.000	0.008	0.006
0.143	0.056	0.030	0.036	0.074	0.047	0.018	0.048	0.008	0.015	0.008	0.003	0.029	0.020
0.000	0.000	0.000	0.000	0.001	0.000	0.000	0.000	0.000	0.001	0.000	0.000	0.001	0.001
0.000	0.000	0.001	0.001	0.000	0.001	0.001	0.001	0.001	0.000	0.000	0.000	0.001	0.001
0.004	0.002	0.000	0.001	0.000	0.002	0.001	0.002	0.001	0.000	0.001	0.001	0.002	0.002
0.000	0.000	0.000	0.000	0.000	0.000	0.000	0.000	0.000	0.000	0.000	0.000	0.000	0.000
0.002	0.001	0.000	0.001	0.000	0.000	0.000	0.000	0.000	0.000	0.000	0.000	0.000	0.000
0.000	0.000	0.000	0.000	0.000	0.000	0.000	0.000	0.000	0.000	0.000	0.000	0.000	0.000

0.002	0.001	0.000	0.000	0.000	0.002	0.001	0.001	0.001	0.001	0.001	0.002	0.002	0.001
0.0246	0.0231	0.0285	0.0204	0.0235	0.0220	0.0282	0.0233	0.0271	0.0197	0.0368	0.0308	0.0332	0.0324
0.003	0.000	0.000	0.000	0.000	0.001	0.000	0.001	0.001	0.000	0.000	0.000	0.001	0.001

0.548	0.601	0.583	0.579	0.583	0.542	0.594	0.580	0.591	0.615	0.589	0.593	0.549	0.579
0.000	0.000	0.000	0.000	0.000	0.001	0.000	0.000	0.000	0.000	0.000	0.000	0.000	0.000
0.001	0.000	0.002	0.004	0.000	0.002	0.001	0.000	0.000	0.005	0.004	0.001	0.041	0.009
0.349	0.516	0.586	0.544	0.462	0.535	0.592	0.502	0.630	0.611	0.607	0.594	0.521	0.574
0.001	0.000	0.000	0.000	0.000	0.000	0.000	0.000	0.000	0.000	0.000	0.000	0.000	0.000
0.021	0.005	0.002	0.003	0.002	0.003	0.000	0.001	0.000	0.001	0.000	0.000	0.008	0.006
0.286	0.112	0.060	0.072	0.149	0.093	0.036	0.095	0.016	0.031	0.015	0.006	0.058	0.041
0.000	0.000	0.000	0.000	0.001	0.000	0.000	0.000	0.000	0.001	0.000	0.000	0.001	0.001
0.000	0.000	0.001	0.001	0.000	0.001	0.001	0.001	0.001	0.000	0.000	0.000	0.001	0.001
0.004	0.002	0.000	0.001	0.000	0.002	0.001	0.002	0.001	0.000	0.001	0.001	0.002	0.002
0.000	0.000	0.000	0.000	0.000	0.000	0.000	0.000	0.000	0.000	0.000	0.000	0.000	0.000
0.002	0.001	0.000	0.001	0.000	0.000	0.000	0.000	0.000	0.000	0.000	0.000	0.000	0.000
0.000	0.000	0.000	0.000	0.000	0.000	0.000	0.000	0.000	0.000	0.000	0.000	0.000	0.000
0.003	0.001	0.001	0.001	0.001	0.003	0.001	0.002	0.002	0.001	0.002	0.004	0.004	0.003

1.370	1.502	1.456	1.449	1.456	1.356	1.486	1.450	1.476	1.537	1.471	1.483	1.373	1.446
0.000	0.000	0.000	0.001	0.000	0.001	0.000	0.000	0.000	0.000	0.000	0.000	0.001	0.000
0.003	0.001	0.003	0.008	0.000	0.005	0.002	0.000	0.000	0.010	0.008	0.002	0.083	0.018
0.523	0.774	0.878	0.816	0.694	0.803	0.888	0.752	0.945	0.917	0.911	0.891	0.782	0.861
0.001	0.000	0.000	0.000	0.000	0.000	0.000	0.000	0.000	0.000	0.000	0.000	0.000	0.000
0.042	0.009	0.004	0.006	0.003	0.006	0.000	0.002	0.000	0.002	0.000	0.000	0.015	0.013
0.429	0.168	0.089	0.108	0.223	0.140	0.054	0.143	0.023	0.046	0.023	0.009	0.087	0.061
0.000	0.000	0.000	0.000	0.001	0.000	0.000	0.000	0.000	0.001	0.000	0.000	0.001	0.001
0.000	0.000	0.001	0.001	0.000	0.001	0.001	0.001	0.001	0.000	0.000	0.000	0.001	0.001
0.004	0.002	0.000	0.001	0.000	0.002	0.001	0.002	0.001	0.000	0.001	0.001	0.002	0.002
0.000	0.000	0.000	0.000	0.000	0.000	0.000	0.000	0.000	0.000	0.000	0.000	0.000	0.000
0.002	0.001	0.000	0.001	0.000	0.000	0.000	0.000	0.000	0.000	0.000	0.000	0.000	0.000
0.000	0.000	0.000	0.000	0.000	0.000	0.000	0.000	0.000	0.000	0.000	0.000	0.000	0.000

0.002	0.001	0.000	0.000	0.000	0.002	0.001	0.001	0.001	0.001	0.001	0.002	0.002	0.001
0.0246	0.0231	0.0285	0.0204	0.0235	0.0220	0.0282	0.0233	0.0271	0.0197	0.0368	0.0308	0.0332	0.0324
0.003	0.000	0.000	0.000	0.000	0.001	0.000	0.001	0.001	0.000	0.000	0.000	0.001	0.001
2.363	2.446	2.420	2.381	2.367	2.304	2.419	2.339	2.433	2.504	2.397	2.373	2.329	2.388
1.693	*1.635*	*1.653*	*1.680*	*1.690*	*1.736*	*1.654*	*1.710*	*1.644*	*1.597*	*1.669*	*1.685*	*1.718*	*1.675*
W5-D1A_ca	**W5-D1A_ca**	**W5-D1A_ca**	**W5-D1A_ca**	**W5-D1A_ca**	**W5-D1A_ca**	**W5-D1A_ca**	**W5-D1A_ca**	**W5-D1A_ca**	**W5-D1A_ca**	**W5-D1A_ca**	**W5-D1A_ca**	**W5-D1A_ca**	**W5-D1A_ca**
0.928	0.983	0.963	0.974	0.985	0.941	0.983	0.992	0.971	0.982	0.982	1.000	0.943	0.969
0.000	0.000	0.000	0.001	0.000	0.001	0.000	0.000	0.000	0.000	0.000	0.000	0.001	0.000
0.002	0.001	0.003	0.007	0.000	0.004	0.002	0.000	0.000	0.008	0.007	0.002	0.071	0.015
0.591	0.844	0.968	0.914	0.782	0.930	0.979	0.858	1.035	0.977	1.014	1.001	0.896	0.961
0.001	0.000	0.000	0.000	0.000	0.001	0.000	0.000	0.000	0.000	0.000	0.000	0.000	0.000
0.036	0.008	0.003	0.005	0.003	0.005	0.000	0.002	0.000	0.002	0.000	0.000	0.013	0.011
0.484	0.183	0.099	0.121	0.252	0.162	0.060	0.163	0.026	0.049	0.025	0.011	0.100	0.069
0.000	0.001	0.000	0.000	0.001	0.000	0.001	0.000	0.001	0.001	0.000	0.000	0.001	0.001
0.000	0.000	0.002	0.001	0.000	0.001	0.001	0.001	0.001	0.000	0.000	0.000	0.001	0.002
0.008	0.003	0.001	0.002	0.001	0.004	0.001	0.003	0.001	0.001	0.001	0.002	0.003	0.003
0.000	0.000	0.000	0.000	0.000	0.000	0.000	0.000	0.000	0.000	0.000	0.000	0.000	0.000
0.004	0.001	0.000	0.002	0.000	0.001	0.000	0.000	0.000	0.000	0.000	0.000	0.000	0.001
0.000	0.000	0.000	0.000	0.000	0.000	0.000	0.000	0.000	0.000	0.000	0.000	0.000	0.000
0.005	0.002	0.002	0.001	0.001	0.005	0.002	0.003	0.004	0.002	0.003	0.006	0.006	0.004
0.042	0.038	0.047	0.034	0.040	0.038	0.047	0.040	0.044	0.032	0.061	0.052	0.057	0.054
0.005	0.000	0.000	0.000	0.001	0.002	0.001	0.002	0.001	0.000	0.000	0.000	0.002	0.001
1.13	1.04	1.07	1.05	1.04	1.11	1.04	1.03	1.07	1.03	1.04	1.02	1.02	1.05
0.93	0.98	0.97	0.98	0.98	0.95	0.98	0.99	0.97	0.99	0.99	1.00	1.01	0.98
excess	ok	ok	ok	ok	excess	ok	ok	ok	ok	ok	ok	ok	ok
ok	ok	ok	ok	ok	ok	ok	ok	ok	ok	ok	ok	ok	ok
menor	menor	menor	menor	menor	menor	menor	menor	menor	menor	menor	menor	menor	menor

W5-D1A_ca	W5-D1A_ca	W5-F1A_ca	W5-F1A_ca	W5-F1A_ca	W5-F1A_ca	W5-F1A_ca	W5-F1A_ca	W5-F1A_ca	W5-F1A_ca	W5-F1A_ca	W5-F1A_ca	W5-F1A_ca	W5-F1A_ca
31	**32**	**1**	**2**	**3**	**4**	**5**	**6**	**7**	**8**	**9**	**10**	**11**	**12**
41.24	41.34	41.99	42.11	41.31	43.54	40.96	40.74	43.51	43.15	39.56	43.66	42.92	44.29
0.00	0.00	0.00	0.00	0.01	0.01	0.04	0.00	0.02	0.00	0.00	0.03	0.03	0.00
0.05	1.13	0.08	0.03	0.03	0.16	0.07	0.41	0.17	0.29	0.00	0.09	0.07	0.07
27.55	28.42	28.07	27.49	31.83	31.17	32.32	30.04	29.80	30.34	31.69	29.42	30.68	30.28
0.00	0.02	0.02	0.00	0.00	0.00	0.00	0.00	0.00	0.00	0.00	0.00	0.00	0.00
0.00	0.68	0.13	0.26	0.00	0.29	0.05	0.28	0.14	0.14	0.05	0.05	0.01	0.02
4.16	3.01	8.19	8.21	1.93	4.48	1.25	4.21	5.38	4.47	2.04	4.62	3.09	4.20
0.00	0.01	0.03	0.03	0.04	0.05	0.02	0.02	0.08	0.05	0.01	0.00	0.03	0.00
0.00	0.02	0.00	0.00	0.00	0.01	0.04	0.00	0.04	0.06	0.11	0.04	0.01	0.08
0.01	0.18	0.13	0.17	0.01	0.09	0.00	0.09	0.11	0.11	0.01	0.01	0.00	0.01
0.00	0.02	0.01	0.00	0.02	0.00	0.00	0.00	0.00	0.00	0.00	0.00	0.00	0.00
0.00	0.07	0.06	0.05	0.00	0.07	0.02	0.05	0.08	0.08	0.00	0.00	0.00	0.04
0.00	0.00	0.00	0.00	0.00	0.00	0.00	0.00	0.00	0.00	0.00	0.00	0.00	0.00
0.03	0.03	0.12	0.05	0.01	0.08	0.01	0.07	0.14	0.06	0.01	0.01	0.00	0.01
0.47	0.44	0.58	0.59	0.53	0.64	0.35	0.70	0.83	0.53	0.61	0.44	0.45	0.58
0.01	0.01	0.01	0.01	0.01	0.02	0.00	0.01	0.02	0.02	0.01	0.00	0.00	0.00
72.89	*74.72*	*78.77*	*78.34*	*75.06*	*79.95*	*74.49*	*75.97*	*79.67*	*78.64*	*73.45*	*77.72*	*76.64*	*78.93*
0.201	*0.186*	*0.245*	*0.252*	*0.223*	*0.273*	*0.146*	*0.297*	*0.352*	*0.227*	*0.259*	*0.184*	*0.188*	*0.244*
72.69	**74.53**	**78.52**	**78.09**	**74.84**	**79.68**	**74.34**	**75.67**	**79.32**	**78.42**	**73.19**	**77.53**	**76.45**	**78.69**
0.291	0.291	0.296	0.297	0.291	0.307	0.289	0.287	0.307	0.304	0.279	0.308	0.302	0.312
0.000	0.000	0.000	0.000	0.000	0.000	0.000	0.000	0.000	0.000	0.000	0.000	0.000	0.000
0.001	0.019	0.001	0.000	0.001	0.003	0.001	0.007	0.003	0.005	0.000	0.001	0.001	0.001
0.270	0.279	0.275	0.270	0.312	0.306	0.317	0.295	0.292	0.298	0.311	0.289	0.301	0.297
0.000	0.000	0.000	0.000	0.000	0.000	0.000	0.000	0.000	0.000	0.000	0.000	0.000	0.000
0.000	0.008	0.002	0.003	0.000	0.004	0.001	0.003	0.002	0.002	0.001	0.001	0.000	0.000
0.026	0.019	0.051	0.051	0.012	0.028	0.008	0.026	0.034	0.028	0.013	0.029	0.019	0.026
0.000	0.000	0.001	0.001	0.001	0.001	0.000	0.001	0.002	0.001	0.000	0.000	0.001	0.000
0.000	0.000	0.000	0.000	0.000	0.000	0.001	0.000	0.001	0.001	0.002	0.001	0.000	0.001
0.000	0.003	0.002	0.003	0.000	0.002	0.000	0.002	0.002	0.002	0.000	0.000	0.000	0.000
0.000	0.000	0.000	0.000	0.000	0.000	0.000	0.000	0.000	0.000	0.000	0.000	0.000	0.000
0.000	0.001	0.001	0.000	0.000	0.001	0.000	0.000	0.001	0.001	0.000	0.000	0.000	0.000
0.000	0.000	0.000	0.000	0.000	0.000	0.000	0.000	0.000	0.000	0.000	0.000	0.000	0.000

0.000	0.000	0.001	0.001	0.000	0.001	0.000	0.001	0.002	0.001	0.000	0.000	0.000	0.000
0.0247	0.0230	0.0303	0.0312	0.0277	0.0336	0.0183	0.0369	0.0436	0.0279	0.0322	0.0229	0.0235	0.0304
0.000	0.000	0.000	0.000	0.000	0.001	0.000	0.000	0.000	0.000	0.000	0.000	0.000	0.000

0.581	0.583	0.592	0.593	0.582	0.613	0.577	0.574	0.613	0.608	0.557	0.615	0.605	0.624
0.000	0.000	0.000	0.000	0.000	0.000	0.001	0.000	0.000	0.000	0.000	0.000	0.000	0.000
0.001	0.019	0.001	0.000	0.001	0.003	0.001	0.007	0.003	0.005	0.000	0.001	0.001	0.001
0.540	0.558	0.551	0.539	0.624	0.611	0.634	0.589	0.585	0.595	0.622	0.577	0.602	0.594
0.000	0.000	0.000	0.000	0.000	0.000	0.000	0.000	0.000	0.000	0.000	0.000	0.000	0.000
0.000	0.008	0.002	0.003	0.000	0.004	0.001	0.003	0.002	0.002	0.001	0.001	0.000	0.000
0.052	0.038	0.103	0.103	0.024	0.056	0.016	0.053	0.067	0.056	0.026	0.058	0.039	0.053
0.000	0.000	0.001	0.001	0.001	0.001	0.000	0.001	0.002	0.001	0.000	0.000	0.001	0.000
0.000	0.000	0.000	0.000	0.000	0.000	0.001	0.000	0.001	0.001	0.002	0.001	0.000	0.001
0.000	0.003	0.002	0.003	0.000	0.002	0.000	0.002	0.002	0.002	0.000	0.000	0.000	0.000
0.000	0.000	0.000	0.000	0.000	0.000	0.000	0.000	0.000	0.000	0.000	0.000	0.000	0.000
0.000	0.001	0.001	0.000	0.000	0.001	0.000	0.000	0.001	0.001	0.000	0.000	0.000	0.000
0.000	0.000	0.000	0.000	0.000	0.000	0.000	0.000	0.000	0.000	0.000	0.000	0.000	0.000
0.001	0.001	0.003	0.001	0.000	0.002	0.000	0.001	0.003	0.001	0.000	0.000	0.000	0.000

1.453	1.456	1.479	1.483	1.455	1.534	1.443	1.435	1.533	1.520	1.393	1.538	1.512	1.560
0.000	0.000	0.000	0.000	0.000	0.000	0.001	0.000	0.000	0.000	0.000	0.001	0.001	0.000
0.002	0.037	0.003	0.001	0.001	0.005	0.002	0.014	0.006	0.010	0.000	0.003	0.002	0.002
0.811	0.836	0.826	0.809	0.936	0.917	0.951	0.884	0.877	0.893	0.932	0.866	0.903	0.891
0.000	0.000	0.000	0.000	0.000	0.000	0.000	0.000	0.000	0.000	0.000	0.000	0.000	0.000
0.000	0.017	0.003	0.006	0.000	0.007	0.001	0.007	0.003	0.003	0.001	0.001	0.000	0.001
0.078	0.056	0.154	0.154	0.036	0.084	0.024	0.079	0.101	0.084	0.038	0.087	0.058	0.079
0.000	0.000	0.001	0.001	0.001	0.001	0.000	0.001	0.002	0.001	0.000	0.000	0.001	0.000
0.000	0.000	0.000	0.000	0.000	0.000	0.001	0.000	0.001	0.001	0.002	0.001	0.000	0.001
0.000	0.003	0.002	0.003	0.000	0.002	0.000	0.002	0.002	0.002	0.000	0.000	0.000	0.000
0.000	0.000	0.000	0.000	0.000	0.000	0.000	0.000	0.000	0.000	0.000	0.000	0.000	0.000
0.000	0.001	0.001	0.000	0.000	0.001	0.000	0.000	0.001	0.001	0.000	0.000	0.000	0.000
0.000	0.000	0.000	0.000	0.000	0.000	0.000	0.000	0.000	0.000	0.000	0.000	0.000	0.000

0.000	0.000	0.001	0.001	0.000	0.001	0.000	0.001	0.002	0.001	0.000	0.000	0.000	0.000
0.0247	0.0230	0.0303	0.0312	0.0277	0.0336	0.0183	0.0369	0.0436	0.0279	0.0322	0.0229	0.0235	0.0304
0.000	0.000	0.000	0.000	0.000	0.001	0.000	0.000	0.000	0.000	0.000	0.000	0.000	0.000
2.331	2.397	2.455	2.442	2.416	2.535	2.414	2.403	2.505	2.501	2.351	2.484	2.465	2.519
1.716	*1.669*	*1.629*	*1.638*	*1.655*	*1.578*	*1.657*	*1.664*	*1.597*	*1.599*	*1.701*	*1.610*	*1.623*	*1.588*
W5-D1A_ca	**W5-D1A_ca**	**W5-F1A_ca**	**W5-F1A_ca**	**W5-F1A_ca**	**W5-F1A_ca**	**W5-F1A_ca**	**W5-F1A_ca**	**W5-F1A_ca**	**W5-F1A_ca**	**W5-F1A_ca**	**W5-F1A_ca**	**W5-F1A_ca**	**W5-F1A_ca**
0.997	0.972	0.964	0.972	0.964	0.968	0.956	0.955	0.979	0.972	0.948	0.990	0.981	0.991
0.000	0.000	0.000	0.000	0.000	0.000	0.001	0.000	0.000	0.000	0.000	0.001	0.001	0.000
0.001	0.031	0.002	0.001	0.001	0.004	0.002	0.011	0.005	0.008	0.000	0.002	0.002	0.002
0.927	0.930	0.897	0.883	1.033	0.965	1.051	0.981	0.934	0.952	1.058	0.929	0.977	0.943
0.000	0.001	0.000	0.000	0.000	0.000	0.000	0.000	0.000	0.000	0.000	0.000	0.000	0.000
0.000	0.014	0.003	0.005	0.000	0.006	0.001	0.006	0.003	0.003	0.001	0.001	0.000	0.000
0.089	0.063	0.167	0.168	0.040	0.089	0.026	0.088	0.108	0.089	0.043	0.093	0.063	0.084
0.000	0.001	0.001	0.001	0.002	0.002	0.001	0.001	0.003	0.002	0.000	0.000	0.001	0.000
0.000	0.000	0.000	0.000	0.000	0.000	0.001	0.000	0.001	0.001	0.003	0.001	0.000	0.002
0.000	0.005	0.004	0.005	0.000	0.003	0.000	0.003	0.003	0.003	0.000	0.000	0.000	0.000
0.000	0.000	0.000	0.000	0.000	0.000	0.000	0.000	0.000	0.000	0.000	0.000	0.000	0.000
0.000	0.001	0.001	0.001	0.000	0.001	0.000	0.001	0.001	0.001	0.000	0.000	0.000	0.001
0.000	0.000	0.000	0.000	0.000	0.000	0.000	0.000	0.000	0.000	0.000	0.000	0.000	0.000
0.001	0.001	0.004	0.002	0.000	0.003	0.000	0.002	0.005	0.002	0.001	0.000	0.000	0.000
0.042	0.038	0.049	0.051	0.046	0.053	0.030	0.061	0.070	0.045	0.055	0.037	0.038	0.048
0.001	0.001	0.001	0.001	0.000	0.001	0.000	0.000	0.001	0.001	0.000	0.000	0.000	0.000
1.02	1.02	1.08	1.07	1.08	1.07	1.08	1.08	1.06	1.05	1.11	1.03	1.04	1.03
1.00	1.00	0.97	0.97	0.96	0.97	0.96	0.97	0.98	0.98	0.95	0.99	0.98	0.99
ok	ok	ok	ok	ok	ok	ok	ok	ok	ok	excess	ok	ok	ok
ok	ok	ok	ok	ok	ok	ok	ok	ok	ok	ok	ok	ok	ok
menor	menor	menor	menor	menor	menor	menor	menor	menor	menor	menor	menor	menor	menor

W5-F1A_ca	W5-F1A_ca	W5-F1A_ca	W5-F1A_ca	W5-F1A_ca	W5-F1A_ca	W5-F1A_ca	W5-F1A_ca	W5-F1A_ca	W5-F1A_ca	W5-F1A_ca	W5-F1A_ca	W5-F1A_ca	W5-F1A_ca
13	**14**	**15**	**17**	**18**	**19**	**20**	**21**	**30**	**31**	**34**	**35**	**36**	**38**
43.64	43.08	43.56	40.02	43.39	40.68	40.74	38.89	38.37	43.36	43.01	41.86	42.13	41.33
0.03	0.00	0.05	0.04	0.00	0.02	0.00	0.02	0.07	0.01	0.01	0.02	0.00	0.02
0.20	0.44	0.11	7.58	1.08	2.65	0.16	3.05	1.43	0.51	0.19	0.12	0.10	0.19
24.41	26.94	26.92	22.47	26.33	24.75	22.93	22.05	21.06	27.28	27.33	27.50	26.34	29.78
0.01	0.00	0.00	0.00	0.00	0.00	0.00	0.01	0.01	0.03	0.00	0.01	0.01	0.00
0.34	0.47	0.30	0.89	0.16	0.09	0.14	0.23	0.14	0.41	0.43	0.45	0.06	0.00
13.59	8.82	9.39	13.39	8.55	12.94	13.72	13.65	14.93	10.12	9.93	9.05	10.00	6.38
0.01	0.00	0.01	0.00	0.03	0.00	0.00	0.02	0.00	0.01	0.03	0.02	0.01	0.01
0.04	0.01	0.06	0.00	0.08	0.02	0.00	0.03	0.06	0.00	0.03	0.07	0.00	0.09
0.12	0.04	0.07	0.11	0.05	0.14	0.02	0.09	0.07	0.07	0.24	0.07	0.02	0.01
0.00	0.00	0.00	0.00	0.00	0.03	0.00	0.00	0.06	0.00	0.04	0.00	0.00	0.00
0.10	0.01	0.00	0.00	0.00	0.00	0.00	0.00	0.00	0.05	0.19	0.02	0.00	0.04
0.00	0.00	0.00	0.00	0.00	0.00	0.00	0.00	0.00	0.00	0.00	0.00	0.00	0.00
0.06	0.11	0.08	0.07	0.14	0.04	0.07	0.12	0.05	0.12	0.11	0.07	0.06	0.04
0.53	0.44	0.58	0.40	0.50	0.43	0.58	0.46	0.34	0.53	0.61	0.42	0.36	0.51
0.00	0.01	0.00	0.00	0.00	0.00	0.00	0.01	0.00	0.01	0.02	0.00	0.01	0.00
82.43	*79.71*	*80.48*	*84.33*	*79.66*	*81.14*	*77.71*	*77.98*	*75.93*	*81.84*	*81.53*	*79.03*	*78.44*	*77.76*
0.221	*0.188*	*0.244*	*0.171*	*0.210*	*0.180*	*0.242*	*0.195*	*0.143*	*0.226*	*0.260*	*0.179*	*0.153*	*0.216*
82.21	**79.52**	**80.23**	**84.16**	**79.45**	**80.96**	**77.47**	**77.78**	**75.79**	**81.62**	**81.27**	**78.85**	**78.29**	**77.54**
0.307	0.303	0.307	0.282	0.306	0.287	0.287	0.274	0.270	0.305	0.303	0.295	0.297	0.291
0.000	0.000	0.000	0.000	0.000	0.000	0.000	0.000	0.000	0.000	0.000	0.000	0.000	0.000
0.003	0.007	0.002	0.126	0.018	0.044	0.003	0.051	0.024	0.008	0.003	0.002	0.002	0.003
0.239	0.264	0.264	0.220	0.258	0.243	0.225	0.216	0.207	0.268	0.268	0.270	0.258	0.292
0.000	0.000	0.000	0.000	0.000	0.000	0.000	0.000	0.000	0.000	0.000	0.000	0.000	0.000
0.004	0.006	0.004	0.011	0.002	0.001	0.002	0.003	0.002	0.005	0.005	0.006	0.001	0.000
0.085	0.055	0.059	0.084	0.054	0.081	0.086	0.085	0.093	0.063	0.062	0.057	0.063	0.040
0.000	0.000	0.000	0.000	0.001	0.000	0.000	0.000	0.000	0.000	0.001	0.000	0.000	0.000
0.001	0.000	0.001	0.000	0.001	0.000	0.000	0.000	0.001	0.000	0.000	0.001	0.000	0.001
0.002	0.001	0.001	0.002	0.001	0.002	0.000	0.002	0.001	0.001	0.004	0.001	0.000	0.000
0.000	0.000	0.000	0.000	0.000	0.000	0.000	0.000	0.000	0.000	0.000	0.000	0.000	0.000
0.001	0.000	0.000	0.000	0.000	0.000	0.000	0.000	0.000	0.000	0.002	0.000	0.000	0.000
0.000	0.000	0.000	0.000	0.000	0.000	0.000	0.000	0.000	0.000	0.000	0.000	0.000	0.000

0.001	0.001	0.001	0.001	0.002	0.000	0.001	0.001	0.001	0.001	0.001	0.001	0.001	0.000
0.0277	0.0233	0.0305	0.0213	0.0262	0.0225	0.0303	0.0240	0.0179	0.0281	0.0319	0.0223	0.0188	0.0271
0.000	0.000	0.000	0.000	0.000	0.000	0.000	0.000	0.000	0.000	0.001	0.000	0.000	0.000
0.615	0.607	0.614	0.564	0.611	0.573	0.574	0.548	0.541	0.611	0.606	0.590	0.594	0.582
0.000	0.000	0.001	0.001	0.000	0.000	0.000	0.000	0.001	0.000	0.000	0.000	0.000	0.000
0.003	0.007	0.002	0.126	0.018	0.044	0.003	0.051	0.024	0.008	0.003	0.002	0.002	0.003
0.479	0.528	0.528	0.441	0.516	0.485	0.450	0.433	0.413	0.535	0.536	0.539	0.517	0.584
0.000	0.000	0.000	0.000	0.000	0.000	0.000	0.000	0.000	0.000	0.000	0.000	0.000	0.000
0.004	0.006	0.004	0.011	0.002	0.001	0.002	0.003	0.002	0.005	0.005	0.006	0.001	0.000
0.170	0.110	0.118	0.168	0.107	0.162	0.172	0.171	0.187	0.127	0.124	0.113	0.125	0.080
0.000	0.000	0.000	0.000	0.001	0.000	0.000	0.000	0.000	0.000	0.001	0.000	0.000	0.000
0.001	0.000	0.001	0.000	0.001	0.000	0.000	0.000	0.001	0.000	0.000	0.001	0.000	0.001
0.002	0.001	0.001	0.002	0.001	0.002	0.000	0.002	0.001	0.001	0.004	0.001	0.000	0.000
0.000	0.000	0.000	0.000	0.000	0.000	0.000	0.000	0.000	0.000	0.000	0.000	0.000	0.000
0.001	0.000	0.000	0.000	0.000	0.000	0.000	0.000	0.000	0.000	0.002	0.000	0.000	0.000
0.000	0.000	0.000	0.000	0.000	0.000	0.000	0.000	0.000	0.000	0.000	0.000	0.000	0.000
0.001	0.002	0.002	0.002	0.003	0.001	0.002	0.003	0.001	0.003	0.002	0.001	0.001	0.001
1.537	1.517	1.534	1.410	1.528	1.433	1.435	1.370	1.351	1.527	1.515	1.474	1.484	1.456
0.001	0.000	0.001	0.001	0.000	0.000	0.000	0.000	0.001	0.000	0.000	0.000	0.000	0.000
0.007	0.015	0.004	0.252	0.036	0.088	0.005	0.101	0.048	0.017	0.006	0.004	0.003	0.006
0.718	0.793	0.792	0.661	0.775	0.728	0.675	0.649	0.620	0.803	0.804	0.809	0.775	0.876
0.000	0.000	0.000	0.000	0.000	0.000	0.000	0.000	0.000	0.001	0.000	0.000	0.000	0.000
0.008	0.012	0.007	0.022	0.004	0.002	0.004	0.006	0.004	0.010	0.011	0.011	0.001	0.000
0.255	0.166	0.176	0.252	0.161	0.243	0.258	0.256	0.280	0.190	0.187	0.170	0.188	0.120
0.000	0.000	0.000	0.000	0.001	0.000	0.000	0.000	0.000	0.000	0.001	0.000	0.000	0.000
0.001	0.000	0.001	0.000	0.001	0.000	0.000	0.000	0.001	0.000	0.000	0.001	0.000	0.001
0.002	0.001	0.001	0.002	0.001	0.002	0.000	0.002	0.001	0.001	0.004	0.001	0.000	0.000
0.000	0.000	0.000	0.000	0.000	0.000	0.000	0.000	0.000	0.000	0.000	0.000	0.000	0.000
0.001	0.000	0.000	0.000	0.000	0.000	0.000	0.000	0.000	0.000	0.002	0.000	0.000	0.000
0.000	0.000	0.000	0.000	0.000	0.000	0.000	0.000	0.000	0.000	0.000	0.000	0.000	0.000

0.001	0.001	0.001	0.001	0.002	0.000	0.001	0.001	0.001	0.001	0.001	0.001	0.001	0.000
0.0277	0.0233	0.0305	0.0213	0.0262	0.0225	0.0303	0.0240	0.0179	0.0281	0.0319	0.0223	0.0188	0.0271
0.000	0.000	0.000	0.000	0.000	0.000	0.000	0.000	0.000	0.000	0.001	0.000	0.000	0.000
2.517	2.492	2.503	2.590	2.495	2.487	2.362	2.375	2.298	2.537	2.516	2.462	2.443	2.448
1.589	*1.605*	*1.598*	*1.545*	*1.603*	*1.608*	*1.693*	*1.685*	*1.740*	*1.577*	*1.590*	*1.625*	*1.637*	*1.634*
W5-F1A_ca	**W5-F1A_ca**	**W5-F1A_ca**	**W5-F1A_ca**	**W5-F1A_ca**	**W5-F1A_ca**	**W5-F1A_ca**	**W5-F1A_ca**	**W5-F1A_ca**	**W5-F1A_ca**	**W5-F1A_ca**	**W5-F1A_ca**	**W5-F1A_ca**	**W5-F1A_ca**
0.977	0.974	0.981	0.871	0.980	0.922	0.972	0.923	0.941	0.963	0.964	0.958	0.972	0.952
0.001	0.000	0.001	0.001	0.000	0.000	0.000	0.000	0.002	0.000	0.000	0.000	0.000	0.000
0.005	0.012	0.003	0.195	0.029	0.071	0.005	0.085	0.041	0.013	0.005	0.003	0.003	0.005
0.761	0.848	0.844	0.681	0.828	0.781	0.762	0.729	0.719	0.844	0.853	0.876	0.846	0.955
0.000	0.000	0.000	0.000	0.000	0.000	0.000	0.000	0.000	0.001	0.000	0.000	0.000	0.000
0.007	0.009	0.006	0.017	0.003	0.002	0.003	0.005	0.003	0.008	0.009	0.009	0.001	0.000
0.270	0.177	0.188	0.259	0.172	0.261	0.291	0.288	0.325	0.200	0.198	0.184	0.205	0.131
0.000	0.000	0.000	0.000	0.001	0.000	0.000	0.001	0.000	0.000	0.001	0.001	0.000	0.000
0.001	0.000	0.001	0.000	0.002	0.000	0.000	0.001	0.001	0.000	0.001	0.001	0.000	0.002
0.004	0.001	0.002	0.003	0.002	0.004	0.001	0.003	0.002	0.002	0.007	0.002	0.001	0.000
0.000	0.000	0.000	0.000	0.000	0.000	0.000	0.000	0.001	0.000	0.000	0.000	0.000	0.000
0.001	0.000	0.000	0.000	0.000	0.000	0.000	0.000	0.000	0.001	0.003	0.000	0.000	0.001
0.000	0.000	0.000	0.000	0.000	0.000	0.000	0.000	0.000	0.000	0.000	0.000	0.000	0.000
0.002	0.004	0.003	0.002	0.005	0.001	0.003	0.004	0.002	0.004	0.004	0.002	0.002	0.001
0.044	0.037	0.049	0.033	0.042	0.036	0.051	0.040	0.031	0.044	0.051	0.036	0.031	0.044
0.000	0.000	0.000	0.000	0.000	0.000	0.000	0.001	0.000	0.000	0.001	0.000	0.001	0.000
1.05	1.04	1.05	0.96	1.01	1.05	1.06	1.03	1.06	1.06	1.07	1.08	1.06	1.09
0.98	0.99	0.98	1.07	1.01	0.99	0.98	1.01	0.98	0.98	0.97	0.96	0.97	0.96
ok	ok	ok	ok	ok	ok	ok	ok	ok	ok	ok	ok	ok	ok
ok	ok	ok	ok	ok	ok	ok	ok	ok	ok	ok	ok	ok	ok
menor	menor	menor	menor	menor	menor	menor	menor	menor	menor	menor	menor	menor	menor

W5-F1A_ca	W5-F1A_ca	W5-F1A_ca	W5-F1A_ca	W5-F1A_ca	W5-F1A_ca	W5-F1A_ca	W6-B7A_ca	W6-B7A_ca	W6-B7A_ca	W6-B7A_ca	W6-B7A_ca	W6-B7A_ca	W6-B7A_ca
39	**40**	**41**	**42**	**43**	**44**	**45**	**6**	**8**	**11**	**13**	**14**	**15**	**17**
41.87	41.17	40.67	40.81	38.17	41.39	40.48	36.24	37.65	39.81	23.35	40.05	39.73	39.66
0.01	0.00	0.00	0.00	0.00	0.00	0.02	0.01	0.04	0.00	0.02	0.00	0.00	0.00
0.15	0.24	0.15	0.32	1.19	0.45	0.00	5.58	0.40	2.38	8.39	0.06	0.04	0.07
30.47	27.18	25.91	25.66	24.92	26.88	26.14	29.59	23.63	29.41	27.78	23.43	30.17	29.51
0.02	0.01	0.05	0.04	0.02	0.00	0.00	0.01	0.01	0.02	0.06	0.01	0.00	0.02
0.00	0.11	0.16	0.27	0.19	0.27	0.02	0.03	0.00	0.08	0.09	0.00	0.00	0.00
1.15	9.68	11.31	9.02	10.57	9.87	11.61	5.37	10.49	5.51	15.15	12.03	1.13	2.78
0.00	0.02	0.01	0.00	0.00	0.01	0.00	0.04	0.00	0.06	0.08	0.05	0.03	0.00
0.01	0.02	0.00	0.09	0.07	0.00	0.00	0.00	0.05	0.01	0.00	0.04	0.04	0.04
0.02	0.07	0.09	0.13	0.13	0.11	0.00	0.03	0.03	0.06	3.29	0.05	0.03	0.03
0.00	0.00	0.01	0.05	0.00	0.02	0.00	0.00	0.00	0.00	0.14	0.00	0.00	0.00
0.02	0.03	0.05	0.13	0.00	0.14	0.04	0.00	0.04	0.00	0.30	0.00	0.00	0.00
0.00	0.00	0.00	0.00	0.00	0.00	0.00	0.00	0.00	0.00	0.00	0.00	0.00	0.00
0.00	0.07	0.12	0.05	0.08	0.08	0.01	0.03	0.02	0.04	0.06	0.08	0.03	0.03
0.57	0.30	0.68	0.44	0.29	0.48	0.49	0.47	0.34	0.40	0.10	0.70	0.68	0.54
0.00	0.01	0.02	0.00	0.00	0.01	0.00	0.00	0.01	0.01	0.03	0.01	0.02	0.02
73.64	*78.26*	*78.58*	*76.36*	*74.96*	*79.07*	*78.18*	*76.75*	*72.05*	*77.12*	*78.19*	*75.85*	*71.25*	*72.04*
0.240	*0.129*	*0.292*	*0.184*	*0.120*	*0.204*	*0.206*	*0.199*	*0.144*	*0.170*	*0.048*	*0.295*	*0.292*	*0.230*
73.40	**78.13**	**78.28**	**76.17**	**74.84**	**78.86**	**77.97**	**76.55**	**71.91**	**76.95**	**78.14**	**75.55**	**70.96**	**71.81**
0.295	0.290	0.287	0.288	0.269	0.292	0.285	0.255	0.265	0.280	0.165	0.282	0.280	0.279
0.000	0.000	0.000	0.000	0.000	0.000	0.000	0.000	0.000	0.000	0.000	0.000	0.000	0.000
0.003	0.004	0.002	0.005	0.020	0.008	0.000	0.093	0.007	0.040	0.140	0.001	0.001	0.001
0.299	0.267	0.254	0.252	0.244	0.264	0.256	0.290	0.232	0.288	0.272	0.230	0.296	0.289
0.000	0.000	0.000	0.000	0.000	0.000	0.000	0.000	0.000	0.000	0.000	0.000	0.000	0.000
0.000	0.001	0.002	0.003	0.002	0.003	0.000	0.000	0.000	0.001	0.001	0.000	0.000	0.000
0.007	0.061	0.071	0.056	0.066	0.062	0.073	0.034	0.066	0.034	0.095	0.075	0.007	0.017
0.000	0.000	0.000	0.000	0.000	0.000	0.000	0.001	0.000	0.002	0.002	0.001	0.001	0.000
0.000	0.000	0.000	0.001	0.001	0.000	0.000	0.000	0.001	0.000	0.000	0.001	0.001	0.001
0.000	0.001	0.002	0.002	0.002	0.002	0.000	0.000	0.001	0.001	0.059	0.001	0.000	0.000
0.000	0.000	0.000	0.000	0.000	0.000	0.000	0.000	0.000	0.000	0.001	0.000	0.000	0.000
0.000	0.000	0.000	0.001	0.000	0.001	0.000	0.000	0.000	0.000	0.003	0.000	0.000	0.000
0.000	0.000	0.000	0.000	0.000	0.000	0.000	0.000	0.000	0.000	0.000	0.000	0.000	0.000

0.000	0.001	0.001	0.001	0.001	0.001	0.000	0.000	0.000	0.000	0.001	0.001	0.000	0.000
0.0300	0.0158	0.0360	0.0229	0.0150	0.0252	0.0257	0.0248	0.0177	0.0210	0.0052	0.0367	0.0360	0.0283
0.000	0.000	0.000	0.000	0.000	0.000	0.000	0.000	0.000	0.000	0.001	0.000	0.001	0.001

0.590	0.580	0.573	0.575	0.538	0.583	0.570	0.511	0.530	0.561	0.329	0.564	0.560	0.559
0.000	0.000	0.000	0.000	0.000	0.000	0.000	0.000	0.000	0.000	0.000	0.000	0.000	0.000
0.003	0.004	0.002	0.005	0.020	0.008	0.000	0.093	0.007	0.040	0.140	0.001	0.001	0.001
0.598	0.533	0.508	0.503	0.489	0.527	0.513	0.580	0.463	0.577	0.545	0.460	0.592	0.579
0.000	0.000	0.001	0.001	0.000	0.000	0.000	0.000	0.000	0.000	0.001	0.000	0.000	0.000
0.000	0.001	0.002	0.003	0.002	0.003	0.000	0.000	0.000	0.001	0.001	0.000	0.000	0.000
0.014	0.121	0.142	0.113	0.132	0.124	0.145	0.067	0.131	0.069	0.190	0.151	0.014	0.035
0.000	0.000	0.000	0.000	0.000	0.000	0.000	0.001	0.000	0.002	0.002	0.001	0.001	0.000
0.000	0.000	0.000	0.001	0.001	0.000	0.000	0.000	0.001	0.000	0.000	0.001	0.001	0.001
0.000	0.001	0.002	0.002	0.002	0.002	0.000	0.000	0.001	0.001	0.059	0.001	0.000	0.000
0.000	0.000	0.000	0.000	0.000	0.000	0.000	0.000	0.000	0.000	0.001	0.000	0.000	0.000
0.000	0.000	0.000	0.001	0.000	0.001	0.000	0.000	0.000	0.000	0.003	0.000	0.000	0.000
0.000	0.000	0.000	0.000	0.000	0.000	0.000	0.000	0.000	0.000	0.000	0.000	0.000	0.000
0.000	0.002	0.003	0.001	0.002	0.002	0.000	0.001	0.000	0.001	0.001	0.002	0.001	0.001

1.475	1.450	1.433	1.438	1.344	1.458	1.426	1.277	1.326	1.402	0.823	1.411	1.399	1.397
0.000	0.000	0.000	0.000	0.000	0.000	0.000	0.000	0.001	0.000	0.000	0.000	0.000	0.000
0.005	0.008	0.005	0.010	0.039	0.015	0.000	0.186	0.013	0.079	0.279	0.002	0.001	0.002
0.896	0.800	0.762	0.755	0.733	0.791	0.769	0.871	0.695	0.865	0.817	0.689	0.888	0.868
0.000	0.000	0.001	0.001	0.000	0.000	0.000	0.000	0.000	0.000	0.001	0.000	0.000	0.000
0.000	0.003	0.004	0.007	0.005	0.007	0.001	0.001	0.000	0.002	0.002	0.000	0.000	0.000
0.022	0.182	0.213	0.169	0.199	0.185	0.218	0.101	0.197	0.103	0.285	0.226	0.021	0.052
0.000	0.000	0.000	0.000	0.000	0.000	0.000	0.001	0.000	0.002	0.002	0.001	0.001	0.000
0.000	0.000	0.000	0.001	0.001	0.000	0.000	0.000	0.001	0.000	0.000	0.001	0.001	0.001
0.000	0.001	0.002	0.002	0.002	0.002	0.000	0.000	0.001	0.001	0.059	0.001	0.000	0.000
0.000	0.000	0.000	0.000	0.000	0.000	0.000	0.000	0.000	0.000	0.001	0.000	0.000	0.000
0.000	0.000	0.000	0.001	0.000	0.001	0.000	0.000	0.000	0.000	0.003	0.000	0.000	0.000
0.000	0.000	0.000	0.000	0.000	0.000	0.000	0.000	0.000	0.000	0.000	0.000	0.000	0.000

0.000	0.001	0.001	0.001	0.001	0.001	0.000	0.000	0.000	0.000	0.001	0.001	0.000	0.000
0.0300	0.0158	0.0360	0.0229	0.0150	0.0252	0.0257	0.0248	0.0177	0.0210	0.0052	0.0367	0.0360	0.0283
0.000	0.000	0.000	0.000	0.000	0.000	0.000	0.000	0.000	0.000	0.001	0.000	0.001	0.001
2.384	2.437	2.403	2.374	2.317	2.448	2.402	2.424	2.225	2.445	2.270	2.313	2.294	2.307
1.678	*1.641*	*1.665*	*1.685*	*1.726*	*1.634*	*1.665*	*1.650*	*1.797*	*1.636*	*1.762*	*1.729*	*1.744*	*1.734*
W5-F1A_ca	**W5-F1A_ca**	**W5-F1A_ca**	**W5-F1A_ca**	**W5-F1A_ca**	**W5-F1A_ca**	**W5-F1A_ca**	**W6-B7A_ca**	**W6-B7A_ca**	**W6-B7A_ca**	**W6-B7A_ca**	**W6-B7A_ca**	**W6-B7A_ca**	**W6-B7A_ca**
0.990	0.952	0.954	0.969	0.928	0.953	0.950	0.843	0.953	0.918	0.580	0.976	0.976	0.969
0.000	0.000	0.000	0.000	0.000	0.000	0.001	0.000	0.001	0.000	0.000	0.000	0.000	0.000
0.004	0.006	0.004	0.009	0.034	0.012	0.000	0.153	0.012	0.065	0.246	0.002	0.001	0.002
1.003	0.875	0.846	0.848	0.844	0.862	0.854	0.958	0.833	0.944	0.960	0.795	1.032	1.003
0.000	0.000	0.001	0.001	0.000	0.000	0.000	0.000	0.000	0.000	0.001	0.000	0.000	0.000
0.000	0.002	0.003	0.006	0.004	0.005	0.000	0.001	0.000	0.002	0.002	0.000	0.000	0.000
0.024	0.199	0.236	0.190	0.229	0.202	0.242	0.111	0.236	0.113	0.334	0.261	0.025	0.060
0.000	0.001	0.000	0.000	0.000	0.000	0.000	0.002	0.000	0.002	0.003	0.002	0.001	0.000
0.000	0.000	0.000	0.002	0.002	0.000	0.000	0.000	0.001	0.000	0.000	0.001	0.001	0.001
0.000	0.002	0.003	0.004	0.004	0.003	0.000	0.001	0.001	0.002	0.103	0.001	0.001	0.001
0.000	0.000	0.000	0.001	0.000	0.000	0.000	0.000	0.000	0.000	0.002	0.000	0.000	0.000
0.000	0.001	0.001	0.002	0.000	0.002	0.001	0.000	0.001	0.000	0.005	0.000	0.000	0.000
0.000	0.000	0.000	0.000	0.000	0.000	0.000	0.000	0.000	0.000	0.000	0.000	0.000	0.000
0.000	0.002	0.004	0.002	0.003	0.003	0.000	0.001	0.001	0.001	0.002	0.003	0.001	0.001
0.050	0.026	0.060	0.039	0.026	0.041	0.043	0.041	0.032	0.034	0.009	0.064	0.063	0.049
0.000	0.001	0.001	0.000	0.000	0.000	0.000	0.000	0.001	0.001	0.001	0.000	0.001	0.001
1.03	1.08	1.09	1.06	1.09	1.08	1.10	1.07	1.07	1.06	1.41	1.06	1.06	1.07
0.99	0.96	0.96	0.98	0.96	0.97	0.95	1.00	0.97	0.98	0.83	0.98	0.98	0.97
ok	ok	ok	ok	ok	ok	ok	ok	ok	ok	excess	ok	ok	ok
ok	ok	ok	ok	ok	ok	ok	ok	ok	ok	ok	ok	ok	ok
menor	menor	menor	menor	menor	menor	menor	menor	menor	menor	menor	menor	menor	menor

W6-B7A_ca	W6-B7A_ca	W6-B7A_ca	W6-B7A_ca	W6-B7A_ca	W6-B7A_ca	W6-B7A_ca	W6-B7A_ca	W6-B7A_ca	W6-B7A_ca	W6-B7A_ca	W6-B7A_ca	W6-B7A_ca	W6-B7A_ca
18	**19**	**21**	**22**	**23**	**24**	**25**	**28**	**29**	**31**	**32**	**33**	**34**	**43**
37.70	40.59	36.77	39.89	38.74	40.47	38.41	38.93	38.34	40.44	38.25	35.25	13.60	38.52
0.00	0.01	0.01	0.00	0.00	0.00	0.03	0.00	0.03	0.00	0.01	0.06	0.08	0.03
0.02	0.07	5.19	0.07	0.04	0.04	0.11	0.00	0.01	0.03	0.87	3.53	4.33	0.41
24.28	31.67	29.37	29.71	26.92	31.07	30.51	31.01	32.00	29.78	29.85	28.80	18.09	26.51
0.00	0.00	0.00	0.00	0.00	0.00	0.00	0.00	0.00	0.00	0.00	0.01	0.08	0.03
0.01	0.00	0.00	0.02	0.02	0.02	0.00	0.00	0.00	0.00	0.04	0.00	0.14	0.00
11.33	1.69	2.18	2.93	7.43	0.74	1.45	1.75	1.57	3.16	3.88	4.56	33.91	7.89
0.00	0.00	0.04	0.01	0.00	0.02	0.02	0.02	0.01	0.01	0.02	0.02	0.09	0.01
0.02	0.00	0.03	0.04	0.05	0.03	0.07	0.00	0.03	0.04	0.01	0.04	0.02	0.00
0.02	0.02	0.09	0.02	0.02	0.01	0.00	0.02	0.04	0.09	0.01	0.04	5.70	0.01
0.00	0.01	0.00	0.00	0.00	0.00	0.00	0.00	0.00	0.01	0.00	0.00	0.14	0.00
0.02	0.00	0.00	0.00	0.00	0.00	0.00	0.04	0.02	0.01	0.02	0.00	0.55	0.03
0.00	0.00	0.00	0.00	0.00	0.00	0.00	0.00	0.00	0.00	0.00	0.00	0.00	0.00
0.02	0.01	0.03	0.01	0.02	0.01	0.01	0.02	0.01	0.01	0.02	0.04	0.07	0.02
0.41	0.53	0.46	0.78	0.57	0.48	0.64	0.52	0.65	0.38	0.48	0.44	0.70	0.54
0.01	0.01	0.01	0.00	0.01	0.00	0.01	0.00	0.00	0.01	0.01	0.01	0.03	0.01
73.20	*73.95*	*73.53*	*72.85*	*73.16*	*72.25*	*70.61*	*71.65*	*72.05*	*73.33*	*72.81*	*72.14*	*76.90*	*73.35*
0.174	*0.223*	*0.198*	*0.329*	*0.243*	*0.204*	*0.269*	*0.217*	*0.273*	*0.162*	*0.203*	*0.187*	*0.302*	*0.228*
73.03	**73.73**	**73.33**	**72.52**	**72.92**	**72.04**	**70.34**	**71.44**	**71.77**	**73.17**	**72.61**	**71.95**	**76.60**	**73.12**
0.266	0.286	0.259	0.281	0.273	0.285	0.271	0.274	0.270	0.285	0.269	0.248	0.096	0.271
0.000	0.000	0.000	0.000	0.000	0.000	0.000	0.000	0.000	0.000	0.000	0.000	0.001	0.000
0.000	0.001	0.086	0.001	0.001	0.001	0.002	0.000	0.000	0.000	0.015	0.059	0.072	0.007
0.238	0.311	0.288	0.291	0.264	0.305	0.299	0.304	0.314	0.292	0.293	0.282	0.177	0.260
0.000	0.000	0.000	0.000	0.000	0.000	0.000	0.000	0.000	0.000	0.000	0.000	0.001	0.000
0.000	0.000	0.000	0.000	0.000	0.000	0.000	0.000	0.000	0.000	0.000	0.000	0.002	0.000
0.071	0.011	0.014	0.018	0.047	0.005	0.009	0.011	0.010	0.020	0.024	0.029	0.212	0.049
0.000	0.000	0.001	0.000	0.000	0.001	0.001	0.000	0.000	0.000	0.000	0.001	0.002	0.000
0.000	0.000	0.000	0.001	0.001	0.000	0.001	0.000	0.000	0.001	0.000	0.001	0.000	0.000
0.000	0.000	0.002	0.000	0.000	0.000	0.000	0.000	0.001	0.002	0.000	0.001	0.102	0.000
0.000	0.000	0.000	0.000	0.000	0.000	0.000	0.000	0.000	0.000	0.000	0.000	0.001	0.000
0.000	0.000	0.000	0.000	0.000	0.000	0.000	0.000	0.000	0.000	0.000	0.000	0.005	0.000
0.000	0.000	0.000	0.000	0.000	0.000	0.000	0.000	0.000	0.000	0.000	0.000	0.000	0.000

0.000	0.000	0.000	0.000	0.000	0.000	0.000	0.000	0.000	0.000	0.000	0.000	0.001	0.000
0.0214	0.0276	0.0244	0.0410	0.0301	0.0255	0.0334	0.0272	0.0342	0.0201	0.0253	0.0232	0.0368	0.0282
0.000	0.000	0.000	0.000	0.000	0.000	0.000	0.000	0.000	0.000	0.000	0.000	0.001	0.000

0.531	0.572	0.518	0.562	0.546	0.570	0.541	0.548	0.540	0.570	0.539	0.497	0.192	0.543
0.000	0.000	0.000	0.000	0.000	0.000	0.000	0.000	0.000	0.000	0.000	0.001	0.001	0.000
0.000	0.001	0.086	0.001	0.001	0.001	0.002	0.000	0.000	0.000	0.015	0.059	0.072	0.007
0.476	0.621	0.576	0.583	0.528	0.609	0.599	0.608	0.628	0.584	0.586	0.565	0.355	0.520
0.000	0.000	0.000	0.000	0.000	0.000	0.000	0.000	0.000	0.000	0.000	0.000	0.001	0.000
0.000	0.000	0.000	0.000	0.000	0.000	0.000	0.000	0.000	0.000	0.000	0.000	0.002	0.000
0.142	0.021	0.027	0.037	0.093	0.009	0.018	0.022	0.020	0.040	0.049	0.057	0.425	0.099
0.000	0.000	0.001	0.000	0.000	0.001	0.001	0.000	0.000	0.000	0.000	0.001	0.002	0.000
0.000	0.000	0.000	0.001	0.001	0.000	0.001	0.000	0.000	0.001	0.000	0.001	0.000	0.000
0.000	0.000	0.002	0.000	0.000	0.000	0.000	0.000	0.001	0.002	0.000	0.001	0.102	0.000
0.000	0.000	0.000	0.000	0.000	0.000	0.000	0.000	0.000	0.000	0.000	0.000	0.001	0.000
0.000	0.000	0.000	0.000	0.000	0.000	0.000	0.000	0.000	0.000	0.000	0.000	0.005	0.000
0.000	0.000	0.000	0.000	0.000	0.000	0.000	0.000	0.000	0.000	0.000	0.000	0.000	0.000
0.000	0.000	0.001	0.000	0.000	0.000	0.000	0.000	0.000	0.000	0.000	0.001	0.002	0.001

1.328	1.430	1.295	1.405	1.364	1.425	1.353	1.371	1.350	1.425	1.347	1.242	0.479	1.357
0.000	0.000	0.000	0.000	0.000	0.000	0.001	0.000	0.001	0.000	0.000	0.001	0.002	0.001
0.001	0.002	0.173	0.002	0.001	0.001	0.004	0.000	0.000	0.001	0.029	0.117	0.144	0.014
0.714	0.932	0.864	0.874	0.792	0.914	0.898	0.912	0.942	0.876	0.878	0.847	0.532	0.780
0.000	0.000	0.000	0.000	0.000	0.000	0.000	0.000	0.000	0.000	0.000	0.000	0.002	0.001
0.000	0.000	0.000	0.001	0.000	0.001	0.000	0.000	0.000	0.000	0.001	0.000	0.004	0.000
0.213	0.032	0.041	0.055	0.140	0.014	0.027	0.033	0.029	0.059	0.073	0.086	0.637	0.148
0.000	0.000	0.001	0.000	0.000	0.001	0.001	0.000	0.000	0.000	0.000	0.001	0.002	0.000
0.000	0.000	0.000	0.001	0.001	0.000	0.001	0.000	0.000	0.001	0.000	0.001	0.000	0.000
0.000	0.000	0.002	0.000	0.000	0.000	0.000	0.000	0.001	0.002	0.000	0.001	0.102	0.000
0.000	0.000	0.000	0.000	0.000	0.000	0.000	0.000	0.000	0.000	0.000	0.000	0.001	0.000
0.000	0.000	0.000	0.000	0.000	0.000	0.000	0.000	0.000	0.000	0.000	0.000	0.005	0.000
0.000	0.000	0.000	0.000	0.000	0.000	0.000	0.000	0.000	0.000	0.000	0.000	0.000	0.000

0.000	0.000	0.000	0.000	0.000	0.000	0.000	0.000	0.000	0.000	0.000	0.000	0.001	0.000
0.0214	0.0276	0.0244	0.0410	0.0301	0.0255	0.0334	0.0272	0.0342	0.0201	0.0253	0.0232	0.0368	0.0282
0.000	0.000	0.000	0.000	0.000	0.000	0.000	0.000	0.000	0.000	0.000	0.000	0.001	0.000
2.247	2.382	2.364	2.318	2.284	2.344	2.267	2.304	2.307	2.354	2.317	2.284	1.892	2.286
1.781	*1.679*	*1.692*	*1.726*	*1.751*	*1.707*	*1.764*	*1.736*	*1.734*	*1.699*	*1.726*	*1.751*	*2.114*	*1.750*
W6-B7A_ca	**W6-B7A_ca**	**W6-B7A_ca**	**W6-B7A_ca**	**W6-B7A_ca**	**W6-B7A_ca**	**W6-B7A_ca**	**W6-B7A_ca**	**W6-B7A_ca**	**W6-B7A_ca**	**W6-B7A_ca**	**W6-B7A_ca**	**W6-B7A_ca**	**W6-B7A_ca**
0.946	0.960	0.877	0.970	0.956	0.973	0.955	0.952	0.937	0.968	0.930	0.870	0.405	0.949
0.000	0.000	0.000	0.000	0.000	0.000	0.001	0.000	0.001	0.000	0.000	0.001	0.002	0.001
0.001	0.002	0.146	0.002	0.001	0.001	0.003	0.000	0.000	0.001	0.025	0.103	0.152	0.012
0.848	1.043	0.975	1.006	0.925	1.040	1.056	1.056	1.088	0.993	1.011	0.989	0.750	0.910
0.000	0.000	0.000	0.000	0.000	0.000	0.000	0.000	0.000	0.000	0.000	0.000	0.002	0.001
0.000	0.000	0.000	0.000	0.000	0.001	0.000	0.000	0.000	0.000	0.001	0.000	0.004	0.000
0.253	0.036	0.046	0.063	0.163	0.016	0.032	0.038	0.034	0.067	0.084	0.100	0.898	0.173
0.000	0.000	0.002	0.000	0.000	0.001	0.001	0.001	0.000	0.001	0.001	0.001	0.005	0.001
0.001	0.000	0.001	0.001	0.001	0.001	0.002	0.000	0.001	0.001	0.000	0.001	0.001	0.000
0.001	0.001	0.003	0.001	0.001	0.000	0.000	0.000	0.001	0.003	0.000	0.001	0.215	0.000
0.000	0.000	0.000	0.000	0.000	0.000	0.000	0.000	0.000	0.000	0.000	0.000	0.002	0.000
0.000	0.000	0.000	0.000	0.000	0.000	0.000	0.001	0.000	0.000	0.000	0.000	0.011	0.000
0.000	0.000	0.000	0.000	0.000	0.000	0.000	0.000	0.000	0.000	0.000	0.000	0.000	0.000
0.001	0.000	0.001	0.000	0.001	0.001	0.000	0.001	0.000	0.000	0.001	0.002	0.003	0.001
0.038	0.046	0.041	0.071	0.053	0.043	0.059	0.047	0.059	0.034	0.044	0.041	0.078	0.049
0.001	0.000	0.001	0.000	0.000	0.000	0.000	0.000	0.000	0.000	0.000	0.000	0.002	0.001
1.10	1.08	1.03	1.07	1.09	1.06	1.09	1.10	1.13	1.06	1.10	1.10	1.89	1.09
0.95	0.96	1.02	0.97	0.96	0.97	0.96	0.95	0.94	0.97	0.96	0.97	0.56	0.96
excess	ok	ok	ok	ok	ok	ok	ok	excess	ok	ok	ok	excess	ok
ok	ok	ok	ok	ok	ok	ok	ok	ok	ok	ok	ok	ok	ok
menor	menor	menor	menor	menor	menor	menor	menor	menor	menor	menor	menor	maior	menor

W6-B7B_ca	W6-B7B_ca	W6-B7B_ca	W6-B7B_ca	W6-B7B_ca	W6-B7B_ca	W6-B7B_ca	W6-B7B_ca	W6-B7B_ca	W6-B7B_ca	W6-B7B_ca	W6-B7B_ca	W6-B7B_ca	W6-B7B_ca
1	**7**	**9**	**12**	**14**	**15**	**16**	**17**	**19**	**20**	**25**	**28**	**29**	**30**
37.63	43.43	42.89	43.30	41.03	32.54	43.18	41.23	42.06	41.94	40.69	35.89	42.06	34.63
0.02	0.00	0.01	0.03	0.01	0.00	0.05	0.00	0.04	0.00	0.00	0.00	0.04	0.00
1.98	0.03	0.18	0.22	0.34	0.74	0.10	0.05	0.07	0.13	7.69	5.05	0.10	9.90
29.24	32.63	31.25	32.05	31.82	36.27	31.40	31.25	31.16	32.10	33.06	32.43	29.15	33.29
0.02	0.00	0.00	0.01	0.01	0.02	0.00	0.00	0.00	0.01	0.00	0.00	0.01	0.00
0.00	0.00	0.00	0.01	0.01	0.04	0.01	0.02	0.00	0.03	0.00	0.00	0.00	0.04
4.77	0.18	1.30	1.87	1.74	2.79	0.48	0.48	0.86	0.77	1.33	1.85	4.16	1.46
0.06	0.03	0.02	0.01	0.00	0.10	0.01	0.02	0.01	0.04	0.03	0.12	0.04	0.03
0.00	0.00	0.03	0.03	0.00	0.00	0.05	0.02	0.00	0.02	0.00	0.00	0.07	0.04
0.02	0.02	0.04	0.06	0.02	3.64	0.05	0.02	0.03	0.02	0.17	1.53	0.01	0.01
0.00	0.00	0.00	0.00	0.00	0.00	0.00	0.00	0.00	0.00	0.01	0.09	0.00	0.00
0.00	0.00	0.00	0.00	0.00	0.00	0.00	0.00	0.00	0.00	0.03	0.37	0.00	0.00
0.00	0.00	0.00	0.00	0.00	0.48	0.00	0.00	0.00	0.00	0.00	0.00	0.00	0.00
0.28	0.02	0.03	0.04	0.01	0.02	0.02	0.02	0.04	0.07	0.10	0.11	0.08	0.07
0.33	0.60	0.33	0.70	0.55	0.36	0.58	0.56	0.51	0.36	0.46	0.42	0.66	0.39
0.00	0.00	0.01	0.01	0.00	0.00	0.00	0.00	0.01	0.00	0.01	0.02	0.01	0.00
73.70	*76.29*	*75.44*	*77.67*	*74.89*	*76.35*	*75.27*	*73.01*	*74.16*	*74.85*	*82.92*	*77.22*	*75.73*	*79.20*
0.140	*0.253*	*0.139*	*0.296*	*0.231*	*0.152*	*0.245*	*0.237*	*0.219*	*0.152*	*0.193*	*0.181*	*0.277*	*0.163*
73.56	**76.03**	**75.30**	**77.38**	**74.66**	**76.20**	**75.03**	**72.77**	**73.94**	**74.69**	**82.73**	**77.04**	**75.45**	**79.04**
0.265	0.306	0.302	0.305	0.289	0.229	0.304	0.290	0.296	0.295	0.287	0.253	0.296	0.244
0.000	0.000	0.000	0.000	0.000	0.000	0.000	0.000	0.000	0.000	0.000	0.000	0.000	0.000
0.033	0.000	0.003	0.004	0.006	0.012	0.002	0.001	0.001	0.002	0.128	0.084	0.002	0.165
0.287	0.320	0.307	0.314	0.312	0.356	0.308	0.306	0.306	0.315	0.324	0.318	0.286	0.326
0.000	0.000	0.000	0.000	0.000	0.000	0.000	0.000	0.000	0.000	0.000	0.000	0.000	0.000
0.000	0.000	0.000	0.000	0.000	0.001	0.000	0.000	0.000	0.000	0.000	0.000	0.000	0.000
0.030	0.001	0.008	0.012	0.011	0.017	0.003	0.003	0.005	0.005	0.008	0.012	0.026	0.009
0.001	0.001	0.000	0.000	0.000	0.002	0.000	0.001	0.000	0.001	0.001	0.003	0.001	0.001
0.000	0.000	0.000	0.000	0.000	0.000	0.001	0.000	0.000	0.000	0.000	0.000	0.001	0.001
0.000	0.000	0.001	0.001	0.000	0.065	0.001	0.000	0.000	0.000	0.003	0.027	0.000	0.000
0.000	0.000	0.000	0.000	0.000	0.000	0.000	0.000	0.000	0.000	0.000	0.001	0.000	0.000
0.000	0.000	0.000	0.000	0.000	0.000	0.000	0.000	0.000	0.000	0.000	0.004	0.000	0.000
0.000	0.000	0.000	0.000	0.000	0.008	0.000	0.000	0.000	0.000	0.000	0.000	0.000	0.000

0.003	0.000	0.000	0.000	0.000	0.000	0.000	0.000	0.000	0.001	0.001	0.001	0.001	0.001
0.0175	0.0316	0.0172	0.0368	0.0288	0.0189	0.0307	0.0295	0.0271	0.0191	0.0239	0.0220	0.0345	0.0204
0.000	0.000	0.000	0.000	0.000	0.000	0.000	0.000	0.000	0.000	0.000	0.001	0.000	0.000

0.530	0.612	0.604	0.610	0.578	0.458	0.608	0.581	0.593	0.591	0.573	0.506	0.593	0.488
0.000	0.000	0.000	0.000	0.000	0.000	0.001	0.000	0.001	0.000	0.000	0.000	0.000	0.000
0.033	0.000	0.003	0.004	0.006	0.012	0.002	0.001	0.001	0.002	0.128	0.084	0.002	0.165
0.573	0.640	0.613	0.629	0.624	0.711	0.616	0.613	0.611	0.630	0.649	0.636	0.572	0.653
0.000	0.000	0.000	0.000	0.000	0.000	0.000	0.000	0.000	0.000	0.000	0.000	0.000	0.000
0.000	0.000	0.000	0.000	0.000	0.001	0.000	0.000	0.000	0.000	0.000	0.000	0.000	0.000
0.060	0.002	0.016	0.023	0.022	0.035	0.006	0.006	0.011	0.010	0.017	0.023	0.052	0.018
0.001	0.001	0.000	0.000	0.000	0.002	0.000	0.001	0.000	0.001	0.001	0.003	0.001	0.001
0.000	0.000	0.000	0.000	0.000	0.000	0.001	0.000	0.000	0.000	0.000	0.000	0.001	0.001
0.000	0.000	0.001	0.001	0.000	0.065	0.001	0.000	0.000	0.000	0.003	0.027	0.000	0.000
0.000	0.000	0.000	0.000	0.000	0.000	0.000	0.000	0.000	0.000	0.000	0.001	0.000	0.000
0.000	0.000	0.000	0.000	0.000	0.000	0.000	0.000	0.000	0.000	0.000	0.004	0.000	0.000
0.000	0.000	0.000	0.000	0.000	0.016	0.000	0.000	0.000	0.000	0.000	0.000	0.000	0.000
0.006	0.000	0.001	0.001	0.000	0.000	0.000	0.000	0.001	0.002	0.002	0.002	0.002	0.001

1.326	1.530	1.511	1.525	1.445	1.146	1.521	1.452	1.482	1.477	1.433	1.264	1.482	1.220
0.000	0.000	0.000	0.001	0.000	0.000	0.001	0.000	0.001	0.000	0.000	0.000	0.001	0.000
0.066	0.001	0.006	0.007	0.011	0.025	0.003	0.002	0.002	0.004	0.256	0.168	0.003	0.330
0.860	0.960	0.920	0.943	0.936	1.067	0.924	0.919	0.917	0.945	0.973	0.954	0.858	0.979
0.000	0.000	0.000	0.000	0.000	0.000	0.000	0.000	0.000	0.000	0.000	0.000	0.000	0.000
0.000	0.000	0.000	0.000	0.000	0.001	0.000	0.000	0.000	0.001	0.000	0.000	0.000	0.001
0.090	0.003	0.024	0.035	0.033	0.052	0.009	0.009	0.016	0.014	0.025	0.035	0.078	0.027
0.001	0.001	0.000	0.000	0.000	0.002	0.000	0.001	0.000	0.001	0.001	0.003	0.001	0.001
0.000	0.000	0.000	0.000	0.000	0.000	0.001	0.000	0.000	0.000	0.000	0.000	0.001	0.001
0.000	0.000	0.001	0.001	0.000	0.065	0.001	0.000	0.000	0.000	0.003	0.027	0.000	0.000
0.000	0.000	0.000	0.000	0.000	0.000	0.000	0.000	0.000	0.000	0.000	0.001	0.000	0.000
0.000	0.000	0.000	0.000	0.000	0.000	0.000	0.000	0.000	0.000	0.000	0.004	0.000	0.000
0.000	0.000	0.000	0.000	0.000	0.008	0.000	0.000	0.000	0.000	0.000	0.000	0.000	0.000

0.003	0.000	0.000	0.000	0.000	0.000	0.000	0.000	0.000	0.001	0.001	0.001	0.001	0.001
0.0175	0.0316	0.0172	0.0368	0.0288	0.0189	0.0307	0.0295	0.0271	0.0191	0.0239	0.0220	0.0345	0.0204
0.000	0.000	0.000	0.000	0.000	0.000	0.000	0.000	0.000	0.000	0.000	0.001	0.000	0.000
2.338	2.480	2.454	2.495	2.412	2.358	2.445	2.369	2.405	2.434	2.680	2.445	2.407	2.549
1.711	*1.613*	*1.630*	*1.603*	*1.658*	*1.697*	*1.636*	*1.688*	*1.663*	*1.643*	*1.493*	*1.636*	*1.662*	*1.569*
W6-B7B_ca	**W6-B7B_ca**	**W6-B7B_ca**	**W6-B7B_ca**	**W6-B7B_ca**	**W6-B7B_ca**	**W6-B7B_ca**	**W6-B7B_ca**	**W6-B7B_ca**	**W6-B7B_ca**	**W6-B7B_ca**	**W6-B7B_ca**	**W6-B7B_ca**	**W6-B7B_ca**
0.907	0.987	0.985	0.978	0.959	0.778	0.995	0.981	0.986	0.971	0.856	0.827	0.985	0.766
0.000	0.000	0.000	0.001	0.000	0.000	0.001	0.000	0.001	0.000	0.000	0.000	0.001	0.000
0.056	0.001	0.005	0.006	0.009	0.021	0.003	0.001	0.002	0.004	0.191	0.138	0.003	0.259
0.981	1.033	0.999	1.008	1.035	1.207	1.008	1.035	1.016	1.035	0.968	1.040	0.950	1.025
0.000	0.000	0.000	0.000	0.000	0.000	0.000	0.000	0.000	0.000	0.000	0.000	0.000	0.000
0.000	0.000	0.000	0.000	0.000	0.001	0.000	0.000	0.000	0.001	0.000	0.000	0.000	0.001
0.102	0.004	0.026	0.037	0.036	0.059	0.010	0.010	0.018	0.016	0.025	0.038	0.087	0.029
0.003	0.001	0.001	0.000	0.000	0.004	0.000	0.001	0.001	0.002	0.001	0.005	0.002	0.001
0.000	0.000	0.001	0.001	0.000	0.000	0.001	0.000	0.000	0.000	0.000	0.000	0.002	0.001
0.001	0.000	0.001	0.002	0.001	0.110	0.001	0.001	0.001	0.001	0.005	0.045	0.000	0.000
0.000	0.000	0.000	0.000	0.000	0.000	0.000	0.000	0.000	0.000	0.000	0.001	0.000	0.000
0.000	0.000	0.000	0.000	0.000	0.000	0.000	0.000	0.000	0.000	0.000	0.006	0.000	0.000
0.000	0.000	0.000	0.000	0.000	0.026	0.000	0.000	0.000	0.000	0.000	0.000	0.000	0.000
0.010	0.001	0.001	0.001	0.000	0.001	0.001	0.001	0.001	0.003	0.003	0.004	0.003	0.002
0.030	0.051	0.028	0.059	0.048	0.032	0.050	0.050	0.045	0.031	0.036	0.036	0.057	0.032
0.000	0.000	0.000	0.000	0.000	0.000	0.000	0.000	0.001	0.000	0.000	0.001	0.000	0.000
1.10	1.04	1.03	1.05	1.07	1.41	1.02	1.05	1.04	1.06	1.00	1.14	1.04	1.06
0.96	0.99	0.99	0.98	0.97	0.80	1.00	0.98	0.99	0.97	1.05	0.96	0.99	1.02
ok	ok	ok	ok	ok	excess	ok	ok	ok	ok	ok	excess	ok	ok
ok	ok	ok	ok	ok	ok	ok	ok	ok	ok	ok	ok	ok	ok
menor	menor	menor	menor	menor	menor	menor	menor	menor	menor	menor	menor	menor	menor

W6-B7B_ca	W6-B7B_ca	W6-B7B_ca	W6-C6_car	W6-C6_car	W6-C6_car	W6-C6_car	W6-C6_car	W6-C6_car	W6-C6_car	W6-C6_car	W6-C6_car	W6-C6_car	W6-C6_car
39	**40**	**41**	**1**	**2**	**3**	**4**	**5**	**6**	**7**	**8**	**9**	**10**	**11**
42.77	38.20	41.42	41.86	42.98	32.60	32.34	29.56	31.25	31.11	27.63	44.41	39.02	45.80
0.01	0.02	0.00	0.03	0.00	0.01	0.00	0.01	0.00	0.02	0.01	0.00	0.00	0.00
0.83	0.18	0.38	0.00	0.00	0.11	0.08	0.10	0.07	0.18	0.06	0.01	0.03	0.02
30.93	29.41	29.58	26.98	28.83	29.97	31.89	27.70	30.24	27.35	25.33	29.52	26.02	30.44
0.00	0.00	0.00	0.02	0.00	0.01	0.03	0.03	0.01	0.05	0.02	0.00	0.00	0.00
0.00	0.00	0.00	0.39	0.03	0.34	0.06	0.22	0.23	0.28	0.41	0.01	0.07	0.01
1.99	5.05	2.24	7.18	5.82	8.12	4.75	5.96	5.56	7.60	6.07	4.24	5.36	4.58
0.00	0.02	0.02	0.01	0.00	0.02	0.02	0.03	0.04	0.05	0.03	0.02	0.00	0.02
0.01	0.00	0.00	0.00	0.02	0.04	0.04	0.06	0.01	0.07	0.01	0.00	0.00	0.03
0.07	1.48	0.02	0.95	0.01	8.28	8.33	7.70	8.29	8.55	8.20	0.02	0.04	0.03
0.00	0.05	0.00	0.12	0.00	0.00	0.01	0.08	0.00	0.00	0.24	0.00	0.00	0.00
0.00	0.31	0.00	0.44	0.00	0.10	0.11	0.11	0.08	0.14	0.81	0.04	0.05	0.02
0.00	0.00	0.00	0.00	0.00	0.00	0.00	0.10	0.00	0.00	0.00	0.00	0.00	0.00
0.04	0.05	0.03	0.06	0.05	0.05	0.05	0.07	0.03	0.07	0.06	0.04	0.05	0.03
0.52	0.55	0.52	0.59	0.50	0.54	0.28	0.36	0.28	0.31	0.40	0.59	0.42	0.58
0.00	0.01	0.01	0.00	0.00	0.01	0.09	0.02	0.04	0.15	0.22	0.00	0.01	0.00
76.52	*74.67*	*73.58*	*77.98*	*77.58*	*79.57*	*77.42*	*71.45*	*75.48*	*75.28*	*68.85*	*78.24*	*70.41*	*80.92*
0.219	*0.234*	*0.220*	*0.249*	*0.211*	*0.231*	*0.136*	0.155	*0.126*	*0.165*	*0.218*	*0.249*	*0.178*	*0.245*
76.30	**74.44**	**73.36**	**77.73**	**77.37**	**79.33**	**77.28**	**71.29**	**75.35**	**75.12**	**68.63**	**78.00**	**70.24**	**80.67**
0.301	0.269	0.292	0.295	0.303	0.230	0.228	0.208	0.220	0.219	0.195	0.313	0.275	0.323
0.000	0.000	0.000	0.000	0.000	0.000	0.000	0.000	0.000	0.000	0.000	0.000	0.000	0.000
0.014	0.003	0.006	0.000	0.000	0.002	0.001	0.002	0.001	0.003	0.001	0.000	0.000	0.000
0.303	0.288	0.290	0.265	0.283	0.294	0.313	0.272	0.297	0.268	0.248	0.290	0.255	0.299
0.000	0.000	0.000	0.000	0.000	0.000	0.000	0.000	0.000	0.000	0.000	0.000	0.000	0.000
0.000	0.000	0.000	0.005	0.000	0.004	0.001	0.003	0.003	0.004	0.005	0.000	0.001	0.000
0.012	0.032	0.014	0.045	0.036	0.051	0.030	0.037	0.035	0.048	0.038	0.027	0.034	0.029
0.000	0.000	0.000	0.000	0.000	0.001	0.001	0.001	0.001	0.001	0.001	0.000	0.000	0.001
0.000	0.000	0.000	0.000	0.000	0.001	0.001	0.001	0.000	0.001	0.000	0.000	0.000	0.000
0.001	0.026	0.000	0.017	0.000	0.148	0.149	0.137	0.148	0.152	0.146	0.000	0.001	0.001
0.000	0.000	0.000	0.001	0.000	0.000	0.000	0.001	0.000	0.000	0.002	0.000	0.000	0.000
0.000	0.003	0.000	0.004	0.000	0.001	0.001	0.001	0.001	0.001	0.008	0.000	0.000	0.000
0.000	0.000	0.000	0.000	0.000	0.000	0.000	0.002	0.000	0.000	0.000	0.000	0.000	0.000

0.000	0.001	0.000	0.001	0.000	0.001	0.000	0.001	0.000	0.001	0.001	0.000	0.001	0.000
0.0273	0.0289	0.0273	0.0311	0.0263	0.0286	0.0145	0.0189	0.0146	0.0165	0.0211	0.0310	0.0221	0.0307
0.000	0.000	0.000	0.000	0.000	0.000	0.002	0.001	0.001	0.004	0.006	0.000	0.000	0.000

0.603	0.538	0.584	0.590	0.606	0.459	0.456	0.417	0.440	0.438	0.389	0.626	0.550	0.645
0.000	0.000	0.000	0.000	0.000	0.000	0.000	0.000	0.000	0.000	0.000	0.000	0.000	0.000
0.014	0.003	0.006	0.000	0.000	0.002	0.001	0.002	0.001	0.003	0.001	0.000	0.000	0.000
0.607	0.577	0.580	0.529	0.565	0.588	0.626	0.543	0.593	0.536	0.497	0.579	0.510	0.597
0.000	0.000	0.000	0.000	0.000	0.000	0.000	0.000	0.000	0.001	0.000	0.000	0.000	0.000
0.000	0.000	0.000	0.005	0.000	0.004	0.001	0.003	0.003	0.004	0.005	0.000	0.001	0.000
0.025	0.063	0.028	0.090	0.073	0.102	0.059	0.075	0.070	0.095	0.076	0.053	0.067	0.057
0.000	0.000	0.000	0.000	0.000	0.001	0.001	0.001	0.001	0.001	0.001	0.000	0.000	0.001
0.000	0.000	0.000	0.000	0.000	0.001	0.001	0.001	0.000	0.001	0.000	0.000	0.000	0.000
0.001	0.026	0.000	0.017	0.000	0.148	0.149	0.137	0.148	0.152	0.146	0.000	0.001	0.001
0.000	0.000	0.000	0.001	0.000	0.000	0.000	0.001	0.000	0.000	0.002	0.000	0.000	0.000
0.000	0.003	0.000	0.004	0.000	0.001	0.001	0.001	0.001	0.001	0.008	0.000	0.000	0.000
0.000	0.000	0.000	0.000	0.000	0.000	0.000	0.003	0.000	0.000	0.000	0.000	0.000	0.000
0.001	0.001	0.001	0.001	0.001	0.001	0.001	0.001	0.001	0.001	0.001	0.001	0.001	0.001

1.507	1.345	1.459	1.474	1.514	1.148	1.139	1.041	1.101	1.096	0.973	1.564	1.374	1.613
0.000	0.000	0.000	0.001	0.000	0.000	0.000	0.000	0.000	0.000	0.000	0.000	0.000	0.000
0.028	0.006	0.013	0.000	0.000	0.004	0.003	0.003	0.002	0.006	0.002	0.000	0.001	0.001
0.910	0.865	0.870	0.794	0.848	0.882	0.938	0.815	0.890	0.805	0.745	0.869	0.766	0.896
0.000	0.000	0.000	0.000	0.000	0.000	0.001	0.001	0.000	0.001	0.000	0.000	0.000	0.000
0.000	0.000	0.000	0.010	0.001	0.009	0.002	0.005	0.006	0.007	0.010	0.000	0.002	0.000
0.037	0.095	0.042	0.135	0.109	0.153	0.089	0.112	0.105	0.143	0.114	0.080	0.101	0.086
0.000	0.000	0.000	0.000	0.000	0.001	0.001	0.001	0.001	0.001	0.001	0.000	0.000	0.001
0.000	0.000	0.000	0.000	0.000	0.001	0.001	0.001	0.000	0.001	0.000	0.000	0.000	0.000
0.001	0.026	0.000	0.017	0.000	0.148	0.149	0.137	0.148	0.152	0.146	0.000	0.001	0.001
0.000	0.000	0.000	0.001	0.000	0.000	0.000	0.001	0.000	0.000	0.002	0.000	0.000	0.000
0.000	0.003	0.000	0.004	0.000	0.001	0.001	0.001	0.001	0.001	0.008	0.000	0.000	0.000
0.000	0.000	0.000	0.000	0.000	0.000	0.000	0.002	0.000	0.000	0.000	0.000	0.000	0.000

0.000	0.001	0.000	0.001	0.000	0.001	0.000	0.001	0.000	0.001	0.001	0.000	0.001	0.000
0.0273	0.0289	0.0273	0.0311	0.0263	0.0286	0.0145	0.0189	0.0146316	0.0164737	0.0210526	0.031	0.0221053	0.0306842
0.000	0.000	0.000	0.000	0.000	0.000	0.002	0.001	0.0011566	0.0041185	0.0061777	8.463E-05	0.0001975	0
2.470	2.328	2.372	2.421	2.460	2.331	2.314	2.111	2.245	2.204	1.989	2.499	2.234	2.583
1.619	*1.718*	*1.687*	*1.652*	*1.626*	*1.716*	*1.729*	*1.895*	*1.781*	*1.815*	*2.011*	*1.601*	*1.791*	*1.549*
W6-B7B_ca	**W6-B7B_ca**	**W6-B7B_ca**	**W6-C6_car**	**W6-C6_car**	**W6-C6_car**	**W6-C6_car**	**W6-C6_car**	**W6-C6_car**	**W6-C6_car**	**W6-C6_car**	**W6-C6_car**	**W6-C6_car**	**W6-C6_car**
0.976	0.925	0.984	0.974	0.985	0.788	0.788	0.789	0.784	0.795	0.783	1.002	0.984	0.999
0.000	0.001	0.000	0.001	0.000	0.000	0.000	0.000	0.000	0.001	0.000	0.000	0.000	0.000
0.022	0.005	0.011	0.000	0.000	0.003	0.002	0.003	0.002	0.005	0.002	0.000	0.001	0.001
0.982	0.991	0.979	0.874	0.920	1.009	1.081	1.030	1.057	0.973	0.999	0.927	0.914	0.925
0.000	0.000	0.000	0.001	0.000	0.000	0.001	0.001	0.000	0.001	0.001	0.000	0.000	0.000
0.000	0.000	0.000	0.008	0.001	0.007	0.001	0.005	0.005	0.006	0.010	0.000	0.002	0.000
0.040	0.109	0.047	0.149	0.118	0.175	0.103	0.141	0.124	0.173	0.153	0.085	0.120	0.089
0.000	0.001	0.001	0.001	0.000	0.001	0.001	0.001	0.002	0.002	0.001	0.001	0.000	0.001
0.000	0.000	0.000	0.000	0.000	0.001	0.001	0.002	0.000	0.002	0.000	0.000	0.000	0.001
0.002	0.045	0.001	0.028	0.000	0.253	0.257	0.260	0.263	0.277	0.294	0.000	0.001	0.001
0.000	0.001	0.000	0.001	0.000	0.000	0.000	0.001	0.000	0.000	0.003	0.000	0.000	0.000
0.000	0.005	0.000	0.007	0.000	0.002	0.002	0.002	0.001	0.002	0.016	0.001	0.001	0.000
0.000	0.000	0.000	0.000	0.000	0.000	0.000	0.006	0.000	0.000	0.000	0.000	0.000	0.000
0.001	0.002	0.001	0.002	0.002	0.002	0.002	0.003	0.001	0.003	0.003	0.001	0.002	0.001
0.044	0.050	0.046	0.051	0.043	0.049	0.025	0.036	0.026	0.030	0.042	0.050	0.040	0.048
0.000	0.001	0.000	0.000	0.000	0.000	0.004	0.001	0.002	0.007	0.012	0.000	0.000	0.000
1.03	1.15	1.03	1.07	1.04	1.45	1.45	1.45	1.45	1.44	1.48	1.02	1.04	1.02
1.00	0.93	0.99	0.97	0.98	0.79	0.79	0.79	0.79	0.80	0.78	1.00	0.99	1.00
ok	excess	ok	ok	ok	excess	excess	excess	excess	excess	excess	ok	ok	ok
ok	ok	ok	ok	ok	ok	ok	ok	ok	ok	ok	ok	ok	ok
menor	menor	menor	menor	menor	menor	menor	menor	menor	menor	menor	menor	menor	menor

W6-C6_car 12	W6-C6_car 13	W6-C6_car 14	W6-C6_car 15	W6-C6_car 16	W6-C6_car 17	W6-C6_car 18	W6-C6_car 19	W6-C6_car 20	W6-C6_car 21	W6-C6_car 22	W6-C6_car 23	W6-C6_car 24	W6-C6_car 25
31.06	31.37	28.34	43.63	28.71	37.05	42.10	31.60	30.90	29.40	30.07	31.02	30.22	28.61
0.04	0.00	0.04	0.01	0.02	0.00	0.01	0.00	0.04	0.02	0.02	0.01	0.00	0.02
0.07	0.10	0.00	0.01	0.00	0.14	0.05	0.07	0.13	0.75	0.06	0.07	0.09	0.00
29.74	29.86	31.74	30.01	32.20	27.94	28.57	31.24	29.23	27.71	29.41	30.76	28.23	30.00
0.02	0.00	0.05	0.00	0.05	0.00	0.00	0.00	0.02	0.01	0.01	0.00	0.00	0.00
0.37	0.48	0.00	0.00	0.00	0.11	0.01	0.15	0.22	0.16	0.36	0.55	0.36	0.00
7.13	7.32	2.41	4.57	2.32	1.77	2.89	6.73	9.19	8.30	7.88	6.73	9.36	5.15
0.07	0.06	0.01	0.00	0.02	0.03	0.01	0.04	0.05	0.05	0.02	0.06	0.06	0.01
0.00	0.08	0.00	0.07	0.01	0.03	0.08	0.04	0.14	0.05	0.08	0.10	0.08	0.00
8.71	7.79	9.44	0.05	10.15	0.66	0.03	7.75	8.23	7.51	7.72	8.12	8.24	7.48
0.00	0.04	1.12	0.01	0.85	0.10	0.03	0.11	0.07	0.05	0.06	0.00	0.04	1.80
0.10	0.16	3.23	0.00	2.61	0.52	0.00	0.36	0.15	0.23	0.11	0.11	0.15	3.70
0.00	0.00	0.00	0.00	0.00	0.00	0.00	0.00	0.00	0.25	0.00	0.00	0.00	0.00
0.04	0.04	0.12	0.03	0.08	0.04	0.03	0.05	0.11	0.14	0.07	0.09	0.09	0.10
0.48	0.50	0.30	0.75	0.35	0.29	0.47	0.41	0.18	0.35	0.14	0.53	0.59	0.42
0.06	0.01	0.01	0.01	0.02	0.00	0.00	0.02	0.02	0.29	0.04	0.02	0.03	0.08
77.25	*77.17*	*76.17*	*78.51*	*76.72*	*68.04*	*73.63*	*77.93*	*78.04*	*74.61*	*75.38*	*77.50*	*76.92*	*76.71*
0.216	*0.213*	*0.128*	*0.318*	*0.149*	*0.122*	*0.198*	*0.178*	*0.081*	*0.211*	*0.069*	*0.227*	*0.257*	*0.194*
77.03	**76.96**	**76.04**	**78.19**	**76.57**	**67.92**	**73.43**	**77.75**	**77.95**	**74.40**	**75.31**	**77.28**	**76.66**	**76.51**
0.219	0.221	0.200	0.307	0.202	0.261	0.297	0.223	0.218	0.207	0.212	0.219	0.213	0.202
0.000	0.000	0.000	0.000	0.000	0.000	0.000	0.000	0.000	0.000	0.000	0.000	0.000	0.000
0.001	0.002	0.000	0.000	0.000	0.002	0.001	0.001	0.002	0.012	0.001	0.001	0.002	0.000
0.292	0.293	0.311	0.294	0.316	0.274	0.280	0.306	0.287	0.272	0.288	0.302	0.277	0.294
0.000	0.000	0.000	0.000	0.000	0.000	0.000	0.000	0.000	0.000	0.000	0.000	0.000	0.000
0.005	0.006	0.000	0.000	0.000	0.001	0.000	0.002	0.003	0.002	0.004	0.007	0.005	0.000
0.045	0.046	0.015	0.029	0.015	0.011	0.018	0.042	0.058	0.052	0.049	0.042	0.059	0.032
0.002	0.002	0.000	0.000	0.000	0.001	0.000	0.001	0.001	0.001	0.001	0.001	0.001	0.000
0.000	0.001	0.000	0.001	0.000	0.000	0.001	0.001	0.002	0.001	0.001	0.001	0.001	0.000
0.155	0.139	0.168	0.001	0.181	0.012	0.001	0.138	0.147	0.134	0.138	0.145	0.147	0.133
0.000	0.000	0.007	0.000	0.006	0.001	0.000	0.001	0.000	0.000	0.000	0.000	0.000	0.012
0.001	0.001	0.031	0.000	0.025	0.005	0.000	0.003	0.001	0.002	0.001	0.001	0.001	0.036
0.000	0.000	0.000	0.000	0.000	0.000	0.000	0.000	0.000	0.004	0.000	0.000	0.000	0.000

0.000	0.000	0.001	0.000	0.001	0.000	0.000	0.001	0.001	0.001	0.001	0.001	0.001	0.001
0.0252	0.0264	0.0156	0.0395	0.0182	0.0153	0.0248	0.0217	0.0096	0.0184	0.0075	0.0278	0.0313	0.0220
0.002	0.000	0.000	0.000	0.000	0.000	0.000	0.001	0.001	0.008	0.001	0.001	0.001	0.002

0.438	0.442	0.399	0.615	0.404	0.522	0.593	0.445	0.435	0.414	0.424	0.437	0.426	0.403
0.001	0.000	0.001	0.000	0.000	0.000	0.000	0.000	0.001	0.000	0.000	0.000	0.000	0.000
0.001	0.002	0.000	0.000	0.000	0.002	0.001	0.001	0.002	0.012	0.001	0.001	0.002	0.000
0.583	0.586	0.623	0.589	0.632	0.548	0.560	0.613	0.573	0.543	0.577	0.603	0.554	0.588
0.000	0.000	0.001	0.000	0.001	0.000	0.000	0.000	0.000	0.000	0.000	0.000	0.000	0.000
0.005	0.006	0.000	0.000	0.000	0.001	0.000	0.002	0.003	0.002	0.004	0.007	0.005	0.000
0.089	0.092	0.030	0.057	0.029	0.022	0.036	0.084	0.115	0.104	0.099	0.084	0.117	0.064
0.002	0.002	0.000	0.000	0.000	0.001	0.000	0.001	0.001	0.001	0.001	0.001	0.001	0.000
0.000	0.001	0.000	0.001	0.000	0.000	0.001	0.001	0.002	0.001	0.001	0.001	0.001	0.000
0.155	0.139	0.168	0.001	0.181	0.012	0.001	0.138	0.147	0.134	0.138	0.145	0.147	0.133
0.000	0.000	0.007	0.000	0.006	0.001	0.000	0.001	0.000	0.000	0.000	0.000	0.000	0.012
0.001	0.001	0.031	0.000	0.025	0.005	0.000	0.003	0.001	0.002	0.001	0.001	0.001	0.036
0.000	0.000	0.000	0.000	0.000	0.000	0.000	0.000	0.000	0.008	0.000	0.000	0.000	0.000
0.001	0.001	0.002	0.001	0.002	0.001	0.001	0.001	0.002	0.003	0.001	0.002	0.002	0.002

1.094	1.105	0.998	1.537	1.011	1.305	1.483	1.113	1.088	1.036	1.059	1.093	1.065	1.008
0.001	0.000	0.001	0.000	0.000	0.000	0.000	0.000	0.001	0.000	0.000	0.000	0.000	0.000
0.002	0.003	0.000	0.000	0.000	0.005	0.002	0.002	0.004	0.025	0.002	0.002	0.003	0.000
0.875	0.879	0.934	0.883	0.948	0.822	0.840	0.919	0.860	0.815	0.865	0.905	0.831	0.883
0.000	0.000	0.001	0.000	0.001	0.000	0.000	0.000	0.000	0.000	0.000	0.000	0.000	0.000
0.009	0.012	0.000	0.000	0.000	0.003	0.000	0.004	0.005	0.004	0.009	0.014	0.009	0.000
0.134	0.138	0.045	0.086	0.044	0.033	0.054	0.126	0.173	0.156	0.148	0.126	0.176	0.097
0.002	0.002	0.000	0.000	0.000	0.001	0.000	0.001	0.001	0.001	0.001	0.001	0.001	0.000
0.000	0.001	0.000	0.001	0.000	0.000	0.001	0.001	0.002	0.001	0.001	0.001	0.001	0.000
0.155	0.139	0.168	0.001	0.181	0.012	0.001	0.138	0.147	0.134	0.138	0.145	0.147	0.133
0.000	0.000	0.007	0.000	0.006	0.001	0.000	0.001	0.000	0.000	0.000	0.000	0.000	0.012
0.001	0.001	0.031	0.000	0.025	0.005	0.000	0.003	0.001	0.002	0.001	0.001	0.001	0.036
0.000	0.000	0.000	0.000	0.000	0.000	0.000	0.000	0.000	0.004	0.000	0.000	0.000	0.000

0.000	0.000	0.001	0.000	0.001	0.000	0.000	0.001	0.001	0.001	0.001	0.001	0.001	0.001
0.0252105	0.0263684	0.0156316	0.0395263	0.0181579	0.0152632	0.0247895	0.0217368	0.0096316	0.0183684	0.0075263	0.0278421	0.0312632	0.022
0.0018054	0.0002539	0.0003667	0.0002257	0.0004795	0	0	0.000536	0.000536	0.0080395	0.0010719	0.0005642	0.0008181	0.0022849
2.261	2.267	2.180	2.489	2.207	2.179	2.370	2.298	2.280	2.167	2.221	2.276	2.220	2.157
1.769	*1.764*	*1.835*	*1.607*	*1.812*	*1.835*	*1.688*	*1.741*	*1.754*	*1.846*	*1.801*	*1.758*	*1.802*	*1.854*
W6-C6_car	**W6-C6_car**	**W6-C6_car**	**W6-C6_car**	**W6-C6_car**	**W6-C6_car**	**W6-C6_car**	**W6-C6_car**	**W6-C6_car**	**W6-C6_car**	**W6-C6_car**	**W6-C6_car**	**W6-C6_car**	**W6-C6_car**
0.774	0.780	0.733	0.988	0.733	0.958	1.001	0.775	0.764	0.765	0.763	0.768	0.767	0.747
0.001	0.000	0.001	0.000	0.000	0.000	0.000	0.000	0.001	0.000	0.001	0.000	0.000	0.000
0.002	0.003	0.000	0.000	0.000	0.004	0.001	0.002	0.004	0.023	0.002	0.002	0.003	0.000
1.032	1.033	1.143	0.946	1.145	1.006	0.946	1.067	1.006	1.003	1.039	1.061	0.998	1.091
0.001	0.000	0.001	0.000	0.001	0.000	0.000	0.000	0.001	0.000	0.000	0.000	0.000	0.000
0.008	0.010	0.000	0.000	0.000	0.002	0.000	0.003	0.005	0.004	0.008	0.012	0.008	0.000
0.158	0.162	0.055	0.092	0.053	0.041	0.061	0.147	0.202	0.192	0.178	0.148	0.211	0.120
0.003	0.003	0.000	0.000	0.001	0.001	0.000	0.002	0.002	0.002	0.001	0.003	0.003	0.001
0.000	0.002	0.000	0.002	0.000	0.001	0.002	0.001	0.003	0.001	0.002	0.002	0.002	0.000
0.275	0.245	0.309	0.002	0.328	0.022	0.001	0.241	0.258	0.247	0.248	0.254	0.265	0.247
0.000	0.001	0.013	0.000	0.010	0.001	0.000	0.001	0.001	0.001	0.001	0.000	0.000	0.022
0.002	0.003	0.057	0.000	0.046	0.009	0.000	0.006	0.003	0.004	0.002	0.002	0.003	0.066
0.000	0.000	0.000	0.000	0.000	0.000	0.000	0.000	0.000	0.015	0.000	0.000	0.000	0.000
0.001	0.002	0.005	0.001	0.003	0.002	0.001	0.002	0.004	0.005	0.003	0.003	0.003	0.004
0.045	0.047	0.029	0.064	0.033	0.028	0.042	0.038	0.017	0.034	0.014	0.049	0.056	0.041
0.003	0.000	0.001	0.000	0.001	0.000	0.000	0.001	0.001	0.015	0.002	0.001	0.001	0.004
1.48	1.46	1.58	1.04	1.59	1.09	1.01	1.47	1.48	1.48	1.48	1.49	1.49	1.55
0.78	0.78	0.73	0.99	0.73	0.96	1.00	0.78	0.77	0.79	0.76	0.77	0.77	0.75
excess	excess	excess	ok	excess	ok	ok	excess	excess	excess	excess	excess	excess	excess
ok	ok	ok	ok	ok	ok	ok	ok	ok	ok	ok	ok	ok	ok
menor	menor	menor	menor	menor	menor	menor	menor	menor	menor	menor	menor	menor	menor

W6-C6_car	W6-C6_car	W6-C6_car	W6-C6_car	W6-C6_car	W6-C6_car	W6-C6_car	W6-C6_car	W6-C6_car	W6-C6_car	W6-C6_car	W6-C6_car	W6-C6_car	W6-C6_car
26	**28**	**29**	**30**	**31**	**33**	**34**	**35**	**36**	**38**	**39**	**40**	**41**	**42**
30.46	43.33	43.38	30.16	30.66	43.93	42.35	30.64	30.46	25.11	21.82	29.41	29.67	30.12
0.01	0.02	0.01	0.00	0.02	0.00	0.04	0.03	0.00	0.04	0.07	0.03	0.00	0.01
0.05	0.04	0.00	0.00	0.04	0.08	0.01	0.23	0.09	0.10	0.18	0.04	0.01	0.10
28.43	32.27	30.55	30.36	30.73	30.85	32.03	25.62	25.78	20.65	16.85	25.20	26.27	26.02
0.00	0.00	0.00	0.00	0.00	0.00	0.00	0.07	0.09	0.16	0.30	0.15	0.11	0.07
0.28	0.02	0.00	0.13	0.14	0.01	0.02	0.25	0.49	0.32	0.63	0.22	0.68	0.28
10.05	2.36	2.41	6.52	8.27	1.48	1.47	12.55	13.88	26.84	35.04	17.58	12.97	12.81
0.01	0.00	0.00	0.03	0.04	0.01	0.01	0.03	0.05	0.04	0.03	0.02	0.03	0.00
0.08	0.01	0.04	0.10	0.11	0.07	0.04	0.04	0.12	0.04	0.04	0.04	0.10	0.00
8.40	0.03	0.05	7.83	8.61	0.01	0.01	7.77	7.87	6.64	5.51	7.48	7.69	8.06
0.06	0.00	0.00	0.63	0.25	0.02	0.00	0.02	0.00	0.02	0.00	0.03	0.00	0.00
0.19	0.00	0.00	1.47	0.65	0.01	0.01	0.07	0.05	0.19	0.13	0.21	0.11	0.10
0.00	0.00	0.00	0.00	0.00	0.00	0.00	0.00	0.00	0.21	0.15	0.00	0.00	0.00
0.09	0.09	0.04	0.12	0.16	0.03	0.03	0.12	0.06	0.18	0.20	0.05	0.04	0.05
0.46	0.52	0.52	0.53	0.19	0.59	0.41	0.60	0.34	0.27	0.32	0.45	0.54	0.46
0.01	0.01	0.00	0.03	0.04	0.00	0.00	0.02	0.01	0.02	0.02	0.01	0.01	0.01
77.95	*78.05*	*76.35*	*77.27*	*79.26*	*76.43*	*75.78*	*77.40*	*78.64*	*80.17*	*80.62*	*80.26*	*77.57*	*77.42*
0.196	*0.219*	*0.218*	*0.229*	*0.090*	*0.247*	*0.172*	*0.256*	*0.145*	*0.117*	*0.138*	*0.190*	*0.229*	*0.194*
77.75	**77.83**	**76.13**	**77.04**	**79.17**	**76.19**	**75.61**	**77.15**	**78.49**	**80.06**	**80.48**	**80.07**	**77.34**	**77.22**
0.215	0.305	0.306	0.212	0.216	0.309	0.298	0.216	0.215	0.177	0.154	0.207	0.209	0.212
0.000	0.000	0.000	0.000	0.000	0.000	0.000	0.000	0.000	0.000	0.000	0.000	0.000	0.000
0.001	0.001	0.000	0.000	0.001	0.001	0.000	0.004	0.002	0.002	0.003	0.001	0.000	0.002
0.279	0.316	0.300	0.298	0.301	0.303	0.314	0.251	0.253	0.202	0.165	0.247	0.258	0.255
0.000	0.000	0.000	0.000	0.000	0.000	0.000	0.000	0.001	0.001	0.002	0.001	0.001	0.000
0.004	0.000	0.000	0.002	0.002	0.000	0.000	0.003	0.006	0.004	0.008	0.003	0.009	0.003
0.063	0.015	0.015	0.041	0.052	0.009	0.009	0.079	0.087	0.168	0.219	0.110	0.081	0.080
0.000	0.000	0.000	0.001	0.001	0.000	0.000	0.001	0.001	0.001	0.001	0.000	0.001	0.000
0.001	0.000	0.001	0.001	0.002	0.001	0.001	0.001	0.002	0.001	0.001	0.001	0.001	0.000
0.150	0.000	0.001	0.140	0.154	0.000	0.000	0.138	0.140	0.118	0.098	0.133	0.137	0.144
0.000	0.000	0.000	0.004	0.002	0.000	0.000	0.000	0.000	0.000	0.000	0.000	0.000	0.000
0.002	0.000	0.000	0.014	0.006	0.000	0.000	0.001	0.000	0.002	0.001	0.002	0.001	0.001
0.000	0.000	0.000	0.000	0.000	0.000	0.000	0.000	0.000	0.003	0.002	0.000	0.000	0.000

0.001	0.001	0.000	0.001	0.002	0.000	0.000	0.001	0.001	0.002	0.002	0.001	0.000	0.000
0.0242	0.0271	0.0273	0.0276	0.0102	0.0309	0.0215	0.0315	0.0178	0.0141	0.0167	0.0235	0.0284	0.0241
0.000	0.000	0.000	0.001	0.001	0.000	0.000	0.001	0.000	0.001	0.001	0.000	0.000	0.000
0.429	0.610	0.611	0.425	0.432	0.619	0.597	0.432	0.429	0.354	0.307	0.414	0.418	0.424
0.000	0.000	0.000	0.000	0.000	0.000	0.001	0.000	0.000	0.001	0.001	0.000	0.000	0.000
0.001	0.001	0.000	0.000	0.001	0.001	0.000	0.004	0.002	0.002	0.003	0.001	0.000	0.002
0.558	0.633	0.599	0.595	0.603	0.605	0.628	0.503	0.506	0.405	0.330	0.494	0.515	0.510
0.000	0.000	0.000	0.000	0.000	0.000	0.000	0.001	0.001	0.002	0.004	0.002	0.002	0.001
0.004	0.000	0.000	0.002	0.002	0.000	0.000	0.003	0.006	0.004	0.008	0.003	0.009	0.003
0.126	0.029	0.030	0.082	0.104	0.019	0.018	0.157	0.174	0.336	0.439	0.220	0.162	0.160
0.000	0.000	0.000	0.001	0.001	0.000	0.000	0.001	0.001	0.001	0.001	0.000	0.001	0.000
0.001	0.000	0.001	0.001	0.002	0.001	0.001	0.001	0.002	0.001	0.001	0.001	0.001	0.000
0.150	0.000	0.001	0.140	0.154	0.000	0.000	0.138	0.140	0.118	0.098	0.133	0.137	0.144
0.000	0.000	0.000	0.004	0.002	0.000	0.000	0.000	0.000	0.000	0.000	0.000	0.000	0.000
0.002	0.000	0.000	0.014	0.006	0.000	0.000	0.001	0.000	0.002	0.001	0.002	0.001	0.001
0.000	0.000	0.000	0.000	0.000	0.000	0.000	0.000	0.000	0.007	0.005	0.000	0.000	0.000
0.002	0.002	0.001	0.003	0.003	0.001	0.001	0.003	0.001	0.004	0.004	0.001	0.001	0.001
1.073	1.526	1.528	1.062	1.080	1.547	1.492	1.079	1.073	0.884	0.769	1.036	1.045	1.061
0.000	0.000	0.000	0.000	0.000	0.000	0.001	0.001	0.000	0.001	0.001	0.001	0.000	0.000
0.002	0.001	0.000	0.000	0.001	0.003	0.000	0.007	0.003	0.003	0.006	0.001	0.000	0.003
0.836	0.949	0.899	0.893	0.904	0.908	0.942	0.754	0.759	0.607	0.496	0.741	0.773	0.766
0.000	0.000	0.000	0.000	0.000	0.000	0.000	0.001	0.002	0.003	0.006	0.003	0.002	0.001
0.007	0.001	0.000	0.003	0.003	0.000	0.000	0.006	0.012	0.008	0.016	0.006	0.017	0.007
0.189	0.044	0.045	0.123	0.155	0.028	0.028	0.236	0.261	0.504	0.658	0.330	0.244	0.241
0.000	0.000	0.000	0.001	0.001	0.000	0.000	0.001	0.001	0.001	0.001	0.000	0.001	0.000
0.001	0.000	0.001	0.001	0.002	0.001	0.001	0.001	0.002	0.001	0.001	0.001	0.001	0.000
0.150	0.000	0.001	0.140	0.154	0.000	0.000	0.138	0.140	0.118	0.098	0.133	0.137	0.144
0.000	0.000	0.000	0.004	0.002	0.000	0.000	0.000	0.000	0.000	0.000	0.000	0.000	0.000
0.002	0.000	0.000	0.014	0.006	0.000	0.000	0.001	0.000	0.002	0.001	0.002	0.001	0.001
0.000	0.000	0.000	0.000	0.000	0.000	0.000	0.000	0.000	0.003	0.002	0.000	0.000	0.000

0.001	0.001	0.000	0.001	0.002	0.000	0.000	0.001	0.001	0.002	0.002	0.001	0.000	0.000
0.0241579	0.0271053	0.0272632	0.0276316	0.0101579	0.0308947	0.0215263	0.0314737	0.0178421	0.0141053	0.0167368	0.0234737	0.0284211	0.0240526
0.0003103	0.0002257	2.821E-05	0.0009591	0.0010719	0	2.821E-05	0.0005078	0.0002821	0.0005642	0.0005642	0.0002539	0.0001693	0.0001693
2.249	2.510	2.461	2.229	2.305	2.472	2.454	2.211	2.245	2.131	2.048	2.243	2.207	2.212
1.778	*1.593*	*1.626*	*1.795*	*1.736*	*1.618*	*1.630*	*1.809*	*1.782*	*1.877*	*1.953*	*1.783*	*1.812*	*1.808*
W6-C6_car	**W6-C6_car**	**W6-C6_car**	**W6-C6_car**	**W6-C6_car**	**W6-C6_car**	**W6-C6_car**	**W6-C6_car**	**W6-C6_car**	**W6-C6_car**	**W6-C6_car**	**W6-C6_car**	**W6-C6_car**	**W6-C6_car**
0.763	0.973	0.994	0.763	0.750	1.001	0.973	0.781	0.765	0.664	0.601	0.739	0.757	0.767
0.000	0.000	0.000	0.000	0.001	0.000	0.001	0.001	0.000	0.001	0.002	0.001	0.000	0.000
0.001	0.001	0.000	0.000	0.001	0.002	0.000	0.007	0.003	0.003	0.006	0.001	0.000	0.003
0.992	1.009	0.974	1.069	1.046	0.979	1.024	0.909	0.901	0.760	0.645	0.881	0.934	0.923
0.000	0.000	0.000	0.000	0.000	0.000	0.000	0.002	0.002	0.004	0.008	0.004	0.003	0.002
0.006	0.000	0.000	0.003	0.003	0.000	0.000	0.006	0.011	0.007	0.015	0.005	0.015	0.006
0.224	0.047	0.049	0.147	0.180	0.030	0.030	0.284	0.310	0.631	0.857	0.393	0.294	0.290
0.001	0.000	0.000	0.001	0.002	0.000	0.000	0.001	0.002	0.002	0.001	0.001	0.001	0.000
0.002	0.000	0.001	0.003	0.003	0.002	0.001	0.001	0.003	0.001	0.001	0.001	0.003	0.000
0.266	0.001	0.001	0.251	0.266	0.000	0.000	0.251	0.250	0.222	0.192	0.238	0.248	0.260
0.001	0.000	0.000	0.007	0.003	0.000	0.000	0.000	0.000	0.000	0.000	0.000	0.000	0.000
0.003	0.000	0.000	0.025	0.011	0.000	0.000	0.001	0.001	0.003	0.002	0.004	0.002	0.002
0.000	0.000	0.000	0.000	0.000	0.000	0.000	0.000	0.000	0.013	0.009	0.000	0.000	0.000
0.003	0.003	0.001	0.005	0.006	0.001	0.001	0.005	0.002	0.007	0.008	0.002	0.002	0.002
0.043	0.043	0.044	0.050	0.018	0.050	0.035	0.057	0.032	0.026	0.033	0.042	0.051	0.043
0.001	0.000	0.000	0.002	0.002	0.000	0.000	0.001	0.001	0.001	0.001	0.000	0.000	0.000
1.50	1.06	1.03	1.51	1.52	1.01	1.06	1.46	1.48	1.65	1.74	1.53	1.50	1.48
0.76	0.97	0.99	0.76	0.75	1.00	0.97	0.79	0.77	0.67	0.61	0.74	0.76	0.77
excess	ok	ok	excess	excess	ok	ok	excess	excess	excess	excess	excess	excess	excess
ok	ok	ok	ok	ok	ok	ok	ok	ok	ok	ok	ok	ok	ok
menor	menor	menor	menor	menor	menor	menor	menor	menor	menor	maior	menor	menor	menor

W6-C6_car	W6-C6_car	W7-A5_car	W7-A5_car	W7-A5_car	W7-A5_car	W7-A5_car	W7-A5_car	W7-A5_car	W7-A5_car	W7-A5_car	W7-A5_car	W7-A5_car	W7-A5_car
43	**44**	**3**	**4**	**6**	**8**	**14**	**15**	**17**	**19**	**23**	**35**	**37**	**39**
42.13	30.91	39.54	38.49	40.04	38.48	38.30	33.50	40.77	21.97	40.02	38.37	36.57	37.83
0.03	0.01	0.06	0.03	0.00	0.00	0.00	0.06	0.02	0.01	0.00	0.00	0.02	0.01
0.06	0.09	0.23	0.11	0.09	1.92	1.23	5.30	0.60	6.73	0.16	1.07	1.63	0.35
27.36	30.49	31.48	32.31	25.78	26.48	30.03	31.96	29.32	31.27	30.87	30.94	29.50	31.06
0.00	0.00	0.00	0.00	0.00	0.03	0.00	0.00	0.00	0.02	0.01	0.00	0.01	0.03
0.03	0.25	0.00	0.00	0.00	0.02	0.01	0.00	0.01	0.00	0.03	0.00	0.03	0.00
8.65	7.10	0.88	0.67	10.47	8.27	3.60	1.91	1.96	1.62	1.95	2.45	3.08	1.94
0.05	0.08	0.00	0.00	0.01	0.02	0.03	0.04	0.00	0.08	0.02	0.03	0.01	0.03
0.03	0.04	0.06	0.01	0.05	0.07	0.04	0.07	0.04	0.05	0.00	0.01	0.04	0.00
0.05	8.91	0.02	0.01	0.02	0.01	0.03	0.04	0.01	8.08	0.04	0.07	0.08	0.03
0.01	0.00	0.00	0.00	0.00	0.02	0.00	0.00	0.00	0.87	0.00	0.00	0.00	0.01
0.02	0.07	0.04	0.03	0.00	0.00	0.01	0.00	0.02	2.20	0.00	0.05	0.00	0.03
0.00	0.00	0.00	0.00	0.00	0.00	0.00	0.00	0.00	0.00	0.00	0.00	0.00	0.00
0.07	0.10	0.03	0.03	0.06	0.09	0.08	0.10	0.08	0.22	0.14	0.10	0.17	0.11
0.56	0.40	0.70	0.64	0.36	0.36	0.53	0.50	0.53	0.26	0.47	0.46	0.54	0.56
0.00	0.01	0.01	0.00	0.00	0.01	0.01	0.02	0.01	0.09	0.02	0.01	0.01	0.02
78.39	*77.82*	*72.40*	*71.67*	*76.21*	*75.12*	*73.25*	*72.84*	*72.70*	*72.82*	*73.08*	*72.90*	*71.05*	*71.35*
0.236	*0.170*	*0.297*	*0.270*	*0.150*	*0.154*	*0.224*	*0.214*	*0.224*	*0.128*	*0.203*	*0.193*	*0.231*	*0.240*
78.16	**77.65**	**72.10**	**71.40**	**76.06**	**74.96**	**73.03**	**72.63**	**72.48**	**72.69**	**72.87**	**72.71**	**70.82**	**71.11**
0.297	0.218	0.279	0.271	0.282	0.271	0.270	0.236	0.287	0.155	0.282	0.270	0.258	0.266
0.000	0.000	0.000	0.000	0.000	0.000	0.000	0.000	0.000	0.000	0.000	0.000	0.000	0.000
0.001	0.001	0.004	0.002	0.001	0.032	0.021	0.088	0.010	0.112	0.003	0.018	0.027	0.006
0.268	0.299	0.309	0.317	0.253	0.260	0.294	0.313	0.288	0.307	0.303	0.303	0.289	0.305
0.000	0.000	0.000	0.000	0.000	0.000	0.000	0.000	0.000	0.000	0.000	0.000	0.000	0.000
0.000	0.003	0.000	0.000	0.000	0.000	0.000	0.000	0.000	0.000	0.000	0.000	0.000	0.000
0.054	0.044	0.006	0.004	0.066	0.052	0.023	0.012	0.012	0.010	0.012	0.015	0.019	0.012
0.001	0.002	0.000	0.000	0.000	0.000	0.001	0.001	0.000	0.002	0.000	0.001	0.000	0.001
0.000	0.001	0.001	0.000	0.001	0.001	0.000	0.001	0.001	0.001	0.000	0.000	0.001	0.000
0.001	0.159	0.000	0.000	0.000	0.000	0.001	0.001	0.000	0.144	0.001	0.001	0.001	0.000
0.000	0.000	0.000	0.000	0.000	0.000	0.000	0.000	0.000	0.006	0.000	0.000	0.000	0.000
0.000	0.001	0.000	0.000	0.000	0.000	0.000	0.000	0.000	0.021	0.000	0.001	0.000	0.000
0.000	0.000	0.000	0.000	0.000	0.000	0.000	0.000	0.000	0.000	0.000	0.000	0.000	0.000

0.001	0.001	0.000	0.000	0.001	0.001	0.001	0.001	0.001	0.002	0.001	0.001	0.002	0.001
0.0295	0.0208	0.0368	0.0338	0.0187	0.0191	0.0278	0.0263	0.0278	0.0136	0.0249	0.0239	0.0286	0.0295
0.000	0.000	0.000	0.000	0.000	0.000	0.000	0.000	0.000	0.002	0.001	0.000	0.000	0.000
0.594	0.435	0.557	0.542	0.564	0.542	0.540	0.472	0.574	0.310	0.564	0.541	0.515	0.533
0.000	0.000	0.001	0.000	0.000	0.000	0.000	0.001	0.000	0.000	0.000	0.000	0.000	0.000
0.001	0.001	0.004	0.002	0.001	0.032	0.021	0.088	0.010	0.112	0.003	0.018	0.027	0.006
0.537	0.598	0.617	0.634	0.506	0.519	0.589	0.627	0.575	0.613	0.606	0.607	0.579	0.609
0.000	0.000	0.000	0.000	0.000	0.000	0.000	0.000	0.000	0.000	0.000	0.000	0.000	0.000
0.000	0.003	0.000	0.000	0.000	0.000	0.000	0.000	0.000	0.000	0.000	0.000	0.000	0.000
0.108	0.089	0.011	0.008	0.131	0.104	0.045	0.024	0.025	0.020	0.024	0.031	0.039	0.024
0.001	0.002	0.000	0.000	0.000	0.000	0.001	0.001	0.000	0.002	0.000	0.001	0.000	0.001
0.000	0.001	0.001	0.000	0.001	0.001	0.000	0.001	0.001	0.001	0.000	0.000	0.001	0.000
0.001	0.159	0.000	0.000	0.000	0.000	0.001	0.001	0.000	0.144	0.001	0.001	0.001	0.000
0.000	0.000	0.000	0.000	0.000	0.000	0.000	0.000	0.000	0.006	0.000	0.000	0.000	0.000
0.000	0.001	0.000	0.000	0.000	0.000	0.000	0.000	0.000	0.021	0.000	0.001	0.000	0.000
0.000	0.000	0.000	0.000	0.000	0.000	0.000	0.000	0.000	0.000	0.000	0.000	0.000	0.000
0.001	0.002	0.001	0.001	0.001	0.002	0.002	0.002	0.002	0.005	0.003	0.002	0.004	0.002
1.484	1.089	1.393	1.356	1.410	1.356	1.349	1.180	1.436	0.774	1.410	1.351	1.288	1.332
0.001	0.000	0.001	0.001	0.000	0.000	0.000	0.001	0.000	0.000	0.000	0.000	0.000	0.000
0.002	0.003	0.008	0.004	0.003	0.064	0.041	0.177	0.020	0.224	0.005	0.036	0.054	0.012
0.805	0.897	0.926	0.951	0.758	0.779	0.883	0.940	0.863	0.920	0.908	0.910	0.868	0.914
0.000	0.000	0.000	0.000	0.000	0.000	0.000	0.000	0.000	0.000	0.000	0.000	0.000	0.001
0.001	0.006	0.000	0.000	0.000	0.000	0.000	0.000	0.000	0.000	0.001	0.000	0.001	0.000
0.162	0.133	0.017	0.013	0.197	0.155	0.068	0.036	0.037	0.031	0.037	0.046	0.058	0.036
0.001	0.002	0.000	0.000	0.000	0.000	0.001	0.001	0.000	0.002	0.000	0.001	0.000	0.001
0.000	0.001	0.001	0.000	0.001	0.001	0.000	0.001	0.001	0.001	0.000	0.000	0.001	0.000
0.001	0.159	0.000	0.000	0.000	0.000	0.001	0.001	0.000	0.144	0.001	0.001	0.001	0.000
0.000	0.000	0.000	0.000	0.000	0.000	0.000	0.000	0.000	0.006	0.000	0.000	0.000	0.000
0.000	0.001	0.000	0.000	0.000	0.000	0.000	0.000	0.000	0.021	0.000	0.001	0.000	0.000
0.000	0.000	0.000	0.000	0.000	0.000	0.000	0.000	0.000	0.000	0.000	0.000	0.000	0.000

0.001	0.001	0.000	0.000	0.001	0.001	0.001	0.001	0.001	0.002	0.001	0.001	0.002	0.001
0.0295263	0.0208421	0.0367895	0.0337895	0.0186842	0.0191053	0.0278421	0.0263158	0.0278421	0.0136316	0.0248947	0.0239474	0.0286316	0.0295263
0	0.0003949	0.0002821	0	2.821E-05	0.000141	0.0001693	0.0004513	0.000141	0.0023977	0.0005078	0.0001693	0.0002539	0.0004231
2.443	2.281	2.328	2.307	2.361	2.348	2.330	2.324	2.344	2.117	2.351	2.335	2.259	2.283
1.637	*1.753*	*1.718*	*1.734*	*1.694*	*1.704*	*1.716*	*1.721*	*1.707*	*1.889*	*1.702*	*1.713*	*1.770*	*1.752*
W6-C6_car	**W6-C6_car**	**W7-A5_car**	**W7-A5_car**	**W7-A5_car**	**W7-A5_car**	**W7-A5_car**	**W7-A5_car**	**W7-A5_car**	**W7-A5_car**	**W7-A5_car**	**W7-A5_car**	**W7-A5_car**	**W7-A5_car**
0.972	0.764	0.957	0.940	0.956	0.924	0.926	0.812	0.980	0.585	0.960	0.926	0.912	0.934
0.001	0.000	0.001	0.001	0.000	0.000	0.000	0.001	0.000	0.000	0.000	0.000	0.000	0.000
0.002	0.003	0.007	0.003	0.002	0.054	0.035	0.152	0.017	0.212	0.005	0.031	0.048	0.010
0.879	1.048	1.061	1.099	0.857	0.885	1.011	1.079	0.981	1.159	1.030	1.040	1.025	1.068
0.000	0.000	0.000	0.000	0.000	0.001	0.000	0.000	0.000	0.000	0.000	0.000	0.000	0.001
0.001	0.005	0.000	0.000	0.000	0.000	0.000	0.000	0.000	0.000	0.001	0.000	0.001	0.000
0.177	0.156	0.019	0.015	0.222	0.177	0.077	0.041	0.042	0.038	0.041	0.052	0.068	0.043
0.002	0.003	0.000	0.000	0.000	0.001	0.001	0.002	0.000	0.004	0.001	0.001	0.001	0.001
0.001	0.001	0.001	0.000	0.001	0.002	0.001	0.002	0.001	0.001	0.000	0.000	0.001	0.000
0.001	0.279	0.001	0.000	0.000	0.000	0.001	0.001	0.000	0.272	0.001	0.002	0.003	0.001
0.000	0.000	0.000	0.000	0.000	0.000	0.000	0.000	0.000	0.011	0.000	0.000	0.000	0.000
0.000	0.001	0.001	0.001	0.000	0.000	0.000	0.000	0.000	0.040	0.000	0.001	0.000	0.000
0.000	0.000	0.000	0.000	0.000	0.000	0.000	0.000	0.000	0.000	0.000	0.000	0.000	0.000
0.002	0.004	0.001	0.001	0.002	0.003	0.003	0.004	0.003	0.009	0.005	0.004	0.007	0.004
0.048	0.037	0.063	0.059	0.032	0.033	0.048	0.045	0.048	0.026	0.042	0.041	0.051	0.052
0.000	0.001	0.000	0.000	0.000	0.000	0.000	0.001	0.000	0.005	0.001	0.000	0.000	0.001
1.06	1.50	1.09	1.12	1.08	1.07	1.10	1.13	1.03	1.54	1.08	1.10	1.10	1.12
0.97	0.77	0.96	0.94	0.96	0.98	0.96	0.96	1.00	0.80	0.96	0.96	0.96	0.94
ok	excess	ok	excess	ok	ok	ok	excess	ok	excess	ok	excess	excess	excess
ok	ok	ok	ok	ok	ok	ok	ok	ok	ok	ok	ok	ok	ok
menor	menor	menor	menor	menor	menor	menor	menor	menor	menor	menor	menor	menor	menor

W7-A5_car	W7-A5_car	W7-A5_car	W7-A5_car	W7-A5_car	W7-C1A_ca	W7-C1A_ca	W7-C1A_ca	W7-C1A_ca	W7-C1A_ca	W7-C1A_ca	W7-C1A_ca	W7-C1A_ca	W7-C2B_ca
46	**47**	**54**	**56**	**57**	**5**	**16**	**18**	**27**	**28**	**30**	**31**	**40**	**4**
34.69	31.86	31.87	35.61	38.33	40.59	38.65	31.20	31.59	30.42	28.50	26.88	41.01	38.37
0.03	0.02	0.00	0.02	0.02	0.02	0.00	0.03	0.00	0.00	0.02	0.00	0.00	0.01
7.05	9.71	7.89	0.79	0.13	3.62	4.74	2.62	9.20	4.46	2.36	7.14	0.80	4.39
29.19	28.98	28.63	24.95	26.28	30.25	30.87	34.48	32.36	36.01	32.54	31.73	30.88	33.06
0.03	0.01	0.00	0.02	0.03	0.00	0.00	0.00	0.00	0.02	0.00	0.01	0.00	0.00
0.00	0.16	0.66	0.00	0.00	0.00	0.03	0.04	0.06	0.00	0.01	0.00	0.03	0.03
4.54	7.48	5.80	10.16	8.76	3.75	3.89	4.63	3.34	3.54	5.58	4.95	2.26	3.16
0.06	0.03	0.08	0.03	0.03	0.06	0.07	0.14	0.40	0.14	0.07	0.20	0.04	0.03
0.01	0.04	0.00	0.01	0.03	0.05	0.06	0.05	0.06	0.00	0.00	0.00	0.02	0.03
0.06	0.05	0.05	0.06	0.02	0.05	0.04	5.14	4.33	2.24	7.95	7.06	0.00	0.42
0.02	0.00	0.00	0.04	0.00	0.00	0.00	0.00	0.00	0.00	0.03	0.00	0.00	0.06
0.00	0.00	0.00	0.00	0.00	0.00	0.00	0.00	0.00	0.00	0.00	0.00	0.00	0.05
0.00	0.00	0.00	0.00	0.00	0.00	0.00	0.61	0.06	0.93	0.00	0.11	0.00	0.00
0.16	0.13	0.16	0.13	0.13	0.09	0.12	0.07	0.14	0.08	0.07	0.10	0.09	0.11
0.27	0.51	0.38	0.52	0.44	0.29	0.36	0.44	0.39	0.55	0.48	0.43	0.25	0.46
0.01	0.01	0.00	0.00	0.01	0.01	0.01	0.02	0.01	0.00	0.02	0.04	0.00	0.01
75.49	*78.33*	*74.88*	*71.69*	*73.56*	*78.11*	*78.17*	*78.83*	*81.27*	*77.73*	*76.97*	*78.02*	*74.72*	*79.56*
0.117	*0.216*	*0.158*	*0.217*	*0.186*	*0.123*	*0.151*	*0.189*	*0.165*	*0.231*	*0.205*	*0.191*	*0.104*	*0.197*
75.37	**78.11**	**74.72**	**71.47**	**73.37**	**77.99**	**78.02**	**78.64**	**81.11**	**77.50**	**76.77**	**77.83**	**74.62**	**79.36**
0.244	0.224	0.225	0.251	0.270	0.286	0.272	0.220	0.223	0.214	0.201	0.189	0.289	0.270
0.000	0.000	0.000	0.000	0.000	0.000	0.000	0.000	0.000	0.000	0.000	0.000	0.000	0.000
0.117	0.162	0.131	0.013	0.002	0.060	0.079	0.044	0.153	0.074	0.039	0.119	0.013	0.073
0.286	0.284	0.281	0.245	0.258	0.297	0.303	0.338	0.317	0.353	0.319	0.311	0.303	0.324
0.000	0.000	0.000	0.000	0.000	0.000	0.000	0.000	0.000	0.000	0.000	0.000	0.000	0.000
0.000	0.002	0.008	0.000	0.000	0.000	0.000	0.000	0.001	0.000	0.000	0.000	0.000	0.000
0.028	0.047	0.036	0.064	0.055	0.023	0.024	0.029	0.021	0.022	0.035	0.031	0.014	0.020
0.001	0.001	0.002	0.001	0.001	0.001	0.002	0.003	0.010	0.003	0.002	0.005	0.001	0.001
0.000	0.001	0.000	0.000	0.000	0.001	0.001	0.001	0.001	0.000	0.000	0.000	0.000	0.000
0.001	0.001	0.001	0.001	0.000	0.001	0.001	0.092	0.077	0.040	0.142	0.126	0.000	0.007
0.000	0.000	0.000	0.000	0.000	0.000	0.000	0.000	0.000	0.000	0.000	0.000	0.000	0.000
0.000	0.000	0.000	0.000	0.000	0.000	0.000	0.000	0.000	0.000	0.000	0.000	0.000	0.000
0.000	0.000	0.000	0.000	0.000	0.000	0.000	0.010	0.001	0.015	0.000	0.002	0.000	0.000

0.002	0.001	0.002	0.001	0.001	0.001	0.001	0.001	0.001	0.001	0.001	0.001	0.001	0.001
0.0143	0.0267	0.0197	0.0272	0.0232	0.0152	0.0188	0.0232	0.0203	0.0288	0.0251	0.0228	0.0129	0.0243
0.000	0.000	0.000	0.000	0.000	0.000	0.000	0.001	0.000	0.000	0.000	0.001	0.000	0.000

0.489	0.449	0.449	0.502	0.540	0.572	0.545	0.440	0.445	0.429	0.402	0.379	0.578	0.541
0.000	0.000	0.000	0.000	0.000	0.000	0.000	0.000	0.000	0.000	0.000	0.000	0.000	0.000
0.117	0.162	0.131	0.013	0.002	0.060	0.079	0.044	0.153	0.074	0.039	0.119	0.013	0.073
0.573	0.568	0.562	0.489	0.515	0.593	0.605	0.676	0.635	0.706	0.638	0.622	0.606	0.649
0.000	0.000	0.000	0.000	0.000	0.000	0.000	0.000	0.000	0.000	0.000	0.000	0.000	0.000
0.000	0.002	0.008	0.000	0.000	0.000	0.000	0.000	0.001	0.000	0.000	0.000	0.000	0.000
0.057	0.094	0.073	0.127	0.110	0.047	0.049	0.058	0.042	0.044	0.070	0.062	0.028	0.040
0.001	0.001	0.002	0.001	0.001	0.001	0.002	0.003	0.010	0.003	0.002	0.005	0.001	0.001
0.000	0.001	0.000	0.000	0.000	0.001	0.001	0.001	0.001	0.000	0.000	0.000	0.000	0.000
0.001	0.001	0.001	0.001	0.000	0.001	0.001	0.092	0.077	0.040	0.142	0.126	0.000	0.007
0.000	0.000	0.000	0.000	0.000	0.000	0.000	0.000	0.000	0.000	0.000	0.000	0.000	0.000
0.000	0.000	0.000	0.000	0.000	0.000	0.000	0.000	0.000	0.000	0.000	0.000	0.000	0.000
0.000	0.000	0.000	0.000	0.000	0.000	0.000	0.020	0.002	0.030	0.000	0.004	0.000	0.000
0.003	0.003	0.003	0.003	0.003	0.002	0.002	0.001	0.003	0.002	0.001	0.002	0.002	0.002

1.222	1.122	1.123	1.254	1.350	1.430	1.361	1.099	1.113	1.071	1.004	0.947	1.444	1.352
0.001	0.000	0.000	0.000	0.000	0.000	0.000	0.001	0.000	0.000	0.000	0.000	0.000	0.000
0.235	0.323	0.263	0.026	0.004	0.120	0.158	0.087	0.306	0.148	0.079	0.238	0.026	0.146
0.859	0.853	0.842	0.734	0.773	0.890	0.908	1.015	0.952	1.060	0.957	0.934	0.909	0.973
0.001	0.000	0.000	0.000	0.000	0.000	0.000	0.000	0.000	0.000	0.000	0.000	0.000	0.000
0.000	0.004	0.017	0.000	0.000	0.000	0.001	0.001	0.001	0.000	0.000	0.000	0.001	0.001
0.085	0.141	0.109	0.191	0.165	0.070	0.073	0.087	0.063	0.066	0.105	0.093	0.042	0.059
0.001	0.001	0.002	0.001	0.001	0.001	0.002	0.003	0.010	0.003	0.002	0.005	0.001	0.001
0.000	0.001	0.000	0.000	0.000	0.001	0.001	0.001	0.001	0.000	0.000	0.000	0.000	0.000
0.001	0.001	0.001	0.001	0.000	0.001	0.001	0.092	0.077	0.040	0.142	0.126	0.000	0.007
0.000	0.000	0.000	0.000	0.000	0.000	0.000	0.000	0.000	0.000	0.000	0.000	0.000	0.000
0.000	0.000	0.000	0.000	0.000	0.000	0.000	0.000	0.000	0.000	0.000	0.000	0.000	0.000
0.000	0.000	0.000	0.000	0.000	0.000	0.000	0.010	0.001	0.015	0.000	0.002	0.000	0.000

0.002	0.001	0.002	0.001	0.001	0.001	0.001	0.001	0.001	0.001	0.001	0.001	0.001	0.001
0.0143158	0.0266842	0.0197368	0.0271579	0.0231579	0.0152105	0.0187895	0.0231579	0.0202632	0.0288421	0.0251053	0.0227895	0.0129474	0.0243158
0.0002821	0.0003385	0	0	0.000141	0.0001975	0.000141	0.0005078	0.0003385	8.463E-05	0.0004795	0.0011283	5.642E-05	0.0003667
2.399	2.433	2.348	2.196	2.284	2.507	2.496	2.384	2.515	2.391	2.277	2.333	2.418	2.529
1.667	*1.644*	*1.703*	*1.821*	*1.751*	*1.595*	*1.602*	*1.678*	*1.590*	*1.673*	*1.757*	*1.714*	*1.654*	*1.582*
W7-A5_car	**W7-A5_car**	**W7-A5_car**	**W7-A5_car**	**W7-A5_car**	**W7-C1A_ca**	**W7-C1A_ca**	**W7-C1A_ca**	**W7-C1A_ca**	**W7-C1A_ca**	**W7-C1A_ca**	**W7-C1A_ca**	**W7-C1A_ca**	**W7-C2B_ca**
0.815	0.738	0.765	0.914	0.946	0.912	0.873	0.738	0.708	0.717	0.705	0.649	0.956	0.855
0.001	0.000	0.000	0.001	0.001	0.000	0.000	0.001	0.000	0.000	0.000	0.000	0.000	0.000
0.196	0.266	0.224	0.024	0.004	0.096	0.127	0.073	0.243	0.124	0.069	0.204	0.022	0.115
0.955	0.934	0.957	0.891	0.903	0.947	0.970	1.135	1.010	1.182	1.121	1.067	1.002	1.026
0.001	0.000	0.000	0.000	0.001	0.000	0.000	0.000	0.000	0.000	0.000	0.000	0.000	0.000
0.000	0.003	0.014	0.000	0.000	0.000	0.001	0.001	0.001	0.000	0.000	0.000	0.001	0.001
0.095	0.154	0.124	0.232	0.192	0.075	0.078	0.097	0.066	0.074	0.123	0.106	0.047	0.063
0.002	0.001	0.004	0.002	0.001	0.002	0.003	0.006	0.016	0.006	0.003	0.009	0.001	0.001
0.000	0.001	0.000	0.000	0.001	0.001	0.001	0.001	0.001	0.000	0.000	0.000	0.001	0.001
0.002	0.002	0.002	0.002	0.001	0.001	0.001	0.154	0.123	0.067	0.249	0.216	0.000	0.012
0.000	0.000	0.000	0.000	0.000	0.000	0.000	0.000	0.000	0.000	0.000	0.000	0.000	0.001
0.000	0.000	0.000	0.000	0.000	0.000	0.000	0.000	0.000	0.000	0.000	0.000	0.000	0.001
0.000	0.000	0.000	0.000	0.000	0.000	0.000	0.033	0.003	0.050	0.000	0.006	0.000	0.000
0.006	0.005	0.006	0.005	0.005	0.003	0.004	0.002	0.005	0.003	0.003	0.004	0.003	0.004
0.024	0.044	0.034	0.049	0.041	0.024	0.030	0.039	0.032	0.048	0.044	0.039	0.021	0.038
0.000	0.001	0.000	0.000	0.000	0.000	0.000	0.001	0.001	0.000	0.001	0.002	0.000	0.001
1.06	1.10	1.11	1.13	1.10	1.03	1.06	1.43	1.22	1.38	1.50	1.41	1.05	1.11
1.01	1.00	0.99	0.94	0.95	1.01	1.00	0.81	0.95	0.84	0.77	0.85	0.98	0.97
ok	excess	excess	excess	excess	ok	ok	excess	excess	excess	excess	excess	ok	excess
ok	ok	ok	ok	ok	ok	ok	ok	ok	ok	ok	ok	ok	ok
menor	menor	menor	menor	menor	menor	menor	menor	menor	menor	menor	menor	menor	menor

W7-C2B_c	**W7-C2B_c**	**W7-C2B_c**	**W7-C2B_c**	**W7-C2B_c**	**W7-C2B_c**	**W7-C2B_c**	**W7-C2B_c**	**W7-C2B_c**	**W7-C2B_c**	**W7-C2B_c**	**W7-C2B_c**	**W7-C2B_c**	**W7-C2B_c**
8	**13**	**16**	**18**	**23**	**24**	**25**	**31**	**34**	**36**	**39**	**41**	**44**	**47**
40.18	37.84	43.01	41.37	39.79	38.61	40.13	39.36	39.70	38.44	39.38	38.62	38.87	36.22
0.00	0.00	0.00	0.00	0.04	0.04	0.00	0.01	0.00	0.01	0.03	0.00	0.01	0.00
3.98	5.21	0.07	0.00	0.51	0.05	0.19	0.03	0.06	0.09	0.12	1.77	0.60	3.40
32.47	31.45	29.97	31.41	31.52	29.56	29.94	30.94	30.50	29.38	30.34	30.51	30.46	30.67
0.00	0.00	0.00	0.00	0.00	0.00	0.00	0.00	0.00	0.01	0.00	0.00	0.00	0.00
0.10	0.00	0.00	0.00	0.00	0.02	0.03	0.01	0.01	0.00	0.01	0.00	0.03	0.00
2.88	2.15	3.32	1.73	2.15	3.93	3.41	2.95	2.66	2.47	4.00	2.94	2.15	3.44
0.05	0.05	0.05	0.03	0.00	0.00	0.01	0.03	0.00	0.04	0.02	0.02	0.02	0.07
0.00	0.02	0.07	0.03	0.02	0.00	0.04	0.00	0.07	0.07	0.00	0.00	0.01	0.09
0.81	0.19	0.04	0.05	0.02	0.02	0.01	0.02	0.04	0.04	0.09	0.21	0.03	0.90
0.09	0.02	0.01	0.00	0.00	0.00	0.00	0.00	0.00	0.00	0.00	0.00	0.00	0.03
0.13	0.00	0.02	0.00	0.00	0.00	0.00	0.03	0.00	0.00	0.00	0.00	0.00	0.01
0.00	0.00	0.00	0.00	0.00	0.00	0.00	0.00	0.00	0.00	0.00	0.00	0.00	0.00
0.11	0.12	0.07	0.03	0.07	0.05	0.07	0.04	0.03	0.13	0.07	0.10	0.06	0.14
0.41	0.41	0.61	0.50	0.51	0.59	0.47	0.52	0.47	0.56	0.58	0.53	0.52	0.40
0.04	0.03	0.00	0.00	0.02	0.01	0.00	0.01	0.04	0.01	0.01	0.03	0.01	0.02
80.57	*76.85*	*76.58*	*74.50*	*74.01*	*72.23*	*73.63*	*73.28*	*72.93*	*70.58*	*73.99*	*74.09*	*72.10*	*74.72*
0.179	*0.180*	*0.257*	*0.210*	*0.218*	*0.251*	*0.198*	*0.219*	*0.208*	*0.236*	*0.248*	*0.230*	*0.220*	*0.172*
80.39	**76.67**	**76.33**	**74.29**	**73.79**	**71.98**	**73.43**	**73.06**	**72.72**	**70.35**	**73.74**	**73.86**	**71.88**	**74.55**
0.283	0.267	0.303	0.291	0.280	0.272	0.283	0.277	0.280	0.271	0.277	0.272	0.274	0.255
0.000	0.000	0.000	0.000	0.000	0.000	0.000	0.000	0.000	0.000	0.000	0.000	0.000	0.000
0.066	0.087	0.001	0.000	0.008	0.001	0.003	0.000	0.001	0.001	0.002	0.029	0.010	0.057
0.318	0.308	0.294	0.308	0.309	0.290	0.294	0.303	0.299	0.288	0.298	0.299	0.299	0.301
0.000	0.000	0.000	0.000	0.000	0.000	0.000	0.000	0.000	0.000	0.000	0.000	0.000	0.000
0.001	0.000	0.000	0.000	0.000	0.000	0.000	0.000	0.000	0.000	0.000	0.000	0.000	0.000
0.018	0.013	0.021	0.011	0.013	0.025	0.021	0.018	0.017	0.015	0.025	0.018	0.013	0.022
0.001	0.001	0.001	0.001	0.000	0.000	0.000	0.001	0.000	0.001	0.001	0.000	0.000	0.002
0.000	0.000	0.001	0.000	0.000	0.000	0.000	0.000	0.001	0.001	0.000	0.000	0.000	0.001
0.014	0.003	0.001	0.001	0.000	0.000	0.000	0.000	0.001	0.001	0.002	0.004	0.001	0.016
0.001	0.000	0.000	0.000	0.000	0.000	0.000	0.000	0.000	0.000	0.000	0.000	0.000	0.000
0.001	0.000	0.000	0.000	0.000	0.000	0.000	0.000	0.000	0.000	0.000	0.000	0.000	0.000
0.000	0.000	0.000	0.000	0.000	0.000	0.000	0.000	0.000	0.000	0.000	0.000	0.000	0.000

0.001	0.001	0.001	0.000	0.001	0.000	0.001	0.000	0.000	0.001	0.001	0.001	0.001	0.001
0.0213	0.0218	0.0321	0.0261	0.0267	0.0312	0.0248	0.0272	0.0248	0.0293	0.0306	0.0280	0.0272	0.0208
0.001	0.001	0.000	0.000	0.001	0.000	0.000	0.000	0.001	0.000	0.000	0.001	0.000	0.001

0.566	0.533	0.606	0.583	0.561	0.544	0.565	0.555	0.559	0.542	0.555	0.544	0.548	0.510
0.000	0.000	0.000	0.000	0.001	0.001	0.000	0.000	0.000	0.000	0.000	0.000	0.000	0.000
0.066	0.087	0.001	0.000	0.008	0.001	0.003	0.000	0.001	0.001	0.002	0.029	0.010	0.057
0.637	0.617	0.588	0.616	0.618	0.580	0.587	0.607	0.598	0.576	0.595	0.598	0.597	0.602
0.000	0.000	0.000	0.000	0.000	0.000	0.000	0.000	0.000	0.000	0.000	0.000	0.000	0.000
0.001	0.000	0.000	0.000	0.000	0.000	0.000	0.000	0.000	0.000	0.000	0.000	0.000	0.000
0.036	0.027	0.042	0.022	0.027	0.049	0.043	0.037	0.033	0.031	0.050	0.037	0.027	0.043
0.001	0.001	0.001	0.001	0.000	0.000	0.000	0.001	0.000	0.001	0.001	0.000	0.000	0.002
0.000	0.000	0.001	0.000	0.000	0.000	0.000	0.000	0.001	0.001	0.000	0.000	0.000	0.001
0.014	0.003	0.001	0.001	0.000	0.000	0.000	0.000	0.001	0.001	0.002	0.004	0.001	0.016
0.001	0.000	0.000	0.000	0.000	0.000	0.000	0.000	0.000	0.000	0.000	0.000	0.000	0.000
0.001	0.000	0.000	0.000	0.000	0.000	0.000	0.000	0.000	0.000	0.000	0.000	0.000	0.000
0.000	0.000	0.000	0.000	0.000	0.000	0.000	0.000	0.000	0.000	0.000	0.000	0.000	0.000
0.002	0.003	0.001	0.001	0.002	0.001	0.001	0.001	0.001	0.003	0.001	0.002	0.001	0.003

1.415	1.333	1.515	1.457	1.402	1.360	1.414	1.386	1.398	1.354	1.387	1.360	1.369	1.276
0.000	0.000	0.000	0.000	0.001	0.001	0.000	0.000	0.000	0.000	0.001	0.000	0.000	0.000
0.132	0.173	0.002	0.000	0.017	0.002	0.006	0.001	0.002	0.003	0.004	0.059	0.020	0.113
0.955	0.925	0.882	0.924	0.927	0.870	0.881	0.910	0.897	0.864	0.893	0.898	0.896	0.902
0.000	0.000	0.000	0.000	0.000	0.000	0.000	0.000	0.000	0.000	0.000	0.000	0.000	0.000
0.002	0.000	0.000	0.000	0.000	0.001	0.001	0.000	0.000	0.000	0.000	0.000	0.001	0.000
0.054	0.040	0.062	0.032	0.040	0.074	0.064	0.055	0.050	0.046	0.075	0.055	0.040	0.065
0.001	0.001	0.001	0.001	0.000	0.000	0.000	0.001	0.000	0.001	0.001	0.000	0.000	0.002
0.000	0.000	0.001	0.000	0.000	0.000	0.000	0.000	0.001	0.001	0.000	0.000	0.000	0.001
0.014	0.003	0.001	0.001	0.000	0.000	0.000	0.000	0.001	0.001	0.002	0.004	0.001	0.016
0.001	0.000	0.000	0.000	0.000	0.000	0.000	0.000	0.000	0.000	0.000	0.000	0.000	0.000
0.001	0.000	0.000	0.000	0.000	0.000	0.000	0.000	0.000	0.000	0.000	0.000	0.000	0.000
0.000	0.000	0.000	0.000	0.000	0.000	0.000	0.000	0.000	0.000	0.000	0.000	0.000	0.000

0.001	0.001	0.001	0.000	0.001	0.000	0.001	0.000	0.000	0.001	0.001	0.001	0.001	0.001
0.0213158	0.0217895	0.0320526	0.0261053	0.0267368	0.0312105	0.0247895	0.0271579	0.0248421	0.0292632	0.0306316	0.028	0.0272105	0.0207895
0.0011001	0.0007334	5.642E-05	0.0001128	0.0005642	0.0002257	0	0.0002257	0.0011001	0.0002821	0.0003385	0.0007334	0.0002821	0.000677
2.567	2.467	2.449	2.403	2.375	2.292	2.354	2.341	2.337	2.257	2.347	2.363	2.314	2.366
1.558	*1.621*	*1.633*	*1.664*	*1.684*	*1.745*	*1.699*	*1.708*	*1.712*	*1.772*	*1.704*	*1.693*	*1.728*	*1.691*
W7-C2B_ca	**W7-C2B_ca**	**W7-C2B_ca**	**W7-C2B_ca**	**W7-C2B_ca**	**W7-C2B_ca**	**W7-C2B_ca**	**W7-C2B_ca**	**W7-C2B_ca**	**W7-C2B_ca**	**W7-C2B_ca**	**W7-C2B_ca**	**W7-C2B_ca**	**W7-C2B_ca**
0.882	0.864	0.990	0.970	0.944	0.949	0.961	0.947	0.957	0.960	0.946	0.921	0.947	0.863
0.000	0.000	0.000	0.000	0.001	0.001	0.000	0.000	0.000	0.000	0.001	0.000	0.000	0.000
0.103	0.141	0.002	0.000	0.014	0.001	0.005	0.001	0.002	0.003	0.003	0.050	0.017	0.096
0.992	1.000	0.960	1.026	1.041	1.012	0.998	1.037	1.024	1.021	1.014	1.013	1.032	1.017
0.000	0.000	0.000	0.000	0.000	0.000	0.000	0.000	0.000	0.000	0.000	0.000	0.000	0.000
0.002	0.000	0.000	0.000	0.000	0.001	0.001	0.000	0.000	0.000	0.000	0.000	0.001	0.000
0.056	0.044	0.068	0.036	0.045	0.086	0.073	0.063	0.057	0.055	0.085	0.062	0.047	0.073
0.002	0.002	0.002	0.001	0.000	0.000	0.000	0.001	0.000	0.002	0.001	0.001	0.001	0.003
0.000	0.000	0.002	0.001	0.000	0.000	0.001	0.000	0.002	0.002	0.000	0.000	0.000	0.002
0.022	0.005	0.001	0.001	0.001	0.001	0.000	0.000	0.001	0.001	0.003	0.006	0.001	0.027
0.001	0.000	0.000	0.000	0.000	0.000	0.000	0.000	0.000	0.000	0.000	0.000	0.000	0.000
0.002	0.000	0.000	0.000	0.000	0.000	0.000	0.000	0.000	0.000	0.000	0.000	0.000	0.000
0.000	0.000	0.000	0.000	0.000	0.000	0.000	0.000	0.000	0.000	0.000	0.000	0.000	0.000
0.003	0.004	0.002	0.001	0.003	0.002	0.002	0.001	0.001	0.005	0.002	0.004	0.002	0.005
0.033	0.035	0.052	0.043	0.045	0.054	0.042	0.046	0.043	0.052	0.052	0.047	0.047	0.035
0.002	0.001	0.000	0.000	0.001	0.000	0.000	0.000	0.002	0.000	0.001	0.001	0.000	0.001
1.08	1.06	1.04	1.07	1.09	1.10	1.07	1.10	1.08	1.09	1.11	1.09	1.08	1.13
0.99	1.00	0.99	0.97	0.96	0.95	0.97	0.95	0.96	0.96	0.95	0.97	0.96	0.96
ok	ok	ok	ok	ok	excess	ok	excess	ok	ok	excess	ok	ok	excess
ok	ok	ok	ok	ok	ok	ok	ok	ok	ok	ok	ok	ok	ok
menor	menor	menor	menor	menor	menor	menor	menor	menor	menor	menor	menor	menor	menor

W7-C2B_ca	W7-C2B_ca	W7-C2B_campo1-22	variscite E	crandallite	strengite E	millisite EM	wardite EM	wavellite E	goyazite E	gorceixite EM
49	**51**	**52**								
32.47	39.02	39.61	44.92	34.28	37.99	34.75	35.67	34.46		
0.00	0.02	0.00	0.00	0.00	0.00	0.00	0.00	0.00		
2.64	1.73	0.03	0.00	0.00	0.00	0.00	0.00	0.00		
30.15	29.58	30.29	32.27	36.94	0.00	37.45	38.43	37.12		
0.00	0.00	0.00	0.00	0.00	0.00	0.00	0.00	0.00		
0.10	0.02	0.01	0.00	0.00	0.00	0.00	0.00	0.00		
2.92	4.07	2.92	0.00	0.00	42.73	0.00	0.00	0.00		
0.05	0.04	0.02	0.00	0.00	0.00	0.00	0.00	0.00		
0.00	0.04	0.00	0.00	0.00	0.00	0.00	0.00	0.00		
2.46	0.03	0.04	0.00	13.55	0.00	6.87	0.00	0.00		
0.00	0.00	0.00	0.00	0.00	0.00	0.00	0.00	0.00		
0.00	0.00	0.00	0.00	0.00	0.00	0.00	0.00	0.00		
0.00	0.00	0.00	0.00	0.00	0.00	2.66	7.79	0.00		
0.09	0.09	0.09	0.00	0.00	0.00	1.73	0.00	0.00		
0.39	0.59	0.59	0.00	0.00	0.00	0.00	0.00	0.00		
0.08	0.01	0.02	0.00	0.00	0.00	0.00	0.00	0.00		
70.69	*74.61*	*72.97*	*77.19*	*84.77*	*80.72*	*83.46*	*81.89*	*71.58*		
0.180	*0.252*	*0.253*	*0.000*	*0.000*	*0.000*	*0.000*	*0.000*	*0.000*		
70.51	**74.35**	**72.71**	**77.19**	**84.77**	**80.72**	**83.46**	**81.89**	**71.58**		
0.229	0.275	0.279	0.316	0.242	0.268	0.245	0.251	0.243		
0.000	0.000	0.000	0.000	0.000	0.000	0.000	0.000	0.000		
0.044	0.029	0.000	0.000	0.000	0.000	0.000	0.000	0.000		
0.296	0.290	0.297	0.316	0.362	0.000	0.367	0.377	0.364		
0.000	0.000	0.000	0.000	0.000	0.000	0.000	0.000	0.000		
0.001	0.000	0.000	0.000	0.000	0.000	0.000	0.000	0.000		
0.018	0.026	0.018	0.000	0.000	0.268	0.000	0.000	0.000		
0.001	0.001	0.000	0.000	0.000	0.000	0.000	0.000	0.000		
0.000	0.001	0.000	0.000	0.000	0.000	0.000	0.000	0.000		
0.044	0.001	0.001	0.000	0.242	0.000	0.123	0.000	0.000		
0.000	0.000	0.000	0.000	0.000	0.000	0.000	0.000	0.000		
0.000	0.000	0.000	0.000	0.000	0.000	0.000	0.000	0.000		
0.000	0.000	0.000	0.000	0.000	0.000	0.043	0.126	0.000		

0.001	0.001	0.001	0.000	0.000	0.000	0.018	0.000	0.000
0.0204	0.0312	0.0313	0.0000	0.0000	0.0000	0.0000	0.0000	0.0000
0.002	0.000	0.000	0.000	0.000	0.000	0.000	0.000	0.000
0.457	0.550	0.558	0.633	0.483	0.535	0.490	0.503	0.486
0.000	0.000	0.000	0.000	0.000	0.000	0.000	0.000	0.000
0.044	0.029	0.000	0.000	0.000	0.000	0.000	0.000	0.000
0.591	0.580	0.594	0.633	0.725	0.000	0.735	0.754	0.728
0.000	0.000	0.000	0.000	0.000	0.000	0.000	0.000	0.000
0.001	0.000	0.000	0.000	0.000	0.000	0.000	0.000	0.000
0.037	0.051	0.037	0.000	0.000	0.535	0.000	0.000	0.000
0.001	0.001	0.000	0.000	0.000	0.000	0.000	0.000	0.000
0.000	0.001	0.000	0.000	0.000	0.000	0.000	0.000	0.000
0.044	0.001	0.001	0.000	0.242	0.000	0.123	0.000	0.000
0.000	0.000	0.000	0.000	0.000	0.000	0.000	0.000	0.000
0.000	0.000	0.000	0.000	0.000	0.000	0.000	0.000	0.000
0.000	0.000	0.000	0.000	0.000	0.000	0.086	0.251	0.000
0.002	0.002	0.002	0.000	0.000	0.000	0.037	0.000	0.000
1.144	1.374	1.395	1.582	1.208	1.338	1.224	1.256	1.214
0.000	0.000	0.000	0.000	0.000	0.000	0.000	0.000	0.000
0.088	0.058	0.001	0.000	0.000	0.000	0.000	0.000	0.000
0.887	0.870	0.891	0.949	1.087	0.000	1.102	1.131	1.092
0.000	0.000	0.000	0.000	0.000	0.000	0.000	0.000	0.000
0.002	0.001	0.000	0.000	0.000	0.000	0.000	0.000	0.000
0.055	0.077	0.055	0.000	0.000	0.803	0.000	0.000	0.000
0.001	0.001	0.000	0.000	0.000	0.000	0.000	0.000	0.000
0.000	0.001	0.000	0.000	0.000	0.000	0.000	0.000	0.000
0.044	0.001	0.001	0.000	0.242	0.000	0.123	0.000	0.000
0.000	0.000	0.000	0.000	0.000	0.000	0.000	0.000	0.000
0.000	0.000	0.000	0.000	0.000	0.000	0.000	0.000	0.000
0.000	0.000	0.000	0.000	0.000	0.000	0.043	0.126	0.000

0.001	0.001	0.001	0.000	0.000	0.000	0.018	0.000	0.000
0.0203684	0.0311579	0.0312632	0	0	0	0	0	0
0.0021721	0.0002821	0.0004231	0	0	0	0	0	0
2.211	2.367	2.329	2.532	2.536	2.141	2.510	2.513	2.306
			4O	8O	4O	24O	8O	8 O
1.809	*1.690*	*1.718*	*1.580*	*3.155*	*1.868*	*9.563*	*3.184*	*3.469*
W7-C2B_ca	**W7-C2B_ca**	**W7-C2B_campo1-22**	**variscite E**	**crandallite**	**strengite E**	**millisite E**	**wardite EM**	**wavellite EM**
0.828	0.929	0.959	1.000	1.524	1.000	4.682	1.600	1.684
0.000	0.000	0.000	0.000	0.000	0.000	0.000	0.000	0.000
0.079	0.049	0.001	0.000	0.000	0.000	0.000	0.000	0.000
1.070	0.980	1.020	1.000	2.286	0.000	7.025	2.400	2.526
0.000	0.000	0.000	0.000	0.000	0.000	0.000	0.000	0.000
0.002	0.000	0.000	0.000	0.000	0.000	0.000	0.000	0.000
0.066	0.086	0.063	0.000	0.000	1.000	0.000	0.000	0.000
0.002	0.002	0.001	0.000	0.000	0.000	0.000	0.000	0.000
0.000	0.001	0.000	0.000	0.000	0.000	0.000	0.000	0.000
0.079	0.001	0.001	0.000	0.762	0.000	1.172	0.000	0.000
0.000	0.000	0.000	0.000	0.000	0.000	0.000	0.000	0.000
0.000	0.000	0.000	0.000	0.000	0.000	0.000	0.000	0.000
0.000	0.000	0.000	0.000	0.000	0.000	0.821	0.800	0.000
0.003	0.003	0.003	0.000	0.000	0.000	0.351	0.000	0.000
0.037	0.053	0.054	0.000	0.000	0.000	0.000	0.000	0.000
0.004	0.000	0.001	0.000	0.000	0.000	0.000	0.000	0.000
1.22	1.07	1.09	1.00	3.05	1.00	9.37	3.20	2.53
0.91	0.98	0.96	1.00	1.52	1.00	4.68	1.60	1.68
excess	ok	ok	ok	excess	ok	excess	excess	excess
ok	ok	ok	ok	excess	ok	excess	excess	excess
menor	menor	menor	menor	menor	maior	menor	menor	menor

Sample	W6-B7A_ca	W6-B7A_ca	W6-B7A_ca	W6-B7A_ca	W6-B7A_ca	W6-B7A_ca	W6-B7A_ca	W6-B7A_ca	W6-B7B_ca	W6-B7B_ca	W6-B7B_ca	W7-A5_can	W7-A5_can
No.	**2**	**3**	**5**	**7**	**9**	**40**	**44**	**45**	**5**	**22**	**27**	**10**	**11**
P2O5	0.08	0.09	0.11	0.10	0.13	0.09	0.08	0.06	0.07	0.11	0.00	0.14	0.13
V2O3	0.01	0.03	0.00	0.02	0.04	0.02	0.03	0.02	0.01	0.02	0.02	0.00	0.01
SiO2	39.25	41.50	40.65	37.25	45.44	39.10	41.05	43.51	39.60	39.26	39.01	41.02	39.37
Al2O3	30.06	32.39	31.16	28.50	35.24	29.17	32.35	34.29	31.06	29.17	26.95	31.39	30.39
Cr2O3	0.00	0.00	0.01	0.00	0.01	0.03	0.00	0.02	0.00	0.02	0.02	0.00	0.02
TiO2	0.00	0.00	0.04	0.00	0.04	0.03	0.04	0.02	0.00	0.00	0.02	0.02	0.00
FeO	1.79	1.98	1.85	1.86	2.08	1.68	1.05	1.55	1.96	1.40	1.03	0.81	0.89
MgO	0.18	0.18	0.21	0.28	0.05	0.23	0.25	0.05	0.07	0.14	0.23	0.15	0.09
MnO	0.00	0.01	0.02	0.02	0.03	0.00	0.00	0.00	0.05	0.00	0.00	0.00	0.01
CaO	0.07	0.07	0.05	0.05	0.02	0.05	0.07	0.02	0.05	0.11	0.10	0.10	0.10
BaO	0.03	0.00	0.00	0.00	0.01	0.00	0.02	0.02	0.00	0.01	0.01	0.01	0.01
SrO	0.00	0.00	0.00	0.00	0.00	0.00	0.00	0.00	0.00	0.00	0.00	0.00	0.00
Na2O	0.01	0.00	0.03	0.02	0.00	0.00	0.04	0.02	0.04	0.34	0.11	0.12	0.13
K2O	0.02	0.02	0.04	0.02	0.02	0.70	0.08	0.03	0.04	0.15	0.11	0.12	0.09
F	0.15	0.00	0.00	0.00	0.03	0.01	0.03	0.00	0.13	0.00	0.00	0.00	0.01
Cl	0.31	0.24	0.32	0.28	0.03	0.19	0.02	0.03	0.16	0.33	0.29	0.22	0.23
Total	71.299	75.875	73.846	67.741	82.517	70.641	74.478	78.976	72.586	70.432	67.243	73.434	70.835
O=F=Cl	0.132	0.054	0.072	0.063	0.021	0.045	0.019	0.008	0.090	0.075	0.065	0.049	0.055
Total 2	**71.17**	**75.82**	**73.77**	**67.68**	**82.50**	**70.60**	**74.46**	**78.97**	**72.50**	**70.36**	**67.18**	**73.38**	**70.78**

anion prop	W6-B7A_ca	W6-B7A_ca	W6-B7A_ca	W6-B7A_ca	W6-B7A_ca	W6-B7A_ca	W6-B7A_ca	W6-B7A_ca	W6-B7B_ca	W6-B7B_ca	W6-B7B_ca	W7-A5_can	W7-A5_can
P	0.011	0.012	0.015	0.015	0.016	0.013	0.011	0.007	0.010	0.016	0.000	0.019	0.019
V	0.001	0.004	0.000	0.002	0.005	0.002	0.004	0.002	0.001	0.003	0.003	0.000	0.001
Si	6.483	6.416	6.462	6.456	6.434	6.510	6.408	6.415	6.414	6.542	6.758	6.498	6.475
Al	5.852	5.902	5.837	5.822	5.881	5.723	5.952	5.957	5.928	5.729	5.502	5.862	5.891
Cr	0.000	0.000	0.001	0.000	0.001	0.004	0.000	0.003	0.000	0.003	0.002	0.000	0.002
Ti	0.000	0.000	0.005	0.000	0.005	0.004	0.005	0.002	0.000	0.000	0.003	0.002	0.000
Fe	0.247	0.255	0.246	0.269	0.247	0.234	0.137	0.191	0.265	0.195	0.149	0.107	0.123
Mg	0.043	0.041	0.050	0.071	0.010	0.056	0.059	0.010	0.018	0.035	0.060	0.035	0.023
Mn	0.000	0.002	0.003	0.002	0.003	0.000	0.000	0.000	0.006	0.000	0.000	0.000	0.001
Ca	0.012	0.012	0.008	0.009	0.003	0.009	0.012	0.002	0.008	0.020	0.019	0.017	0.018
Ba	0.002	0.000	0.000	0.000	0.001	0.000	0.001	0.001	0.000	0.001	0.001	0.000	0.000
Sr	0.000	0.000	0.000	0.000	0.000	0.000	0.000	0.000	0.000	0.000	0.000	0.000	0.000
Na	0.003	0.001	0.008	0.007	0.000	0.001	0.011	0.005	0.013	0.111	0.037	0.036	0.042

K	0.003	0.004	0.009	0.005	0.003	0.149	0.016	0.005	0.008	0.032	0.024	0.024	0.019
F	0.076	0.000	0.000	0.000	0.015	0.003	0.016	0.000	0.066	0.000	0.000	0.000	0.004
Cl	0.087	0.063	0.086	0.082	0.007	0.053	0.006	0.008	0.044	0.094	0.084	0.059	0.064
Si	6.483	6.416	6.462	6.456	6.434	6.510	6.408	6.415	6.414	6.542	6.758	6.498	6.475
P	0.011	0.012	0.015	0.015	0.016	0.013	0.011	0.007	0.010	0.016	0.000	0.019	0.019
AlIV	1.506	1.573	1.524	1.530	1.550	1.477	1.581	1.578	1.576	1.443	1.242	1.483	1.506
sumT	*8.000*	*8.000*	*8.000*	*8.000*	*8.000*	*8.000*	*8.000*	*8.000*	*8.000*	*8.000*	*8.000*	*8.000*	*8.000*
AlVI	4.346	4.329	4.313	4.292	4.331	4.246	4.372	4.379	4.353	4.286	4.260	4.379	4.385
Cr	0.000	0.000	0.001	0.000	0.001	0.004	0.000	0.003	0.000	0.003	0.002	0.000	0.002
Ti	0.000	0.000	0.005	0.000	0.005	0.004	0.005	0.002	0.000	0.000	0.003	0.002	0.000
Fe	0.247	0.255	0.246	0.269	0.247	0.234	0.137	0.191	0.265	0.195	0.149	0.107	0.123
Mg	0.043	0.041	0.050	0.071	0.010	0.056	0.059	0.010	0.018	0.035	0.060	0.035	0.023
Mn	0.000	0.002	0.003	0.002	0.003	0.000	0.000	0.000	0.006	0.000	0.000	0.000	0.001
Sum	*4.637*	*4.626*	*4.619*	*4.635*	*4.596*	*4.544*	*4.573*	*4.585*	*4.641*	*4.520*	*4.474*	*4.522*	*4.534*
Ca	0.012	0.012	0.008	0.009	0.003	0.009	0.012	0.002	0.008	0.020	0.019	0.017	0.018
Ba	0.002	0.000	0.000	0.000	0.001	0.000	0.001	0.001	0.000	0.001	0.001	0.000	0.000
Sr	0.000	0.000	0.000	0.000	0.000	0.000	0.000	0.000	0.000	0.000	0.000	0.000	0.000
Na	0.003	0.001	0.008	0.007	0.000	0.001	0.011	0.005	0.013	0.111	0.037	0.036	0.042
K	0.003	0.004	0.009	0.005	0.003	0.149	0.016	0.005	0.008	0.032	0.024	0.024	0.019
sum	*0.020*	*0.018*	*0.025*	*0.020*	*0.006*	*0.159*	*0.040*	*0.014*	*0.029*	*0.164*	*0.081*	*0.077*	*0.080*
F	0.076	0.000	0.000	0.000	0.015	0.003	0.016	0.000	0.066	0.000	0.000	0.000	0.004
Cl	0.087	0.063	0.086	0.082	0.007	0.053	0.006	0.008	0.044	0.094	0.084	0.059	0.064
Si/Si+Al	0.811	0.597	0.600	0.601	0.598	0.605	0.594	0.594	0.596	0.604	0.613	0.597	0.596

W7-A5_can	W7-A5_can	W7-A5_can	W7-A5_can	W7-A5_can	W7-A5_can	W7-A5_can	W7-A5_can	W7-A5_can	W7-A5_can	W7-C1A_ca	W7-C1A_ca	W7-C1A_ca	W7-C1A_ca
13	**18**	**22**	**38**	**41**	**48**	**49**	**52**	**53**	**55**	**3**	**4**	**7**	**8**
0.15	0.16	0.17	0.04	0.07	0.14	0.09	0.07	0.12	0.18	0.44	0.24	0.32	0.55
0.00	0.03	0.01	0.02	0.00	0.01	0.01	0.00	0.00	0.00	0.00	0.00	0.00	0.01
36.96	38.02	39.91	40.00	39.52	38.69	39.38	39.27	39.32	38.30	39.61	37.03	41.14	41.52
29.53	28.85	30.72	30.76	28.26	29.86	29.14	28.56	30.46	29.76	29.80	28.06	31.71	31.82
0.02	0.01	0.00	0.00	0.01	0.00	0.00	0.04	0.01	0.00	0.01	0.01	0.02	0.00
0.01	0.00	0.00	0.03	0.04	0.01	0.02	0.00	0.00	0.00	0.00	0.00	0.00	0.00
1.03	0.86	0.67	0.70	0.62	1.21	1.47	1.15	1.39	1.12	0.82	0.93	0.82	0.97
0.08	0.11	0.13	0.21	0.24	0.12	0.10	0.25	0.17	0.10	0.25	0.38	0.43	0.34
0.00	0.01	0.00	0.04	0.00	0.00	0.00	0.00	0.01	0.00	0.00	0.00	0.00	0.00
0.08	0.03	0.04	0.05	0.09	0.04	0.08	0.06	0.02	0.06	0.24	0.11	0.17	0.35
0.00	0.02	0.00	0.00	0.02	0.00	0.00	0.02	0.01	0.00	0.00	0.00	0.00	0.00
0.00	0.00	0.00	0.00	0.00	0.00	0.00	0.00	0.00	0.00	0.00	0.00	0.00	0.00
0.15	0.19	0.10	0.14	0.12	0.04	0.10	0.04	0.08	0.11	0.15	0.05	0.11	0.08
0.13	0.36	0.13	0.15	0.20	0.18	0.08	0.06	0.04	0.08	0.44	0.69	0.37	0.17
0.03	0.00	0.04	0.00	0.03	0.04	0.00	0.06	0.00	0.09	0.10	0.08	0.00	0.11
0.29	0.21	0.25	0.24	0.20	0.14	0.15	0.12	0.12	0.16	0.10	0.19	0.17	0.09
67.791	68.223	71.511	71.724	68.744	69.828	69.949	69.040	71.109	69.306	71.306	67.095	74.612	75.369
0.077	0.046	0.072	0.053	0.055	0.050	0.035	0.051	0.028	0.076	0.065	0.074	0.038	0.065
67.71	**68.18**	**71.44**	**71.67**	**68.69**	**69.78**	**69.91**	**68.99**	**71.08**	**69.23**	**71.24**	**67.02**	**74.57**	**75.30**

W7-A5_can	W7-A5_can	W7-A5_can	W7-A5_can	W7-A5_can	W7-A5_can	W7-A5_can	W7-A5_can	W7-A5_can	W7-A5_can	W7-C1A_ca	W7-C1A_ca	W7-C1A_ca	W7-C1A_ca
0.022	0.023	0.023	0.006	0.010	0.020	0.012	0.010	0.016	0.026	0.061	0.035	0.042	0.071
0.000	0.004	0.002	0.003	0.000	0.001	0.002	0.000	0.000	0.000	0.000	0.000	0.000	0.002
6.378	6.503	6.495	6.491	6.676	6.464	6.565	6.620	6.446	6.451	6.487	6.474	6.431	6.428
6.007	5.816	5.891	5.885	5.627	5.878	5.725	5.673	5.884	5.908	5.752	5.781	5.840	5.805
0.002	0.002	0.000	0.000	0.001	0.000	0.000	0.005	0.002	0.000	0.001	0.001	0.002	0.000
0.002	0.000	0.000	0.004	0.004	0.001	0.002	0.000	0.000	0.000	0.000	0.000	0.000	0.000
0.148	0.123	0.091	0.095	0.088	0.169	0.205	0.162	0.191	0.157	0.112	0.135	0.107	0.126
0.020	0.028	0.031	0.052	0.060	0.029	0.024	0.064	0.042	0.025	0.061	0.100	0.101	0.079
0.000	0.002	0.000	0.005	0.000	0.000	0.000	0.000	0.002	0.000	0.000	0.000	0.000	0.000
0.014	0.006	0.007	0.008	0.016	0.008	0.014	0.011	0.004	0.010	0.042	0.021	0.029	0.059
0.000	0.001	0.000	0.000	0.001	0.000	0.000	0.001	0.000	0.000	0.000	0.000	0.000	0.000
0.000	0.000	0.000	0.000	0.000	0.000	0.000	0.000	0.000	0.000	0.000	0.000	0.000	0.000
0.049	0.064	0.030	0.043	0.039	0.014	0.031	0.013	0.024	0.037	0.047	0.016	0.034	0.025

0.029	0.078	0.027	0.032	0.043	0.038	0.017	0.012	0.008	0.017	0.091	0.153	0.073	0.033
0.016	0.000	0.018	0.000	0.013	0.022	0.000	0.031	0.000	0.050	0.052	0.042	0.000	0.052
0.084	0.060	0.070	0.065	0.057	0.040	0.044	0.033	0.034	0.046	0.028	0.056	0.044	0.024

6.378	6.503	6.495	6.491	6.676	6.464	6.565	6.620	6.446	6.451	6.487	6.474	6.431	6.428
0.022	0.023	0.023	0.006	0.010	0.020	0.012	0.010	0.016	0.026	0.061	0.035	0.042	0.071
1.599	1.473	1.482	1.503	1.313	1.516	1.422	1.370	1.538	1.523	1.452	1.492	1.527	1.500
8.000	*8.000*	*8.000*	*8.000*	*8.000*	*8.000*	*8.000*	*8.000*	*8.000*	*8.000*	*8.000*	*8.000*	*8.000*	*8.000*
4.407	4.343	4.409	4.382	4.314	4.363	4.303	4.303	4.346	4.385	4.300	4.290	4.314	4.305
0.002	0.002	0.000	0.000	0.001	0.000	0.000	0.005	0.002	0.000	0.001	0.001	0.002	0.000
0.002	0.000	0.000	0.004	0.004	0.001	0.002	0.000	0.000	0.000	0.000	0.000	0.000	0.000
0.148	0.123	0.091	0.095	0.088	0.169	0.205	0.162	0.191	0.157	0.112	0.135	0.107	0.126
0.020	0.028	0.031	0.052	0.060	0.029	0.024	0.064	0.042	0.025	0.061	0.100	0.101	0.079
0.000	0.002	0.000	0.005	0.000	0.000	0.000	0.000	0.002	0.000	0.000	0.000	0.000	0.000
4.579	*4.498*	*4.531*	*4.537*	*4.467*	*4.561*	*4.533*	*4.533*	*4.583*	*4.567*	*4.474*	*4.526*	*4.524*	*4.510*
0.014	0.006	0.007	0.008	0.016	0.008	0.014	0.011	0.004	0.010	0.042	0.021	0.029	0.059
0.000	0.001	0.000	0.000	0.001	0.000	0.000	0.001	0.000	0.000	0.000	0.000	0.000	0.000
0.000	0.000	0.000	0.000	0.000	0.000	0.000	0.000	0.000	0.000	0.000	0.000	0.000	0.000
0.049	0.064	0.030	0.043	0.039	0.014	0.031	0.013	0.024	0.037	0.047	0.016	0.034	0.025
0.029	0.078	0.027	0.032	0.043	0.038	0.017	0.012	0.008	0.017	0.091	0.153	0.073	0.033
0.092	*0.149*	*0.065*	*0.083*	*0.098*	*0.059*	*0.062*	*0.038*	*0.037*	*0.064*	*0.180*	*0.190*	*0.136*	*0.116*
0.016	0.000	0.018	0.000	0.013	0.022	0.000	0.031	0.000	0.050	0.052	0.042	0.000	0.052
0.084	0.060	0.070	0.065	0.057	0.040	0.044	0.033	0.034	0.046	0.028	0.056	0.044	0.024

0.591	0.600	0.596	0.597	0.607	0.597	0.604	0.606	0.597	0.595	0.601	0.601	0.599	0.599

W7-C1A_ca	W7-C1A_ca	W7-C1A_ca	W7-C1A_ca	W7-C1A_ca	W7-C1A_ca	W7-C1A_campo3-1	kaolinite	halloysite	dickite	nacrite	beidellite
9	**11**	**12**	**14**	**15**	**17**	**33**	**EM**	**EM**	**EM**	**EM**	
0.21	0.48	0.54	0.93	0.98	0.50	0.32	0.000	0.00	0.00	0	0
0.00	0.00	0.00	0.02	0.03	0.00	0.00	0.000	0.00	0.00	0	0
38.01	38.94	39.66	36.79	37.44	38.17	44.16	45.800	43.98	48.86	46.55	55.8
29.17	29.36	31.63	29.16	28.49	29.99	35.30	39.550	38.46	37.12	39.5	28.6
0.00	0.00	0.01	0.01	0.00	0.01	0.00	0.000	0.00	0.00	0	0.4
0.00	0.00	0.00	0.00	0.01	0.00	0.00	0.000	0.01	0.51	0	0
0.56	0.66	1.00	1.52	1.50	1.03	0.47	0.693	0.03	1.35	0	0
0.20	0.20	0.29	0.30	0.30	0.20	0.17	0.140	0.00	0.09	0	2.03
0.00	0.00	0.00	0.01	0.01	0.00	0.04	0.000	0.00	0.00	0	0
0.12	0.38	0.41	0.58	0.55	0.30	0.11	0.410	0.32	0.22	0	2.23
0.00	0.00	0.00	0.00	0.00	0.01	0.00	0.000	0.00	0.00	0	0
0.00	0.00	0.00	0.00	0.00	0.00	0.00	0.000	0.00	0.00	0	0
0.06	0.05	0.06	0.06	0.03	0.08	0.10	0.000	0.14	0.07	0	0.09
1.31	0.08	0.20	0.13	0.12	0.11	0.11	0.030	0.48	0.60	0	0.48
0.04	0.04	0.00	0.00	0.03	0.08	0.05	0.000	0.00	0.00	0	0
0.10	0.12	0.24	0.28	0.24	0.18	0.27	0.000	0.00	0.00	0	0
69.138	69.670	73.379	69.156	69.086	70.003	80.461	85.976	82.773	88.170	85.403	88.952
0.037	0.042	0.054	0.064	0.066	0.075	0.082	0.000	0.000	0.000	0.000	0.000
69.10	**69.63**	**73.32**	**69.09**	**69.02**	**69.93**	**80.38**	**85.98**	**82.77**	**88.17**	**85.40**	**88.95**

W7-C1A_ca	W7-C1A_ca	W7-C1A_ca	W7-C1A_ca	W7-C1A_ca	W7-C1A_ca	W7-C1A_campo3-1	kaolinite	halloysite	dickite	nacrite	beidellite
0.031	0.067	0.072	0.134	0.141	0.070	0.039	0.000	0.000	0.000	0.000	0.000
0.000	0.000	0.000	0.003	0.004	0.000	0.000	0.000	0.000	0.000	0.000	0.000
6.448	6.490	6.320	6.256	6.359	6.373	6.389	6.191	6.172	6.473	6.286	7.289
5.831	5.766	5.940	5.842	5.703	5.901	6.019	6.300	6.361	5.796	6.286	4.403
0.000	0.000	0.001	0.001	0.000	0.001	0.000	0.000	0.000	0.000	0.000	0.038
0.001	0.001	0.000	0.001	0.002	0.000	0.000	0.000	0.001	0.051	0.000	0.000
0.079	0.092	0.133	0.216	0.213	0.144	0.057	0.078	0.004	0.149	0.000	0.000
0.051	0.051	0.068	0.076	0.075	0.050	0.037	0.028	0.000	0.018	0.000	0.395
0.000	0.000	0.000	0.002	0.001	0.000	0.005	0.000	0.000	0.000	0.000	0.000
0.021	0.067	0.070	0.106	0.100	0.054	0.018	0.059	0.048	0.031	0.000	0.312
0.000	0.000	0.000	0.000	0.000	0.000	0.000	0.000	0.000	0.000	0.000	0.000
0.000	0.000	0.000	0.000	0.000	0.000	0.000	0.000	0.000	0.000	0.000	0.000
0.021	0.016	0.019	0.021	0.011	0.027	0.027	0.000	0.038	0.018	0.000	0.023

0.284	0.018	0.040	0.029	0.027	0.023	0.021	0.005	0.086	0.101	0.000	0.080
0.020	0.019	0.000	0.000	0.016	0.043	0.024	0.000	0.000	0.000	0.000	0.000
0.028	0.032	0.065	0.082	0.069	0.051	0.065	0.000	0.000	0.000	0.000	0.000
6.448	6.490	6.320	6.256	6.359	6.373	6.389	6.191	6.172	6.473	6.286	7.289
0.031	0.067	0.072	0.134	0.141	0.070	0.039	0.000	0.000	0.000	0.000	0.000
1.522	1.443	1.608	1.610	1.500	1.557	1.572	1.809	1.828	1.527	1.714	0.711
8.000	*8.000*	*8.000*	*8.000*	*8.000*	*8.000*	*8.000*	*8.000*	*8.000*	*8.000*	*8.000*	*8.000*
4.309	4.323	4.332	4.232	4.203	4.344	4.447	4.491	4.532	4.269	4.571	3.693
0.000	0.000	0.001	0.001	0.000	0.001	0.000	0.000	0.000	0.000	0.000	0.038
0.001	0.001	0.000	0.001	0.002	0.000	0.000	0.000	0.001	0.051	0.000	0.000
0.079	0.092	0.133	0.216	0.213	0.144	0.057	0.078	0.004	0.149	0.000	0.000
0.051	0.051	0.068	0.076	0.075	0.050	0.037	0.028	0.000	0.018	0.000	0.395
0.000	0.000	0.000	0.002	0.001	0.000	0.005	0.000	0.000	0.000	0.000	0.000
4.440	*4.467*	*4.534*	*4.527*	*4.494*	*4.539*	*4.546*	*4.597*	*4.537*	*4.487*	*4.571*	*4.126*
0.021	0.067	0.070	0.106	0.100	0.054	0.018	0.059	0.048	0.031	0.000	0.312
0.000	0.000	0.000	0.000	0.000	0.000	0.000	0.000	0.000	0.000	0.000	0.000
0.000	0.000	0.000	0.000	0.000	0.000	0.000	0.000	0.000	0.000	0.000	0.000
0.021	0.016	0.019	0.021	0.011	0.027	0.027	0.000	0.038	0.018	0.000	0.023
0.284	0.018	0.040	0.029	0.027	0.023	0.021	0.005	0.086	0.101	0.000	0.080
0.326	*0.102*	*0.129*	*0.155*	*0.138*	*0.104*	*0.066*	*0.065*	*0.172*	*0.151*	*0.000*	*0.415*
0.020	0.019	0.000	0.000	0.016	0.043	0.024	0.000	0.000	0.000	0.000	0.000
0.028	0.032	0.065	0.082	0.069	0.051	0.065	0.000	0.000	0.000	0.000	0.000
0.599	0.600	0.593	0.596	0.602	0.595	0.590	0.580	0.577	0.603	0.579	0.664

Sample	W5-D1A_ca	W5-D1A_ca	W5-D1A_ca	W5-D1A_ca	W5-D1A_ca	W5-D1A_ca	W5-D1A_ca	W5-D1A_ca	W5-D1A_ca	W5-D1A_ca	W5-D1A_ca	W5-F1A_ca	W5-F1A_ca
No.	22	25	29	34	35	36	37	38	39	40	41	22	23
P2O5	0.02	0.00	0.00	0.05	0.00	0.02	0.00	0.00	0.07	0.02	0.00	0.03	0.04
V2O3	0.00	0.02	0.00	0.00	0.00	0.01	0.05	0.00	0.00	0.00	0.00	0.00	0.00
SiO2	96.14	99.61	98.30	97.90	94.31	95.58	96.66	99.56	96.79	93.83	97.61	96.81	98.56
Al2O3	0.05	0.09	0.02	0.07	0.36	0.92	0.07	0.01	0.04	0.04	0.52	0.04	0.05
Cr2O3	0.00	0.00	0.00	0.00	0.00	0.00	0.00	0.00	0.00	0.00	0.00	0.01	0.00
TiO2	0.00	0.00	0.00	0.03	0.01	0.00	0.00	0.04	0.01	0.00	0.00	0.00	0.00
FeO	0.01	0.02	0.00	0.03	0.05	0.06	0.04	0.02	0.01	0.03	0.06	0.02	0.00
MgO	0.00	0.00	0.00	0.00	0.01	0.04	0.00	0.00	0.00	0.01	0.02	0.00	0.02
MnO	0.07	0.07	0.03	0.02	0.00	0.01	0.03	0.05	0.00	0.01	0.01	0.01	0.02
CaO	0.00	0.02	0.00	0.02	0.03	0.14	0.01	0.01	0.03	0.03	0.02	0.00	0.00
BaO	0.00	0.01	0.07	0.00	0.01	0.02	0.00	0.00	0.00	0.00	0.00	0.02	0.00
SrO	0.00	0.00	0.00	0.00	0.00	0.00	0.00	0.00	0.00	0.00	0.00	0.00	0.00
Na2O	0.05	0.02	0.05	0.04	0.12	0.08	0.15	0.01	0.07	0.12	0.12	0.09	0.04
K2O	0.06	0.04	0.04	0.02	0.11	0.11	0.05	0.03	0.03	0.05	0.13	0.04	0.03
F	0.02	0.23	0.00	0.01	0.00	0.00	0.00	0.00	0.00	0.00	0.00	0.01	0.00
Cl	0.06	0.04	0.01	0.01	0.02	0.00	0.01	0.01	0.01	0.02	0.02	0.00	0.00
Total	96.47	100.05	98.51	98.18	95.01	96.99	97.07	99.73	97.07	94.13	98.49	97.09	98.76

W5-F1A_ca	W5-F1A_ca	W5-F1A_ca	W5-F1A_ca	W5-F1A_ca	W5-F1A_ca	W6-B7A_ca	W6-B7A_ca	W6-B7A_ca	W6-B7A_ca	W6-B7A_ca	W6-B7A_ca	W6-B7A_ca	W6-B7A_ca
24	25	26	27	29	33	1	10	12	16	26	27	30	39
0.00	0.04	0.05	0.04	0.02	0.17	0.00	0.01	0.02	0.00	0.02	0.04	0.01	0.02
0.04	0.00	0.00	0.00	0.00	0.01	0.04	0.04	0.01	0.00	0.00	0.01	0.00	0.03
96.99	97.55	93.44	97.41	95.75	95.54	97.02	99.66	96.26	99.07	100.07	99.03	97.90	100.03
0.16	0.18	0.27	0.22	0.22	2.58	0.00	0.01	0.47	0.17	0.01	0.03	0.03	0.00
0.00	0.00	0.01	0.00	0.00	0.02	0.00	0.00	0.00	0.00	0.00	0.01	0.00	0.00
0.00	0.00	0.02	0.00	0.00	0.05	0.04	0.00	0.01	0.00	0.03	0.02	0.05	0.01
0.02	0.00	0.00	0.00	0.03	0.67	0.00	0.06	0.07	0.11	0.04	0.01	0.03	0.01
0.00	0.01	0.01	0.00	0.01	0.01	0.00	0.01	0.01	0.00	0.00	0.01	0.00	0.01
0.03	0.07	0.02	0.00	0.03	0.05	0.02	0.04	0.01	0.01	0.00	0.06	0.00	0.04
0.03	0.03	0.06	0.02	0.03	0.07	0.03	0.02	0.03	0.02	0.01	0.01	0.00	0.02
0.00	0.00	0.00	0.01	0.00	0.02	0.04	0.02	0.00	0.00	0.01	0.00	0.02	0.02
0.00	0.00	0.00	0.00	0.00	0.00	0.00	0.00	0.00	0.00	0.00	0.00	0.00	0.00
0.09	0.15	0.42	0.11	0.18	0.00	0.00	0.00	0.05	0.01	0.00	0.00	0.00	0.02
0.06	0.07	0.18	0.07	0.09	0.12	0.00	0.01	0.10	0.04	0.02	0.01	0.01	0.00
0.02	0.08	0.14	0.01	0.22	0.00	0.06	0.00	0.03	0.10	0.00	0.00	0.07	0.00
0.01	0.01	0.01	0.02	0.01	0.01	0.00	0.00	0.01	0.02	0.00	0.00	0.01	0.01
97.44	98.15	94.58	97.90	96.50	99.32	97.20	99.87	97.06	99.50	100.20	99.22	98.10	100.20

W6-B7A_ca	W6-B7B_ca	W6-B7B_ca	W6-B7B_ca	W6-B7B_ca	W6-B7B_ca	W6-B7B_ca	W6-B7B_ca	W6-B7B_ca	W6-B7B_ca	W6-B7B_ca	W6-B7B_ca	W6-B7B_ca	W6-B7B_ca
42	2	3	8	10	11	13	18	21	23	32	33	34	35
0.03	0.02	0.00	0.02	0.01	0.00	0.00	0.00	0.02	0.02	0.00	0.00	0.02	0.02
0.00	0.00	0.01	0.00	0.00	0.00	0.00	0.00	0.00	0.04	0.02	0.00	0.00	0.01
99.91	93.93	100.73	98.43	99.03	99.73	99.10	98.38	99.35	100.79	99.73	101.97	97.43	99.88
0.09	1.78	0.18	0.57	0.24	0.10	0.33	0.08	0.04	0.00	0.01	0.05	0.02	0.01
0.00	0.00	0.02	0.00	0.00	0.00	0.00	0.00	0.00	0.00	0.00	0.00	0.00	0.03
0.02	0.04	0.00	0.04	0.00	0.00	0.03	0.01	0.00	0.00	0.00	0.01	0.00	0.02
0.04	1.07	0.06	0.08	0.07	0.05	0.06	0.05	0.01	0.01	0.01	0.01	0.02	0.00
0.00	1.24	0.02	0.01	0.00	0.00	0.00	0.02	0.01	0.00	0.01	0.01	0.00	0.00
0.00	0.05	0.00	0.02	0.02	0.01	0.04	0.00	0.00	0.02	0.07	0.00	0.02	0.00
0.01	0.02	0.04	0.01	0.01	0.02	0.09	0.02	0.03	0.01	0.00	0.00	0.04	0.01
0.00	0.00	0.00	0.01	0.01	0.00	0.00	0.00	0.00	0.00	0.00	0.05	0.00	0.00
0.00	0.00	0.00	0.00	0.00	0.00	0.00	0.00	0.00	0.00	0.00	0.00	0.00	0.00
0.00	0.05	0.02	0.09	0.06	0.02	0.07	0.02	0.05	0.03	0.01	0.00	0.09	0.02
0.01	0.08	0.01	0.13	0.04	0.03	0.08	0.03	0.02	0.01	0.01	0.00	0.03	0.01
0.00	0.07	0.00	0.02	0.00	0.08	0.03	0.00	0.12	0.00	0.00	0.02	0.00	0.00
0.00	0.00	0.01	0.01	0.00	0.00	0.01	0.00	0.02	0.01	0.01	0.00	0.02	0.00
100.12	98.32	101.09	99.41	99.49	100.01	99.83	98.60	99.61	100.94	99.87	102.11	97.70	100.01

W6-B7B_ca	W6-B7B_ca	W6-B7B_ca	W6-B7B_ca	W6-B7B_ca	W6-C6_can	W6-C6_can	W7-A5_can	W7-A5_can	W7-A5_can	W7-A5_can	W7-A5_can	W7-A5_can	W7-A5_can
36	37	38	42	43	27	32	1	2	7	9	16	21	25
0.01	0.00	0.00	0.06	0.01	0.00	0.04	0.01	0.02	0.02	0.00	0.07	0.03	0.01
0.01	0.01	0.02	0.00	0.00	0.00	0.00	0.01	0.00	0.00	0.00	0.02	0.00	0.00
99.02	99.34	98.73	97.04	98.48	101.55	100.61	100.94	97.50	98.24	99.81	100.14	99.87	90.15
0.04	0.02	0.10	0.28	0.15	0.00	0.00	0.03	0.07	0.08	0.04	0.13	0.05	4.34
0.00	0.00	0.01	0.00	0.00	0.00	0.00	0.01	0.00	0.00	0.00	0.00	0.00	0.01
0.00	0.00	0.00	0.04	0.02	0.00	0.00	0.00	0.00	0.00	0.00	0.03	0.00	0.02
0.00	0.00	0.01	0.04	0.00	0.12	0.05	0.06	0.17	0.10	0.02	0.03	0.05	0.26
0.00	0.02	0.03	0.00	0.00	0.01	0.00	0.00	0.00	0.01	0.01	0.01	0.02	0.16
0.00	0.01	0.05	0.06	0.03	0.03	0.01	0.02	0.00	0.00	0.09	0.02	0.00	0.00
0.02	0.02	0.01	0.01	0.02	0.02	0.03	0.03	0.02	0.06	0.02	0.01	0.04	0.04
0.00	0.00	0.00	0.00	0.00	0.03	0.00	0.02	0.01	0.01	0.05	0.00	0.00	0.00
0.00	0.00	0.00	0.00	0.00	0.00	0.00	0.00	0.00	0.00	0.00	0.00	0.00	0.00
0.06	0.04	0.05	0.08	0.06	0.02	0.05	0.00	0.03	0.16	0.01	0.03	0.02	0.02
0.02	0.02	0.02	0.07	0.04	0.00	0.02	0.01	0.01	0.03	0.01	0.02	0.01	0.08
0.00	0.14	0.00	0.00	0.09	0.00	0.00	0.00	0.02	0.00	0.02	0.00	0.00	0.00
0.02	0.01	0.01	0.00	0.00	0.00	0.01	0.00	0.00	0.01	0.00	0.00	0.01	0.07
99.20	99.56	99.03	97.67	98.84	101.78	100.81	101.13	97.85	98.71	100.06	100.51	100.10	95.14

W7-A5_can	W7-A5_can	W7-A5_can	W7-A5_can	W7-A5_can	W7-A5_can	W7-A5_can	W7-A5_can	W7-A5_can	W7-A5_can	W7-C1A_ca	W7-C1A_ca	W7-C1A_ca	W7-C1A_ca
28	30	31	32	33	34	36	40	50	58	13	26	32	35
0.08	0.01	0.03	0.02	0.00	0.00	0.01	0.01	0.04	0.04	0.00	0.01	0.00	0.05
0.00	0.00	0.01	0.03	0.00	0.00	0.02	0.00	0.00	0.00	0.01	0.00	0.01	0.01
98.20	97.74	98.92	96.98	95.24	97.88	99.43	96.42	99.47	99.16	101.85	100.14	99.99	99.54
0.07	0.00	0.02	0.03	0.08	0.00	0.00	0.05	0.04	0.00	0.01	0.01	0.05	0.00
0.00	0.01	0.01	0.00	0.00	0.00	0.00	0.00	0.00	0.00	0.00	0.00	0.00	0.00
0.00	0.00	0.02	0.00	0.03	0.00	0.00	0.00	0.02	0.04	0.00	0.02	0.00	0.01
0.02	0.01	0.00	0.01	0.00	0.03	0.00	0.00	0.05	0.01	0.01	0.04	0.00	0.00
0.00	0.00	0.02	0.00	0.00	0.00	0.01	0.01	0.00	0.01	0.00	0.01	0.00	0.00
0.06	0.02	0.00	0.00	0.03	0.00	0.00	0.01	0.00	0.00	0.02	0.00	0.03	0.00
0.02	0.00	0.00	0.03	0.00	0.04	0.02	0.02	0.00	0.00	0.00	0.03	0.02	0.02
0.02	0.00	0.00	0.00	0.00	0.01	0.00	0.00	0.00	0.00	0.05	0.02	0.03	0.00
0.00	0.00	0.00	0.00	0.00	0.00	0.00	0.00	0.00	0.00	0.00	0.00	0.00	0.00
0.09	0.02	0.02	0.04	0.03	0.02	0.01	0.05	0.00	0.03	0.00	0.01	0.01	0.02
0.07	0.01	0.02	0.02	0.04	0.02	0.00	0.04	0.01	0.01	0.01	0.01	0.01	0.01
0.00	0.00	0.08	0.00	0.00	0.22	0.04	0.03	0.00	0.00	0.00	0.00	0.00	0.00
0.02	0.00	0.00	0.02	0.02	0.01	0.01	0.02	0.00	0.00	0.01	0.00	0.00	0.00
98.65	97.83	99.13	97.17	95.46	98.14	99.52	96.64	99.62	99.31	101.97	100.29	100.16	99.67

W7-C1A_ca	W7-C2B_ca	W7-C2B_ca	W7-C2B_ca	W7-C2B_ca	W7-C2B_ca	W7-C2B_ca	W7-C2B_ca	W7-C2B_ca	W7-C2B_ca	W7-C2B_ca	W7-C2B_ca	W7-C2B_ca	W7-C2B_ca
37	19	21	22	26	27	28	29	30	35	37	38	40	42
0.03	0.00	0.02	0.01	0.04	0.02	0.00	0.02	0.01	0.00	0.00	0.06	0.00	0.03
0.00	0.00	0.01	0.00	0.01	0.04	0.01	0.01	0.00	0.00	0.00	0.02	0.00	0.02
100.13	98.80	96.71	98.48	96.90	100.27	100.03	99.80	96.26	100.13	100.10	100.04	99.99	99.85
0.07	0.07	0.02	0.03	0.93	0.02	0.02	0.02	0.22	0.06	0.02	0.00	0.05	0.07
0.00	0.00	0.00	0.00	0.01	0.00	0.00	0.00	0.00	0.01	0.00	0.00	0.00	0.00
0.00	0.01	0.00	0.02	0.00	0.01	0.00	0.03	0.00	0.00	0.01	0.00	0.03	0.04
0.01	0.06	0.03	0.03	0.22	0.00	0.00	0.02	0.02	0.06	0.00	0.02	0.04	0.04
0.00	0.03	0.00	0.00	0.10	0.01	0.02	0.01	0.01	0.01	0.01	0.00	0.00	0.00
0.00	0.00	0.01	0.03	0.04	0.02	0.05	0.02	0.00	0.00	0.00	0.01	0.00	0.01
0.01	0.01	0.03	0.01	0.20	0.01	0.02	0.00	0.04	0.01	0.00	0.01	0.00	0.02
0.00	0.03	0.00	0.00	0.00	0.00	0.00	0.00	0.00	0.02	0.00	0.01	0.01	0.01
0.00	0.00	0.00	0.00	0.00	0.00	0.00	0.00	0.00	0.00	0.00	0.00	0.00	0.00
0.02	0.19	0.13	0.04	0.11	0.03	0.03	0.06	0.28	0.05	0.04	0.05	0.05	0.05
0.01	0.08	0.04	0.04	0.40	0.01	0.02	0.03	0.07	0.05	0.02	0.01	0.05	0.04
0.00	0.02	0.00	0.04	0.00	0.00	0.00	0.00	0.00	0.03	0.02	0.00	0.00	0.06
0.01	0.02	0.01	0.01	0.02	0.00	0.00	0.01	0.02	0.03	0.01	0.01	0.03	0.02
100.27	99.31	97.02	98.72	98.97	100.43	100.19	100.03	96.94	100.45	100.21	100.23	100.24	100.24

W7-C2B_ca	W7-C2B_ca	W7-C2B_ca	W5-D1A_ca	W5-F1A_ca	W7-A5_can	W7-C1A_campo1-6
45	46	50	18	28	44	6
0.00	0.00	0.00	0.08	0.04	0.02	0.05
0.00	0.03	0.00	0.00	0.00	0.00	0.00
100.31	101.76	100.91	79.15	88.97	74.84	99.03
0.02	0.01	0.01	0.06	0.60	1.49	0.01
0.00	0.00	0.00	0.00	0.00	0.01	0.00
0.01	0.04	0.02	0.05	0.02	0.05	0.00
0.04	0.00	0.02	0.06	0.14	0.09	0.00
0.00	0.00	0.00	0.02	0.01	0.00	0.01
0.03	0.00	0.04	0.01	0.00	0.00	0.00
0.01	0.01	0.01	0.02	0.04	0.05	0.02
0.00	0.04	0.00	0.01	0.01	0.00	0.00
0.00	0.00	0.00	0.00	0.00	0.00	0.00
0.01	0.01	0.04	0.09	0.12	0.03	0.06
0.03	0.01	0.02	0.08	0.13	0.04	0.03
0.00	0.00	0.00	0.00	0.04	0.06	0.00
0.03	0.00	0.01	0.38	0.10	0.21	0.00
100.48	101.91	101.08	79.92	90.18	76.81	99.22

Laboratório de Microscopia e Microanálises (LMIc)
Microssonda Eletrônica JEOL JXA-8230, 5 WDS e 1 EDS
15kV, 20nA, 5nm spot size

No.	Na2O	F	SiO2	Al2O3	MgO	BaO	FeO	Cl	V2O3	SrO	TiO2	CaO	P2O5
1	0	0	100.004	0.033	0.023	0	0.02	0.002	0	0.004	0	0.013	0
2	0	0.676	0.027	33.332	0.017	0	1.47	0.002	0	0.02	0.004	0.021	48.989
3	0	0.307	0	33.299	0.018	0	1.488	0.002	0.03	0	0	0.022	48.663
4	0	0.475	0.01	33.164	0	0	1.21	0	0.047	0.017	0	0.018	48.815
5	0	0.61	0.016	33.524	0.006	0	1.341	0.006	0	0	0	0.014	48.293
6	0	0.384	0.032	33.311	0.012	0	2.833	0.012	0.019	0.066	0	0.236	48.817
7	0	0.481	0.003	33.126	0.017	0.009	1.61	0.011	0	0	0.009	0.045	48.18
8	0	0.486	0.016	33.062	0.019	0	3.37	0.009	0.002	0.003	0.032	0.025	48.785
9	0	0.443	0.008	33.428	0.001	0	2.215	0.004	0.015	0.022	0	0.044	48.622
10	0.03	0.071	98.443	0.076	0.005	0	0.05	0.006	0.055	0	0.028	0.014	0.038
11	0.056	0	96.669	0.605	0.018	0.03	0.163	0.028	0	0	0	0.063	0.037
12	0	0.391	0.017	32.027	0	0	2.703	0.002	0.029	0	0.034	0.116	48.936
13	0	0.587	0	33.111	0.022	0.036	2.24	0.003	0.011	0.044	0	0.154	48.056
14	0	0.252	0.05	33.169	0.02	0	1.941	0.002	0	0.013	0.023	0.045	48.507
15	0	0.473	0.018	33.454	0	0.017	2.294	0.01	0	0	0	0.044	48.882
16	0	0.532	0.033	33.951	0.017	0.03	1.379	0.009	0.028	0	0.007	0.009	49.306
17	0	0.633	0	33.02	0	0.011	1.794	0.005	0.007	0.008	0.025	0.038	48.814
18	0	0.393	0.016	33.739	0.004	0	1.98	0.019	0	0.006	0.014	0.029	48.207
19	0	0.4	0.031	33.805	0.014	0.022	1.832	0.008	0.004	0	0	0.13	48.564
20	0	0	99.866	0.047	0	0	0.022	0.015	0	0	0.018	0.004	0
21	0.062	0.027	99.48	0.208	0.017	0	0.063	0.024	0.018	0	0.034	0.021	0
22	0	0.624	0.055	33.884	0.033	0.002	2.883	0.017	0.039	0	0.022	0.027	47.618
23	0	0.575	1.465	32.64	0.029	0	4.104	0	0.005	0.011	0	0.03	46.84
24	0.015	0.03	100.624	0.146	0	0	0.07	0	0.019	0	0	0.013	0.003
25	0	0.383	7.478	30.995	0.033	0.01	3.43	0.012	0	0.009	0	0.015	43.413
Minimum	0	0	0	0.033	0	0	0.02	0	0	0	0	0.004	0
Maximum	0.062	0.676	100.624	33.951	0.033	0.036	4.104	0.028	0.055	0.066	0.034	0.236	49.306
Average	0.007	0.369	24.174	25.246	0.013	0.007	1.7	0.008	0.013	0.009	0.01	0.048	36.655

Sigma	0.017	0.224	43.05	14.386	0.011	0.011	1.172	0.008	0.016	0.016	0.013	0.055	21.046
No. of data	25												

Cr2O3	K2O	MnO	Total	Comment	
0.012	0.006	0.004	100.121	W6-B7A_campo2-1	**Quartzo**
0.021	0.018	0.039	84.351	W6-B7A_campo2-2	
0.036	0.017	0	83.753	W6-B7A_campo2-3	
0.025	0.013	0.006	83.6	W6-B7A_campo2-4	
0.035	0.023	0	83.61	W6-B7A_campo2-5	
0.043	0.029	0.013	85.642	W6-B7A_campo2-6	
0.029	0.033	0	83.348	W6-B7A_campo2-7	
0.035	0.028	0	85.665	W6-B7A_campo2-8	
0.026	0.008	0	84.648	W6-B7A_campo2-9	
0.017	0.016	0	98.818	W6-B7A_campo2-10	
0	0.135	0.016	97.814	W6-B7A_campo2-11	
0.038	0.015	0.002	84.145	W6-B7A_campo2-12	
0.043	0.014	0	84.073	W6-B7A_campo2-13	
0.016	0.012	0	83.944	W6-B7A_campo2-14	
0.028	0.021	0.023	85.063	W6-B7A_campo2-15	
0.006	0.019	0.031	85.131	W6-B7A_campo2-16	
0.018	0.019	0.012	84.136	W6-B7A_campo2-17	
0.007	0.04	0.013	84.298	W6-B7A_campo2-18	
0.025	0.024	0	84.689	W6-B7A_campo2-19	
0.023	0.005	0	99.997	W6-B7A_campo2-20	
0.01	0.046	0	99.994	W6-B7A_campo2-21	
0.021	0.033	0.006	84.997	W6-B7A_campo2-22	
0.026	0.04	0	85.523	W6-B7A_campo2-23	
0	0.003	0.025	100.935	W6-B7A_campo2-24	
0.036	0.043	0	85.693	W6-B7A_campo2-25	
0	0.003	0	83.348		
0.043	0.135	0.039	100.935		
0.023	0.026	0.008	88.16		

0.012	0.026	0.011	6.622

Laboratório de Microscopia e Microanálises (LMIc)
Microssonda Eletrônica JEOL JXA-8230, 5 WDS e 1 EDS
15kV, 20nA, 5nm spot size

No.	Na2O	F	SiO2	Al2O3	MgO	BaO	FeO	Cl	V2O3	SrO	TiO2	CaO	P2O5	Cr2O3
1	0.067	0.065	33.051	25.726	0.234	0.004	0.502	0.373	0.031	0	0	0.035	0.119	0
2	0.039	0.047	31.065	23.718	0.236	0.03	0.462	0.344	0	0	0	0.051	0.103	0.001
3	0.101	0.028	30.788	24.661	0.153	0.012	0.44	0.27	0.051	0	0.245	0.088	0.239	0.007
4	0.062	0	31.652	24.685	0.229	0.007	0.744	0.287	0	0.01	0	0.071	0.08	0
5	0.101	0	31.324	23.692	0.258	0.019	0.552	0.333	0	0	0	0.064	0.117	0.019
6	0.051	0.019	32.034	25.092	0.257	0	0.433	0.305	0	0	0.026	0.069	0.157	0
7	0.083	0	36.155	29.71	0.176	0	0.497	0.233	0.042	0	0.037	0.052	0.163	0.004
8	0.099	0.056	36.05	29.076	0.181	0	0.522	0.185	0.025	0.033	0.003	0.051	0.079	0.006
9	0.091	0.066	36.786	29.879	0.229	0	0.593	0.176	0.021	0.016	0.001	0.081	0.133	0
10	0	0.025	99.509	0.038	0.009	0.03	0.026	0.004	0.037	0.02	0	0.02	0.042	0.021
11	0	0.451	1.392	33.385	0.139	0	2.184	0.012	0	0	0.013	1.383	46.363	0.049
12	0	0.566	1.839	33.032	0.109	0.02	2.299	0.059	0.023	0	0.02	1.53	46.71	0.043
13	0.043	0	37.222	30.439	0.281	0.006	0.537	0.281	0.01	0	0.024	0.075	0.118	0
14	0.058	0	37.302	30.419	0.203	0	0.52	0.29	0.018	0	0	0.038	0.097	0
15	0.049	0.018	37.468	30.094	0.2	0	0.576	0.378	0	0	0	0.06	0.053	0
16	0.052	0	33.801	26.542	0.222	0.001	0.474	0.364	0.043	0.03	0	0.073	0.134	0.013
17	0.916	0.178	11.317	33.818	0.264	0	4.302	0.053	0.016	0.041	0.075	4.122	31.033	0.035
18	1.459	0.266	9.21	34.226	0.141	0	3.404	0.027	0	0.012	0.048	2.821	32.108	0.035
19	0.077	0	37.643	29.169	0.277	0.004	0.615	0.395	0	0	0.03	0.074	0.153	0.007
20	0.166	0.04	28.318	21.442	0.151	0	0.423	0.452	0	0	0.031	0.088	0.141	0.007
21	1.196	0.273	10.498	32.61	0.138	0.004	3.667	0.172	0	0.05	0.022	3.408	30.212	0.036
22	0.053	0.047	32.829	25.919	0.18	0	0.487	0.326	0	0.005	0	0.092	0.331	0
23	0.554	0.199	8.941	32.533	0.219	0	3.615	0.091	0.019	0.012	0.035	5.734	30.912	0.022
24	0.105	0	33.686	26.276	0.172	0	0.526	0.442	0	0	0.014	0.04	0.124	0.007
25	0.053	0.058	31.893	24.39	0.146	0	0.463	0.519	0.001	0.003	0.033	0.036	0.108	0
Minimum	0	0	1.392	0.038	0.009	0	0.026	0.004	0	0	0	0.02	0.042	0
Maximum	1.459	0.566	99.509	34.226	0.281	0.03	4.302	0.519	0.051	0.05	0.245	5.734	46.71	0.049

Average	0.219	0.096	30.071	27.223	0.192	0.005	1.155	0.255	0.013	0.009	0.026	0.806	8.793	0.012
Sigma	0.389	0.149	18.764	6.766	0.062	0.009	1.264	0.148	0.017	0.015	0.049	1.548	16.152	0.016
No. of data	25													

K2O	MnO	Total	Comment
0.083	0	60.179	W7-C1A_campo2-1
0.115	0	56.113	W7-C1A_campo2-2
0.078	0	57.088	W7-C1A_campo2-3
0.377	0.016	58.155	W7-C1A_campo2-4
0.239	0	56.643	W7-C1A_campo2-5
0.092	0	58.458	W7-C1A_campo2-6
0.074	0	67.173	W7-C1A_campo2-7
0.147	0.051	66.498	W7-C1A_campo2-8
0.137	0.01	68.151	W7-C1A_campo2-9
0.007	0.012	99.788	W7-C1A_campo2-10
0.112	0	85.29	W7-C1A_campo2-11
0.081	0.038	86.118	W7-C1A_campo2-12
0.07	0	69.043	W7-C1A_campo2-13
0.067	0	68.947	W7-C1A_campo2-14
0.071	0.013	68.887	W7-C1A_campo2-15
0.072	0.02	61.759	W7-C1A_campo2-16
0.284	0.003	86.37	W7-C1A_campo2-17
0.118	0	83.757	W7-C1A_campo2-18
0.101	0	68.456	W7-C1A_campo2-19
0.1	0	51.24	W7-C1A_campo2-20
0.121	0.006	82.259	W7-C1A_campo2-21
0.056	0.005	60.236	W7-C1A_campo2-22
0.096	0.019	82.896	W7-C1A_campo2-23
0.098	0	61.39	W7-C1A_campo2-24
0.079	0	57.641	W7-C1A_campo2-25
0.007	0	51.24	
0.377	0.051	99.788	

0.115	0.008	68.901
0.078	0.013	12.589